EXPERIMENTAL AND NUMERICAL INVESTIGATION OF THE DESIGN AND CONTROL OF VAPOR-COMPRESSION SYSTEMS WITH INTEGRATION OF TWO-PHASE EJECTORS FOR PERFORMANCE ENHANCEMENT THROUGH EXPANSION WORK RECOVERY

BY

NEAL D. LAWRENCE

DISSERTATION

Submitted in partial fulfillment of the requirements
for the degree of Doctor of Philosophy in Mechanical Engineering
in the Graduate College of the
University of Illinois at Urbana-Champaign, 2016

Urbana, Illinois

Doctoral Committee:

Adjunct Assistant Professor Stefan Elbel, Chair
Research Professor Predrag S. Hrnjak
Professor Anthony M. Jacobi
Professor J. Craig Dutton

ABSTRACT

The use of ejectors to improve the efficiency and capacity of vapor-compression refrigeration cycles by means of expansion work recovery has received significant attention in the past decade. Research has focused primarily on the design and performance of the ejector and the effect the ejector has on cycle performance. However, recent research has shown that additional factors, such as cycle architecture, improvement in evaporator performance, and cycle control, can also have significant influence on ejector cycle performance. While these factors have been noted in several studies, they have yet to be thoroughly investigated. Thus, the objective of this research is to investigate how to properly integrate an ejector into a vapor-compression cycle (how to choose the proper cycle architecture and proper use of the ejector) and how to design and operate other system components in addition to the ejector, such as the evaporator and cycle controls, in order to gain the maximum benefit from the ejector in the given system.

Two ejector cycles are investigated through the use of numerical modeling and experiments. The cycles of interest are the standard ejector cycle, which uses the ejector pressure increase to directly increase compressor suction pressure and reduce compressor power, and the ejector recirculation cycle, which uses the ejector to recirculate excess liquid through the evaporator and improve evaporator performance. The numerical results have shown that refrigerants and systems with inherently high throttling loss, such as transcritical CO_2 (R744) systems, should use the ejector to directly supplement compressor power using the pressure increase provided by the ejector, while systems using lower-pressure refrigerants should use the ejector to improve the performance of the evaporator by means of liquid recirculation (overfeed).

An experimental investigation of the two ejector cycles using R410A has been performed; two different microchannel evaporators with the same air-side geometry but different refrigerant-side cross-sectional area are used in the experimental investigation. The experimental results have shown that the more favorable ejector cycle depends on the design of the evaporator and on the operating conditions. The standard ejector cycle is more favorable at conditions of higher ambient temperature and with an evaporator with lower refrigerant-side cross-sectional area, achieving up to 9 % greater COP at matched capacity compared to an expansion valve cycle without an ejector. On the other hand, the ejector recirculation cycle is more favorable at lower ambient temperature and with an evaporator with greater refrigerant-side cross-sectional area (achieving up to 16 % greater COP at matched capacity). Further numerical investigation of the R410A system has provided additional insight into proper evaporator design and operation in ejector cycles. It has been found that the standard ejector cycle should operate with a low amount of evaporator overfeed to achieve greater ejector pressure increase and use the design

of the evaporator to improve evaporator effectiveness. The ejector recirculation cycle, which cannot directly utilize the ejector pressure increase, should operate with higher overfeed and use the evaporator design to optimize mass flux by balancing pressure drop and heat transfer effectiveness.

Finally, an experimental investigation of a transcritical CO_2 standard ejector cycle has been performed in order to investigate ejector cycle control. The high-side pressure of the transcritical system has been controlled and optimized by changing the effective nozzle throat size of the ejector through use of an adjustable position needle. Compared to using an expansion valve upstream of a fixed geometry ejector to control high-side pressure, the adjustable ejector results in slightly higher expansion work recovery efficiency and slightly higher COP. A loss in COP of up to 4 % has been observed for not properly controlling high-side pressure, while a loss in COP of up to 11 % has been observed for not properly controlling evaporator flow rate, meaning that it is important to also control and optimize evaporator flow rate in addition to high-side pressure when using a transcritical CO_2 standard ejector cycle. It has also been demonstrated that the high-side pressure optimization concept used to maximize COP under transcritical conditions can be extended and used to optimize the performance of the same system when it is operating under subcritical conditions as well.

ACKNOWLEDGEMENTS

I would first like to thank my advisor and friend, Professor Stefan Elbel, for his guidance throughout my time as a graduate student. His patience, knowledge, and input has been critical in helping me grow and improve my engineering and research skills. I would also like to thank my doctoral committee, Professor Pega Hrnjak, Professor Anthony M. Jacobi, and Professor J. Craig Dutton of the University of Illinois at Urbana-Champaign and Professor Armin Hafner of the Norwegian University of Science and Technology, for their input on improving my research.

I would like to acknowledge the member companies of the Air Conditioning and Refrigeration Center at the University of Illinois at Urbana-Champaign, whose support has helped make this research possible. I would also like to thank Creative Thermal Solutions, Inc. of Urbana, Illinois for their technical support and help with experiments and equipment.

Finally, I would like to thank my family, friends, and colleagues for their continuous support and encouragement throughout my engineering education.

TABLE OF CONTENTS

LIST OF FIGURES

LIST OF TABLES

NOMENCLATURE

Symbols

A	area	(mm^2)
C	constant	(-)
$\dot{C}$	capacitance rate	(kW K^{-1})
c_p	specific heat at constant pressure	(kJ kg^{-1} K^{-1})
d	diameter	(mm)
d_h	hydraulic diameter	(mm)
f	Darcy friction factor	(-)
Fr	Froude number	(-)
g	acceleration due to gravity	(m s^{-2})
G	mass flux	(kg m^{-2} s^{-1})
h	specific enthalpy	(kJ kg^{-1})
	heat transfer coefficient	(W m^{-2} K^{-1})
	height	(mm)
h_{fg}	specific enthalpy of vaporization	(kJ kg^{-1})
j	Chilton-Colburn j-factor	(-)
k	thermal conductivity	(W m^{-1} K^{-1})
L	length	(mm)
$\dot{m}$	mass flow rate	(g s^{-1})
n	circulation number	(-)
N	rotational speed	(min^{-1})
	quantity of given parameter	(-)
NTU	number of transfer units of heat exchanger	(-)
OR	overfeed ratio	(-)
P	pressure	(kPa, bar)
	pitch	(mm)
Pr	Prandtl number	(-)
q	specific heat transfer rate	(kJ kg^{-1})
q''	heat flux rate	(kW m^{-2})
$\dot{Q}$	heat transfer rate	(kW)
r	ratio of ejector motive to total mass flow rate	(-)

R	recirculation ratio	(-)
Re	Reynolds number	(-)
RH	relative humidity	(-)
s	specific entropy	(kJ kg^{-1} K^{-1})
T	temperature	(°C)
U	overall heat transfer coefficient	(kW m^{-2} K^{-1})
v	velocity	(m s^{-1})
$\dot{V}$	volumetric flow rate	(m^3 s^{-1})
w	specific compression work	(kJ kg^{-1})
$\dot{W}$	power	(kW)
We	Weber number	(-)
x	vapor mass fraction, two-phase quality	(-)
X	Lockhart-Martinelli parameter	(-)
z	axial direction of tube	

Abbreviations

CFD	computational fluid dynamics	
COP	Coefficient of Performance	(-)
COS	condenser outlet split	
DEM	delayed equilibrium model	
DX	direct expansion	
FGB	flash gas bypass	
HEM	homogeneous equilibrium model	
HTC	heat transfer coefficient	(W m^{-2} K^{-1})
IHX	internal heat exchanger	
LMTD	logarithmic mean temperature difference	(K)
LT	low-temperature	
MT	medium-temperature	
PAG	polyalkylene glycol	
PTFE	polytetrafluoroethylene	
PVE	polyvinyl ether	
VFD	variable frequency drive	

Greek Symbols

α	void fraction	(-)
	full angle	(°)
Δ	change in quantity	
ΔP	pressure drop	(kPa)
ΔT	temperature difference	(K)
ε	heat exchanger effectiveness	(-)
	absolute roughness	(mm)
η	component efficiency	(-)
θ	angle	(°)
μ	dynamic viscosity	(Pa s)
Π_s	suction pressure ratio	(-)
ρ	density	(kg m^{-3})
$\bar{\rho}$	average mass-weighted density of two-phase fluid	(kg m^{-3})
σ	surface tension	(N m^{-1})
ϕ	phase	
	specific availability	(kJ kg^{-1})
	two-phase multiplier	(-)
$\dot{\Phi}$	availability destruction rate	(kW)
Φ_m	mass entrainment ratio	(-)

Subscripts

1, 2, . . .	points in thermodynamic cycle
acc	acceleration
air	air-side of heat exchanger
amb	ambient, difference to ambient
app	approach temperature of heat exchanger
atm	atmospheric
c	critical
cp	compressor, compression
cond	condenser
conv	converging
dest	destruction
diff	diffuser of ejector

div	diverging
DP	dew point
E	equilibrium state
ejec	ejector
element	element in finite volume model
evap	evaporator
exp	expansion process
fin	heat exchanger fin
fr	frictional
gc	gas cooler
gr	gravitational
i	referring to a given thermodynamic state
in	inlet of component
l	liquid phase
lift	increase provided by ejector
lo	liquid only
louver	louver of heat exchanger fin
macro	macroscopic contribution to flow boiling
max	maximum
mech	mechanical
micro	microscopic contribution to flow boiling
min	minimum
mn	motive nozzle of ejector
ms	mixing section of ejector
n	flow nozzle
port	microchannel port
o	stagnation state
	dead state
opt	optimum
out	outlet of component
r	ratio
rec	recovery in ejector
ref	refrigerant-side of heat exchanger

s	ejector suction stream
	isentropic (process)
sat	saturation state
SC	subcooling
SH	superheat
sn	suction nozzle of ejector
t	throat of nozzle
tp	two-phase
tot	total
tt	turbulent-turbulent
tube	microchannel tube
v	vapor phase
vo	vapor only
vol	volumetric
w	wall

CHAPTER 1: INTRODUCTION

1.1 Background and Motivation

Vapor-compression systems are commonly used to achieve cooling (transfer of energy from a lower-temperature source to a higher-temperature sink) in air-conditioning and refrigeration applications. The most common thermodynamic cycle used in vapor-compression systems is the Evans-Perkins cycle, which consists of four processes: Isentropic compression; isobaric heat rejection; isenthalpic expansion; and isobaric heat addition. The isenthalpic expansion process in the Evan-Perkins cycle is irreversible, meaning that it simultaneously decreases cycle cooling capacity and increases cycle work input. Both of these effects contribute to lower cycle efficiency, as measured by the Coefficient of Performance (COP), compared to an ideal refrigeration cycle such as the Carnot cycle. Figure 1.1 shows the ideal Evans-Perkins and Carnot refrigeration cycles on a temperature-specific entropy diagram. The magnitude of capacity loss due to isenthalpic expansion compared to an isentropic expansion is equal to the magnitude of increase in cycle work input; this loss is commonly referred to as the throttling loss. The throttling loss is shown graphically on the temperature-specific entropy diagram of Figure 1.1. Throttling loss is a strong function of the operating conditions and thermodynamic properties of the working fluid.

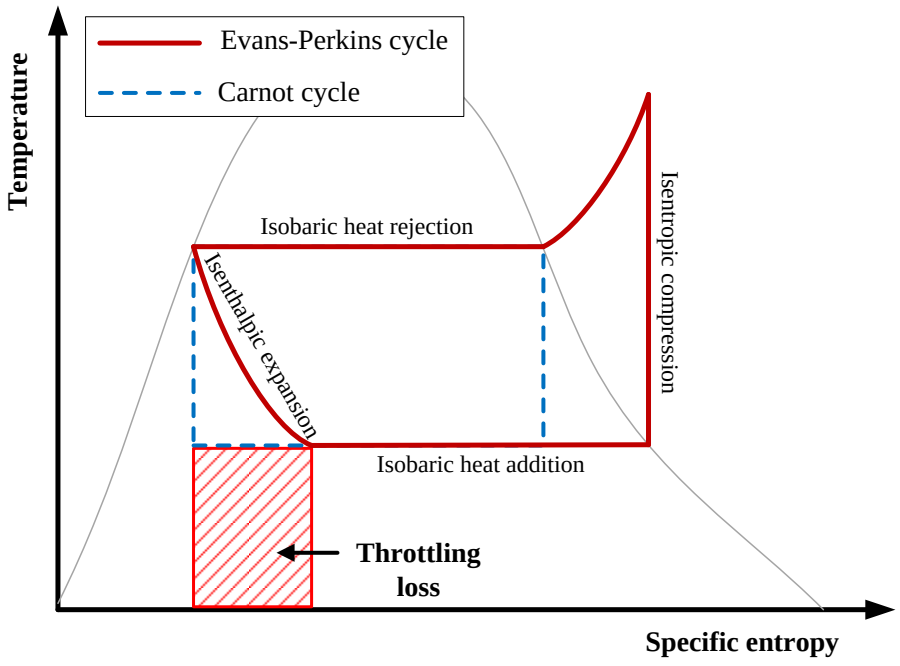

Figure 1.1: Temperature-specific entropy diagram comparing the ideal Evans-Perkins and Carnot refrigeration cycles; processes of the ideal Evans-Perkins cycle are noted on the diagram.

In conventional vapor-compression systems using the Evans-Perkins cycle, devices such as expansion valves, capillary tubes, and orifice plates/tubes are commonly used to expand the refrigerant from the high-pressure side to the low-pressure side of the system. While these devices are inexpensive and reliable, they result in an isenthalpic expansion rather than an isentropic expansion and thus cause throttling loss, as described above. To improve the performance of conventional vapor-compression systems, a device capable of theoretically producing an isentropic expansion can be used to expand the refrigerant rather than a throttling (isenthalpic) device. One such device theoretically capable of producing an isentropic expansion is a refrigerant expander, in which the enthalpy of the fluid is converted to mechanical work. This mechanical work produced by the expander can be used to directly supplement the compressor work and thus reduce the required work input of the cycle; the extraction of enthalpy from the fluid also results in lower enthalpy at the start of heat absorption, which increases the cooling capacity of the cycle. However, expanders are complex and costly to implement in vapor-compression systems. A potentially simpler and less expensive option would be to use an ejector, in which the enthalpy released by the expanding fluid is directly used as compression work for a second fluid. The integration of ejectors into vapor-compression systems is the subject of this dissertation.

1.2 Ejector Background and Operation

An ejector is a device that uses the enthalpy released during the expansion of a high-pressure fluid to provide compression work to a low-pressure fluid. A diagram of fluid flow through an ejector is shown in Figure 1.2. The high-pressure (motive or primary) fluid is expanded through a nozzle to low pressure and high velocity and is mixed with a low-pressure (suction or secondary) fluid. The two fluids do not have to be of the same composition but often are for refrigeration applications. The mixed flow is then decelerated in the diffuser, and the momentum is converted to static pressure. Thus, the net effect of the ejector is a pressure increase of the suction fluid provided by the expansion of and mixing with the motive fluid. The ejector can theoretically approach an isentropic expansion because the enthalpy of the motive stream is converted to kinetic energy, which is then transferred to the suction stream, ultimately reducing the enthalpy of the motive stream as it passes through the ejector. An isentropic expansion represents the ideal limiting case when no irreversibility is present and no entropy generation occurs. The operation of an ejector is similar to that of a pump. For a given amount of work or power that is provided by the expanding motive stream, requiring the ejector to compress or pump a greater amount of mass will result in lower pressure increase that the ejector can provide; there is a trade-off between the two effects of mass entrainment and pressure increase that the ejector provides. Ejectors are of interest as expansion devices in vapor-compression systems because they are inexpensive, robust, and involve no moving parts.

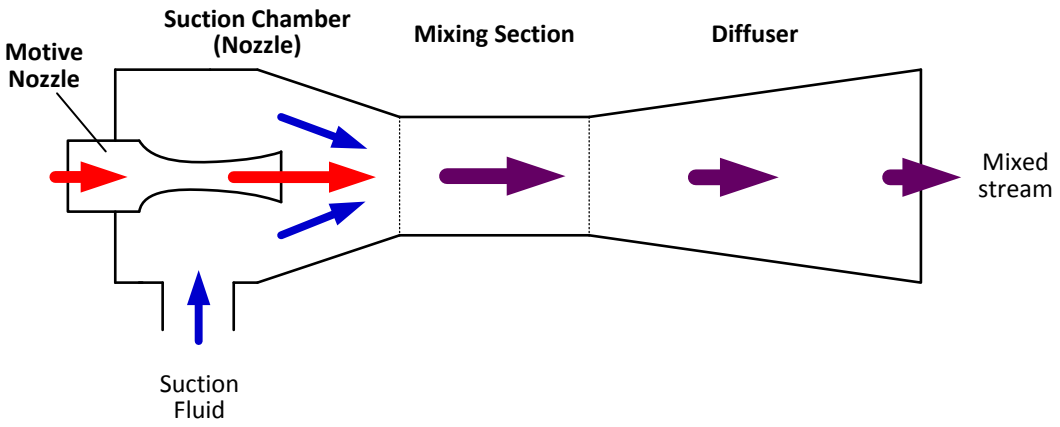

Figure 1.2: Diagram of flow through an ejector.

Ejector performance is often quantified in terms of the mass entrainment ratio and the suction pressure ratio. The mass entrainment ratio, shown in Equation (1.1), is defined as the mass flow rate of suction fluid (pumped by the ejector) divided by the mass flow rate of motive fluid; it is a dimensionless measure of the rate at which the ejector can entrain mass. The suction pressure ratio, shown in Equation (1.2), is defined as the pressure at the diffuser outlet divided by the pressure of the suction fluid; it is a dimensionless measure of the pressure increase that the ejector provides to the suction fluid.

$$\Phi_m = \frac{\dot{m}_{sn}}{\dot{m}_{mn}} \qquad (1.1)$$

$$\Pi_s = \frac{P_{diff,out}}{P_{sn,in}} \qquad (1.2)$$

The entrainment ratio and pressure ratio of an ejector must be considered simultaneously because they measure two separate effects of the ejector. It is often more convenient to have a single parameter to quantify ejector performance such as an ejector efficiency. The work recovery efficiency of a two-phase ejector is shown in Equation (1.3); it is defined as the amount of work recovered in the ejector, assuming an isentropic compression of the suction stream from suction inlet to diffuser outlet pressure, divided by the theoretical maximum amount of work available for recovery as the motive stream expands isentropically from motive inlet to diffuser outlet pressure (Elbel and Hrnjak, 2008).

$$\eta_{ejec} = \frac{\dot{W}_{rec}}{\dot{W}_{rec,max}} = \Phi_m \frac{h\left(P_{diff,out}, s_{sn,in}\right) - h_{sn,in}}{h_{mn,in} - h\left(P_{diff,out}, s_{mn,in}\right)} \qquad (1.3)$$

1.3 Structure of Dissertation

Chapter 1 of this dissertation has provided background information on throttling loss and work recovery, thus motivating research on the use of ejectors for work recovery in vapor-compression systems. Chapter 2 of the dissertation reviews the relevant literature on the use of ejectors for expansion work recovery in vapor-compression systems. Chapter 3 discusses the shortcomings of the current state of ejector technology and thus presents the objectives and the contributions to the field of ejector technology that is made by the research presented in this dissertation.

Chapter 4 describes the numerical model that is used to simulate the performance of different ejector cycles in the presented research. The evaporator is modeled with a finite volume model, while the remaining cycle components were modeled with thermodynamic state point analysis. Further details of the evaporator model are provided in Appendix B. Chapter 5 describes the experimental facilities and ejector designs that were used to obtain experimental results. Separate facilities were constructed for experiments with R410A and with CO_2, although the basic components of the two facilities were the same. Further details of the experimental facility are provided in Appendix C.

Chapter 6 presents numerical results comparing the performance of two different ejector cycles with several different refrigerants. Chapter 7 presents experimental and numerical results with R410A, investigating the effect of evaporator design in different ejector cycles and how to design and operate an evaporator to gain the most benefit from an ejector cycle. Chapter 8 presents experimental results with CO_2 investigating different ejector cycle control methods, discusses control strategies for ejector cycles, and compares transcritical and subcritical cycle operation. Finally, Chapter 9 presents a summary of the presented research, important conclusions, and recommendations for further work.

CHAPTER 2: REVIEW OF EJECTORS IN REFRIGERATION APPLICATIONS

This chapter reviews the relevant literature on ejectors with a focus on their application as work recovery devices in vapor-compression systems. Portions of the literature review presented in this chapter have been previously published in an invited review paper by Elbel and Lawrence (2016).

2.1 Ejectors in Early Refrigeration Applications

A thorough review of historical development of ejectors can be found in Elbel (2007, 2011); a brief summary of ejectors in early refrigeration systems will be given here. The first known use of an ejector was by Henri Giffard in 1858 for pumping water into the boiler of a steam locomotive, while the first known use of an ejector in a refrigeration application was in 1910 by Maurice Leblanc. The cycle used by Leblanc has become known as the steam-jet ejector cycle, in which the ejector is driven by low-grade heat and used in place of a mechanical compressor. A schematic and pressure-specific enthalpy diagram can be seen in Figure 2.1. This cycle is also known as the single-phase ejector cycle or vapor-jet ejector cycle when used with a fluid other than steam; a detailed review of relevant research on this cycle can be found in Chunnanond and Aphornratana (2004) and more recently in Chen *et al.* (2015) and Besagni *et al.* (2016). Steam-jet ejector refrigeration reached its peak in the 1930's for air conditioning of large buildings, but the technology has since been replaced by vapor-compression systems with mechanical compressors (Stoecker, 1958). Ejectors have not been considered again for use in refrigeration applications until more recently, as will be discussed in the next section. However, Elbel (2011) noted that ejectors have also been applied for many years in the power generation industry to remove non-condensable gases from steam condensers and provide emergency cooling water to nuclear reactors as well as in the chemical processing industry to pump hazardous or combustible substances.

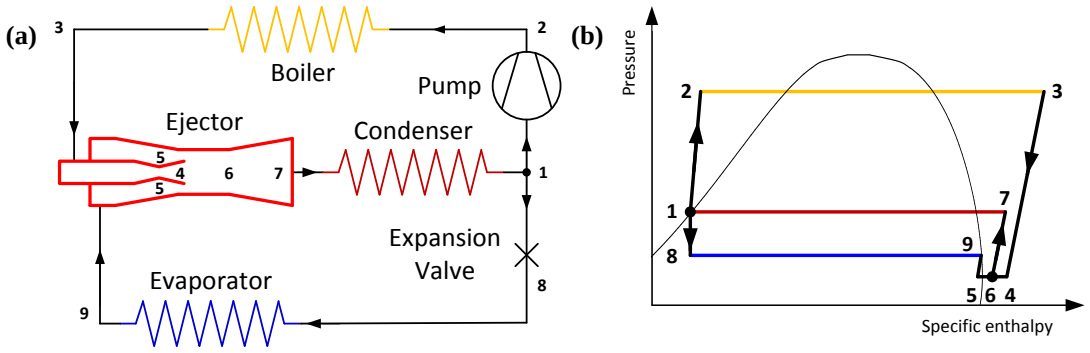

Figure 2.1: Single-phase (vapor-jet) ejector cycle for subcritical operation shown as (a) schematic diagram and (b) pressure-specific enthalpy diagram.

2.2 Overview of Ejectors for Expansion Work Recovery

The focus of this research concerns vapor-compression refrigeration cycles using an ejector for expansion work recovery. The most commonly considered cycle using an ejector for expansion work recovery is shown in Figure 2.2 for transcritical operation. This cycle will be referred to as the standard ejector cycle throughout this dissertation. This cycle was first patented by Gay (1931) but was largely neglected for many years until Kornhauser (1990) reported the first theoretical analysis of the cycle.

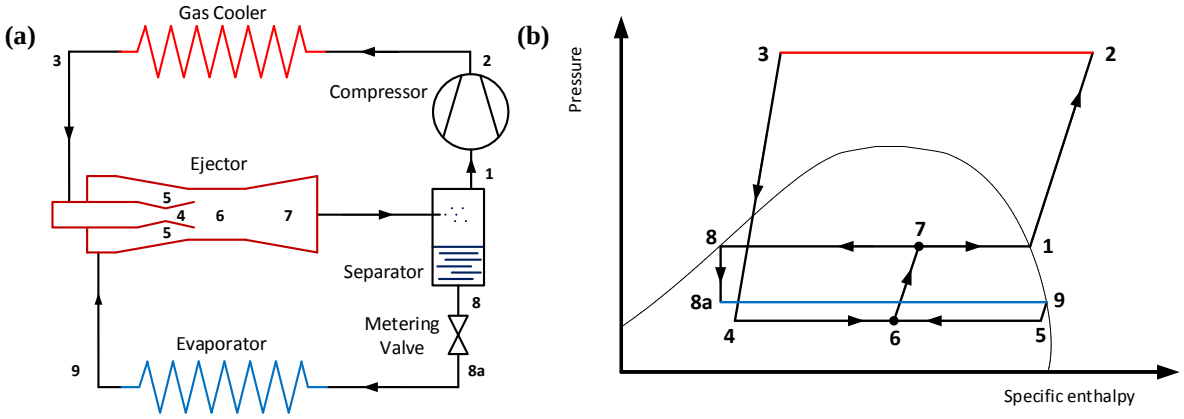

Figure 2.2: Standard ejector cycle for transcritical operation represented as (a) schematic diagram and (b) pressure-specific enthalpy diagram.

A review of over 150 publications on ejectors for work recovery in vapor-compression systems has been conducted, and an in-depth review of the studies that offer important contributions to the field of ejector technology will be presented here. Other recent review papers on ejectors in work recovery applications include Sarkar (2012), Sumeru *et al.* (2012), Chen *et al.* (2015), and Besagni *et al.* (2016). The review presented here will draw specific attention to many of the key practical issues that real systems using ejectors face, which were of lesser focus in the previously noted review papers by other researchers.

Figure 2.3 shows an outline of the progression of research on two-phase ejectors. Research on two-phase ejectors began in the early 1990's with theoretical performance predictions of the standard ejector cycle using simple cycle models. Experimental testing of two-phase ejectors was then performed with conventional refrigerants (R134a, R12) in order to see realistic results for two-phase ejector performance; this allowed for a more realistic prediction of ejector cycle performance improvement, which was much smaller than what was predicted by the theoretical models. Because of the renewed interest in the use of CO_2 as an alternative refrigerant, significant research began on the application of a two-phase ejector in a transcritical CO_2 cycle in the early 2000's. The transcritical CO_2 ejector cycle was first investigated

numerically, and several experimental studies on the cycle were then published mainly between 2008 and 2012; the results of these studies were very encouraging, showing up to 15 – 30 % COP improvement. Current research on two-phase ejectors seems to be focused in multiple directions. Experimental studies on CO_2 ejectors have given way to development of multi-dimensional (CFD) models of CO_2 ejectors. The success of the ejector in transcritical CO_2 systems also seems to have motivated researchers to apply ejectors to subcritical cycles with conventional refrigerants (R134a, R1234yf, and R410A) again. Several of the studies with conventional refrigerants have opted for alternate ejector cycles, as will be discussed in greater detail below. Finally, researchers have recently begun addressing the issue of ejector cycle control, which is critical in allowing ejectors to be applied in real systems.

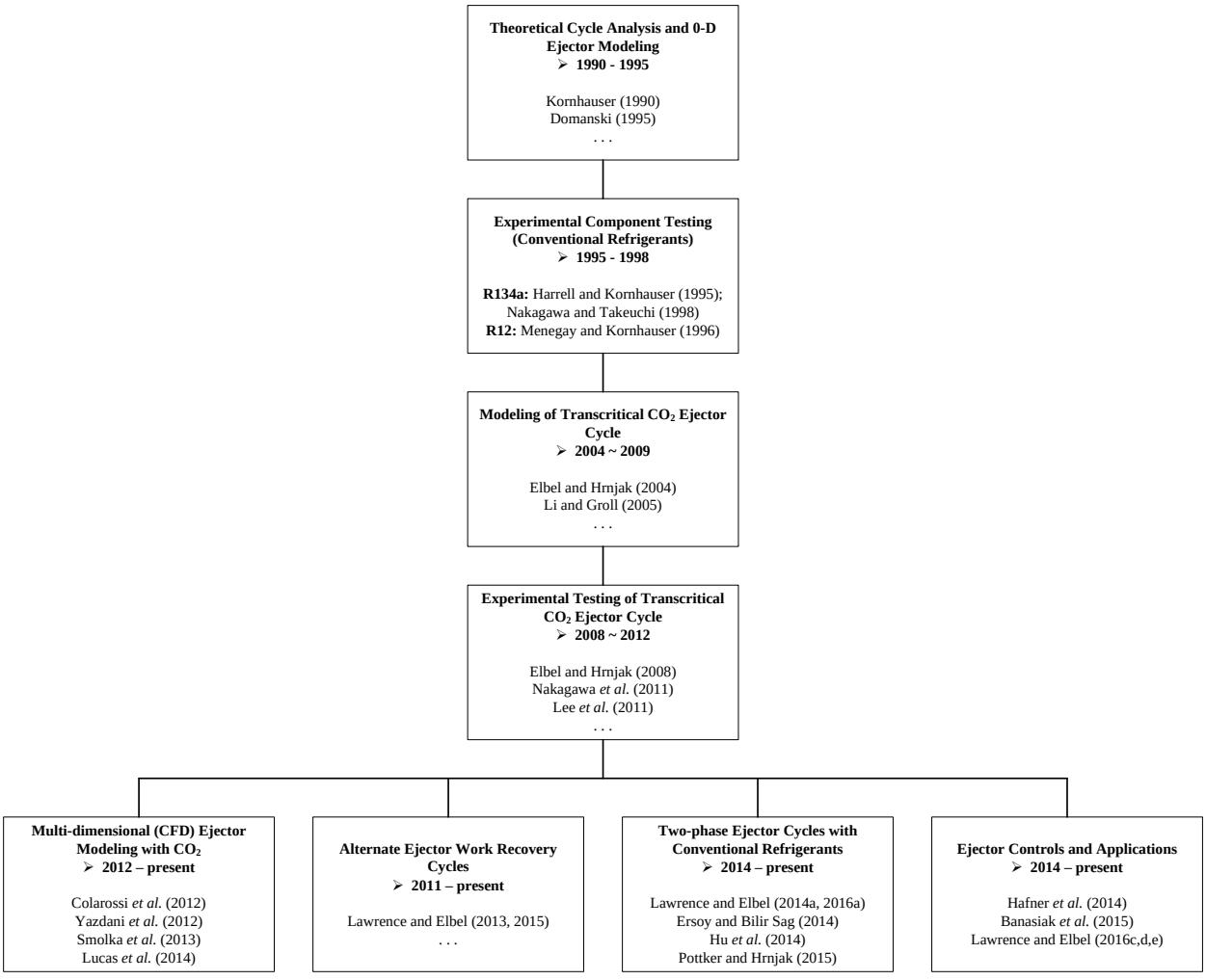

Figure 2.3: Diagram showing the progression of research on two-phase ejectors and ejector cycles; use of ". . ." indicates additional relevant studies that are not listed.

2.3 Ejector Modeling

2.3.1 Zero-dimensional Ejector Modeling

Various modeling procedures have been developed to predict the performance of two-phase ejectors. The simplest models are zero-dimensional models, which assign an efficiency and apply relevant conservation equations to each of the components of the ejector (motive nozzle, suction nozzle, mixing section, and diffuser) to simulate performance. Zero-dimensional models nearly always assume homogeneous equilibrium flow, meaning that the fluid is at thermodynamic and mechanical equilibrium at all locations. These models are sometimes referred to as one-dimensional models because they account for the relative location of the different ejector components as flow proceeds through the ejector. However, they are not one-dimensional models in the sense of a model that is able to calculate flow characteristics and account for geometric effects at each point along the flow path. Zero-dimensional ejector models can generally be categorized by whether the mixing process is assumed to occur at constant pressure or through a constant cross-sectional area passage. Kornhauser (1990) developed the first model of a two-phase ejector based on the assumption of constant-pressure mixing, while Li and Groll (2005) introduced a model of a two-phase ejector based on the assumption of constant-area mixing. Detailed equation listings for the constant-pressure mixing and constant-area mixing ejector models can be found in these papers.

The majority of ejector cycle simulation papers have employed the zero-dimensional modeling approach described above. The major drawback of this approach is specifying a proper value for the efficiency of each ejector component for each operating condition. The performance of the ejector is strongly dependent on the efficiency of its components, but these efficiencies are known to be highly dependent on geometry and operating conditions. Many studies in the literature have employed zero-dimensional ejector models without proper justification for the component efficiencies that were used and have assumed that the component efficiencies remain constant as ejector operating conditions vary. Additionally, while zero-dimensional models do have limited ability to estimate certain flow cross-section areas, they do not have the ability to predict any of the important lengths or angles that affect two-phase ejector performance.

Several recent papers have demonstrated simple methods to improve upon the accuracy of zero-dimensional models while still retaining computational simplicity. To address the issue of how ejector component efficiencies vary with ejector geometry and operating conditions, Liu and Groll (2013) developed empirical correlations based on their experimental data for the efficiencies of the motive nozzle, suction nozzle, and mixing section of a transcritical CO_2 ejector. The correlations were functions of the ratio of motive to suction pressure, ratio of nozzle throat to mixing diameter, and entrainment ratio.

It should be noted that the motive nozzle of the ejector used to obtain the experimental data was a converging-only nozzle. The model used to simulate ejector performance was a constant-area mixing model similar to that of Li and Groll (2005) mentioned above; however, a significant improvement is offered by the formulation of Liu and Groll (2013) because realistic values of component efficiencies can be applied over a range of operating conditions.

Lucas *et al.* (2013) used the idea of an ejector performance map for predicting the characteristics of an ejector. A performance map of an ejector calculates the overall performance of the ejector for the given operating conditions based on experimentally determined performance correlations. They developed an empirical correlation for ejector work recovery efficiency as a function of several ejector dimensions and operating conditions. The correlation was not a function of entrainment ratio, meaning that by specifying the ejector entrainment ratio and calculating ejector efficiency from the inlet states and necessary dimensions, the performance of the ejector could be fully specified. Thus, with the required inputs, the efficiency correlation of Lucas *et al.* (2013) can be used as a simple method to simulate ejector performance based on experimental data.

2.3.2 One-dimensional and Multi-dimensional Ejector Modeling

Due to the above mentioned limitations of zero-dimensional ejector modeling, one focus of ejector research for the past few years has been on developing CFD models capable of accounting for different ejector geometry and operating conditions, as well as providing local flow characteristics throughout the ejector. The studies discussed below generally use commercial CFD software to model the turbulent mixing process between motive and suction streams, and in some cases, the models are able to account for the non-equilibrium flow in the nozzle and shock waves in the ejector.

Banasiak and Hafner (2011) developed a one-dimensional model of a transcritical CO_2 ejector in which the flow path was discretized along the axial direction of the ejector and the flow was assumed uniform over a cross-section; the model was able to account for ejector geometry, metastability effects, mixing of the two flows, and shock waves in the mixing section and diffuser. The model generally predicted motive flow rate and pressure lift to within 5 %. They used their model to show that smaller mixing diameter results in larger maximum pressure lift but lower maximum entrainment ratio. Banasiak and Hafner (2013) continued the study focusing on different phase change models in the motive nozzle. They compared the homogeneous equilibrium model (HEM) to the delayed equilibrium model (DEM) with both homogeneous and heterogeneous nucleation and developed an empirical correlation to model the strength of heterogeneous nucleation.

Colarossi *et al.* (2012) developed a two-dimensional CFD model of a transcritical CO_2 ejector using the homogeneous relaxation model to account for non-equilibrium effects. They used their model to predict the data of Nakagawa *et al.* (2011a) and found that their model could match the data to within 35 % while predicting similar trends with respect to varying mixing length. Colarossi *et al.* (2012) also found that the instantaneous quality was very close to the equilibrium quality throughout the nozzle, meaning that the expansion in the nozzle was nearly at thermodynamic equilibrium according to their model; they concluded that the turbulence model and motive inlet condition have a more significant effect on the pressure recovery and accuracy of the ejector model than the relaxation model.

Yazdani *et al.* (2012) developed a three-dimensional CFD model of a transcritical CO_2 ejector using boiling-controlled heat transfer and inertia-controlled cavitation models to predict phase change; they found that phase change is dominated by boiling near the center of the nozzle and by cavitation near the walls. They also found that accounting for slip between phases has a minor impact on overall ejector performance but does produce a shock train at the exit of the motive nozzle. They used their model to show that reducing the mixing section diameter for the same nozzle diameter resulted in a reduction of the shock train amplitude at the outlet of the nozzle but a stronger shock wave downstream in the mixing section, resulting in lower overall pressure recovery with the ejector. Yazdani *et al.* (2014) continued the study with a focus on the motive nozzle. They found that choking occurred in the nozzle downstream of the throat due to increasing velocity and decreasing speed of sound as liquid changes to vapor. Their model also showed that wider nozzle diverging angle results in more rapid phase change, choking closer to the nozzle throat, and flow behavior closer to equilibrium.

Smołka *et al.* (2013) developed a three-dimensional CFD model of a transcritical CO_2 ejector but assumed homogeneous equilibrium flow throughout. They were able to predict experimental data for motive flow rates to within 14 % and suction flow rates to within 20 %, and pressure lift was also generally predicted accurately. They also accounted for the position of the suction inlet to the ejector and noted that doing so resulted in non-symmetric flow through the ejector mixing section and diffuser, meaning that depending on the particular ejector design, it may not be accurate to simplify the ejector model to axisymmetric geometry. Banasiak *et al.* (2014) continued the study of Smołka *et al.* (2013) by investigating the irreversibility of the flow at different locations in the ejector. Banasiak *et al.* (2014) found that the greatest irreversibility was caused by the shock train at the nozzle outlet and the turbulent mixing process in the mixing section, while the expansion in the motive nozzle generally accounted for only a small portion of the total irreversibility in the ejector. They also used their model to show that optimizing the geometry of one ejector section may not reduce overall ejector irreversibility but instead

may just shift it to another section of the ejector; this means that all ejector dimensions must be considered simultaneously when optimizing ejector geometry. Palacz *et al.* (2015) used a similar model to investigate the accuracy of the homogeneous equilibrium model over a larger range of conditions. They found that for operating conditions near or above the critical point, the model generally predicted motive mass flow rate to within 10 % compared to the experimental data. However, for operating conditions at lower pressure or lower temperature, the accuracy of the model decreased.

Lucas *et al.* (2014) also used a three-dimensional transcritical CO_2 ejector CFD model assuming homogeneous equilibrium flow throughout. They first compared their model results to experimental results for an ejector without suction flow and found that the model predicted motive flow rate and pressure rise to within 10 %; an ejector with only motive flow still has frictional losses but does not have mixing losses. They then compared their model results to experimental results for the ejector with suction flow and found that the model only predicted pressure lift accurately to within 20 % when suction flow was considered; this means that the model was not able to account for mixing losses as accurately as frictional losses.

It can be seen from the above studies that the most challenging aspect of developing an accurate CFD model of a two-phase ejector seems to be accurate modeling of the turbulent mixing process. Colarossi *et al.* (2012) concluded that modeling of turbulence had a more significant effect on model accuracy than modeling of non-equilibrium motive flow expansion, while Lucas *et al.* (2014) showed that losses caused by the mixing process were more difficult to predict than frictional losses. Additionally, the recent studies of Smołka *et al.* (2013), Banasiak *et al.* (2014), and Lucas *et al.* (2014) all assumed homogenous equilibrium flow throughout the ejector and still achieved reasonable accuracy, which again indicates that accounting for non-equilibrium effects may not be as important as other aspects of the flow in the ejector. It should be noted, however, that the study of Palacz *et al.* (2015) found the homogeneous equilibrium approach was less accurate at nozzle inlet conditions of lower pressure and lower temperature, meaning that for certain applications, such as refrigeration, a different approach may be necessary.

It should also be noted that many of the above studies do not always predict shock waves in the ejector or do not validate the prediction of shock waves. Shock waves are known to occur in the mixing section and diffuser of two-phase CO_2 ejectors based on experimental observations (Elbel, 2011) and are believed to occur at the outlet of the nozzle (shock train). A shock wave is an irreversible process, meaning that it decreases the overall efficiency of an ejector compared to an isentropic pressure rise; this means that an accurate two-phase ejector model should be able to accurately predict location, shape, and strength of

shock waves. The difficulty in model prediction of shock waves is in part due to the difficulty in determining shock structure experimentally, especially for the two-phase shock train at the outlet of the nozzle. The position and strength of shock waves is a function of the Mach number of the flow throughout the ejector. However, it is difficult to determine the Mach number for two-phase flow, as the speed of sound of a two-phase flow is highly dependent on the flow regime, and the flow regime throughout two-phase ejectors is generally not well known (Banasiak *et al.*, 2015a). This adds further difficulty to accurate prediction of shock waves in two-phase ejectors. It should be noted, however, that many of the above models have predicted the overall performance of the ejector accurately without necessarily predicting shock waves accurately.

Little and Garimella (2016) provide a detailed review of zero-, one-, and multi-dimensional ejector modeling, emphasizing single-phase (heat recovery) ejectors. Banasiak *et al.* (2015a) provide a more detailed review of one- and multi-dimensional modeling of transcritical CO_2 ejectors. They also review several experimental studies that attempt to characterize the physics of the flow inside the ejector, noting that no study has successfully identified the two-phase flow patterns or velocity profiles inside the ejector. It is concluded in the study of Banasiak *et al.* (2015a) that greater knowledge of the flow pattern in each ejector passage, turbulence modeling, shock wave shape and strength, metastability effects, and effect of lubricant in CO_2 ejectors is needed in order to improve the accuracy of multi-dimensional models. More recently, Deng *et al.* (2016) visualized the flow inside a transcritical CO_2 ejector and identified flow patterns, focusing on the existence of vortices in the suction chamber. Further studies of this type would greatly aid in the development of accurate ejector models.

The objective of developing a multi-dimensional CFD model is not only to accurately predict ejector performance but also to aid in the design of a high-efficiency ejector. In order to be a useful tool for ejector design, the model should be able to accurately model ejector performance for all ejector geometries and operating conditions; however, the models presented here are generally adjusted to match a single set of data but have not necessarily been shown to be accurate when compared to data from multiple studies. Future studies will need to focus on developing CFD models that can accurately predict the performance of ejectors from multiple studies over a wide range of geometries and operating conditions. Additionally, all of the CFD ejector models that have been developed and discussed here have used CO_2 as the working fluid. It may be interesting to see in future studies if the models developed for transcritical CO_2 ejectors can be applied to low-pressure refrigerants. The obvious advantage of using a multi-dimensional CFD model as opposed to a zero-dimensional model of an ejector is that all ejector dimensions and operating conditions can be accounted for by an accurate CFD model; however, this

comes at the cost of far greater computational requirements. The zero-dimensional modeling methods presented by Liu and Groll (2013) and Lucas *et al.* (2013) provide interesting opportunities to accurately account for different operating conditions and ejector geometries without requiring the computational complexity of multi-dimensional CFD models. Expanding the procedures of these studies to account for additional ejector dimensions and wider ranges of operating conditions could be a focus of future studies and may allow zero-dimensional modeling to be of similar accuracy and applicability as multi-dimensional CFD modeling.

2.4 Ejector Cycle Modeling and Performance

2.4.1 Standard Two-phase Ejector Cycle

The simplest method of modeling cycle performance is with a thermodynamic state point model; the vast majority of ejector cycle modeling studies have used this approach. Thermodynamic state point models are implemented by specifying the outlet state of each component or determining outlet state by zero-dimensional modeling of the component. Condensing and evaporation temperature are specified rather than determined by heat source/sink temperatures and heat transfer rate equations. These models also generally neglect pressure drop in heat exchangers and tubing between components and neglect heat transfer to or from surroundings in the tubing between components. Despite the significant simplifications of thermodynamic state point models compared to real systems, these models are able to provide reasonable prediction of the COP improvement that an ejector cycle can offer if the ejector is modeled such that its performance is realistic. However, as noted above, it is difficult to accurately simulate the performance of an ejector with the zero-dimensional modeling approach described above, especially as operating conditions vary. Ejector cycle modeling studies often assume values for the ejector component efficiencies that are too large, meaning that these studies will often over-predict the COP improvement that an ejector cycle can achieve compared to the improvement that has been observed experimentally.

Kornhauser (1990) was the first to analyze the performance of the standard ejector cycle. He used a thermodynamic state point model for the cycle and the zero-dimensional constant- pressure mixing model for the ejector to investigate the ability of the standard ejector cycle to improve COP with several different refrigerants. He observed that the COP of the ejector cycle was strongly dependent on the specified efficiencies of the ejector components and that the maximum COP improvement achieved by the ejector cycle compared to a cycle with an isenthalpic expansion (DX cycle) ranged from 12 to 30 % depending on the refrigerant. A similar study was performed by Domanski (1995) with 38 different refrigerants, predicting up to 80 % COP improvement. Numerous additional studies have theoretically analyzed the standard ejector cycle with similar zero-dimensional ejector models using various

refrigerants, providing insight into the operation and performance of the standard ejector similar to that provided by Kornhauser (1990).

Transcritical CO_2 systems offer the opportunity for significantly greater COP improvement, compared to low-pressure refrigerants, when using a work recovery device such as an ejector. CO_2 is seen as a possible alternative for more conventional synthetic refrigerants currently used in many air conditioning and refrigeration applications due to its low global warming potential and non-toxic and non-flammable properties, but it suffers from significant reductions in capacity and COP if the refrigerant is expanded isenthalpically, especially for transcritical operation. The critical temperature of CO_2 is 31°C, meaning that for an air conditioning application, the cycle will very often operate in transcritical mode. As a result, much of the recent work on two-phase ejectors has focused on transcritical CO_2 systems. Elbel and Hrnjak (2004a) and Li and Groll (2005) used numerical models to analyze the performance of a transcritical CO_2 ejector cycle; both of these studies showed that, similar to a transcritical CO_2 DX cycle, the COP of a transcritical CO_2 ejector cycle can be maximized by optimizing gas cooler pressure. Further discussion of gas cooler pressure optimization in CO_2 ejector cycles will be provided in the sections on experimental studies and ejectors in real systems below. It will also be one of the focuses of the experimental investigation reported in this study. Numerous additional studies have also theoretically investigated the transcritical CO_2 ejector cycle, though the conclusions of these studies were similar to those of Elbel and Hrnjak (2004a) and Li and Groll (2015).

CO_2 cycles very commonly employ an internal heat exchanger (IHX) between the gas cooler outlet and the compressor suction because the capacity and COP of a CO_2 cycle are known to improve significantly with an IHX. When applying an IHX to a CO_2 cycle with an ejector, it has been seen by numerical studies (Elbel and Hrnjak, 2004a) that the highest COP for a given capacity is achieved by an ejector cycle without an IHX if the ejector recovers all of the available expansion work. This is because using an IHX in an ejector cycle decreases the ejector motive inlet enthalpy, which results in less work that can be recovered by the ejector and less opportunity for COP improvement. However, as will be seen below, experimental studies often find that an IHX improves the performance of a CO_2 system with an ejector. Zhang *et al.* (2013) used a numerical model to show that whether an IHX helps or hurts an ejector cycle depends on the efficiency of the ejector. A real ejector will not recover all of the available work, meaning that there will still be throttling loss as the flow expands through the ejector. If the ejector efficiency is low, it will be more beneficial to use the IHX to reduce this throttling loss, even though it also reduces ejector work recovery. For higher ejector efficiency, as is often assumed in numerical studies, the reduced work recovery will penalize the cycle more than the reduced throttling loss aids the cycle.

2.4.2 Ejectors in Liquid Recirculation Cycles

The standard ejector cycle uses the ejector to lift the pressure of the fluid at the evaporator outlet, which results in higher compressor suction pressure. In this sense, the work recovered in the ejector is used to directly supplement the work of the compressor. However, this is not the only way that the work recovered by the ejector can be used to improve cycle performance, as the work recovered in the ejector can be used to pump excess liquid through the evaporator, resulting in an evaporator that is overfed with liquid. This liquid overfeed or liquid recirculation effect increases the mass flux through the evaporator and eliminates evaporator dryout, resulting in improved evaporator performance. Thus, the work recovered in the ejector can also be used to improve evaporator performance, which indirectly unloads the compressor. Figure 2.4 shows a schematic of the ejector recirculation cycle in which the ejector is used to recirculate liquid through the evaporator. This cycle was patented by Phillips (1938).

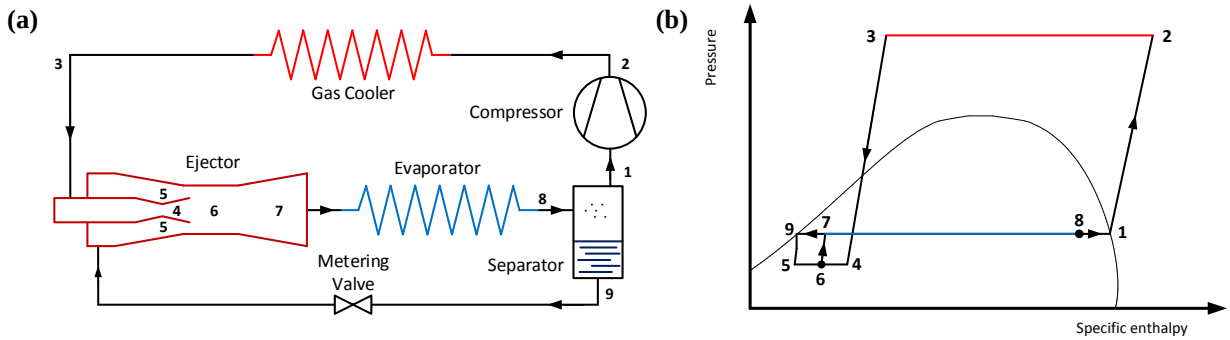

Figure 2.4: Ejector recirculation cycle shown as (a) schematic and (b) pressure-specific enthalpy diagram.

Liquid overfeed was actually the first widely used application of ejectors for work recovery before research began on the standard ejector cycle (Lorentzen, 1983). However, only a limited amount of research can be found on the ejector recirculation cycle in the open literature, possibly because the operation and performance of the cycle are thought to be well understood already. Furthermore, the positive effects of this indirect method of utilizing expansion work to improve the cycle are not directly visible from simple state point models since the improvement mechanism relies on improving evaporator effectiveness by eliminating or reducing dryout. Industrial refrigeration systems utilizing refrigerant pumps for liquid overfeeding target the same improvement mechanism; however, in those cycles electric power has to be spent to operate the pump, while in the ejector recirculation cycle, expansion work is used to achieve overfeed. Note that the standard ejector cycle can also use the ejector to recirculate liquid and improve evaporator performance while simultaneously using the ejector to directly unload the compressor. With the exception of the present study, no research has focused on modeling of the ejector recirculation cycle or comparing the standard ejector and ejector recirculation cycles.

One factor that affects the amount of COP improvement that can be achieved with a recirculation cycle is the amount of additional liquid being fed into the evaporator. The amount of additional liquid being fed into the evaporator (the amount of recirculation) can be quantified by the circulation number (*n*), defined as the total mass flow rate of liquid supplied to the evaporator divided by the mass flow rate of refrigerant that is vaporized in the evaporator, as defined by (ASHRAE, 2014) and shown in Equation (2.1). By performing an energy balance on the refrigerant that is vaporized in the evaporator, an expression for mass flow rate of vaporized refrigerant can be obtained and used to calculate circulation number, as also shown in Equation (2.1). ASHRAE (2014) also defines the overfeed ratio (*OR*) as the mass ratio of liquid to vapor at the evaporator outlet, as shown in Equation (2.2).

$$n = \frac{\dot{m}_{evap,total}}{\dot{m}_{evap,vaporized}} = \frac{\dot{m}_{evap,total}\left(h_v\left(P_{evap,out}\right) - h_{evap,in}\right)}{\dot{Q}_{evap}} \qquad (2.1)$$

$$OR = \frac{\dot{m}_{liquid,evap,out}}{\dot{m}_{vapor,evap,out}} = \frac{1 - x_{evap,out}}{x_{evap,out}} \qquad (2.2)$$

When using the ejector recirculation cycle, it must be determined if the total mass flow rate at the evaporator inlet or the mass flow rate of liquid at the evaporator inlet should be used in the numerator of the circulation number definition, as there will often be a significant amount of vapor present at the evaporator inlet in this cycle. For the forced standard ejector cycle, this would not be a problem as the amount of vapor at the evaporator inlet is generally very small and would not have a significant effect on the calculated value of circulation number. In this study, the total evaporator inlet mass flow rate (liquid and vapor) is used in the numerator of the circulation number for all cycles.

The amount of overfeed can also be measured with the recirculation ratio (*R*), defined as the evaporator mass flow rate over the condenser/gas cooler mass flow rate, as shown in Equation (2.3). It is easy to see that for the standard ejector cycle, the recirculation ratio is equivalent to the entrainment ratio, Equation (1.1), which is defined as the ejector suction mass flow rate divided by the ejector driving or motive mass flow rate, as shown in Equation (2.4). It can also be seen that for the ejector recirculation cycle, the recirculation ratio is equal to the ejector entrainment ratio plus one, as also pointed out by Li *et al.* (2014) and shown in Equation (2.5).

$$R = \frac{\dot{m}_{evap}}{\dot{m}_{cond}} \qquad (2.3)$$

$$R_{StandardEjecCycle} = \Phi_m \qquad (2.4)$$

$$R_{EjecRecircCycle} = 1 + \Phi_m \qquad (2.5)$$

In comparison to the circulation number, the recirculation ratio is relatively easy to understand and use, and its definition is valid for any evaporator outlet state. Furthermore, as shown above, the recirculation ratio can be directly related to the entrainment ratio of the ejector for both of the ejector cycles. However, the recirculation ratio is simply a ratio of mass flow rates and does not provide any direct information about the amount of overfeed in the evaporator like the circulation number does. Similarly, the overfeed ratio only describes the state of the fluid at the outlet of the evaporator, as it is only a function of evaporator outlet quality, and does not provide any direct information about the amount of overfeed in the evaporator. The circulation number directly measures the amount of overfeed in the evaporator, as it is the ratio of total evaporator mass flow rate to mass flow rate of vaporized refrigerant. Thus, while the circulation number may be more difficult to understand and calculate, it does provide better description of the operation of a recirculation cycle. Note that while the circulation number can be calculated for any outlet state using the formula shown in Equation (2.1), it is technically not defined for a superheated evaporator outlet state. For the standard ejector cycle, the circulation number can be approximated as the inverse of the evaporator outlet quality, though this is not the case for the ejector recirculation cycle due to the presence of the vapor at the inlet of the evaporator. Note that for the cycles considered in this study, there is no simple relation between circulation number and recirculation ratio, as the relation between the two depends on the evaporator and condenser pressures in each of the cycles.

2.4.3 Alternate Two-phase Ejector Cycles

Numerous examples of alternate vapor-compression cycles using an ejector for work recovery can be found in the open literature. One example of an alternate ejector work recovery cycle is shown in Figure 2.5. The flow at the outlet of the condenser or gas cooler is split; one stream becomes the motive flow of the ejector while the other stream is isenthalpically expanded and sent to an evaporator before becoming the suction flow of the ejector. The two-phase flow at the outlet of the ejector is sent to a second, higher temperature evaporator before entering the suction of the compressor. Because the flow at the outlet of the condenser (subcritical operation) is split, this cycle will be referred to as the COS (condenser outlet split) ejector cycle (Lawrence and Elbel, 2013). The pressure lift provided by the ejector causes a lift in saturation temperature between the two evaporators, meaning that the COS ejector cycle offers the opportunity to provide cooling capacity at two different temperatures. This may initially seem like an attractive cycle for systems that require two different evaporation temperatures, such as refrigeration

systems with medium-temperature (MT) and low-temperature (LT) evaporators. However, it must be noted that the difference in temperature between the evaporators and the ratio of capacities of the evaporators are not independent but are a function of ejector operation. The temperature difference is controlled by the pressure lift of the ejector, while the ratio of capacities is related to the entrainment ratio of the ejector; because ejector pressure lift and entrainment are related, there is a trade-off between greater temperature separation between the evaporators and greater low-temperature evaporator capacity. In addition, depending on the fluid, the achievable temperature difference between the two evaporators, which is the temperature lift achieved by the ejector, may only be about 1 to 2 K, which is too small for what is needed in typical two-temperature applications. Thus, despite the two different evaporation temperatures, the two evaporators in this cycle may be best suited for cooling the same stream of fluid; note that the two evaporators may allow for separation of latent and sensible loads in this case.

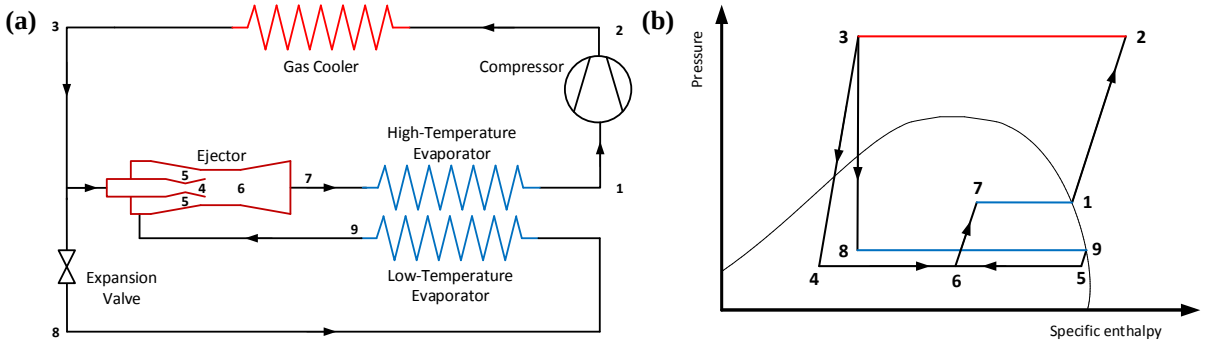

Figure 2.5: Alternate ejector cycle for transcritical operation represented as (a) schematic diagram and (b) pressure-specific enthalpy diagram.

Lawrence (2012) and Lawrence and Elbel (2013) noted several advantages that the COS ejector cycle offers in comparison to the standard ejector cycle. The COS ejector cycle does not have a liquid-vapor separator; the large size and potential inefficiency of a separator may not be allowable for some applications. The COS ejector cycle is also better suited for off-design performance. If the ejector in the standard ejector cycle fails to entrain sufficient mass flow, due to poor ejector design or conditions of low work recovery, then the cycle will lose significant capacity and COP; the COS ejector cycle would not lose capacity in either evaporator if the ejector failed to entrain properly because all flow passes through the compressor. The COS ejector cycle could also potentially offer better oil return than the standard ejector cycle because there is no opportunity for oil separation in parallel loops.

There are numerous additional alternate ejector cycle options that have been proposed and analyzed in the open literature. The majority of these alternate cycles have been proposed more recently, mainly since

2012 once the operation and performance of the standard ejector cycle was better understood. Chen *et al.* (2015) provide an overview of many of the different cycle options that use an ejector for work recovery. However, it should be noted that few of the alternate ejector cycles sufficiently address issues such as off-design operation, separator inefficiency, or oil return that likely limit the use of ejector cycles in real applications. Nonetheless, it may be worth considering the COS ejector cycle or other alternate ejector cycles that offer practical advantages for real applications in future experimental studies, especially when working with fluids that offer less improvement from expansion work recovery.

2.5 Ejector Experiments

2.5.1 Ejector Component Testing

Harrell and Kornhauser (1995) reported some of the first experimental results with a two-phase ejector for work recovery using R134a as the refrigerant. They observed ejector pressure lift in the range of 19 – 32 kPa, estimating that this would result in 4 – 8 % higher COP with the ejector cycle; however, they also noted that an ideal ejector would achieve up to 100 kPa pressure lift, indicating significant deviation from ideal performance in the ejector. Nakagawa and Takeuchi (1998) also investigated a two-phase ejector with R134a and estimated up to 10 % higher COP with the ejector cycle based on the experimentally determined ejector component performance. Menegay and Kornhauser (1996) tested a two-phase ejector in an R12 system. They initially observed no COP improvement with the ejector cycle but did observe COP improvement up to 4 % when providing a slight amount of throttling upstream of the ejector; the explanation of this was that a small amount of throttling before the nozzle would generate a small amount of vapor and reduce metastability, increasing nozzle efficiency. These results showed that the ejector cycle COP improvement was not nearly as large as predicted by the theoretical studies, largely due to significant inefficiencies of the ejector and possibly due to non-ideal design of other system components. Nakagawa *et al.* (1996) also tested an R12 ejector, observing that increasing mixing section length and decreasing mixing section diameter resulted in greater ejector pressure increase (lift) due to better mixing between the motive and suction streams.

2.5.2 Transcritical CO_2 Ejector Cycle Studies

Several detailed experimental studies of two-phase ejectors in transcritical CO_2 systems were reported mainly between 2008 and 2012. Elbel and Hrnjak (2008) investigated a transcritical CO_2 ejector system with an adjustable ejector in order to control high-side pressure in the transcritical system. An adjustable ejector (Figure 2.6) is an ejector in which an adjustable position needle is used to control the effective motive nozzle throat size. Elbel and Hrnjak (2008) showed experimentally that the COP of the system can be maximized by using the adjustable needle to find the optimum high-side pressure. However, they also

showed that using a needle to control nozzle size decreased ejector efficiency due to greater friction between the fluid and the needle as the fluid expands through the nozzle; more use of the needle (smaller nozzle size) resulted in lower ejector efficiency. An important finding, however, was that despite decreasing ejector efficiency, system performance could still increase with greater use of the needle. They also found that the COP of the ejector cycle increased with internal heat exchanger (IHX) effectiveness while ejector efficiency was not significantly affected by IHX effectiveness. Elbel and Hrnjak (2008) observed simultaneous COP and capacity improvements of 7 and 8 %, respectively, and they estimated that COP improvement could reach as high as 18 % if capacity were matched; they observed ejector work recovery efficiency of up to 15 %. Elbel (2011) continued the study by investigating system performance at different ambient temperatures and observed a linear relation between optimum gas cooler pressure and ambient temperature. He also observed that diffuser angle and mixing section length can have a significant effect on the performance of the ejector. A similar study was performed by Xu *et al.* (2012).

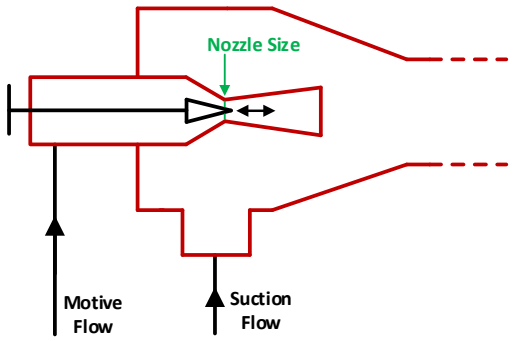

Figure 2.6: Diagram of adjustable ejector with variable position needle used to control effective nozzle size and high-side pressure.

Liu *et al.* (2012a) also used an adjustable ejector with a converging-only nozzle and observed an optimum throat size that maximized system performance; they also adjusted the position of the motive nozzle outlet with respect to the mixing section inlet and observed that there was an optimum nozzle position. A remarkable ejector cycle COP improvement of up to 147 % was reported in this study. Liu *et al.* (2012b) investigated the same ejector and developed a method by which the efficiencies of the (converging-only) motive nozzle, suction nozzle, and mixing section could be determined. They showed that the efficiencies of the motive and suction nozzles generally ranged from about 50 – 90 % while the mixing section efficiency ranged from about 50 – 100 %. Note that the theoretical modeling studies described above generally assume efficiency values of 80 – 100 %, which does not represent the full range observed in Liu *et al.* (2012b). They observed that motive nozzle efficiency decreased with decreasing nozzle size; as the needle is inserted further into the nozzle to decrease nozzle opening, more friction between the fluid and

needle occurs, lowering nozzle efficiency. This observation agrees with the finding of Elbel and Hrnjak (2008). The work by Liu *et al.* (2012b) was an important study because it presented realistic results for ejector component efficiencies over a range of operating conditions and variations in ejector geometry.

Numerous studies have investigated the performance of transcritical CO_2 ejector cycles using fixed geometry ejectors without any means of high-side pressure control. Lee *et al.* (2011) used a fixed geometry ejector and investigated the effects of motive nozzle throat diameter, motive nozzle outlet position, and mixing diameter, and they observed an optimum value for each of these parameters. They noted that the highest COP was achieved with the motive nozzle size for which the flow just becomes choked. They also observed that the cycle performance was not very sensitive to motive nozzle position for small variations from the optimum position; however, cycle performance could decrease rapidly if this parameter deviated significantly from its optimum. An optimum in entrainment ratio was observed near 0.9, where the evaporator outlet was close to a saturated vapor state. Lee *et al.* (2011) observed ejector cycle COP improvement of 15 % at matched capacity. Lee *et al.* (2014) continued the study by investigating how optimum entrainment ratio varied for different ambient temperatures and compressor speeds and observed that optimum entrainment ratio was generally in the range of 0.7 to 0.9.

Nakagawa *et al.* (2011a) investigated the effect of mixing section length on the performance of a cycle with a fixed geometry ejector; they observed that there was an optimum in mixing section length and that this optimum was the same for the cycle both with and without an IHX. They observed COP improvement up to 26 % but noted that improper mixing length could decrease COP by as much as 10 %. Nakagawa *et al.* (2011b) investigated the effect of different IHX size (effectiveness) in a CO_2 ejector cycle. Similar to Elbel and Hrnjak (2008), they found that a larger IHX (greater effectiveness) increased ejector cycle COP and COP improvement compared to a DX cycle with the same IHX. They observed ejector work recovery efficiency up to 22 % with the largest IHX, while ejector efficiency decreased as IHX effectiveness decreased.

The study of Nakagawa *et al.* (2011b) also noted the fact that the liquid-vapor separator in the ejector cycle does not always separate the two phases perfectly. Separator inefficiency can decrease cycle performance because liquid that leaves the separator at the vapor outlet results in lower evaporator capacity and greater compressor work while vapor that leaves the separator at the liquid outlet results in additional mass flow that the ejector must entrain without increasing cooling capacity. Additionally, too much liquid being sent to the compressor can damage the compressor if an IHX is not included in the cycle; note also that the lost capacity due to liquid being sent to the compressor can be partially recovered

if an IHX is used in the cycle. Nakagawa *et al.* (2011b) estimated that the quality of refrigerant leaving the separator at the vapor port was approximately 0.9, meaning that a significant amount of liquid was not being separated properly. Thus, when designing and operating an ejector cycle, one should be aware of the effect that poor liquid-vapor separation can have on the cycle.

Additional fixed geometry, CO_2 ejector cycle studies include those of Banasiak *et al.* (2012), Lucas and Koehler (2012), and Minetto *et al.* (2013). Banasiak *et al.* (2012) investigated the effects of mixing diameter and length and diffuser angle on ejector performance; they also showed that ejector efficiency can be maximized by varying high-side pressure (changing compressor speed). Banasiak *et al.* (2012) observed ejector cycle COP improvements in the range of 6 – 8 % at matched capacity over a large range of capacities; they achieved ejector work recovery efficiency of up to 31 %. In comparison to other studies, the ejector efficiency observed by Banasiak *et al.* (2012) was relatively high, though the COP improvement was relatively low; this demonstrates that there are other factors in an ejector system in addition to the design and performance of the ejector that have a significant effect on the improvement offered by the ejector cycle. Lucas and Koehler (2012) showed how compressor speed can be used to control high-side pressure with a fixed geometry ejector and thus maximize COP for a given operating condition; it should be noted that significant capacity variation would also occur in this case as well. Lucas and Koehler (2012) observed ejector cycle COP improvement of up to 17 % at matched capacity while achieving ejector work recovery efficiency of up to 22 %.

Minetto *et al.* (2013) highlighted the importance of proper oil return in the ejector cycle. The oil will tend to collect at the bottom of the separator with the liquid and flow to the evaporator; an excessive amount of oil in the evaporator will reduce the heat transfer performance of the evaporator. Additionally, not returning sufficient oil to the compressor will damage the compressor over time. Minetto *et al.* (2013) observed that the UA value of the evaporator (plate heat exchanger) in the ejector cycle was nearly 50 % lower than the UA value of the evaporator in the DX cycle for the same range of evaporator mass flow rates and attributed this effect to an excessive amount of oil being circulated through the evaporator and not returned to the compressor. They calculated that the ejector cycle would achieve 25 % COP improvement if the UA values of the two cycles were the same, but they showed that the improvement was significantly reduced because of the lower UA value of the ejector cycle evaporator. The issue of proper management of oil in ejector cycles must be addressed before ejectors cycles can be applied to real systems. It should be noted that some ejector cycles, such as the alternate ejector cycle shown in Figure 2.5, could potentially be less susceptible to oil return problems.

The above experimental studies investigating the performance of the transcritical CO_2 standard ejector cycle have shown very promising COP improvements mostly in the range of 15 – 30 %. However, these experimental studies have also highlighted very important practical issues, such as high-side pressure control, liquid-vapor separator design, and compressor oil return, which need to be addressed in order for ejector systems to be suitable for real applications. Future experimental studies should focus not only on ejector geometry and the COP improvement of the ejector cycle but also on how to effectively address these practical system issues. Additionally, the COP improvements reported in these studies, while promising, are generally the maximum observed in each study and only occur at conditions of high ejector efficiency and high work recovery; future studies will need to investigate how to achieve these COP improvements not only at the design condition of the system but at off-design conditions as well.

2.5.3 Low-pressure Refrigerant Ejector Cycle Studies

The past several years have seen less of a focus experimentally on CO_2 ejector systems and more of a focus on ejector systems using refrigerants that operate at lower-pressure compared to CO_2. It has been well established by the above CO_2 ejector cycle studies that COP improvements in the range of 15 - 30 % can be achieved with a transcritical CO_2 ejector cycle. The focus of recent experimental studies seems to be on what COP improvement can be achieved with low-pressure fluids. Fluids that operate at lower pressure compared to CO_2, such as R134a and R410A, have significantly lower throttling loss than transcritical CO_2, meaning that there is significantly less opportunity for improvement with an ejector when using a low-pressure fluid. A fluid being lower in pressure for a given saturation temperature does not necessarily mean that it will have lower throttling loss. However, it can generally be observed that lower-pressure fluids often have lower throttling loss and less opportunity for work recovery, especially in comparison to CO_2.

Ersoy and Bilir Sag (2014) investigated the standard ejector cycle using R134a and observed COP improvement in the range of 6 – 14 % at matched capacity, while in a similar study, Bilir Sag *et al.* (2015) observed COP improvement in the range of 7 – 13 % at matched capacity. It was observed in both of these studies that the ejector cycle resulted a very significant reduction in evaporator pressure drop compared to the DX cycle, using what appeared to be a brazed-plate heat exchanger as an evaporator. Ersoy and Bilir Sag (2014) observed that the evaporator pressure drop was reduced from 96 – 133 kPa in the DX cycle to 2 – 4 kPa in the ejector cycle. This reduction in pressure drop certainly has a noticeable influence on system performance for a fluid such as R134a and must contribute to the COP improvement that is observed with the ejector cycle.; this may help explain why the COP improvement observed in these two R134a studies may be higher than what would be expected. Further review of the effect of

evaporator design in ejector cycles will be presented in Section 2.6. Investigation of evaporator design in ejector cycles will also be a major point of interest in this dissertation.

Pottker and Hrnjak (2015a) also focused on the ability of the ejector cycle to improve evaporator performance by comparing the COP improvement of the standard ejector cycle to that of a flash-gas-bypass (FGB) cycle with R410A. An FGB cycle is a cycle in which the vapor from the expansion process (flash vapor) is bypassed around the evaporator in order to improve refrigerant distribution and reduce pressure drop in the evaporator, but no work is recovered. Note that the ejector cycle also bypasses the vapor from the expansion process around the evaporator. Thus, this comparison allowed Pottker and Hrnjak (2015a) to quantify the improvements that came from bypassing vapor and from work recovery. They observed that the ejector cycle achieved COP improvements of 5 – 9 % over the FGB cycle (COP improvement due only to work recovery) while the FGB cycle achieved COP improvements of 2 – 8 % over the DX cycle (COP improvement due only to bypassing flash vapor); this meant that the ejector cycle improved COP by 8 – 15 % compared to the DX cycle. Based on the findings of this study, it seems that the ejector cycle can achieve similar improvements from improving the evaporator and from work recovery, though it should be noted that this comparison is highly dependent on evaporator design, fluid, and operating conditions.

Hu *et al.* (2014) investigated an R410A ejector system using several different size motive nozzles as well as an adjustable ejector (Figure 2.6). They tested each nozzle and the adjustable ejector at several different ambient temperatures and capacities and observed that the highest capacity and COP were achieved with a different nozzle at each condition, which clearly demonstrated the need for active control of motive nozzle size. They also showed that the adjustable ejector could achieve capacity and COP that was very close to that of the best nozzle for each of the three conditions when the optimal needle position was used at each condition, meaning that using an adjustable ejector offers significant benefit when optimizing the performance of subcritical cycles as well as transcritical cycles. They observed COP improvement of up to 9 % with the adjustable ejector, though details of ejector performance for different needle positions were not reported.

2.5.4 Alternate Ejector Cycle Studies

Recent years, and mainly since 2014, have also seen more of a focus of experimental studies on cycles other than the standard ejector cycle. Lawrence and Elbel (2014a) performed an experimental investigation of the COS ejector cycle (Figure 2.4) described above with refrigerants R134a and R1234yf using the two evaporators to cool a single stream of air. They found that R134a and R1234yf achieved

COP improvements of 5 and 6 %, respectively, compared to a single evaporation temperature DX cycle at matched capacity, though R134a achieved 4 – 6 % higher absolute COP than R1234yf at matched capacity. This was also observed theoretically by Boumaraf *et al.* (2014); they investigated the COS cycle using a thermodynamic model and saw that R134a achieves slightly higher COP than R1234yf, but R1234yf achieves slightly higher COP improvement than R134a compared to a two evaporation temperature DX cycle. Lawrence and Elbel (2014a) showed that the COS ejector cycle achieved higher COP improvement when the capacity of the low-temperature evaporator was smaller and the temperature difference between evaporators was larger, meaning the ejector was used to provide a relatively large pressure lift to a small amount of mass flow. They also tested different combinations of evaporators and showed that the COP of the COS ejector cycle was fairly sensitive to pressure drop in the high-temperature evaporator, again indicating the important effect of evaporator performance when using low-pressure refrigerants.

There have been several recent experimental studies investigating the use of ejectors in liquid recirculation cycles. Dopazo and Fernández-Seara (2011) investigated the ejector recirculation cycle using a commercially available ejector for liquid recirculation and a plate evaporator with ammonia as the refrigerant, though no comparison to a baseline cycle was made; they used a valve upstream of the ejector motive nozzle to control the motive flow rate and the capacity of the system. Li *et al.* (2014) investigated the ejector recirculation cycle using R134a as the refrigerant and a falling film evaporator. They observed using the ejector to recirculate liquid could yield simultaneous COP and capacity improvements of 2 and 5 %, respectively, when the optimal amount of recirculation was used compared to the same cycle but with no liquid recirculation. Minetto *et al.* (2014a) investigated a cycle that could operate as an ejector recirculation cycle with a round tube evaporator and CO_2 as the refrigerant; in their cycle, a liquid-vapor separator was placed at the outlet of the ejector so that the evaporator could be fed liquid and the flash vapor could be bypassed around the evaporator. They observed COP improvement of approximately 13 % compared to DX operation of the evaporators.

Disawas and Wongwises (2004) showed that the standard ejector cycle can also be used as a liquid recirculation cycle. As noted above, the ejector can pump a two-phase fluid; this allows the evaporator to be overfed and its performance improved in the standard ejector cycle. However, the more mass flow the ejector must pump, the lower the pressure lift that it can provide. Disawas and Wongwises (2004) performed an experimental investigation of the standard ejector cycle with R134a and a plate evaporator; the ejector was used to entrain the maximum amount of mass flow rate, meaning that the evaporator performance was improved by recirculating liquid with the ejector, but the cycle gained little direct

pressure lift benefit. They observed COP improvement generally in the range of 5 – 10 % while capacity increased by a similar magnitude with the ejector cycle. They also noted that the COP improvement of the ejector cycle decreased at higher condenser temperature, even though the work recovery of ejectors is generally seen to increase at higher condenser temperatures.

It can be seen from the experimental studies reviewed here that about half of the studies with low-pressure refrigerants use an alternate ejector cycle (COS ejector cycle or ejector recirculation cycle), indicating the strong interest in the use of alternate ejector cycles for low-pressure refrigerants; the results suggest that these alternate ejector cycles are still able to achieve reasonable COP improvement. Based on the above studies with low-pressure refrigerants, it is not clear whether the standard ejector or ejector recirculation cycle would offer better performance. It is very difficult to directly compare the different studies because of the significant effect of evaporator performance on COP. Each of the above studies uses a different evaporator, and many of the studies do not even use the same type of heat exchanger as the evaporator. Comparison of the standard ejector and ejector recirculation cycles will be a major focus of the research presented in this dissertation. It is also seen that many studies with low-pressure refrigerants seem to give special focus to the performance of the evaporator because evaporator improvement can be a significant contributor to COP improvement with low-pressure refrigerants. Even the study on the COS ejector cycle by Lawrence and Elbel (2014a), in which the ejector was not used to recirculate any liquid, still paid careful attention to pressure drop in the evaporator and showed that this can significantly affect COP. As noted above, the research in this dissertation will provide further insight into evaporator design in ejector cycles.

2.6 Evaporator Operation and Performance in Ejector Cycles

As mentioned in the studies of Minetto *et al.* (2013) and Pottker and Hrnjak (2015a) above, the performance of the evaporator in the ejector and DX cycles can differ significantly. Table 2.1 lists the information that can be gathered from the open literature on evaporator performance in ejector cycles. This table was previously published in Lawrence and Elbel (2016a). It should be noted that the majority of these cycles provide little or no comment on evaporator performance and how it affects the comparison of ejector and DX cycles. Furthermore, none of these cycles have investigated how evaporator design or geometry actually affects this comparison.

Table 2.1: Summary of reported evaporator performance in ejector cycles available from open literature (Lawrence and Elbel, 2016a).

Study	Refrigerant	Cycle	Evaporator	Comments
Bilir Sag *et al.* (2015)	R134a	Standard Ejector	Plate-type	• ΔP_{evap} was 50.6 – 65.5 kPa in DX cycle and 3.7 – 4.0 kPa in ejector cycle. • Average evaporator pressure was 6 – 9 kPa lower in ejector cycle.
Disawas and Wongwises (2004)	R134a	Standard Ejector (circulation number of 1.5 to 3.5)	Plate	• Average P_{evap} approximately 15 – 20 kPa higher in ejector cycle. • Improvement in P_{evap} did not seem to be affected by amount of recirculation.
Ersoy and Bilir Sag (2014)	R134a	Standard Ejector	Plate-type	• ΔP_{evap} was 96.2 – 133.7 kPa in DX cycle and 2.2 – 3.8 kPa in ejector cycle. • Average evaporator pressure was 31.9 – 104.6 kPa lower in ejector cycle.
Li *et al.* (2014)	R134a	Ejector Recirculation	Horizontal-tube falling-film	• T_{evap} increased by 0.4 K as recirculation ratio increased from 1.00 to 1.13.
Minetto *et al.* (2013)	CO_2	Standard Ejector	Plate	• UA_{evap} was 41 – 45 % lower in ejector cycle for same evaporator mass flow rate as DX cycle (due to effect of oil in evaporator).
Minetto *et al.* (2014a)	CO_2	Ejector Recirculation	Round-tube-plate-fin	• T_{evap} was approximately 2 K higher in ejector cycle.
Minetto *et al.* (2014b)	CO_2	Ejector Recirculation (feeding both MT and LT evaporators)	Unknown (supermarket system)	• LT T_{evap} increased by approximately 9 K in ejector cycle, and increase in MT T_{evap} seemed similar.
Pottker and Hrnjak (2015a)	R410A	Standard Ejector	Round-tube-plate-fin	• ΔP_{evap} was 86 – 110 kPa in DX cycle and 24 – 26 kPa in ejector cycle. • Average P_{evap} was 10 – 48 kPa higher in ejector cycle. • Observed similar COP improvement contributions from ejector work recovery and flash vapor bypass.
Schönenberger *et al.* (2014)	CO_2	Standard Ejector (supermarket system)	Unknown (supermarket system)	• T_{evap} increased from -8°C to -2°C when ejector was implemented.

2.7 Ejector Geometry Variation and Control

While ejector systems offer promising improvements at the design conditions of the cycle, COP and capacity are known to suffer at conditions of varying capacity and/or ambient temperature due to reduced ejector performance at these varying conditions (referred to as off-design ejector operation). To address this issue of off-design operation, methods to control and vary ejector geometry must be investigated. Motive nozzle size (throat area) is known to have a significant effect on ejector cycle performance, as it directly affects the motive mass flow rate and the system high-side pressure. This effect is known to be particularly important for transcritical CO_2 cycles where the high-side pressure can be actively controlled. One method to vary motive nozzle size in order to control flow rate and high-side pressure is to use an adjustable ejector (Figure 2.6), as described above. While this has been shown to be an effective method for achieving optimal high-side pressure for the given conditions, it also reduces ejector efficiency due to the presence of the needle in the motive nozzle, as shown by Elbel and Hrnjak (2008). Hu *et al.* (2014) showed that active control of motive nozzle size is very important for achieving optimal performance of subcritical cycles as well in their investigation of an R410A system with an adjustable ejector. In addition to the motive nozzle size, control of other ejector components, such as the mixing section and suction chamber, can also have a very significant impact on ejector performance. However, there have yet to be any successful ejector designs capable of controlling several different dimensions simultaneously for refrigeration applications.

Another method for varying effective motive nozzle size is to use a combination of multiple ejectors arranged in parallel, as described by Hafner *et al.* (2014) and shown in Figure 2.7. Each ejector can have different geometry (such as different motive nozzle size and different mixing section diameter) and can be turned on or off independently by use of solenoid valves in order to achieve different high-side pressures for different operating conditions. The advantage of parallel ejector arrangements compared to the adjustable ejector is that with parallel ejectors, the high-side pressure can be varied without a loss in efficiency due to the control mechanism (such as the needle in the case of the adjustable ejector), though only discrete values of high-side pressure can be achieved this way. Additionally, the geometry of the mixing section and the suction nozzle can essentially be adjusted by using different ejectors for different conditions. The number of parallel ejectors and how much variation in size between the ejectors is an area that needs further research. Parallel ejector arrangements generally also include an expansion valve in parallel with the ejectors so that high-side pressure can be continuously controlled at the expense of some of the potential for work recovery.

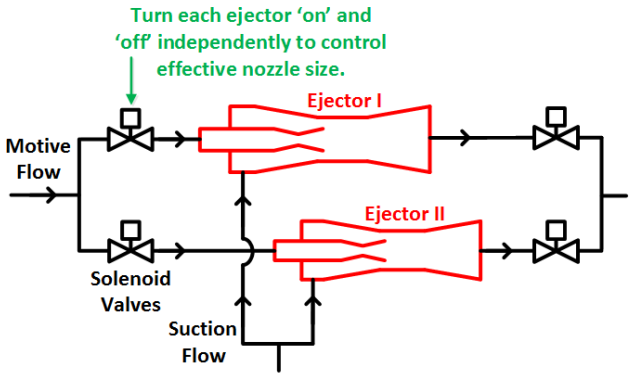

Figure 2.7: Diagram of simplified parallel ejector arrangement control strategy.

Banasiak *et al.* (2015b) performed a detailed laboratory investigation of a CO_2 system using three parallel vapor ejectors and an expansion valve in parallel for high-side pressure control. They observed that ejector efficiency (determined overall for the entire parallel ejector arrangement) generally decreased as motive and suction flow rates through the ejectors increased due to greater frictional losses; they observed up to 33 % work recovery efficiency for the entire parallel ejector assembly. They also observed that the variation of compressor efficiency for different ejector combinations could have significant effect on cycle efficiency; this again highlights the importance of carefully designing or choosing other components of ejector systems in addition to the ejector in order to maximize system efficiency. A maximum COP improvement of 9.8 % compared to a cycle without ejectors was observed at a point where only 50 % of the total flow rate passed though the ejectors but compressor efficiency was highest. The ejectors were not used to pump liquid in the study, so this result does not account for the improvement in evaporator performance due to overfeed. The system also did not have a lower-temperature set of evaporators, as is common in large refrigeration applications where these devices are starting to be applied. Haida *et al.* (2016) performed a similar laboratory study with three parallel ejectors. A maximum COP improvement of 8 % was observed with the parallel ejector assembly compared to a parallel-compression (economizer) cycle, though a maximum COP degradation of 6 % was also observed due to reduced compressor isentropic efficiency when the ejectors were used.

2.8 Ejectors in Commercialized Systems

There are several challenges related to the operation of ejector cycles that must be overcome in order for ejectors to be applied in commercialized systems. Large systems such as commercial and industrial refrigeration systems (discussed further below) often have less restrictive space and cost constraints, meaning that a large liquid-vapor separator would not be an issue; however, other systems, which are generally much smaller and require high levels of compactness, generally cannot have a large separator.

Most systems are subject to varying capacity and/or ambient conditions, meaning that some means of ejector and cycle control must be added to the system. Additionally, all systems require proper oil return, an issue that must still be addressed in ejector cycles with liquid vapor separators. Future work on ejector cycles must address these issues in order for ejector systems to be suitable for real applications.

There have been several different ejector systems that have been successfully commercialized, mostly very recently. As mentioned above, the original use of an ejector for work recovery was to recirculate liquid as in the ejector recirculation cycle. Liquid recirculation is common in large-scale industrial and commercial refrigeration systems; using an ejector to provide liquid recirculation provides a simple alternative to the mechanical pump that is more commonly found in these systems. Ejectors have actually been used in this application for many years and are common enough that liquid recirculation ejectors are commercially available; the studies of Dopazo and Fernández-Seara (2011) and Li *et al.* (2014) both used commercially available liquid recirculation ejectors. In comparison to a two-phase ejector for the standard ejector cycle, which must be carefully designed in order to achieve sufficient performance and pressure lift at the desired entrainment, the design of a liquid recirculation ejector is not as critical, as only a small amount of power is required to pump enough liquid to sufficiently overfeed the evaporator. This may help explain why liquid recirculation ejectors are commercially available and can be purchased and applied to a system without much difficulty. Combined with the fact that an ejector recirculation cycle will still provide capacity even if the ejector does not entrain any mass, this may also help explain why the first use of an ejector for work recovery was for liquid recirculation.

Brodie *et al.* (2012) described the implementation of the COS ejector cycle in a commercially available passenger vehicle cabin cooling system. They showed that both evaporators and the ejector can be integrated into a single unit with one inlet and one outlet that is the same size as a conventional evaporator unit; this unit is shown in Figure 2.8. The cycle could be controlled by automatically adjusting the expansion valve upstream of the low-temperature evaporator in order to ensure superheat at the high-temperature evaporator outlet and protect the compressor. Brodie *et al.* (2012) stated that this system was first introduced to the market in May 2009. They reported a reduction in compressor power consumption of 25 %, though many important details of the study were not included; though not clearly stated, it is likely that the refrigerant in this system was R134a because of the application. It is interesting that the COS ejector cycle was chosen for this automotive cabin cooling application rather than the standard ejector cycle; at the time that this product was introduced, there was almost no research openly available on the COS ejector cycle, and there is still only a limited amount available today. As noted above, the COS ejector cycle has several important advantages in terms of improved off-design operation and

compressor oil return and no liquid-vapor separator, all of which would be important in an automotive system. Thus, despite the significant amount of research done on the standard ejector cycle, one of the first commercialized ejector systems has opted for an alternate ejector cycle. It will be interesting to see if future commercialized ejector systems with low-pressure refrigerants follow the same trend. It should be noted that the same group also worked on similar ejector cycle concepts for refrigerated delivery trucks (Yamada *et al.*, 2009), a chilled beverage box for passenger cars (Oshitani *et al.*, 2008), as well as heat pump water heaters.

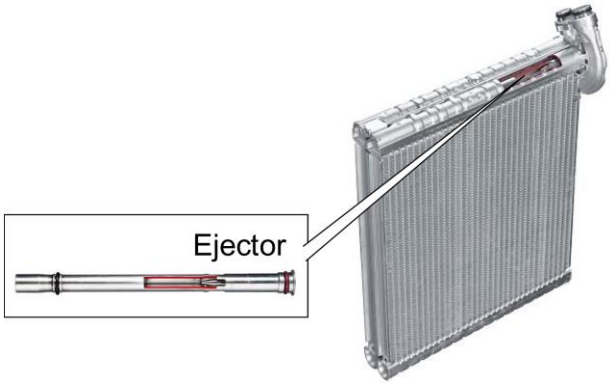

Figure 2.8: Evaporator unit with integrated ejector for automotive cabin cooling (Brodie *et al.*, 2012).

The past few years have seen ejectors applied in CO_2 supermarket refrigeration systems. The use of CO_2 booster systems in supermarkets has been gaining popularity recently, and it is hoped that the implementation of ejectors in these systems will provide reasonable efficiency in a wide range of climates. Hafner *et al.* (2014) introduced a transcritical CO_2 booster cycle using the parallel ejector concept for supermarket systems, as shown in Figure 2.9. In this cycle, the ejectors are used to compress the fluid at the outlet of the medium-temperature (MT) evaporators and thus unload the MT compressors; the ejectors are not used to unload the low-temperature (LT) evaporators or compressors. It can be seen that one of the ejectors is dedicated to pumping liquid and thus overfeeding the MT evaporators, which are controlled to have an outlet quality of 95 %, while the other three ejectors are used to compress vapor and thus unload the MT compressors. The liquid pumping ejectors could also aid in compressor oil return. The ejectors in this cycle are used to increase the pressure of the liquid and a portion of the vapor from the MT evaporators, which is then compressed in the parallel compressors (X and 2), while any vapor that the ejectors cannot compress (due to too little work recovery) is compressed from lower pressure in compressor 1. Note that CO_2 supermarket systems generally do not include an IHX in the compressor suction line, likely due to concerns about compressor discharge temperature. Hafner *et al.* (2014) simulated the performance of this CO_2 booster ejector cycle and calculated cooling COP improvements

for the summer in the range of 5 – 17 % depending on climate; however, they noted that COP increase is very dependent on having the correct system control strategy.

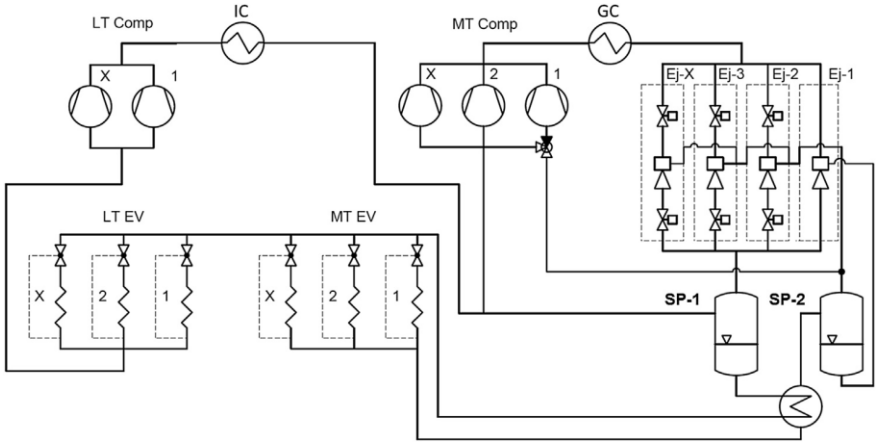

Figure 2.9: Proposed transcritical CO_2 booster cycle with parallel ejectors for supermarket refrigeration systems (Hafner *et al.*, 2014).

A block of six ejectors in parallel is now commercially available for use in CO_2 supermarkets. An image of the ejector block can be seen in Figure 2.10. In the figure, the motive inlet, suction inlet, and diffuser outlet ports for all ejectors are on the left-hand side of the block, while pressure sensors for each of the ports are on the right-hand side of the block. Six ports on the top of the block allow for different ejectors to be used in the ejector block. These blocks are generally implemented with four ejectors for compressing vapor and two ejectors for pumping liquid, allowing the MT evaporators to be overfed.

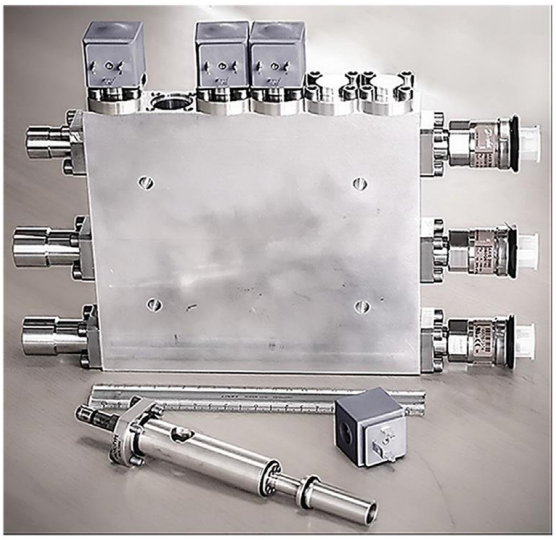

Figure 2.10: Parallel ejector block available for CO_2 supermarket systems (Banasiak *et al.*, 2015b).

Schönenberger *et al.* (2014) reported on a field installation of a transcritical CO_2 booster cycle with parallel ejectors (two vapor compressing ejectors and one liquid pumping ejector) in the region of Fribourg, Switzerland that began operation in the summer of 2013. An expansion valve was installed in parallel with the ejectors, allowing for continuous control of high-side pressure. They reported that the MT evaporator temperature increased by 6 K compared to superheated operation due to overfeeding liquid and operating with a two-phase outlet, and the ejectors further lifted the compressor suction pressure by 3 K. Compared to a parallel compression (economizer) system without ejectors operating in the same region, the ejector system reduced energy consumption by 14 % over a 20 week period during spring and summer.

Schoenenberger (2016) reported additional results from a separate CO_2 supermarket installation with parallel ejectors (three vapor compressing ejectors and two liquid pumping ejectors) in central Switzerland that began operation in 2014. An IHX was placed between the low-pressure liquid line that fed the evaporators (before the evaporator control valves) and the LT evaporator outlet line, allowing the LT evaporators to be overfed as well; this increased the temperature of the LT evaporators by 7 K, while similar improvements in MT evaporator and compressor suction pressures as observed in Schönenberger *et al.* (2014) were observed by Schoenenberger (2016). Schoenenberger (2016) reported 15 to 20 % COP improvement using the ejectors compared to the same system without ejectors.

Additional results were reported by Hafner *et al.* (2016) for a CO_2 supermarket with parallel ejectors (four vapor compressing ejectors and two liquid pumping ejectors) in Spiazzo, Italy from May to October, 2015. This system was also able to supply the full building air-conditioning load in addition to the refrigeration loads. Hafner *et al.* (2016) reported that COP improvement was generally between 15 and 30 % at most operating conditions. Fredslund *et al.* (2016) analyzed data from 7 unspecified locations using parallel ejectors in CO_2 supermarkets. They summarized their findings by noting that systems without integrated air-conditioning could be expected to improve COP by about 4 % with ejectors, while systems with integrated air-conditioning could be expected to improve COP by 10 to 15 % with ejectors. They also reported that the expansion work recovery efficiency of the ejector block was often around 25 %, meaning that the ejector performance observed in laboratory investigations was similar to what is observed in real applications. It should be noted here that the different studies on actual field installations reviewed here generally reported data during the warmer summer months when improvement from the ejector would be greater; less improvement would be expected when averaging for the entire year.

It is not too surprising that supermarket refrigeration systems with CO_2 have been one of the first successful commercialization attempts of ejector systems. As discussed above, the majority of two-phase ejector research has been on transcritical CO_2 cycles. Additionally, the large size of supermarket refrigeration systems helps justify the more complex control strategies that seem necessary to optimize performance of transcritical CO_2 ejector cycles. Both of these factors help make the use of ejectors in supermarket systems an easy choice. Installations of ejectors in CO_2 supermarket systems will likely grow in the coming years as the technology becomes more accepted; it is very possible this ejector technology could spread to other large applications such as industrial or commercial cold storage refrigeration systems as well.

Of greater current interest, however, is what additional systems and applications ejectors could be applied in. Smaller systems such as light commercial refrigeration, household refrigeration, automotive air conditioning, and residential air conditioning and mini-split systems could all benefit from the use of ejectors. However, the smaller size of these systems means that a simpler control strategy than that used in the supermarket systems, or a system that requires no active control, will be needed. These systems also currently use low-pressure refrigerants, meaning that there is less potential benefit from using an ejector cycle. Very small systems could be presented with an additional challenge in terms of manufacturing the very small nozzle throat and keeping it free of clogging; systems of only several hundred watts capacity or less would require nozzle throats of less than 0.5 mm. Thus, further work will need to be done to investigate different simple control strategies and cycle layouts that will allow ejectors to be applied to simpler systems than large-scale refrigeration. Lawrence and Elbel (2016b) presented a design concept and prototype of a 1 kW capacity CO_2 refrigeration system with a simplified ejector design and simplified control, though much more research is needed on integrating ejectors into small-scale refrigeration systems. It is somewhat surprising that an automotive manufacturer was able to successfully commercialize an ejector system given the small system size and the use of low-pressure refrigerants in this application; it is likely the choice of cycle and careful attention to other components in the system, such as the multi-temperature evaporator design in this case, in addition to the design of the ejector that has allowed this commercialization attempt to be a success.

CHAPTER 3: OBJECTIVES OF RESEARCH

The above literature review has shown that significant advances in fundamental research on the use of ejectors for expansion work recovery in vapor-compression cycles has occurred in the last approximately 10 years. This previous research has shown that ejectors certainly offer significant opportunity to improve the COP and capacity of vapor-compression systems. The majority of studies (both experimental and theoretical) have focused on the standard ejector cycle. However, several studies have investigated the ejector recirculation cycle and observed similar performance improvements. It can be seen by looking into these two cycles that the work recovered in the ejector can be used to improve the cycle in two very different ways, namely:

1. To directly supplement compressor power by using the ejector pressure lift to directly increase compressor suction pressure.
2. To improve evaporator performance by using the ejector to pump or recirculate excess liquid through the evaporator.

It should be noted that these are not the only two possible uses of the expansion work recovered in the ejector, though it is these two uses of the ejector that will be of significant interest in this study. It can also be seen from the literature review that there are additional factors, such as evaporator design and performance and cycle control, that can also have a significant effect on ejector cycle performance. While these issues are noted in several studies, they have yet to be thoroughly investigated. Furthermore, no study has investigated and compared the two different uses of the expansion work recovered in the ejector listed above. *Thus, the overall objective of the research in this dissertation is to investigate how to properly integrate an ejector into a vapor-compression cycle (how to choose the proper cycle architecture and proper use of the ejector) and how to design and operate other system components in addition to the ejector, such as the evaporator and cycle controls, in order to gain the maximum benefit from the ejector in the given system.*

The specific objectives of this dissertation are as follows:

- Compare the two uses of the expansion work recovered in the ejector listed above numerically to determine the better use of the ejector and the more favorable ejector cycle for different systems and fluids.
- Compare the standard ejector and ejector recirculation cycles experimentally with R410A.
- Investigate the effect that evaporator design and operation (liquid feeding rate) has on the COP and the COP improvement of the standard ejector and ejector recirculation cycles numerically and experimentally with R410A.

- Develop guidelines on how to properly design and operate evaporators for the standard ejector cycle and for the ejector recirculation cycle.
- Investigate the use of an adjustable ejector and of expansion valves in series and parallel with the ejector to control high-side pressure of a transcritical CO_2 ejector cycle experimentally.
- Investigate the effect of evaporator flow rate and overfeed in a transcritical CO_2 standard ejector cycle experimentally.
- Determine experimentally the loss in standard ejector cycle performance due to improper control of high-side pressure and evaporator flow rate with CO_2.
- Compare the control of transcritical and subcritical CO_2 cycles experimentally using an adjustable ejector to control high-side pressure.

CHAPTER 4: NUMERICAL MODEL DESCRIPTION

This chapter describes the numerical modeling procedure used to analyze the performance of ejector cycles in this study. The microchannel evaporator was simulated using a finite volume model, and the ejector was simulated using a zero-dimensional model. Thermodynamic state-point analysis was used to simulate the remaining cycle components. Additional details of the evaporator model can be found in Appendix B. The numerical model was implemented and solved using computer software.

4.1 Microchannel Evaporator Model

In order to see the effect of liquid recirculation on cycle performance, a finite volume model of a single-pass cross-flow microchannel evaporator based on the conservation of mass, momentum, and energy and able to account for heat transfer and refrigerant-side pressure drop effects was developed. A drawing and the specific dimensions of the microchannel evaporator simulated in this study will be given in later chapters. The evaporator was divided into finite volumes or elements along the length of each tube, and the flow through the evaporator was simulated and solved numerically. The properties of the refrigerant (pressure and specific enthalpy) at the inlet of each element of the evaporator were used to perform heat transfer and pressure drop calculations in each element. The outlet specific enthalpy of the element was determined by performing an energy balance on the element, as shown in Equation (4.1), and the outlet pressure of the element was determined by performing a momentum balance on the element, as shown in Equation (4.2). The refrigerant pressure and specific enthalpy at the inlet to the evaporator were supplied by the cycle model and used as the inputs to the first element. The outlet properties of each element were used as the input properties of the next downstream element, and the calculation proceeded through each element until the outlet of the tube was reached, which marked the outlet state of the evaporator.

$$h_{ref,out} = h_{ref,in} + \frac{\dot{Q}_{element}}{\dot{m}_{tube}} \qquad (4.1)$$

$$P_{ref,out} = P_{ref,in} - \Delta P_{element} \qquad (4.2)$$

Heat transfer and pressure drop in the inlet and outlet headers of the evaporator were assumed to be negligible. It was assumed that refrigerant distribution was uniform in the inlet header of the evaporator, meaning that each of the parallel microchannel tubes received the same refrigerant mass flow rate and inlet quality. The inlet air temperature and volumetric flow rate were assumed to be the same for each element due to the cross-flow configuration of the evaporator, and these parameters were specified as

inputs to the model. Each tube was divided into 200 equally sized elements, for which the evaporator model was found to be grid independent; details on evaporator model grid independence can be found in Appendix B.

The heat transfer and refrigerant-side pressure were calculated separately for each element. The effectiveness-NTU method for heat exchanger analysis was used to calculate the heat transfer $\dot{Q}_{element}$ from air to refrigerant in each element of the evaporator, as shown in Equation (4.3). The heat exchanger effectiveness ε was calculated for each element, as shown in Equation (4.4), using the equation for effectiveness of a cross-flow heat exchanger with both fluids unmixed (Incropera *et al.*, 2007). In this equation, the effectiveness is a function of the capacitance ratio C_r and the number of transfer units *NTU*; the calculation of these parameters is shown in Equations (4.5) through (4.7). Note that these equations assume that no dehumidification occurs in the evaporator; a modified approach accounting for the effect of water vapor on the enthalpy of moist air would be needed in order to analyze dehumidification.

$$\dot{Q}_{element} = \varepsilon \dot{C}_{min}\left(T_{air,in} - T_{ref,in}\right) \qquad (4.3)$$

$$\varepsilon = 1 - \exp\left[\left(\frac{1}{C_r}\right) NTU^{0.22}(\exp[-C_r NTU^{0.78}] - 1)\right] \qquad (4.4)$$

$$C_r = \frac{\dot{C}_{min}}{\dot{C}_{max}} \qquad (4.5)$$

$$\dot{C}_{min} = \text{Min}\left(\dot{m}_{ref} c_{p,ref}, \dot{m}_{air} c_{p,air}\right);\ \dot{C}_{max} = \text{Max}\left(\dot{m}_{ref} c_{p,ref}, \dot{m}_{air} c_{p,air}\right) \qquad (4.6)$$

$$NTU = \frac{UA}{\dot{C}_{min}} \qquad (4.7)$$

For the case of the refrigerant stream being two-phase, the capacitance ratio C_r is zero, and the expression for heat exchanger effectiveness reduces to that shown in Equation (4.8).

$$\varepsilon = 1 - \exp[-NTU] \qquad (4.8)$$

The effectiveness calculation also requires determination of the overall heat transfer coefficient-area product *UA*, which requires knowledge of the air- and refrigerant-side heat transfer coefficients as well as

the air- and refrigerant-side heat transfer areas, as shown in Equation (4.9). This equation neglects the thermal resistance of the tube, which is generally negligible. The air-side heat transfer coefficient was determined based on the correlation of Park and Jacobi (2009) for flat-tube louvered-fin heat exchangers. The heat transfer coefficient for single-phase refrigerant was determined using Gnielinski (1976). The flow boiling correlation of Chen (1966) was used to determine the two-phase heat transfer coefficient for R134a and R410A, while the flow pattern-based correlation of Cheng *et al.* (2006) was used to determine the two-phase heat transfer coefficient for CO_2. Details of these empirical correlations can be found in Appendix B. A summary of the empirical correlations used in the evaporator model is shown in Table 4.1. The air- and refrigerant-side heat transfer areas were determined based on the geometry of the evaporator (specified in later chapters). The surface efficiency η_{air} accounts for temperature variation along the fins on the air-side of the heat exchanger. Further information on surface efficiency can be found in Incropera *et al.* (2007).

$$\frac{1}{UA} = \frac{1}{h_{air}A_{air}\eta_{air}} + \frac{1}{h_{ref}A_{ref}} \qquad (4.9)$$

The pressure drop term $\Delta P_{element}$ in Equation (4.2) represents the total refrigerant-side pressure drop, which is the sum of friction, gravitational, and acceleration pressure drops. The total pressure drop in the element is simply the total pressure gradient, shown in Equation (4.10), multiplied by the length of the element. The frictional pressure drop was calculated using the curve fit of Churchill (1977) for single-phase refrigerant and the correlation of Friedel (1979) for two-phase refrigerant. Details of these correlations can be found in Appendix B. The gravitational and acceleration pressure drops are shown in Equations (4.11) and (4.12), respectively. For all calculations, it was assumed that the microchannel tubes were oriented vertically so that the angle θ in Equation (4.11) was 90°. The vapor volume fraction or void fraction α was determined assuming homogeneous flow, as shown in Equation (4.13).

$$\frac{dP}{dz} = \left(\frac{dP}{dz}\right)_{fr} + \left(\frac{dP}{dz}\right)_{gr} + \left(\frac{dP}{dz}\right)_{acc} \qquad (4.10)$$

$$\left(\frac{dP}{dz}\right)_{gr} = [(1-\alpha)\rho_l + \alpha\rho_v]g\sin\theta \qquad (4.11)$$

$$\left(\frac{dP}{dz}\right)_{acc} = \frac{G^2}{\Delta L}\left[\left(\frac{x^2}{\rho_v\alpha} + \frac{(1-x)^2}{\rho_l(1-\alpha)}\right)_{out} - \left(\frac{x^2}{\rho_v\alpha} + \frac{(1-x)^2}{\rho_l(1-\alpha)}\right)_{in}\right] \qquad (4.12)$$

$$\alpha = \frac{\frac{x}{\rho_v}}{\frac{x}{\rho_v} + \frac{1-x}{\rho_l}} \qquad (4.13)$$

Table 4.1: Summary of empirical correlations used in finite volume evaporator model.

Parameter	Reference
Refrigerant-side 1ϕ pressure drop	Churchill (1977)
Refrigerant-side 1ϕ heat transfer coefficient	Gnielinski (1976)
2ϕ pressure drop	Friedel (1979)
2ϕ heat transfer coefficient	R134a, R410A: Chen (1966) CO_2: Cheng *et al.* (2006)
Air-side heat transfer coefficient	Park and Jacobi (2009)

4.2 Ejector Model

The ejector was simulated using the zero-dimensional, constant-pressure mixing model of Kornhauser (1990). The model performs mass, momentum, and energy balances on the individual ejector components and requires the assumption of the isentropic efficiency of the ejector motive nozzle, suction nozzle, and diffuser as well as the assumption of an ejector mixing section pressure (assumed to be constant through the mixing section). The motive nozzle, suction nozzle, and diffuser isentropic efficiency definitions are shown in Equations (4.14) through (4.16), respectively. Figure 4.1 provides a detailed equation listing for the ejector simulation procedure. The procedure requires specification of the motive and suction inlet states, assumed mixing section pressure, assumed ejector component efficiencies, and ratio of motive to total mass flow rate *r*, Equation (4.17), as inputs. The procedure provides the outlet state of the ejector (pressure and specific enthalpy) as the output.

$$\eta_{mn} = \frac{h_{mn,in} - h_{mn,out}}{h_{mn,in} - h_{mn,out,s}} \qquad (4.14)$$

$$\eta_{sn} = \frac{h_{sn,in} - h_{sn,out}}{h_{sn,in} - h_{sn,out,s}} \qquad (4.15)$$

$$\eta_{diff} = \frac{h_{diff,out} - h_{diff,in}}{\frac{1}{2}v_{diff,in}^2} \qquad (4.16)$$

$$r = \frac{\dot{m}_{mn}}{\dot{m}_{mn} + \dot{m}_{sn}} \qquad (4.17)$$

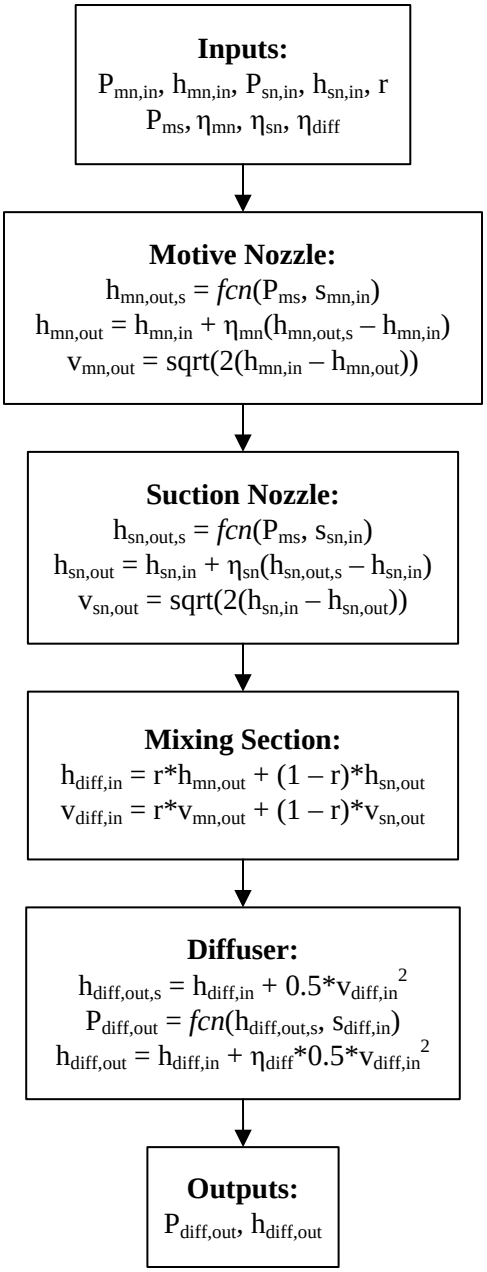

Figure 4.1: Ejector simulation procedure based on zero-dimensional, constant-pressure mixing ejector model of Kornhauser (1990).

The values of component efficiencies were chosen in order to achieve overall ejector work recovery efficiency similar to what is observed experimentally for different fluids, as ejectors seem to achieve different ranges of work recovery efficiency with different fluids. The assumed values of ejector

component efficiencies will be specified in later chapters. The mixing section pressure was set by assuming a specified pressure drop across the suction nozzle; the specified pressure drop corresponded to approximately a 1 K drop in saturation temperature for the given fluid. This assumption is consistent with the experimental observations of Elbel (2011) and Harrell and Kornhauser (1995); very little additional experimental data is available on the mixing section pressure in two-phase ejectors.

4.3 Cycle Model

The finite volume evaporator model and zero-dimensional ejector model were incorporated into thermodynamic state point models of the different ejector cycles in order to simulate the remaining components of the cycle. The condenser temperature and subcooling or gas cooler pressure and outlet temperature were specified as inputs to the model. An internal heat exchanger was not included in any of the cycles. Heat transfer and pressure drop in the tubing between components were neglected. The evaporator air inlet temperature and volumetric flow rate were also specified as inputs to the cycle model. Dry air-side conditions were assumed in the evaporator. For cases where evaporator overfeed was investigated, the refrigerant mass flow rate through the evaporator was specified as well. The compressor compression and mechanical efficiencies, defined in Equations (4.18) and (4.19), respectively, were also specified as inputs to the cycle model and were assumed to be constant for all conditions. The specified values of operating conditions (cycle model inputs) will be given in later chapters.

$$\eta_{cp} = \frac{h_{out,s} - h_{in}}{h_{out} - h_{in}} \qquad (4.18)$$

$$\eta_{mech} = \frac{\dot{m}(h_{out} - h_{in})}{\dot{W}} \qquad (4.19)$$

A mass balance on the liquid-vapor separator in the ejector cycle shows that the ratio of motive to total ejector mass flow rate must equal the ejector outlet quality, as shown in Equation (4.20); this constraint applies to both the standard ejector and ejector recirculation cycles. It was also assumed that the liquid-vapor separator achieved perfect separation, meaning that all vapor that entered the separator exited at the vapor port (leading to the compressor) and all liquid that entered the separator exited at the liquid port (leading to the metering valve in each cycle). Lawrence and Elbel (2012, 2014a) showed cycle performance could be dramatically decreased if the separator did not separate the phases properly.

$$r = x_{diff,out} \qquad (4.20)$$

4.4 Solution Method

The computer program Engineering Equation Solver or EES (F-Chart Software, 2015) was used to obtain property information for the different refrigerants and to iteratively solve the generally non-linear systems of equations. This program uses the Newton-Raphson method to iteratively solve a set of non-linear equations; Stoecker (1989) provides further description of the Newton-Raphson solution method. The iteration proceeded until the relative residuals were less than 10^{-6} and the change in variables was less than 10^{-9}. Equations were programmed in EES based on the above description of the evaporator, ejector, and cycle modeling, and the built-in non-linear equation-solving ability of EES was used to obtain the solution for each specified set of inputs.

CHAPTER 5: EXPERIMENTAL FACILITY DESCRIPTION

This chapter presents a description of the facility that was used to obtain experimental results reported in this dissertation. Experimental results are reported for both an R410A ejector system and a CO_2 ejector system. The same facility was used to run tests for both refrigerants, but different components for the refrigeration system were used for the two different refrigerants. The ejector design procedure is described, and the dimensions of the R410A ejector and the CO_2 ejector are given. The uncertainty of the results reported in this dissertation is also given.

5.1 Experimental Facility and Methods

The vapor-compression cycles of interest in this study were constructed on an experimental air conditioning test bench. The standard ejector cycle, ejector recirculation cycle, and DX cycle were constructed for the experiments with R410A, while the standard ejector cycle and DX were constructed for the experiments with CO_2. A picture of the experimental facility can be seen in Figure 5.1.

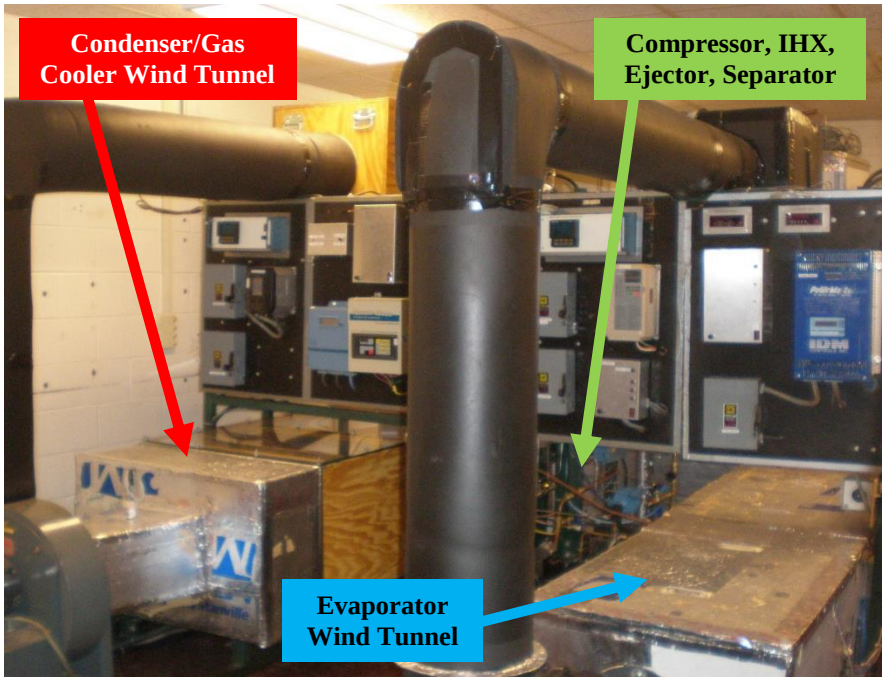

Figure 5.1: Facility for R410A and CO_2 experiments used in this study.

The same basic facility was used for both the R410A and CO_2 systems, but different refrigerant system components were used for the two different refrigerants. Two closed-loop wind tunnels housed the evaporator and condenser/gas cooler. Variable-speed blowers and electric heaters were used to control air

flow rate and inlet temperature to the condenser and evaporator. An additional heat exchanger with chilled water flowing through was included in the condenser/gas cooler wind tunnel to reject heat from the wind tunnel. Type-T thermocouples, absolute and differential pressure transducers, and Coriolis-type mass flow meters were used to obtain refrigerant-side measurements. Type-T thermocouples, differential pressure transducers, capacitive relative humidity sensors, and flow nozzles were used to obtain air-side measurements. A power transducer was used to measure the electrical power input to the compressor; electrical losses in the variable frequency drive were not accounted for in the compressor power measurement but can be assumed small. The power to the air blowers was not measured and was not used when calculating system performance because the power required to blow air through closed-loop wind tunnels is much higher than blower power in real systems. Further description of the components used for the R410A and CO_2 systems can be found in the following sections and in Appendix C. Further details regarding the general construction and operation of the experimental facility can be found in Elbel (2007).

Data was collected at steady-state conditions at 6 second intervals for 10 consecutive minutes, and the data was averaged over the collection period. Two independent energy balances (air- and refrigerant-side) could be obtained for the capacity of the evaporator. When both balances were available, they generally agreed to within 4 % for the majority of data points. Because one of the main objectives of this study is to investigate evaporator overfeeding in ejector cycles, the refrigerant at the evaporator outlet was often two-phase; as a result, the refrigerant-side energy balance often could not be used. For consistency, capacity determined by air-side measurements is reported throughout this dissertation. Repeatability of data points was shown to be within 2 %.

5.1.1 R410A Experimental Facility

The R410A system was constructed using components that would be found in a small-scale air-conditioning system (similar to a 1 to 2 kW capacity mini-split system). The condenser was a round-tube-plate-fin heat exchanger. A liquid receiver was installed at the outlet of the condenser. A fixed geometry ejector (described below) was used as the expansion device. A fixed displacement, rolling-piston compressor suitable for use with R410A was used. A variable frequency drive was used to control compressor speed in order to obtain the desired capacity. PVE oil was used for compressor lubrication. Additional details of the condenser and compressor can be found in Appendix C. Two different microchannel heat exchangers were used for the evaporator, as will be described below. The liquid-vapor separator was large enough that inefficient phase separation was not a concern in this system. A metering valve was installed downstream of the liquid-vapor separator in the ejector cycles in order to control evaporator flow rate and overfeed. Oil was returned to the compressor by means of a bypass line from the

liquid outlet of the separator to the vapor outlet (compressor suction line). A valve was included in the oil return line; this valve was closed (no liquid/oil return to the suction line) while recording data. Tubing length between components was kept approximately the same for the different cycles. Figure 5.2 shows a schematic of the R410A experimental facility for the standard ejector cycle configuration.

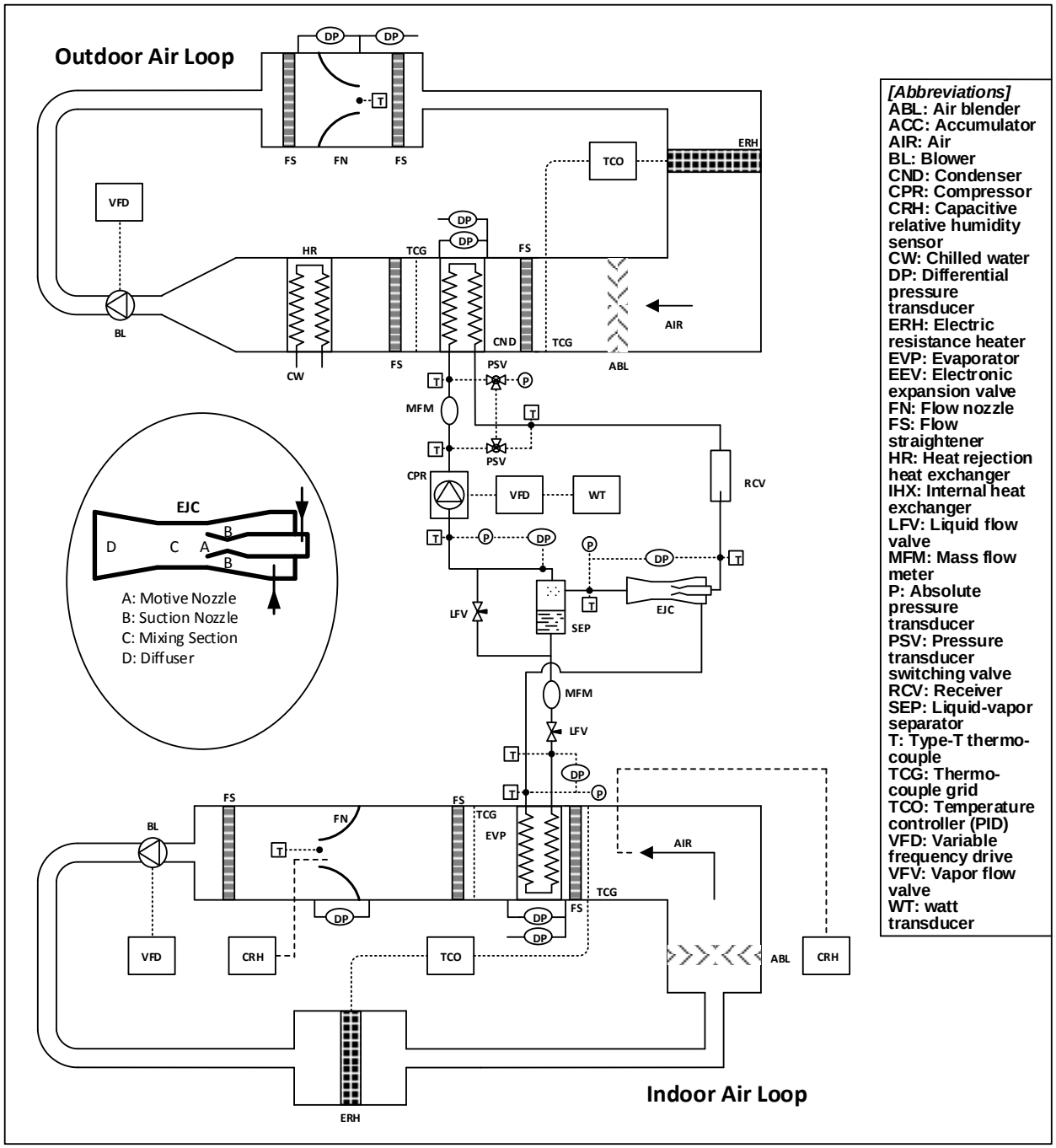

Figure 5.2: Schematic of R410A experimental facility detailing the layout of equipment and sensors for the standard ejector cycle.

Two different microchannel heat exchangers were used as the evaporator in the experiments. The evaporators were of a cross-flow configuration and were single-pass, single-slab with 23 parallel microchannel tubes. Both evaporators (referred to as A and B) had the same air-side characteristics, but Evaporator B had about half the number of microchannel ports per tube on the refrigerant-side (same port size), resulting in half the refrigerant-side cross-sectional area and half the heat transfer area compared to Evaporator A. The shape of the microchannel ports was triangular. The dimensions of the two evaporators are shown in Table 5.1, and a drawing of Evaporator A with important dimensions noted is shown in Figure 5.3. This set of evaporators was chosen in order to experimentally investigate the effect of refrigerant mass flux on ejector cycle performance for the same air-side resistance.

Table 5.1: Dimensions and overall areas of two microchannel evaporators used in R410A experiments.

	Evaporator A	**Evaporator B**
Overall tube length	265 mm	
Overall width	241 mm	
Overall depth	21 mm	
Fin pitch	1.6 mm	
Fin height	8.0 mm	
Louver angle	27°	
Louver pitch	1.4 mm	
Louver height	7.4 mm	
Number of tubes	23	
Tube pitch	9.8 mm	
Tube major diameter	18.8 mm	
Tube minor diameter	1.9 mm	
Number of ports per tube	19	10
Port hydraulic diameter	0.8 mm	
Air-side area	1.573 m^2	
Refrigerant-side area	0.282 m^2	0.148 m^2
Refrigerant-side cross-section area	208.8 mm^2	109.9 mm^2

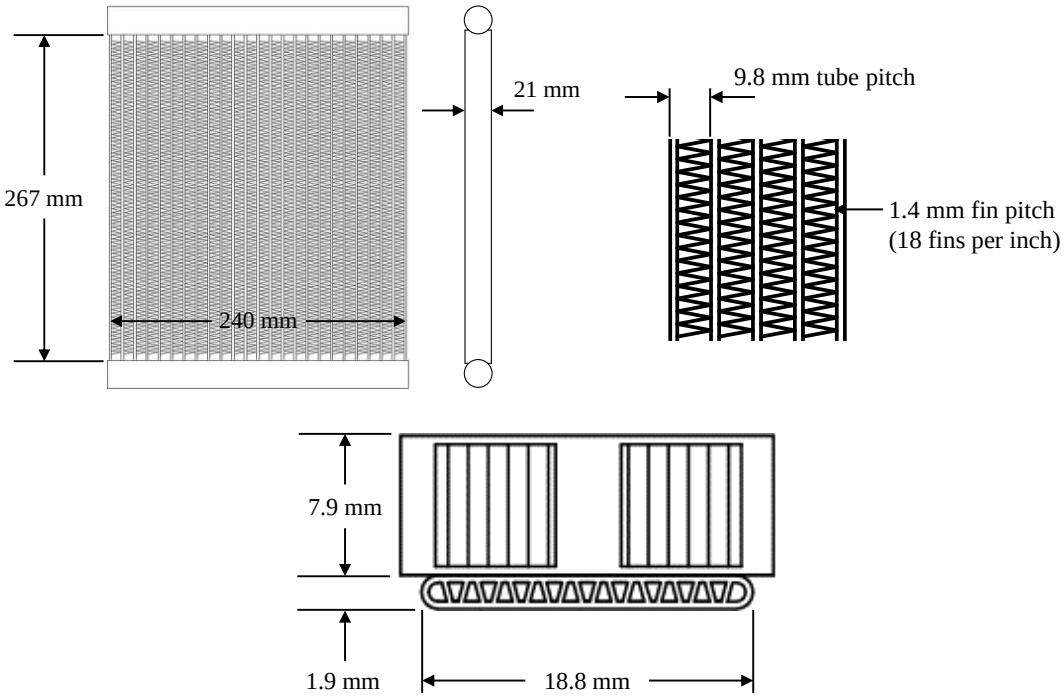

Figure 5.3: Drawing of evaporators used in R410A experiments; only difference between evaporators was the number of ports on the refrigerant-side.

5.1.2 CO_2 Experimental Facility

The CO_2 system was constructed using components similar to what would be found in proposed CO_2 automotive air-conditioning systems for mid-sized vehicles. The gas cooler was a cross-counterflow, microchannel heat exchanger. A fixed displacement, reciprocating, transcritical CO_2 compressor was used. A variable frequency drive was used to control compressor speed. PAG oil was used for compressor lubrication. A cross-counterflow, microchannel heat exchanger was used as the evaporator. A microchannel-plate, counterflow heat exchanger was used as the internal heat exchanger (IHX). A bypass line with a metering valve was installed around the IHX on the low-pressure-side to control IHX effectiveness. Additional details of the gas cooler, compressor, evaporator, and IHX can be found in Appendix C. The liquid-vapor separator was large enough that inefficient phase separation was not a concern in this system at low capacities, but some inefficiency in phase separation may have occurred at the highest capacities. An adjustable ejector (described below) or a fixed ejector in combination with an expansion valve was used as the expansion device depending on the test; further information on ejector control methods will be given in Chapter 8. A metering valve was installed downstream of the liquid-vapor separator in the ejector in order to control evaporator flow rate. Oil was returned to the compressor by means of a bypass line from the liquid outlet of the separator to the vapor outlet (compressor suction line). A metering valve was included in the oil return line, and the valve was closed (no liquid/oil return

to the suction line) while recording data. Tubing length between components was kept approximately the same when implementing the ejector and DX cycles. Figure 5.4 shows a schematic of the CO_2 experimental facility for the standard ejector cycle configuration.

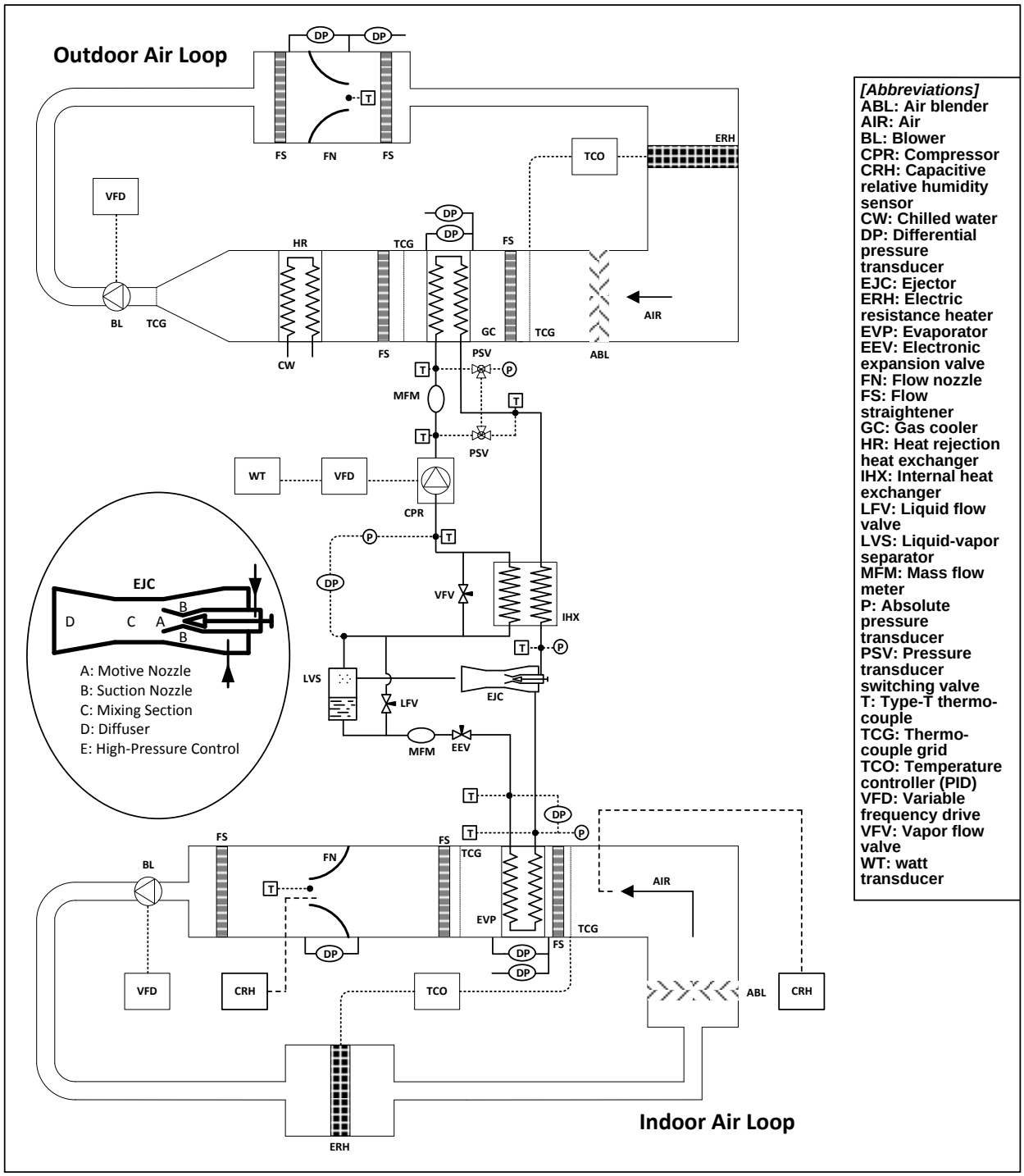

Figure 5.4: Schematic of CO_2 experimental facility detailing the layout of equipment and sensors for the standard ejector cycle.

5.2 Ejector Design

5.2.1 Ejector Design Guidelines

The ejectors for the R410A and CO_2 systems were designed based on a series of calculations and recommendations from the review of Lawrence and Elbel (2014b). A drawing the ejector used in the experiments of this study with relevant geometric parameters noted can be seen in Figure 5.5.

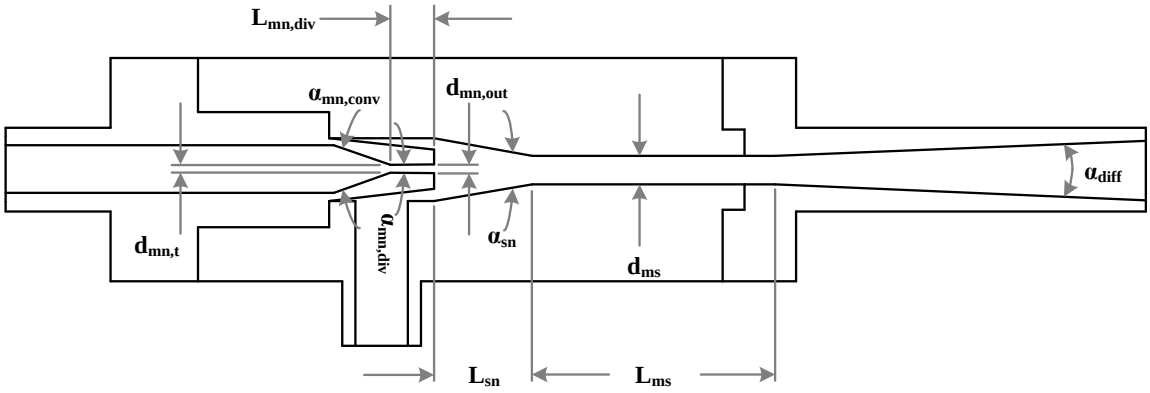

Figure 5.5: Drawing of modular ejector cross-section with relevant geometric parameters noted.

The motive nozzle throat diameter was designed using the empirical correlation for non-homogenous expansion of two-phase flow through a nozzle from Henry and Fauske (1971). Motive nozzle size is an important parameter in ejector design because it sets the high-side pressure and flow rate of the system. The iterative set of equations for this correlation are shown in Equations (5.1) through (5.4). The calculation returns the critical (choked) mas flux at the nozzle throat and the pressure at the throat. The diameter can then be determined based on the calculated critical mass flux and the desired mass flow rate.

$$G_c{}^2 = \left((v_{vE} - v_o) \frac{N}{s_{vE} - s_{lE}} \frac{ds_{lE}}{dP} \right)^{-1} \qquad (5.1)$$

$$\frac{P_t}{P_o} = 1 - \frac{v_o G_c{}^2}{2P_o} \qquad (5.2)$$

$$x_{Et} = \frac{s_o - s_{lE}}{s_{vE} - s_{lE}} \qquad (5.3)$$

$$N = \frac{x_{Et}}{0.14} \leq 1 \qquad (5.4)$$

Additional approaches for sizing the nozzle throat include assuming complete phase change with homogeneous equilibrium flow (HEM) and assuming incompressible (constant density, no phase change) flow. A comparison of these approaches is presented in Figure 5.6. It can be seen that the HEM approach predicts lower mass flow rate than the Henry and Fauske (1971) correlation because the complete phase change results in a greater vapor mass fraction at the throat. The Henry and Fauske (1971) correlation assumes non-equilibrium expansion, meaning that the amount of vapor formed during expansion is reduced compared to the case of thermodynamic equilibrium due to the rate of pressure drop being greater than the rate of heat transfer and phase change in the fluid. The incompressible approach predicts much higher mass flow rate than the Henry and Fauske (1971) correlation because it assumes only high-density liquid and no vapor at the throat. Elbel (2007) showed that the Henry and Fauske (1971) correlation under-predicts nozzle flow rate by 5 to 10 % but is still more accurate than the HEM approach.

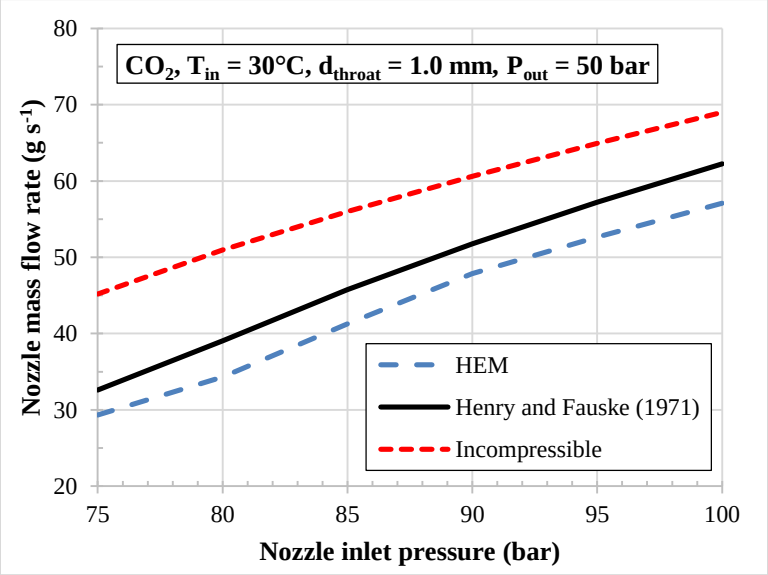

Figure 5.6: Comparison of motive nozzle mass flow rate determined assuming homogenous equilibrium flow (HEM), with the empirical correlation of Henry and Fauske (1971), and assuming incompressible flow.

The motive nozzle diverging section controls the expansion of the motive flow to the mixing section pressure. Too long of a diverging section will result in excessive pressure loss, while too short of a diverging section will not allow enough time for the flow to expand to the mixing section pressure and may result in flow separation if the angle is too large; all of these effects will reduce nozzle and ejector efficiency. ASHRAE (1983) recommends nozzle diverging angles in the range of 5° to 12° (full) for steam ejectors. As shown in the review of Lawrence and Elbel (2014b), two-phase ejectors generally use motive nozzle diverging angles in the range of 1° to 4° (full) for all refrigerants. The smaller angle (larger diverging length) needed for two-phase ejectors is likely due to the fact that flow requires time to change

phase and come to equilibrium before the nozzle outlet while the flow in a single-phase ejector nozzle does not change phase. The ejectors in this study were designed to have a diverging angle of 2.3° (full), as this angle has been seen to yield reasonable ejector performance previously (Elbel, 2007; Lawrence and Elbel, 2014a). The nozzle outlet diameter was calculated assuming equilibrium expansion of the motive flow to the nozzle outlet pressure; the nozzle outlet pressure was assumed to be the pressure corresponding to a 1 K drop in saturation temperature of the suction flow. Motive nozzle diverging length was determined once nozzle outlet diameter and diverging angle were specified. Nozzle converging angle and converging length are generally seen to be less critical than diverging angle and diverging length.

The suction nozzle is designed to pre-accelerate the suction flow slightly and then begin the mixing between the motive and suction flows. Suction nozzle angles and lengths (distance between nozzle outlet and beginning of constant-area mixing section) are often not reported in two-phase ejector studies, so it is difficult to draw any general conclusions about proper suction nozzle design based on previous ejector studies. A suction nozzle (converging) angle of 20° (full) has been seen to yield reasonable ejector performance previously (Elbel 2007; Lawrence and Elbel, 2014a) and will be used again in this study.

ASHRAE (1983) recommends a slight converging angle (taper) in the mixing section, though two-phase ejectors generally use only a constant-area mixing section combined with a short suction nozzle. The diameter of the constant-area mixing section is generally set by the ejector area ratio, shown in Equation (5.5). Too large of a mixing diameter will not force the motive and suction streams to mix (motive stream expands straight through the ejector without entraining suction flow). Too small of a mixing diameter will not allow a large enough cross-sectional area for the suction flow, resulting in a choked suction stream and limited suction flow rate. The optimal ejector area ratio is strongly dependent on the refrigerant and the operating conditions; recommendations for different refrigerants are given in Table 5.2.

$$Area\ Ratio = \frac{A_{ms}}{A_{mn,t}} \qquad (5.5)$$

Table 5.2: Recommended two-phase ejector area ratio (mixing to nozzle throat) depends on the refrigerant.

Refrigerant	Recommended Area Ratio
CO_2	5 – 10
R410A	15 – 20
R134a	25 +

The length of the mixing section is generally set by the mixing ratio, shown in Equation (5.6). Too long of a mixing length will result in excess pressure frictional pressure loss, while too short of a mixing length will not provide enough time for the motive and suction streams to mix. ASHRAE (1983) recommends a mixing ratio of 10 to 15 for ejectors with tapered mixing sections, though most two-phase ejector studies use a mixing length closer to 10.

$$Mixing\ Ratio = \frac{L_{ms}}{d_{ms}} \qquad (5.6)$$

ASHRAE (1983) recommends diffuser angles of 5° to 12° (full) for steam ejectors. The diffuser angle of two-phase ejectors is generally similar; as seen in the review of Lawrence and Elbel (2014b), two-phase ejector studies generally use diffuser angles between 4° and 8° (full). Too large of a diffuser angle can result in flow separation, while too small of a diffuser angle can result in excessive frictional pressure loss, both of which result in lower pressure recovery. It seems that a diffuser angle of 5° (full) is most common for two-phase ejectors; this is the diffuser angle used in the ejectors of this study.

5.2.2 Ejector Assembly

A modular design was used so that dimensions of individual components could be changed without constructing an entirely new ejector. The individual components (motive nozzle, suction chamber and mixing section, and diffuser) were machined out of brass. PTFE gaskets were used to provide a seal between components. The components used for the CO_2 ejector can be seen in Figure 5.7. The individual components were held together using a set of flanges, threaded rods, and nuts. The assembled CO_2 ejector can be seen in Figure 5.8.

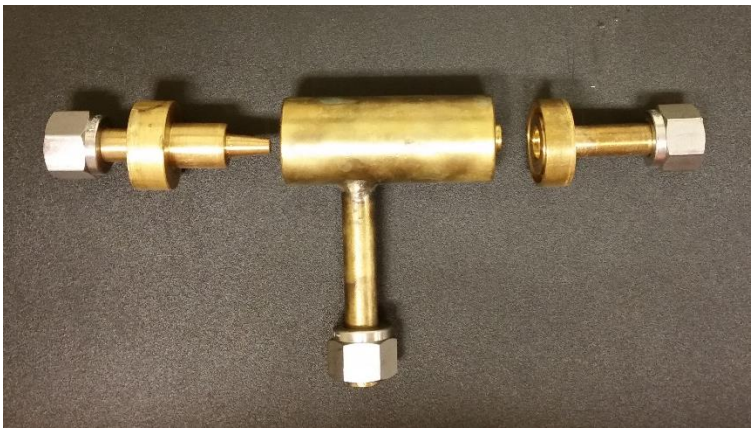

Figure 5.7: Components of modular CO_2 ejector (left to right): Motive nozzle; suction chamber and mixing section; diffuser.

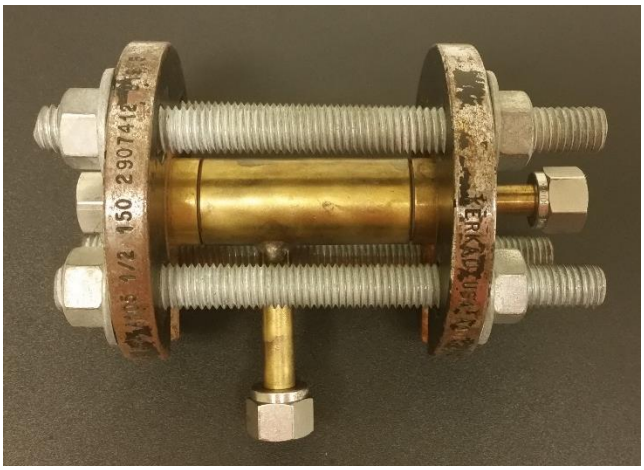

Figure 5.8: CO_2 ejector assembly.

5.2.3 R410A Ejector Design

The R410A ejector was designed for an air-conditioning system of approximately 1 kW capacity using the guidelines provided in Section 5.2.1 above. Table 5.3 shows the internal dimensions of the R410A ejector, and Figure 5.9 shows a drawing of the R410A ejector with important dimensions specified.

Table 5.3: Internal dimensions of ejector for 1 kW R410A air-conditioning system.

Parameter	Symbol	Value
Motive nozzle throat diameter	$d_{mn,t}$	0.7 mm
Motive nozzle converging angle	$\alpha_{mn,conv}$	36° (full)
Motive nozzle outlet diameter	$d_{mn,out}$	1.1 mm
Motive nozzle diverging angle	$\alpha_{mn,div}$	2.3° (full)
Motive nozzle diverging length	$L_{mn,div}$	10 mm
Suction nozzle angle	α_{sn}	20° (full)
Suction nozzle length	L_{sn}	11 mm
Mixing section diameter	d_{ms}	3 mm
Mixing section length	L_{ms}	24 mm
Mixing ratio	L_{ms}/d_{ms}	8.0
Ejector area ratio	$A_{ms}/A_{mn,t}$	18.4
Diffuser angle	α_{diff}	5° (full)

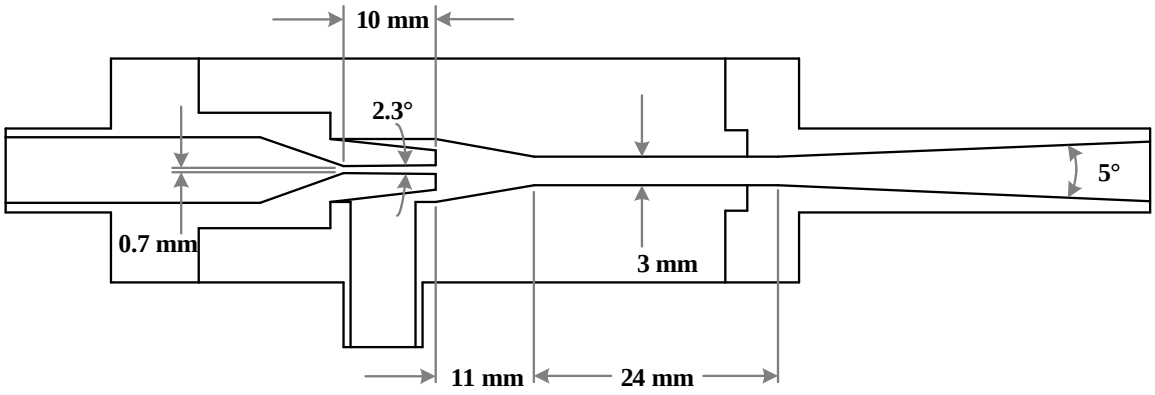

Figure 5.9: Drawing of R410A ejector with important dimensions specified.

5.2.4 CO_2 Ejector Design

The CO_2 ejector was designed for an air-conditioning system of approximately 5-7 kW capacity using the guidelines provided in Section 5.2.1 above. Table 5.4 shows the internal dimensions of the CO_2 ejector, and Figure 5.10 shows a drawing of the CO_2 ejector with important dimensions specified.

Table 5.4: Internal dimensions of ejector for 5-7 kW CO_2 air-conditioning system.

Parameter	Symbol	Value
Motive nozzle throat diameter	$d_{mn,t}$	1.0 mm
Motive nozzle converging angle	$\alpha_{mn,conv}$	36° (full)
Motive nozzle outlet diameter	$d_{mn,out}$	1.2 mm
Motive nozzle diverging angle	$\alpha_{mn,div}$	2.3° (full)
Motive nozzle diverging length	$L_{mn,div}$	5 mm
Suction nozzle angle	α_{sn}	20° (full)
Suction nozzle length	L_{sn}	11 mm
Mixing section diameter	d_{ms}	3 mm
Mixing section length	L_{ms}	24 mm
Mixing ratio	L_{ms}/d_{ms}	8.0
Ejector area ratio	$A_{ms}/A_{mn,t}$	9.0
Diffuser angle	α_{diff}	5° (full)

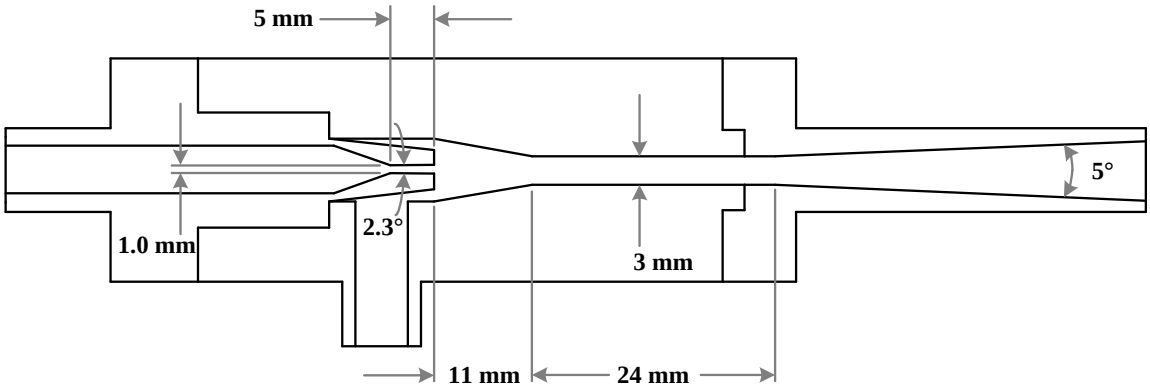

Figure 5.10: Drawing of CO_2 ejector with important dimensions specified.

The length and diameter of the constant-area mixing section happen to be the same for the R410A and CO_2 ejectors used in this study. The mixing diameter is a function of both fluid and operating conditions. CO_2 ejectors require smaller area ratio than R410A ejectors (as shown in Table 5.2) because the ratio of liquid phase to vapor phase density is much lower for CO_2 (primarily due to the very higher vapor density of CO_2). When the flow expands through the motive nozzle and low density vapor is generated, the volume flow rate increases; the higher vapor density of CO_2 compared to R410A means that its volume increase between nozzle throat and mixing section will be lower, resulting in a smaller area ratio. However, the CO_2 system in this study is a larger (higher capacity) system, which increases the flow rates through the ejector and thus the required cross-sectional area. As a result of these two effects, the necessary mixing diameter for the CO_2 and R410A ejectors appears to be about the same.

5.3 Uncertainty Analysis

Error propagation was performed using Engineering Equation Solver (F-Chart Software, 2015). The uncertainty values of the individual sensors used in the R410A and CO_2 experimental facilities can be found in Appendix C. The determined uncertainty values of the calculated parameters in the R410A experiments are listed in Table 5.5. The parameters $COP\ Ratio$ and Q_{evap} are reported as relative uncertainties, and the remaining parameters are reported as absolute uncertainties. The uncertainty of the ejector temperature lift (T_{lift}) in the R410A facility was determined using measured pressures. The determined uncertainty values of the calculated parameters in the CO_2 experiments are listed in Table 5.6. The parameters COP, Q_{evap}, $P_{lift,ejec}$, $\dot{W}_{rec}$, $\dot{W}_{rec,max}$, and UA_{evap} are reported as relative uncertainties, and the remaining parameters are reported as absolute uncertainties. The uncertainty values reported in Tables 5.5 and 5.6 are calculated for a given data point but are generally representative of the uncertainty of their respective systems.

Table 5.5: Uncertainty of calculated parameters reported in R410A experiments.

Parameter	Uncertainty
$\boldsymbol{COP\ Ratio}$ (-)	±8.9 %
$\boldsymbol{Q_{evap}}$ (kW)	±6.3 %
$\boldsymbol{\eta_{ejec}}$ (-)	±0.029
$\boldsymbol{R}$ (-)	±0.088
$\boldsymbol{\Pi_s}$ (-)	±0.006
$\boldsymbol{T_{lift}}$ (K)	±0.2 K

Table 5.6: Uncertainty of calculated parameters reported in CO_2 experiments.

Parameter	Uncertainty
$\boldsymbol{COP}$ (-)	±6.0 %
$\boldsymbol{Q_{evap}}$ (kW)	±6.0 %
$\boldsymbol{\eta_{ejec}}$ (-)	±0.020
$\boldsymbol{P_{lift,ejec}}$ (kPa)	±6.1 %
$\boldsymbol{\dot{W}_{rec}}$ (W)	±8.6 %
$\boldsymbol{\dot{W}_{rec,max}}$ (W)	±1.8 %
$\boldsymbol{\Phi_m}$ (-)	±0.047
$\boldsymbol{UA_{evap}}$ (kW K^{-1})	±7.3 %
$\boldsymbol{x_{evap,out}}$ (-)	±0.052
$\boldsymbol{\Delta T_{SH}}$ (K)	±0.5 K

CHAPTER 6: APPLICATION OF EJECTOR EXPANSION WORK RECOVERY

As discussed in Chapter 3, two possible uses of the expansion work recovered in the ejector are:

1. To directly supplement compressor power by using the ejector pressure lift to directly increase compressor suction pressure.
2. To improve evaporator performance by using the ejector to pump or recirculate excess liquid through the evaporator.

This chapter presents the results of a numerical analysis comparing the performance of the standard ejector and ejector recirculation cycles, thus comparing the two uses of the ejector described above. The results of this chapter have been previously published in Lawrence and Elbel (2015). The analysis is performed with three different refrigerants (CO_2, R410A, and R134a) in order to demonstrate how different fluid properties affect the comparison of the two uses of ejector work recovery. Comparison is also made to a forced recirculation cycle in which a mechanical pump is used to overfeed the evaporator rather than an ejector. For reference, the three recirculation cycles of interest are shown in Figure 6.1.

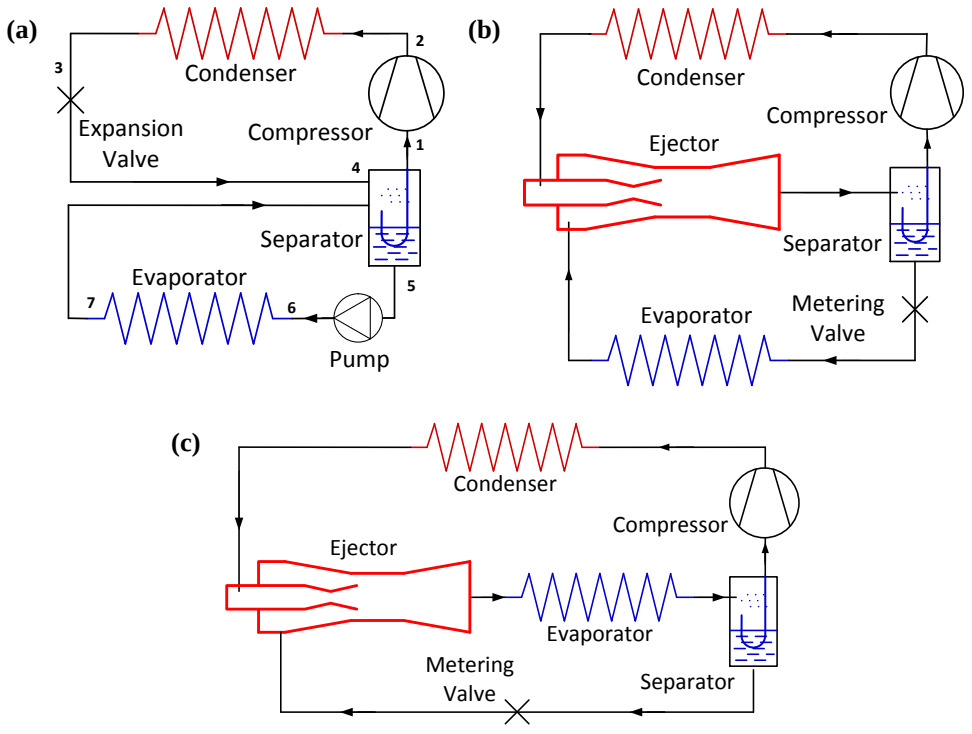

Figure 6.1: Cycle layout diagrams of (a) forced recirculation cycle, (b) standard two-phase ejector cycle, and (c) ejector recirculation cycle.

6.1 COP Improvement by Expansion Work Recovery

A two-phase ejector is an expansion work recovery device in that the energy released from the motive stream during expansion (converted from enthalpy to kinetic energy) can be transferred to the suction stream and ultimately used to reduce cycle work input. The expansion process can theoretically approach isentropic, rather than isenthalpic as in the conventional expansion valve (DX) cycle. The theoretical maximum amount of work than can be recovered (transferred to suction stream) by the ejector, often referred to as the throttling loss of the cycle, is a function of the fluid and the operating conditions.

A basic thermodynamic model was used to calculate the COP improvement that can be achieved with each fluid (CO_2, R410A, and R134a) through expansion work recovery with an ejector. The capacity of the cycle was 2.0 kW for all cases. The condensing temperature was set to 45°C and subcooling was set to 5 K for the R410A and R134a cases. For CO_2, it was assumed that the gas cooler pressure was 10 MPa, and the gas cooler refrigerant outlet temperature was 40°C. An internal heat exchanger (IHX) was not included in the CO_2 cycles in order to simplify the comparison of the different cycles for the three different refrigerants; as mentioned below, the inclusion of an IHX in the CO_2 cycles would not be expected to change the relative comparisons between different recirculation cycles. The finite volume evaporator model described above was not used in this section. Instead, the evaporation temperature was fixed at 10°C and the evaporator outlet was saturated vapor. Constant compressor isentropic and mechanical efficiencies of 70 and 80 %, respectively, were assumed.

The ejector was simulated with the model of Kornhauser (1990), as described in Section 4.2. The isentropic efficiency of each of the components and the mixing section pressure were different for each fluid, as shown in Table 6.1. Lawrence and Elbel (2014b) noted that low pressure fluids have been seen to generally achieve lower work recovery efficiency, likely due to their greater sensitivity to frictional pressure loss in the ejector. Thus, the values of ejector parameters were adjusted in order to produce simulated ejector efficiency close to what has been observed experimentally with each fluid.

Table 6.1: Assumed ejector parameters used in the model of Kornhauser (1990) for different refrigerants; values were chosen in order to achieve overall ejector performance close to that observed experimentally.

Refrigerant	η_{mn}	η_{sn}	η_{diff}	$P_{sn,in} - P_{ms}$
CO_2	0.80	0.80	0.75	100 kPa
R410A	0.70	0.70	0.65	20 kPa
R134a	0.60	0.60	0.55	10 kPa

Table 6.2 compares the throttling loss and theoretical COP improvement obtainable with the standard ejector cycle (compared to a DX cycle at the same conditions) for the three refrigerants using thermodynamic state point analysis. The specific throttling loss is defined as the difference in specific enthalpy between isenthalpic and isentropic expansion processes between high-side and low-side pressures. Total throttling loss is the product of specific throttling loss and the mass flow rate required to produce the specified cooling capacity (2.0 kW). The total throttling loss is the measure of what can be recovered in the ejector and used to improve COP, not the specific throttling loss. The theoretical COP improvement offered by the standard ejector cycle using ejector efficiency parameters from Table 6.1 to model the ejector for each fluid is also shown. Higher ejector component efficiencies result in higher overall ejector efficiency and thus a greater portion of the available expansion work that is actually recovered and used to improve COP. Because the ejector and DX cycles have the same evaporation temperature and outlet state, the COP improvement shown in the table is a result only of using the work recovered to directly supplement compressor power; no improvement in evaporator performance or benefit from using the ejector for liquid recirculation is reflected in these results.

Table 6.2: Comparison of throttling loss and realistic standard ejector cycle COP improvement obtainable with different refrigerants at 2.0 kW cooling capacity.

Refrigerant	Specific Throttling Loss (kJ kg^{-1})	Mass Flow Rate (g s^{-1})	Total Throttling Loss (kW)	Standard Ejector Cycle COP Improvement (%)
CO_2	11.44	18.2	0.208	20.8 (no IHX)
R410A	5.04	13.5	0.068	5.9
R134a	3.51	14.3	0.050	2.3

It can be seen from Table 6.2 that while all three fluids have relatively similar mass flow rates, the properties of CO_2 result in significantly higher specific and total throttling loss for this fluid compared to the other two fluids, particularly at the elevated ambient temperature (condenser/gas cooler outlet temperature) used for these calculations. R134a is seen to have only slightly lower throttling loss than R410A. While greater throttling loss generally results in lower DX cycle COP, it also means greater opportunity for improvement when using an expansion work recovery device such as an ejector. It can be seen that CO_2 provides the greatest potential for COP improvement of 20.8 % with the standard ejector cycle due to its very high throttling loss and higher ejector efficiency compared to R410A and R134a, which is why CO_2 is the most commonly used fluid in two-phase ejector studies. The inclusion of an IHX in the CO_2 ejector and DX cycles would likely reduce the amount of COP improvement achieved by the ejector cycle, though CO_2 would still be expected to achieve significantly higher COP improvement than

the other two fluids. R134a has the lowest throttling loss and lower ejector efficiency, resulting in a COP improvement of only 2.3 % at the given conditions, while R410A achieves a COP improvement of 5.9 %.

6.2 COP Improvement by Liquid Recirculation

The above results have shown the improvement in COP that can be achieved using the expansion work recovered in the ejector solely to directly supplement compressor work. In order to determine the potential for COP improvement through liquid recirculation for each refrigerant, the numerical model of the microchannel evaporator can be used with a cycle model of the forced recirculation cycle to simulate performance. The forced recirculation cycle does not have an ejector and does not recover any expansion work, meaning that it cannot gain any benefit from directly supplementing compressor work; thus, the COP improvement of the forced recirculation cycle represents the COP improvement solely due to improving evaporator performance by means of liquid recirculation.

The same simulation conditions used in the previous section were also used in this section except that the finite volume evaporator model was used rather than fixing the evaporator temperature and outlet state. The evaporator air inlet state was set to be dry air at 27°C, and the evaporator air flow rate was set to 0.150 $m^3 s^{-1}$. The evaporator outlet state was set to 5 K of superheat in the DX cycle, while the outlet state varied with the amount of recirculation for the three recirculation cycles. Additionally, an isentropic efficiency for the pump of 45 %, also used by Stoecker (1998), was assumed for the forced recirculation cycle. A different choice of pump efficiency would not be expected to significantly affect the results, as pumping power was found to generally be negligible in the COP calculation. The highest pumping power was observed with CO_2 due to the larger refrigerant-side pressure drop with CO_2; pumping power reached a maximum of 1.0 % of compressor power for CO_2, which has a small but noticeable effect on COP.

The microchannel evaporator geometry used for the simulations in this section was the same as Evaporator A from Table 5.1 with the exception of the microchannel port hydraulic diameter. When choosing a microchannel evaporator for each of the refrigerants considered here, one would not choose the same refrigerant-side cross-sectional area for each refrigerant. In order to choose a reasonable refrigerant-side cross-sectional area for each refrigerant, an analysis was conducted with the evaporator model described here to determine the microchannel port hydraulic diameter which resulted in a 1 % decrease in DX cycle COP compared to an ideal cycle without pressure drop at matched evaporator capacity and logarithmic-mean temperature difference (LMTD). This was done in order to provide a comparison of the different refrigerants with a reasonable DX cycle mass flux for each refrigerant. Further details of this method can be found in Padilla Fuentes and Hrnjak (2012).

The resulting hydraulic diameter for each refrigerant and the corresponding refrigerant-side total and cross-sectional areas are shown in Table 6.3. The required mass flow rates of the refrigerants to achieve the specified cooling capacity are relatively similar, though CO_2 does require higher mass flow rate than the other two refrigerants due to its lower evaporator specific enthalpy difference, as seen in Table 6.2. CO_2 is seen to have the smallest hydraulic diameter. Because of the high operating pressure of CO_2, its COP is relatively insensitive to pressure drop in the evaporator; additionally, the high vapor density of CO_2 means that for a given mass flux, the velocity and resulting frictional pressure drop of CO_2 will be lower compared to other refrigerants. These effects combine to result in the smallest hydraulic diameter for CO_2. R134a has much lower vapor density, resulting in greater velocity and frictional pressure drop for a given mass flux, as well as lower operating pressure (greater effect of evaporator pressure drop on cycle COP); these result in a much larger hydraulic diameter for R134a. The vapor density and operating pressure of R410A are between those of CO_2 and R134a, resulting in an intermediate hydraulic diameter for R410A.

Table 6.3: Evaporator refrigerant-side dimensions for different refrigerants.

Refrigerant	Hydraulic Diameter (mm)	Refrigerant-side Surface Area (m^2)	Refrigerant-side Cross-sectional Area (mm^2)
CO_2	0.25	0.092	22.0
R410A	0.42	0.151	59.4
R134a	0.78	0.283	208.8

Figure 6.2 presents the performance of the forced recirculation cycle as a function of circulation number, Equation (2.5), for the three different refrigerants. Results are presented in terms of the COP Ratio, defined as the ratio of recirculation cycle COP to DX cycle COP and shown in Equation (6.1). The DX cycle operated with 5 K of superheat at the evaporator outlet. The COP improvement of the forced recirculation cycle is due only to the benefit of liquid recirculation (no ejector work recovery or benefit from directly supplementing compressor work) and thus demonstrates the COP improvement potential achievable through liquid recirculation with an ejector. The improvement due to liquid recirculation of these refrigerants would be different for a different evaporator design or different operating conditions, though the COP improvements calculated here seem to be reasonable for a microchannel evaporator.

$$COP\ Ratio = \frac{COP_{Cycle}}{COP_{DX}} \qquad (6.1)$$

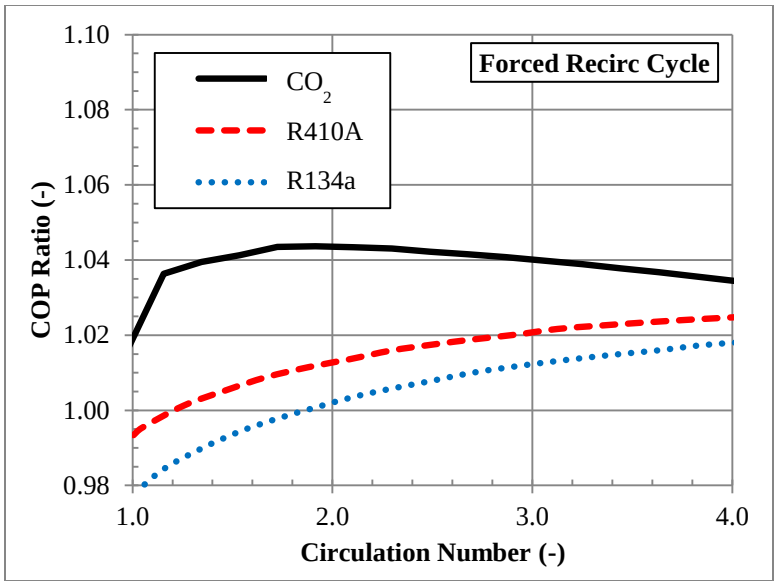

Figure 6.2: Potential for COP improvement using forced recirculation cycle for different refrigerants.

It can be seen from Figure 6.2 that R410A and R134a can both achieve upwards of 2 % COP improvement with liquid recirculation as circulation number increases to a value of 4. The COP of both fluids increases with increasing circulation number due to the increase of heat transfer coefficient with increasing mass flux. The pumping power and refrigerant pressure drop were both taken into account in the model for the forced recirculation cycle; however, the pumping power and pressure drop were generally negligible for R410A and R134a at the lower values of circulation number considered here. Note that the COP Ratio for both fluids would be expected to continue to increase beyond a circulation number of 4; the results in Figure 6.2 show the general behavior and relative magnitude of COP Ratio for R410A and R134a. The COP Ratio for both of these fluids would be expected to show a maximum at some higher value of circulation number once pressure drop and pump work become more significant.

The amount of COP improvement that can be achieved with liquid recirculation depends on the refrigerant mass flux and heat transfer coefficient of the baseline DX cycle that the liquid recirculation cycle is being compared to. A different evaporator geometry, particularly an evaporator with a different refrigerant-side cross-sectional area, would result in a different liquid recirculation COP improvement potential. Microchannel heat exchangers can potentially have higher baseline refrigerant-side heat transfer coefficient due to their small tube size; this would result in better baseline evaporator performance and less opportunity to improve COP with liquid recirculation. Other types of heat exchangers, such as a round-tube heat exchanger, may offer greater opportunity for COP improvement with liquid recirculation if the initial evaporator mass flux in the baseline cycle is relatively low. Additionally, DX cycles that

operate with a larger amount of superheat would also offer greater opportunity for improvement with liquid recirculation. This may help explain why a smaller COP improvement (approximately 2 %) was achieved with R410A and R134a in Figure 6.2.

Figure 6.2 also shows that R410A and R134a actually achieve COP Ratios less than unity at low values of circulation number. This effect is due to the low refrigerant mass fluxes and thus low heat transfer coefficients experienced by the forced recirculation cycle at low circulation numbers. Because the vapor generated during expansion is bypassed around the evaporator, refrigerant enters the evaporator very near a saturated liquid state in the forced recirculation cycle. This very low inlet quality results in larger specific enthalpy difference across the evaporator (at very low recirculation ratio when nearly all refrigerant is evaporated) and thus lower mass flow rate required to achieve the given cooling capacity. Lower mass flow rate will result in lower mass flux and lower refrigerant flow boiling heat transfer coefficient, and thus lower evaporator and cycle performance for the forced recirculation cycle compared to the DX cycle. At high enough circulation number, when evaporator mass flow rate is greater in the forced recirculation cycle than in the DX cycle, the forced recirculation cycle achieves a COP Ratio greater than unity. This means that when operating a cycle that bypasses vapor around the evaporator, the evaporator refrigerant-side geometry may need to be adjusted to ensure that the evaporator mass flux is not so low that it actually decreases evaporator performance and possibly COP compared to a DX cycle.

Note that the effect of poor refrigerant distribution was not accounted for in this analysis. Feeding a two-phase refrigerant into an evaporator may result in a significantly non-uniform distribution of a liquid among parallel tubes in the evaporator; this would result in poor utilization of evaporator heat transfer area and decreased evaporator performance. Using a cycle that bypasses the vapor generated during expansion around the evaporator can result in significantly improved evaporator performance, especially for microchannel evaporators (Elbel and Hrnjak, 2004b). As discussed above, the forced recirculation cycle is one such cycle which bypasses vapor around the evaporator. If the DX cycle were to suffer from poor refrigerant distribution in the evaporator, the forced recirculation cycle would likely improve COP at any circulation number.

As also seen in the figure, CO_2 shows different behavior compared to the other fluids, as it shows a maximum COP improvement of about 4.5 % near a circulation number of approximately 1.8. Unlike most common refrigerants, CO_2 achieves very high flow boiling heat transfer coefficient at low quality (due to its strong nucleate boiling compared to other refrigerants); the heat transfer coefficient of CO_2 may also be reduced at higher mass flux due to nucleate boiling suppression effects, meaning that there is less

opportunity to improve evaporator heat transfer by increasing mass flux when using CO_2. Park and Hrnjak (2007) presented the results of an experimental study in which they compared the flow boiling heat transfer behavior of CO_2 and R410A. They showed that the heat transfer coefficient of CO_2 decreased with increasing mass flux at low quality due to nucleate boiling suppression, whereas R410A heat transfer coefficient increased with increasing mass flux for all qualities. They also showed that the heat transfer coefficient of CO_2 generally did not increase significantly or even decreased as quality increased, whereas their results for R410A showed that heat transfer coefficient significantly increased with increasing quality. Unlike R410A and R134a, the pumping power for the forced recirculation cycle with CO_2 did have noticeable effect on COP (up to 1.0 % of compressor power). As a result, the COP of the CO_2 forced recirculation cycle peaks at lower circulation number and then decreases due to increased pressure drop, increased pumping power, and the effect of nucleate boiling suppression at higher circulation numbers.

6.3 Comparison of COP Improvement Mechanisms

As discussed at the beginning of this chapter, the work recovered in the ejector can be used to directly supplement compressor work (investigated in Section 6.1) or to improve evaporator performance through liquid recirculation (investigated in Section 6.2). From the results presented in the previous two sections, it can be seen that how the magnitudes of COP improvement from these two effects compare is different for the different refrigerants. CO_2 gains significantly greater benefit from direct compressor unloading than from liquid recirculation while R410A and R134a seem to gain similar improvements from direct compressor unloading and liquid recirculation.

It can be noted that the forced recirculation cycle can only gain benefit from liquid recirculation as this cycle does not have an ejector. Similarly, the ejector recirculation cycle, despite recovering expansion work with the ejector, can still only gain benefit from liquid recirculation, as the ejector is not able to directly lift the compressor suction pressure due to the layout of this cycle; the compressor suction pressure is set by the evaporation pressure, and the ejector can only improve the cycle by improving the evaporator performance and increasing evaporator pressure. On the other hand, in the standard ejector cycle, the ejector can actually be used to both directly increase compressor suction pressure through pressure lift and to provide liquid recirculation to the evaporator. Greater evaporator mass flow rate means greater liquid recirculation benefit and higher evaporator pressure but also less ejector pressure lift due to the greater amount of mass that the ejector must pump. Thus, there are two competing effects in the standard ejector cycle as circulation number increases, and the trade-off between these two effects will ultimately result in an optimum circulation number for the standard ejector cycle.

Thus, the fundamental question to be answered by the numerical analysis of the ejector cycles is as follows: For a given fluid, how should the ejector be used; is it better to use the pressure lift of the ejector to directly increase compressor suction pressure or to use the ejector to recirculate liquid through the evaporator, which would indirectly increase compressor suction pressure by increasing evaporation pressure? Comparison of the COP improvement gained by the different fluids by means of liquid recirculation and by means of direct compressor unloading through ejector pressure lift (presented in the previous sections) can be used to gain an idea of which use of the ejector and thus which ejector cycle would be the best choice for each fluid. CO_2 gains far greater benefit from ejector pressure lift, which can only be provided by the standard ejector cycle, than from liquid recirculation; this means that the standard ejector cycle would be expected to offer far greater COP improvement potential for CO_2. However, for R410A and R134a, the two benefits seem to be of similar magnitude, so it is not entirely clear which use of the ejector and which cycle would offer greater COP improvement potential with these fluids. Numerical results will be presented in the following section to further investigate the performance of the recirculation cycles with the different fluids.

6.4 Comparison of Recirculation Cycle Performance

Figure 6.3 compares the performance of the three different recirculation cycles for CO_2. Performance is again reported in terms of COP Ratio, shown in Equation (6.1). It can be seen that the ejector recirculation cycle has lower COP than the forced recirculation cycle until a circulation number of nearly 4. This is due to the presence of vapor at the inlet of the evaporator created by the expansion of the fluid through the ejector in the ejector recirculation cycle. As discussed above, CO_2 achieves very high heat transfer coefficient at low quality, meaning that the presence of vapor at the evaporator inlet reduces the CO_2 boiling heat transfer coefficient, resulting in lower ejector recirculation cycle performance. As circulation number increases, the ejector pumps more liquid back to the evaporator inlet, resulting in lower evaporator inlet quality and improved evaporator and cycle performance at higher circulation number. Despite the large amount of work that can be recovered with the CO_2 ejector, the ejector recirculation cycle can still only achieve approximately 3 % COP improvement. This is because no matter how much work the ejector provides to pump additional liquid through the evaporator, the ejector recirculation cycle is still limited by CO_2's low potential for COP improvement through liquid recirculation. On the other hand, if the work recovered by the CO_2 ejector were used for pressure increase rather than to provide recirculation effect, as is the case in the standard ejector cycle, then the COP improvement can reach as high as 25 % at a circulation number just greater than unity. As discussed above, the optimum circulation number of about 1.1 results from the trade-off between decreasing pressure lift and increasing evaporator pressure as circulation number increases.

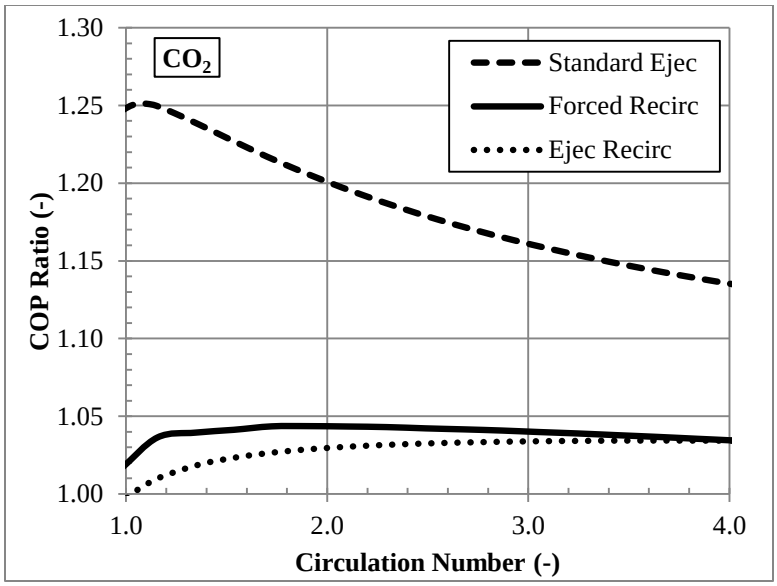

Figure 6.3: Comparison of standard ejector, ejector recirculation, and forced recirculation cycle performance using CO_2 as the refrigerant.

It can be concluded from these results that fluids that gain little benefit from recirculation compared to the benefit they gain from expansion work recovery, such as CO_2, should use the ejector to directly lift the compressor suction pressure. This conclusion would not be expected to change if an IHX were included in the CO_2 cycle; the use of an IHX would result in lower work available for recovery in the ejector but also lower liquid recirculation improvement potential due to lower evaporator inlet quality of the DX cycle and thus higher DX cycle heat transfer coefficient. The results for CO_2 also indicate that even for a fluid that gains significantly greater benefit from ejector pressure lift, it is still beneficial to operate with a slight amount of overfeed in order to at least eliminate the dryout region at the end of the evaporator; this agrees with the evaporator operation implemented in a recent CO_2 ejector supermarket refrigeration system installation described by Schönenberger *et al.* (2014) and Hafner *et al.* (2014).

Figure 6.4 compares the performance of the three different recirculation cycles for R410A. It can be seen that both of the ejector cycles achieve greater COP than the forced recirculation cycle over the range of circulation numbers. The standard ejector cycle gains the same liquid recirculation benefit as the forced recirculation cycle, but it gains additional benefit from the pressure lift provided by the ejector. It can be seen from the figure that as circulation number increases, the difference between the standard ejector cycle and forced recirculation cycle decreases, indicating that, as already known, the pressure lift of the ejector decreases with increasing circulation number. The standard ejector cycle does show a very slight maximum in COP near a circulation number of approximately 2.1, though for the given simulation

parameters, the COP seems to show very little sensitivity to circulation number for circulation number greater than about 1.5. As circulation number increases, the benefit of liquid recirculation increases while the benefit of ejector pressure lift decreases. In this particular case, the changes of these two effects seem to have equal and opposite magnitudes; the increase in evaporator pressure as circulation number increases is about the same as the decrease in ejector pressure lift, resulting in approximately the same compressor suction pressure and COP over a large range of circulation numbers. It should be noted that this trend of standard ejector cycle COP is not a general result for this cycle or fluid but is only true for the specific case presented here; higher or lower ejector efficiency or a different evaporator design would very likely yield a case for which the standard ejector cycle COP does show significant variation with circulation number.

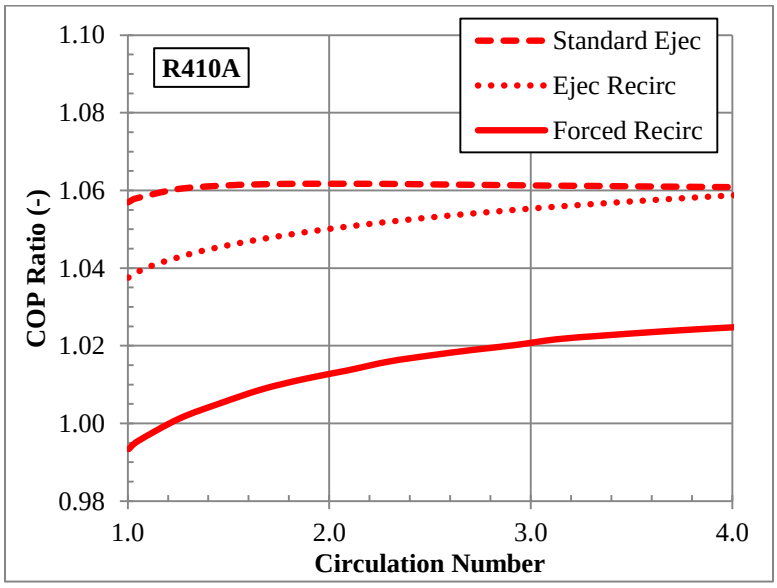

Figure 6.4: Comparison of standard ejector, ejector recirculation, and forced recirculation cycle performance using R410A as the refrigerant.

The ejector recirculation cycle with R410A still only gains benefit from the liquid recirculation effect provided by the ejector; it cannot use the ejector to directly increase compressor suction pressure. However, the presence of vapor at the inlet of the evaporator (higher evaporator inlet quality) in the ejector recirculation cycle results in increased velocity in the tube and increased flow boiling heat transfer coefficient (opposite behavior compared with CO_2). Increased heat transfer coefficient increases evaporation pressure and cycle COP above that of the forced recirculation cycle. Note that because of the presence of vapor and improved heat transfer at the evaporator inlet, the ejector recirculation cycle does not suffer a COP Ratio less than unity at very low circulation number. Note also that refrigerant

distribution was assumed to be uniform in the evaporator in the model. The presence of vapor in the evaporator inlet header may result in some amount of refrigerant maldistribution in the ejector recirculation cycle; this would likely decrease the performance of the evaporator and the cycle, though not below that of the DX cycle which can also suffer from maldistribution. From the results for R410A, it seems that the standard ejector cycle and ejector recirculation cycle can achieve approximately the same COP improvement (about 6 % for the range of circulation numbers considered here), so it is not clear what the best use of the ejector or most favorable cycle choice would be for R410A.

Figure 6.5 compares the performance of the three recirculation cycles for R134a. It can be seen that the standard ejector cycle cannot achieve a circulation number greater than about 2.7. Beyond a circulation number of 2.7, the ejector is not able to provide enough pressure lift to overcome the pressure drop in the evaporator, which is a result of the low work recovery of the R134a ejector. This means that in a realistic system with the given operating parameters, the standard ejector cycle would not be physically able to operate above the limiting circulation number, at least not at the given capacity. The ejector recirculation cycle, on the other hand, is able to provide enough pressure increase to overcome the pressure drop in the evaporator over the range of circulation numbers considered here. The ejector in the ejector recirculation cycle is more effective at entraining mass flow because it entrains fluid that is mostly liquid while the ejector in the standard ejector cycle entrains fluid that has much more vapor; compressing vapor requires significantly greater power than compressing the same mass flow rate of liquid because of the significantly greater specific enthalpy change for a given pressure difference of vapor. This is why the ejector recirculation cycle is able to operate over the entire range of recirculation ratios considered in this analysis while the standard ejector cycle cannot. As mentioned above for R410A, the ejector recirculation cycle gains additional benefit above the forced recirculation cycle due to the presence of vapor at the evaporator inlet, while the standard ejector cycle gains additional benefit above the forced recirculation cycle due to the pressure lift of the ejector.

It can be seen from Figure 6.5 that the ejector recirculation cycle with R134a can achieve COP improvement upwards of 7 % for the range of circulation numbers considered here. Note that based on the results presented in Table 6.2, R134a would only be expected to achieve 2.3 % COP improvement with the standard ejector cycle with a saturated evaporator outlet (benefit only from using ejector pressure increase). However, if an ejector cycle is used such that the evaporator gains liquid recirculation benefit, the COP improvement with an R134a ejector cycle can be significantly higher. Lawrence and Elbel (2014c) showed that a similar conclusion is reached when ammonia, which also has large liquid recirculation potential but low work recovery potential, is used as the working fluid in this analysis.

Notice that even for the standard ejector cycle, the COP continually increases with greater amount of recirculation until the limiting circulation number, meaning that with R134a the liquid recirculation benefit is always greater than the ejector pressure lift benefit. Thus, it can be concluded that fluids that gain significantly greater benefit from liquid recirculation than from expansion work recovery, such as R134a or ammonia, should use the work recovered by the ejector to provide liquid recirculation effect. This conclusion is important because it means that despite the large amount of information that is available in the open literature on applying ejectors to CO_2 systems, it may be best to apply an ejector in a different way when working with lower-pressure fluids.

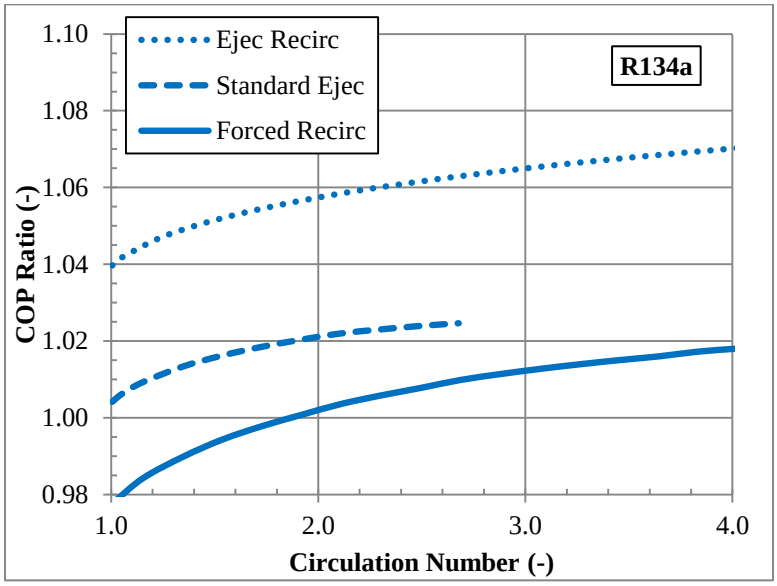

Figure 6.5: Comparison of standard ejector, ejector recirculation, and forced recirculation cycle performance using R134a as the refrigerant.

6.5 Effect of Reduced Ejector Efficiency

One potential challenge of using an ejector in a realistic application is finding an ejector design that can achieve sufficient efficiency to actually improve the COP of the cycle, especially for a system that operates over a range of conditions. The calculation of the COP of the two ejector cycles can be repeated for the case of lower ejector component efficiency and compared to the case of higher ejector component efficiency. For the case of lower ejector component efficiency, the motive nozzle, suction nozzle, and diffuser had efficiencies of 0.65, 0.65, and 0.60, respectively, and mixing section pressure was as shown in Table 6.1. The results comparing the COP of the R410A ejector cycles for the cases of higher and lower ejector component efficiency are shown in Figure 6.6. This case of lower ejector efficiency can represent an ejector that is not designed well, such that it achieves lower performance at all operating

conditions compared to the case of higher ejector efficiency presented above. Recall that the results for R410A showed that the standard ejector and ejector recirculation cycles could achieve approximately the same maximum COP for the range of circulation numbers considered; however, these results may change when the ejector is less efficient. The results in Figure 6.6 demonstrate how ejector efficiency affects the COP of the two different ejector cycles.

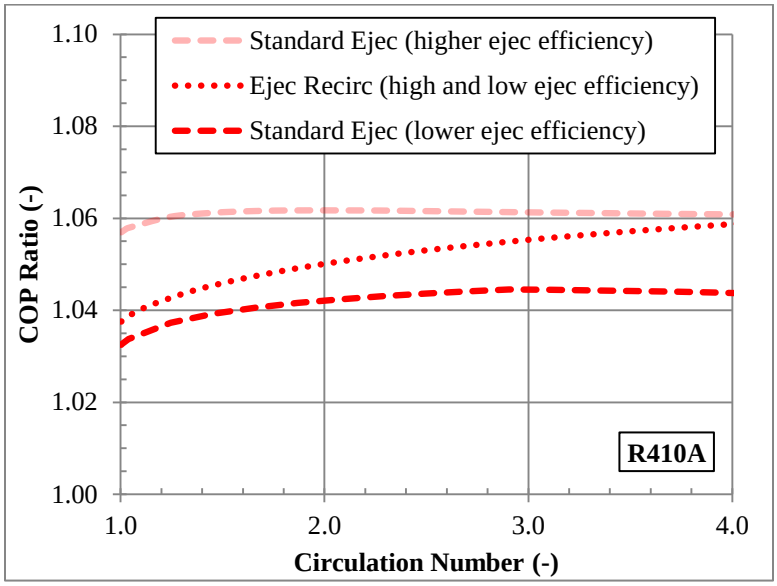

Figure 6.6: Comparison of the performance of ejector cycles for higher and lower ejector efficiency using R410A as the refrigerant.

It can be seen from Figure 6.6 that lower ejector efficiency noticeably reduces the COP of the standard ejector cycle such that it can only achieve up to 4.5 % COP improvement compared to about 6 % COP improvement at higher ejector efficiency. Even though the evaporator performance for a given amount of recirculation is not changed by lower ejector efficiency, as long as the ejector can still overcome the evaporator pressure drop, a less efficient ejector still results in lower pressure lift for a fixed amount of entrainment compared to a more efficient ejector. Thus, in the standard ejector cycle, a lower ejector pressure lift will directly result in lower compressor suction pressure and lower cycle COP, which explains why the standard ejector cycle is seen to have lower COP at lower ejector efficiency.

The standard ejector cycle with lower ejector efficiency shows a maximum in COP at a circulation number of approximately 3.0 (compared to an optimum circulation number of 2.1 for the case of higher ejector efficiency), meaning that a cycle with a less efficient ejector requires a greater amount of recirculation to optimize performance. A less efficient ejector with a lower pressure lift will make the

benefit of using the ejector to directly supplement compressor power less significant compared to the benefit of using the ejector for liquid recirculation; as a result, the maximum COP will be achieved at higher circulation number, where the benefit liquid of recirculation is greater.

Interestingly, the calculation results in Figure 6.6 show that the ejector recirculation cycle COP is completely unchanged by the reduced ejector efficiency (trend only shown once in Figure 6.6). This is because in the ejector recirculation cycle, the compressor suction pressure is determined by the evaporator outlet pressure, and the ejector is used to provide recirculation effect (which increases evaporation pressure) rather than directly lift the compressor suction pressure. The pressure lift of the ejector in this cycle is only used to overcome the pressure drop through the evaporator, and any additional pressure increase provided by the ejector is simply lost in the metering valve. For the same amount of entrainment, a more efficient ejector that provides higher pressure lift will only result in larger pressure drop across the metering valve, as it cannot be used to directly supplement compressor power in this cycle; the large pressure lift will have no effect on the evaporation or compressor suction pressures. Thus, as long as the efficiency of the ejector is high enough to overcome evaporator pressure drop, the performance of the ejector recirculation cycle does not depend on ejector pressure lift or efficiency, making the ejector recirculation cycle more suitable for lower expansion work recovery fluids (such as R410A or R134a) and off-design ejector operation than the standard ejector cycle.

Table 6.4 shows the results of a Second Law analysis of the two expansion processes in the ejector recirculation cycle for the cases of higher and lower ejector efficiency. The irreversibility (availability loss or destruction) of a component without work or heat transfer operating at steady-state is shown in Equation (6.2). This equation was used to calculate the irreversibility of the ejector and expansion valve for each case. Equation (6.3) shows the specific flow availability of a fluid neglecting kinetic, potential, and chemical contributions; subscript ‘o’ refers to the dead state. The dead state was defined as R410A at 25°C and 1 bar. Further information on availability analysis can be found in Moran *et al.* (2014).

$$\dot{\Phi}_{component} = \sum \dot{m}_{in}\phi_{in} - \sum \dot{m}_{out}\phi_{out} \qquad (6.2)$$

$$\phi_i = h_i - h_o - T_o(s_i - s_o) \qquad (6.3)$$

It can be seen from Table 6.4 for the given conditions (R410A at circulation number of 2.0) that when the ejector efficiency decreases, the irreversibility in the ejector ($\dot{\Phi}_{\mathrm{dest,ejec}}$) increases. It can also be seen that

when ejector efficiency decreases, the irreversibility in the expansion valve ($\dot{\Phi}_{dest,valve}$) decreases; this is because the required pressure drop across the expansion valve is lower as a result of the lower ejector pressure lift when ejector efficiency is lower. The increase of irreversibility in the ejector is equal to the decrease of irreversibility of the expansion valve, and the total irreversibility of the expansion processes ($\dot{\Phi}_{dest,exp}$) is the same regardless of how efficient the ejector is; this shows why the COP of the cycle is the same for the ejector recirculation cycle regardless of the losses in the ejector as long as the ejector can still provide the required amount of overfeed.

Table 6.4: Comparison of irreversibility (availability destruction) of the two expansion processes in the ejector recirculation cycle with R410A at *n* = 2.0 for both higher and lower ejector efficiency.

	Higher η_{ejec}	**Lower η_{ejec}**
COP (-)	3.75	3.75
$\dot{\Phi}_{dest,ejec}$ (kW)	0.0376	0.0422
$\dot{\Phi}_{dest,valve}$ (kW)	0.0283	0.0236
$\dot{\Phi}_{dest,exp}$ (kW)	0.0659	0.0659

In an extreme case where the ejector in the ejector recirculation cycle does not provide any overfeed (no entrainment), the ejector would essentially become an expansion valve and result in an isenthalpic expansion (as it is recovering zero expansion work), and the cycle would be the same as a DX cycle. Thus, even for an ejector that has an efficiency of zero and provides no entrainment, the capacity and COP of the ejector recirculation cycle would theoretically be the same as the DX cycle. On the other hand, the standard ejector cycle would result in zero capacity and COP if the ejector were to provide no entrainment. This again demonstrates that the ejector recirculation cycle may be more suitable for lower expansion work recovery fluids (such as R410A or R134a) and off-design ejector operation than the standard ejector cycle.

6.6 Chapter Summary and Conclusions

This chapter has used a numerical model to investigate two different uses of the expansion work recovered by an ejector in a vapor-compression system, namely directly supplementing compressor work by directly lifting compressor suction pressure and improving evaporator performance by liquid recirculation. The standard ejector cycle can use the ejector both ways (though there is a trade-off between the two benefits) while the ejector recirculation cycle can only use the ejector to improve the evaporator. The results have shown that a fluid with very large throttling loss (such as CO_2) should use

the ejector to directly supplement compressor power with the standard ejector cycle. Low-pressure fluids (such as R134a or ammonia) that do not achieve very large pressure lift with the ejector but can gain noticeable benefit from liquid recirculation should use the ejector for liquid recirculation. It has also been seen that the ejector recirculation cycle COP does not depend on ejector efficiency as long as the ejector can overcome the pressure drop in the evaporator. While the numbers presented in this chapter may change for a different type of heat exchanger, it is expected that the overall conclusions on how the recovered work is best used would still hold regardless of the evaporator that is used.

It can be concluded from the results of this chapter that despite the large amount of research that has been done on CO_2 ejector systems, applying ejectors to systems using low pressure refrigerants may require the ejector to be applied and used in the system in a very different way; what was learned from CO_2 ejector studies should not necessarily be directly applied to systems with low-pressure refrigerants. The ejector recirculation cycle has been seen to be more suitable for conditions in which ejector work recovery would not be very large (due to a low-throttling loss fluid being used or low ejector efficiency), which again would make this cycle a more favorable choice for systems with low-pressure refrigerants. Additionally, this cycle may offer the opportunity to use a simpler ejector design and a simplified cycle control strategy, both of which would make this cycle more suitable for smaller and less expensive applications. Further discussion and investigation of the control of ejector cycles will be presented in Chapter 8. The results of this chapter have compared the ejector cycles for only a single evaporator geometry; while the general conclusions of this chapter would still be expected to hold, it is important to investigate how evaporator geometry can affect ejector cycle performance, especially when using the ejector to recirculate liquid and improve evaporator performance. The effect of evaporator geometry and operation on ejector cycle performance will be the subject of the next chapter (Chapter 7).

CHAPTER 7: EFFECT OF EVAPORATOR DESIGN IN EJECTOR CYCLES

The previous section has demonstrated that for certain systems, particularly systems using low-pressure refrigerants that cannot achieve significant work recovery, it is beneficial to use the ejector to improve evaporator performance by overfeeding the evaporator. In this case, a critical factor affecting the improvement an ejector cycle can achieve in comparison to a baseline cycle is the geometry of the evaporator. This chapter will present experimental and numerical results, both with R410A, investigating the effect that evaporator geometry can have on ejector cycle COP and COP improvement. The numerical investigation will also be used to develop guidelines on the design and operation (meaning how much liquid to feed) of the evaporator in the two ejector cycles of interest.

7.1 Experimental Investigation of Ejector Cycles with R410A

This section presents experimental results comparing the performance of the standard ejector cycle and the ejector recirculation cycle. The comparison is performed with both Evaporator A and with Evaporator B in order to see the effect that refrigerant-side cross-sectional area can have on the performance of the cycles. Comparison is also made to a DX cycle. The results of this section have been previously published in Lawrence and Elbel (2016a).

7.1.1 Experimental Conditions

Description of the R410A experimental facility and details of the ejector design can be found in Chapter 5. Table 7.1 shows the system conditions that were used in this section. Evaporator air inlet temperature and flow rate were the same for all tests. Condenser air flow rate was the same for all tests, but condenser air inlet temperature was varied for some tests. The condenser outlet state (ejector inlet state) was approximately saturated liquid due to the presence of the receiver at the condenser outlet. The capacity was kept the same for all tests (1.0 kW) by adjusting compressor speed; this value of capacity was chosen to ensure that the compressor could achieve the desired capacity for all cycles and conditions. In order to investigate different amounts of evaporator overfeed, the evaporator flow rate (outlet state) was adjusted for different tests using the metering valve in each of the ejector cycles. The DX cycle was operated with 3 K of superheat at the evaporator outlet. The system was charged with enough refrigerant to ensure a reasonable liquid level in the liquid-vapor separator for all conditions; this ensured that only liquid would flow to the evaporator in the standard ejector cycle.

Table 7.1: Operating conditions used in R410A experiments.

Parameter	Unit	Value
$T_{evap,air,in}$	°C	27
$\dot{V}_{evap,air}$	$m^3 s^{-1}$	0.100
$T_{cond,air,in}$	°C	35, 39, 42
$\dot{V}_{cond,air}$	$m^3 s^{-1}$	0.200
$\dot{Q}_{evap}$	kW	1.0
$x_{cond,out}$	-	0.0
R	-	0.67 – 1.64
$\Delta T_{SH,DX}$	K	3

7.1.2 Comparison of Standard Ejector and Ejector Recirculation Cycles

The results comparing the performance of the two ejector cycles with Evaporator A are shown in Figure 7.1 with the evaporator outlet state for each point indicated (same capacity for each point). Performance is reported in terms of the COP Ratio, Equation (6.1); capacity was the same for each test. The amount of recirculation is measured with the Recirculation Ratio, Equation (2.3). It can be seen that the ejector recirculation cycle can achieve up to 16 % COP improvement, though COP of this cycle increases only slightly beyond a recirculation ratio of 1.1. As discussed previously, the improvement in COP obtained with the ejector recirculation cycle comes solely from improving the performance of the evaporator; the pressure lift of the ejector is only used to overcome pressure drop in the low-pressure circuit and cannot be used to directly lift compressor suction pressure. The performance of the evaporator in the ejector recirculation cycle is improved in comparison to that of the DX cycle because dryout is eliminated and mass flux is increased by the additional liquid being recirculated by the ejector. Theoretically, the ejector recirculation cycle should have the same performance as the DX cycle if the metering valve is closed (recirculation ratio of 1.0) and the evaporator is operated with the same superheat as the DX cycle. This case is shown in the figure where the ejector recirculation cycle has a recirculation ratio of 1.0 and an evaporator outlet superheat of 3.7 K; the COP is within 1 % of the DX cycle COP. Note that this comparison is only shown to demonstrate that the ejector recirculation cycle without any recirculation and the DX cycle are essentially the same; the ejector recirculation cycle would never be operated this way in a real application. If some amount of recirculation is used and the superheat at the end of the evaporator is eliminated, then the ejector recirculation can achieve significantly higher COP than the DX cycle.

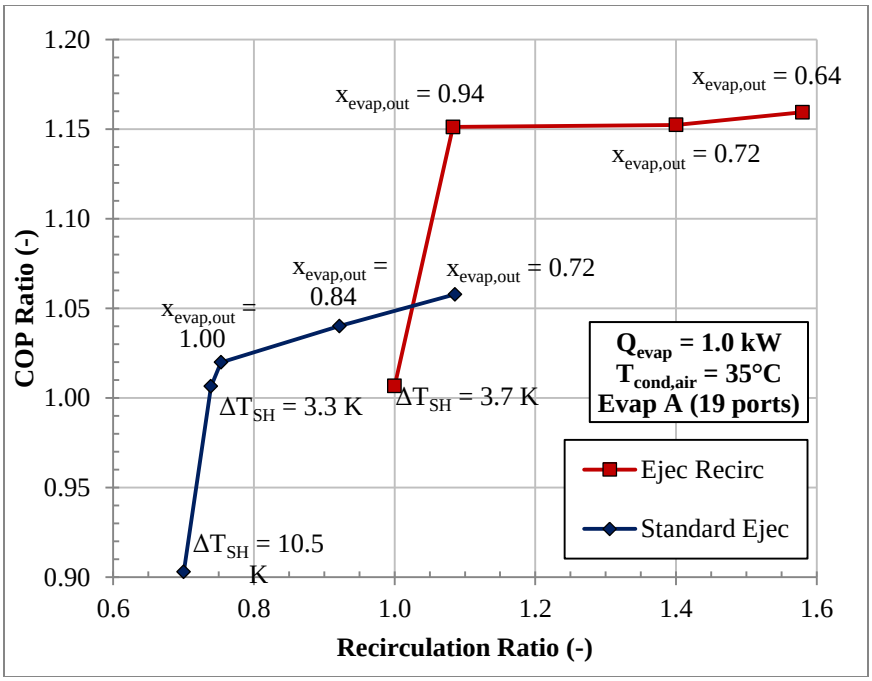

Figure 7.1: COP improvement obtained with standard ejector and ejector recirculation cycles as a function of recirculation ratio using Evaporator A.

Figure 7.1 also shows that the standard ejector cycle achieves noticeably lower COP despite being the more commonly considered of the two ejector cycles. If the standard ejector cycle is operated with 3 K superheat to match the evaporator outlet state of the DX cycle, it is only able to achieve about 1 % COP improvement over the DX cycle. On the other hand, if the ejector is used to recirculate excess liquid through the evaporator in addition to lifting compressor suction pressure, then the standard ejector cycle is able to achieve up to 6 % COP improvement at an evaporator outlet quality of 0.72. These results for both ejector cycles indicate that with Evaporator A, it is better to use the ejector to eliminate superheat and overfeed the evaporator rather than directly lift compressor suction pressure. Note that difficulty was encountered in obtaining readings at higher evaporator mass flow rates, as the mass flow meter upstream of the evaporator in the standard ejector cycle produced unstable readings at higher flow rates; as a result, data could not be obtained for higher recirculation ratios than shown in Figure 6.7. It would be expected that the COP of each ejector cycle reaches a maximum and then begins to decrease at higher recirculation ratio as refrigerant pressure drop becomes more significant.

Figure 7.2 shows the evaporation temperature for each of the data points with Evaporator A as well as the temperature lift of the ejector for the standard ejector cycle. Because capacity and air inlet temperature were the same for all tests, the evaporation temperature can be used as a measure of evaporator performance; higher evaporation temperature indicates higher overall heat transfer coefficient-area

product (UA) of the evaporator. The temperature lift of the ejector is the increase in temperature of saturated vapor at the given pressure between evaporator outlet and diffuser outlet pressures. The pressure lift of the ejector in the ejector recirculation cycle does not directly improve cycle performance because the compressor suction pressure is set by the evaporation pressure; thus, ejector temperature lift is not shown for the ejector recirculation cycle.

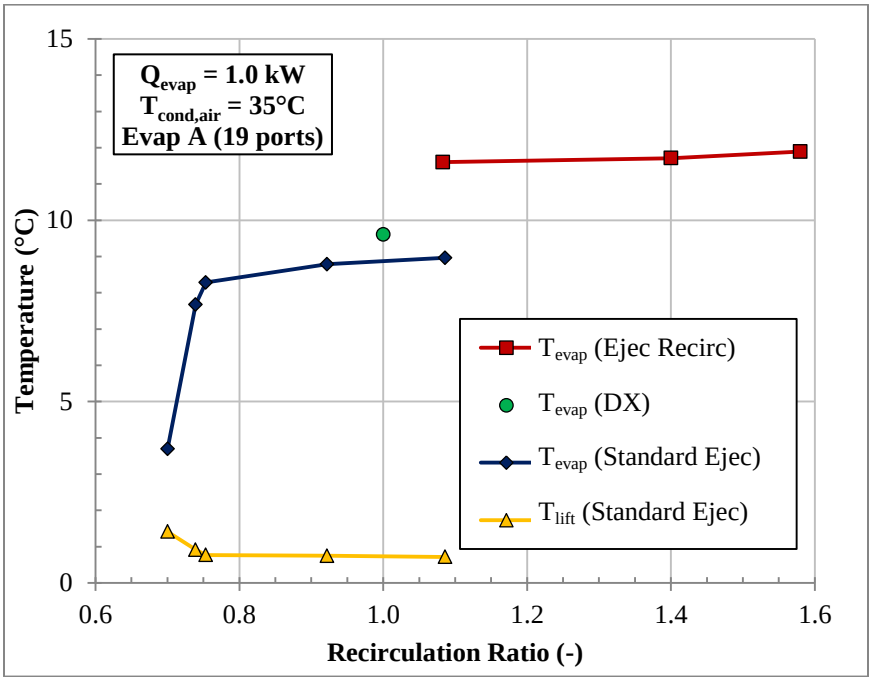

Figure 7.2: Evaporation temperature of ejector cycles and DX cycle and ejector temperature lift of standard ejector cycle as a function of recirculation ratio using Evaporator A.

It can be seen in Figure 7.2 that the evaporation temperature of the ejector recirculation cycle is more than 2 K higher than that of the DX cycle and at least 3 K higher than that of the standard ejector cycle, indicating significantly better evaporator performance in the ejector recirculation cycle. As mentioned above, the ejector recirculation cycle eliminates dryout and provides additional mass flow through the evaporator, both of which contribute to increased refrigerant-side heat transfer coefficient and increased evaporator UA compared to the DX cycle. Increasing recirculation ratio beyond 1.1 seems to only increase evaporation temperature slightly, which indicates that only small improvements in refrigerant-side heat transfer coefficient and evaporator UA are obtainable by further increasing the refrigerant mass flux through the evaporator with this cycle and evaporator; Stoecker (1998) also showed that evaporator UA increased very rapidly at first but then increased only very slightly once dryout was eliminated. It can be concluded that the majority of improvement from overfeeding this microchannel evaporator is from eliminating dryout.

It can also be seen from Figure 7.2 that the evaporation temperature of the standard ejector cycle is in fact noticeably lower than that of the DX cycle. In comparison to the DX cycle, the standard ejector cycle has lower mass flow rate through the evaporator and nearly all liquid at the evaporator inlet due to the vapor being bypassed around the evaporator. While this may improve refrigerant distribution in some heat exchangers, it also results in lower mass flux and lower average quality in the evaporator of the standard ejector cycle, both of which contribute to lower refrigerant-side heat transfer coefficient and lower evaporator UA. This explains why feeding liquid only in the standard ejector cycle can actually result in worse evaporator performance than the DX cycle even if refrigerant distribution can be improved. Note that even for a recirculation ratio of 1.0, for which the evaporator mass flow rate is about the same as that of the DX cycle, the standard ejector cycle still has lower evaporation temperature than the DX cycle; this again is likely due to the presence of vapor at the evaporator inlet in the DX cycle, which increases velocity and heat transfer coefficient throughout the evaporator in the DX cycle in comparison to the ejector cycle. The ejector recirculation cycle does not suffer from this effect because the vapor from the expansion in the ejector still passes through the evaporator. As mentioned in Chapter 2, Minetto *et al.* (2013) also observed significantly lower evaporator performance with the standard ejector cycle using CO_2 compared to a DX cycle and attributed it to an excessive amount oil in the evaporator of the standard ejector cycle. Note that oil would likely have a similar effect on the ejector recirculation cycle, meaning that the lower performance of the standard ejector cycle is not solely due to excessive oil in the evaporator. Note also that for a refrigerant with very strong nucleate boiling, such as CO_2, for which the flow boiling heat transfer coefficient is often higher at low quality especially at lower mass flux (Park and Hrnjak, 2007), the evaporator performance in this cycle would likely not be penalized due to the bypassing of flash vapor. The pressure drop was generally seen to be small (less than 2.0 kPa for most cases) and likely had a negligible effect on the performance of the evaporator and cycle.

Figure 7.3 plots flow boiling heat transfer coefficient of Chen (1966) for example cases of the ejector recirculation and standard ejector cycles. It can be seen from Figure 7.3 that the trend of heat transfer coefficient as a function of quality is similar for both cycles; the heat transfer coefficient is dominated by nucleate boiling at low quality and increases due to increasing convective contribution as more vapor is generated and velocity is greater at higher quality. However, the heat transfer coefficient throughout the evaporator in the standard ejector cycle is lower than in the ejector recirculation cycle for the same refrigerant quality due to lower mass flux (caused by bypassing flash vapor around the evaporator). Additionally, refrigerant enters the evaporator at lower quality in the standard ejector cycle, again resulting in lower heat transfer coefficient, as can be seen from the figure. See Appendix B for further information on the Chen (1966) correlation.

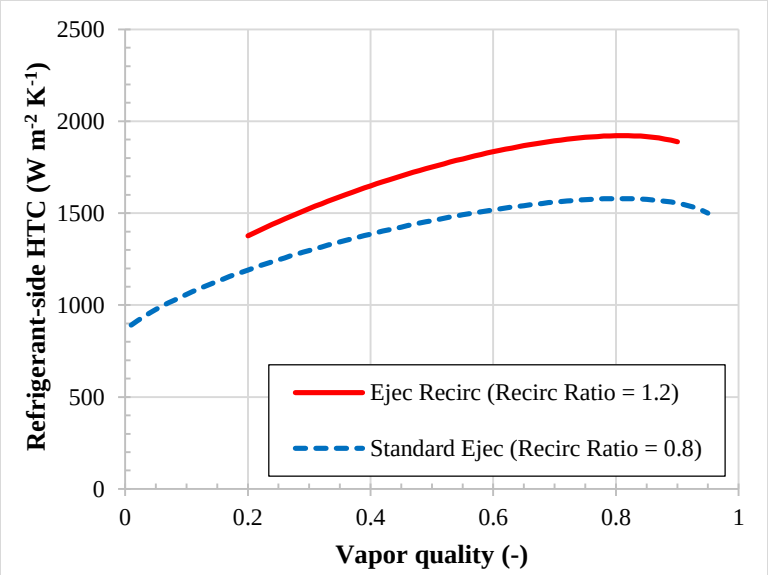

Figure 7.3: Flow boiling heat transfer coefficient from Chen (1966) correlation for example cases of standard ejector and ejector recirculation cycles using tube dimensions and conditions from experiment.

Figures 7.1 and 7.2 also show that unlike the ejector recirculation cycle, the evaporator performance and COP of the standard ejector cycle can depend significantly on recirculation ratio. The increase in evaporation temperature due to eliminating dryout by reducing superheat from 10.5 K to 0 K (recirculation ratios between 0.70 and 0.75) is 4.6 K, while the increase in evaporation temperature due to overfeeding the evaporator (recirculation ratios greater than 0.75) is only 0.7 K. This indicates the importance of always using the ejector cycle to eliminate evaporator dryout even if the ejector pressure lift is reduced slightly as dryout is being eliminated. Figure 7.2 also shows that the total improvement in evaporation temperature is significantly greater than the ejector temperature lift (maximum of 1.4 K lift), and the decrease in ejector temperature lift as recirculation ratio is increased is only 0.6 K, which is much smaller than the change in evaporation temperature over that range. It can also be noted that the temperature lift of the ejector does not change significantly after evaporator superheat has been eliminated (recirculation ratio greater than 0.75); at this point, the additional flow through the ejector is only in the form of more liquid. This means that very little is lost in terms of ejector pressure lift when the ejector is used to pump additional liquid and overfeed the evaporator, but a noticeable improvement in evaporator performance is gained. This again indicates that with R410A and this evaporator, it is better to use the ejector to circulate excess liquid through the evaporator rather than directly unload the compressor. Despite the lower evaporation temperature, the standard ejector cycle is still able to provide some improvement in COP due to the pressure lift of the ejector as well as the fact that the compressor draws saturated vapor from the separator in the ejector cycle, as opposed to superheated vapor in the DX cycle.

However, with improved evaporator performance, the COP improvements of the standard ejector cycle could still be better. This investigation of ejector cycles will be repeated in the Section 7.1.4 with a different evaporator.

7.1.3 Relation between Ejector Performance and Cycle Performance

The experimentally determined ejector performance of the standard ejector and ejector recirculation cycles for the cycle tests discussed in the previous section is shown in Figure 7.4. Ejector performance is measured with ejector pressure ratio, Equation (1.2), and work recovery efficiency, Equation (1.3), as functions of entrainment ratio, Equation (1.1). Recall that the entrainment ratio is equivalent to the recirculation ratio for the standard ejector cycle, while it is equal to recirculation ratio less one for the ejector recirculation cycle. The figure shows that the maximum observed ejector efficiency with the standard ejector cycle was 16.5 % at an entrainment ratio of 0.70, where ejector pressure lift is the largest and entrainment is the lowest; this value of ejector efficiency is similar to the 19 % ejector efficiency observed with an R410A ejector in the study of Pottker and Hrnjak (2015a). This point of highest ejector efficiency was also the point of lowest cycle COP, indicating that higher ejector efficiency does not necessarily mean higher COP; the highest COP with the standard ejector cycle was observed at a recirculation ratio of 1.09 where ejector efficiency was only 10.5 %.

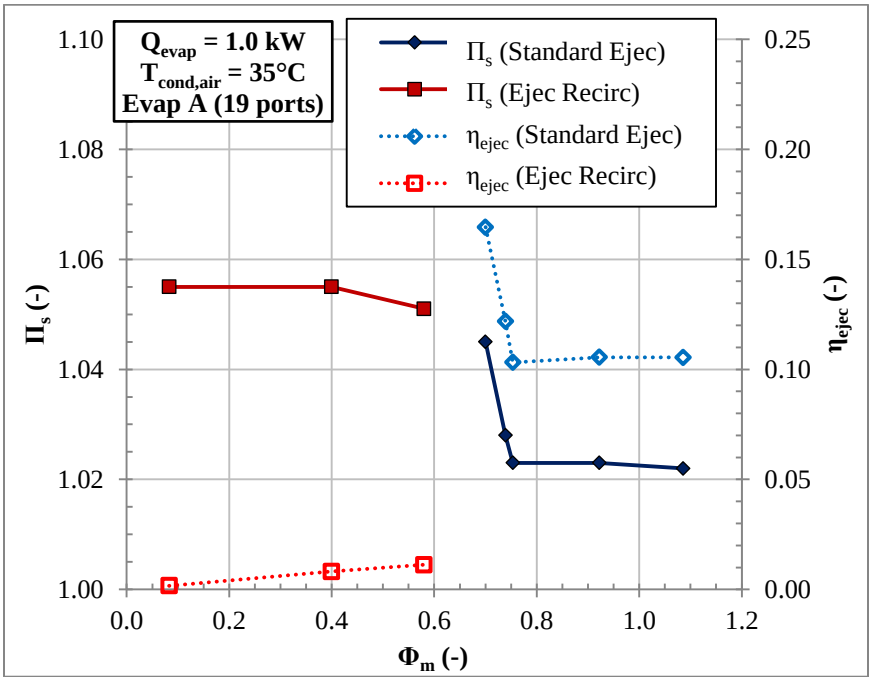

Figure 7.4: Comparison of ejector entrainment ratio, pressure ratio, and work recovery efficiency for the two ejector cycles.

Figure 7.4 also shows that despite the fact that much higher COP was obtained with the ejector recirculation cycle, the maximum observed ejector efficiency for this cycle was only 1.1 % at an entrainment ratio of 0.58. The reason for such low ejector efficiency with the ejector recirculation cycle is unclear. It should be noted that the work required to compress a mass of liquid is much less than the work required to compress the same mass of vapor, which may help explain why so little work is recovered when the ejector is used in the ejector recirculation cycle. It is also possible that greater shearing losses occur when using a high-speed motive stream to accelerate a mostly liquid suction stream compared to a mostly vapor stream. Figure 7.4 also shows that the pressure ratio of the ejector recirculation cycle is higher than that of the standard ejector cycle. However, as noted above, the compressor suction pressure in the ejector recirculation cycle is set by the evaporation pressure; the pressure lift of the ejector is only used to overcome the pressure drop in the evaporator and separator in this cycle, and any additional pressure lift is lost in the metering valve. Thus, the large pressure lift provided to the liquid in the ejector recirculation cycle does not provide any direct benefit to the cycle.

The results presented here indicate that how the work recovered in the ejector is used is just as important as how much expansion work is recovered in the ejector; it is important to recover sufficient work to operate each ejector cycle, but if the work is not used properly, the ejector cycle will provide little or no COP improvement. If too much of the recovered expansion work is used for directly supplementing compressor power (directly using the pressure lift) and not enough for overfeeding the evaporator (pumping extra liquid), as is the case in the standard ejector cycle at low recirculation ratio, then the performance of the evaporator can suffer, ultimately decreasing the overall performance of the cycle. It is better with this cycle and evaporator to use this work to increase mass flow rate through the evaporator even if the efficiency of the ejector decreases somewhat in this case. Greater work recovery would always be beneficial to the standard ejector cycle but only if the additional recovered work is properly distributed between providing additional evaporator overfeed and providing additional direct pressure lift. On the other hand, the ejector in the ejector recirculation cycle is operating with very low efficiency and recovering very little expansion work, but the cycle is using the recovered work in the best way possible, namely to improve the performance of the evaporator by overfeeding liquid.

As noted above, the same ejector geometry was used in both cycles. The geometry was chosen for the standard ejector cycle, though this is likely not the optimal geometry for the ejector recirculation cycle. However, the ejector pressure lift does not affect ejector recirculation cycle performance as long as it is sufficient to overcome pressure drop in the low-pressure circuit. A better liquid recirculation ejector would be able to overfeed a greater amount while still overcoming pressure drop in the low-pressure

circuit. However, as can be seen in Figure 7.2, the evaporation temperature does not increase significantly with increasing evaporator overfeed (ejector entrainment), meaning that only a small amount of ejector entrainment is necessary to obtain reasonable COP improvement with this cycle; a greater amount of overfeed would not offer a significant improvement in COP. Even though the ejector was not designed for use in the ejector recirculation cycle, it still can easily provide the entrainment required to achieve significant COP improvement. Thus, it is not likely that the non-optimal design or low efficiency of the ejector in the ejector recirculation cycle noticeably affects cycle performance. This agrees with the finding of Section 6.5, where the numerical results showed that the performance of the ejector recirculation cycle is independent of ejector efficiency. It can be concluded from this that the design of ejectors intended for liquid recirculation is not as critical as that of ejectors designed to lift pressure in the standard ejector cycle. This may help when designing ejector systems for applications with significant variation in operating conditions (ejector off-design conditions), as the performance of fixed geometry ejectors has been seen to decrease as operating conditions vary.

7.1.4 Effect of Evaporator Design on Ejector Cycle Comparison

The results of Section 7.1.2 have shown that an evaporator with too large refrigerant-side cross-sectional area and too low refrigerant mass flux can have a negative impact on the performance of the evaporator in the standard ejector cycle, limiting the opportunity to improve COP with this cycle; for the present case, the standard ejector cycle mass flux was less than 50 kg m^{-2} s^{-1} with Evaporator A for a saturated outlet. However, if a different evaporator that was not penalized as severely by reduced mass flux were used, it is possible that greater COP improvements could be achieved. Thus, the comparison of the ejector cycles was repeated with Evaporator B, which had 10 microchannel ports in each tube (same port size) rather than 19. Using Evaporator B results in approximately half the refrigerant-side cross-sectional and heat transfer area but double the evaporator mass flux for a given mass flow rate, which increases the refrigerant-side heat transfer coefficient. The COP Ratio obtained with the two ejector cycles with Evaporator B is shown in Figure 7.5 along with the previously presented Evaporator A results for comparison. It can be seen that with Evaporator B, the standard ejector cycle achieves up to 9 % COP improvement, meaning that, as intended, the evaporator with lower refrigerant-side cross-sectional area has improved standard ejector cycle performance. Note again that difficulty was encountered obtaining stable evaporator mass flow rate readings for higher values of recirculation number; a slight further increase in COP would be expected in this case if the evaporator were overfed in the standard ejector cycle. Interestingly, the ejector recirculation cycle achieves up to 13 % COP improvement with Evaporator B, meaning that an evaporator with lower refrigerant-side cross-sectional area hurts ejector recirculation cycle performance; this will be discussed further below.

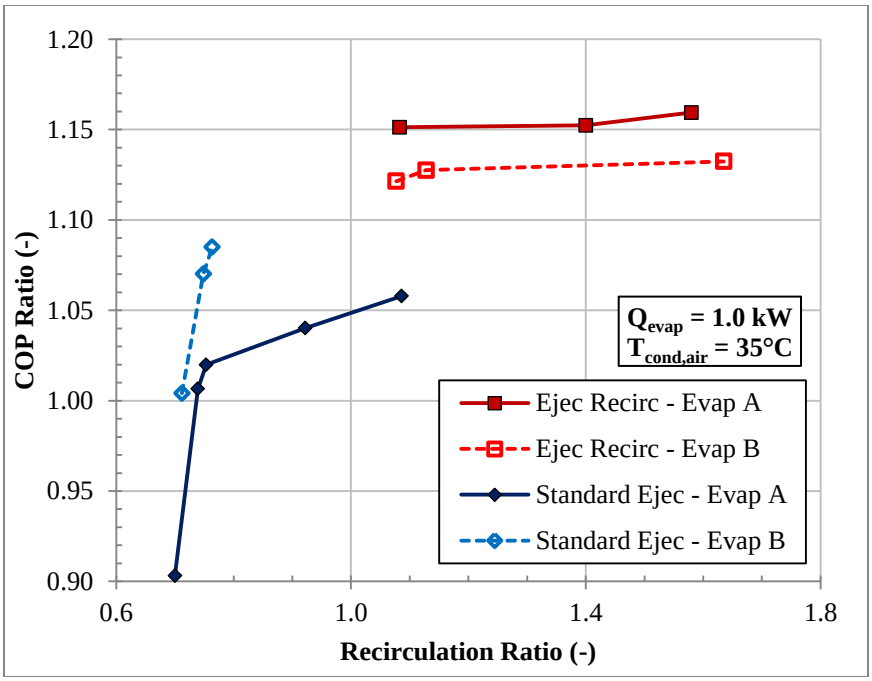

Figure 7.5: Comparison of performance of ejector cycles with different evaporators.

Figure 7.6 compares the performance of the evaporators, measured in terms of evaporation temperature, for the two ejector cycles and DX cycle. The figure shows that Evaporator B results in slightly lower DX cycle evaporation temperature (9.6°C with Evaporator A compared to 8.7°C with Evaporator B). Evaporator B has lower refrigerant-side heat transfer area, which reduces evaporator UA, but also increased mass flux through the evaporator, which increases refrigerant-side heat transfer coefficient and evaporator UA. As a result of this trade-off, the DX cycle with Evaporator B has approximately 1 K lower evaporation temperature than with Evaporator A, meaning that the decrease in refrigerant-side heat transfer area outweighs the increase in refrigerant-side heat transfer coefficient when changing to Evaporator B. Figure 7.6 also shows that a similar observation can be made about the ejector recirculation cycle, as it also results in approximately 1 K lower evaporation temperature with Evaporator B because of the decrease in refrigerant-side heat transfer area. Unlike the ejector recirculation and DX cycles, the standard ejector cycle actually achieves approximately 2 K higher evaporation temperature for a saturated vapor outlet with Evaporator B compared to Evaporator A. Despite the lower refrigerant-side heat transfer area of Evaporator B, the evaporator UA is actually improved due to significantly improved refrigerant-side heat transfer coefficient at increased mass flux. The standard ejector cycle also has the opportunity to improve refrigerant distribution because of the very low quality fluid being fed into the evaporator. As can be seen in Figure 7.6, the standard ejector cycle with Evaporator B is able to achieve higher evaporation temperature than the DX cycle despite having lower evaporator mass flux, which may be

explained by improved refrigerant distribution. Pottker and Hrnjak (2015a) showed that improved distribution can be a significant contribution to COP improvement in the R410A standard ejector cycle, though this comparison would be very dependent on evaporator design.

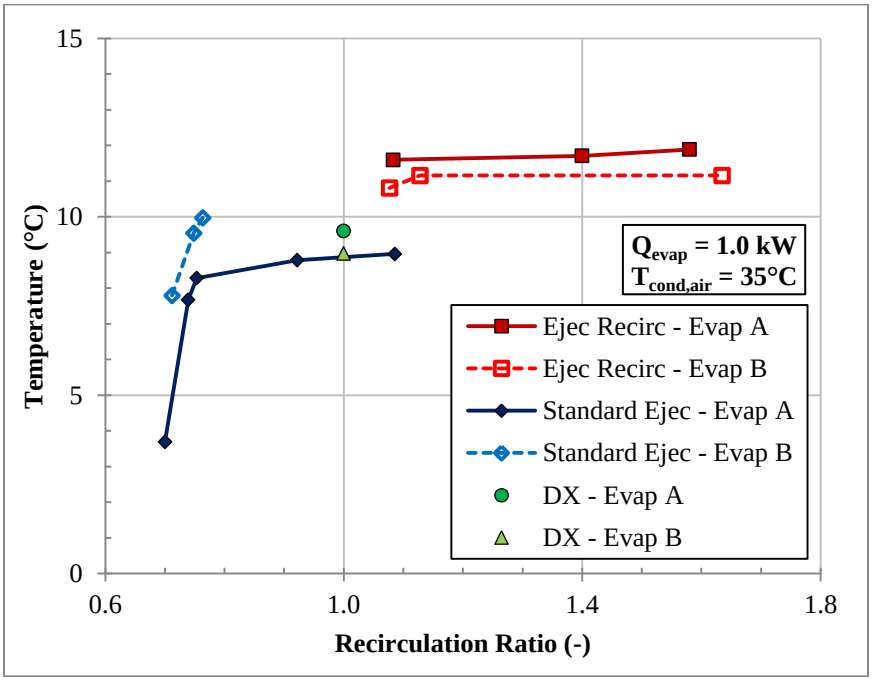

Figure 7.6: Comparison of evaporator performance (evaporation temperature) of ejector cycles and DX cycle with different evaporators.

Figure 7.7 presents numerical results showing how evaporator UA would be expected to vary as a function of refrigerant mass flux through microchannel tubes. The correlation of Chen (1966) was used to calculate refrigerant flow boiling heat transfer coefficient while the correlation of Park and Jacobi (2009) was used to calculate air-side heat transfer coefficient. The overall evaporator UA was obtained as shown in Equation (4.9) using the geometry of Evaporator A and assuming refrigerant quality of 0.5 for demonstration. As can be seen in the figure, evaporator UA increases with increasing mass flux, though the rate of increase is lower once mass flux is already sufficiently high (greater than approximately 50 – 100 kg m^{-2} s^{-1} for this example). This trend is caused by the fact that refrigerant heat transfer coefficient generally shows similar behavior with respect to mass flux. Additionally, because the majority of thermal resistance in the evaporator is due to convection on the air side, the increase in UA that can be achieved by improving refrigerant-side heat transfer coefficient is limited. This relation between evaporator UA and refrigerant mass flux means that if the DX and ejector recirculation cycle mass flux and heat transfer coefficient are already high with Evaporator A, there will not be as much opportunity to improve heat transfer coefficient by decreasing the refrigerant-side cross-sectional area and increasing mass flux with

Evaporator B. On the other hand, if the mass flux with Evaporator A is lower (less than 100 kg m^{-2} s^{-1} as is common in non-overfed microchannel heat exchangers), which is the case with the standard ejector cycle, there will be much greater opportunity to improve heat transfer coefficient by increasing mass flux. This explains why the standard ejector cycle can actually achieve better evaporator performance with Evaporator B than with Evaporator A despite the reduced refrigerant-side heat transfer area.

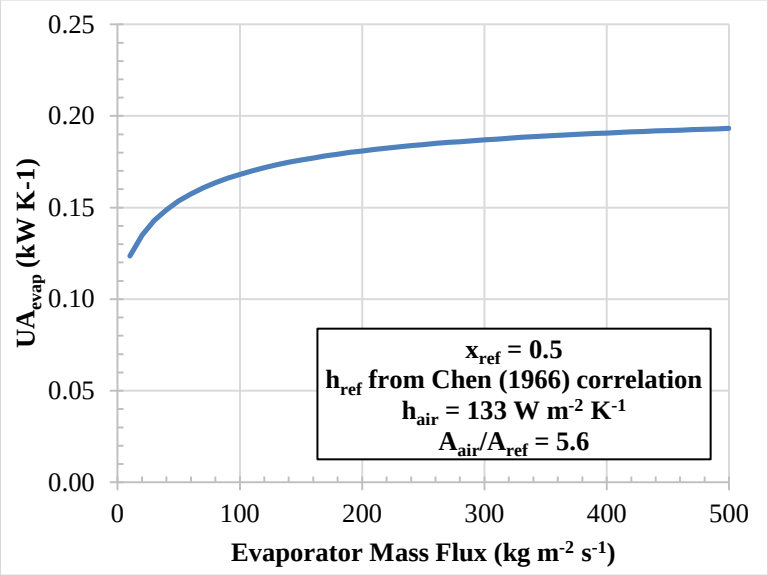

Figure 7.7: Variation of evaporator UA as a function of refrigerant-side mass flux through tube.

7.1.5 Effect of Ambient Temperature on Ejector Cycle Performance

The above results have shown that at the given conditions, it is better to use the ejector to recirculate liquid through the evaporator than to directly unload the compressor, as demonstrated by the ejector recirculation cycle having the highest COP and the improved performance of the standard ejector cycle when operated at higher recirculation ratios. However, if the operating conditions of the system were changed such that a larger amount of expansion work could be recovered by the ejector, this would allow for greater pressure lift and greater opportunity to directly supplement compressor power with the standard ejector cycle; in this case, it is possible that the standard ejector cycle could have higher COP than the ejector recirculation cycle. This can be accomplished experimentally by increasing ambient (condenser air inlet) temperature, resulting in higher condenser pressure and temperature and greater expansion work available to recover in the ejector. The experimental results for the COP Ratio of the two ejector cycles at three different ambient temperatures (35°C, 39°C, and 42°C) with Evaporator B are shown in Figure 7.8. The results for 35°C are the same as those presented in the previous section. The figure shows that at 39°C ambient temperature, the COP Ratio of the two ejector cycles is approximately

equal, as the standard ejector cycle achieves approximately 9 % COP improvement while the ejector recirculation cycle achieves approximately 10 % COP improvement. At 42°C ambient temperature, the standard ejector cycle can achieve higher COP than the ejector recirculation cycle; the standard ejector cycle achieves up to 11 % COP improvement while the ejector recirculation cycle achieves only 6 % COP improvement at this condition. It can also be seen from the figure that the COP improvement of the standard ejector cycle increases with increasing ambient temperature. Higher ambient temperature means greater expansion work recovery and greater opportunity to supplement compressor power with ejector pressure lift. This trend is commonly observed in ejector studies.

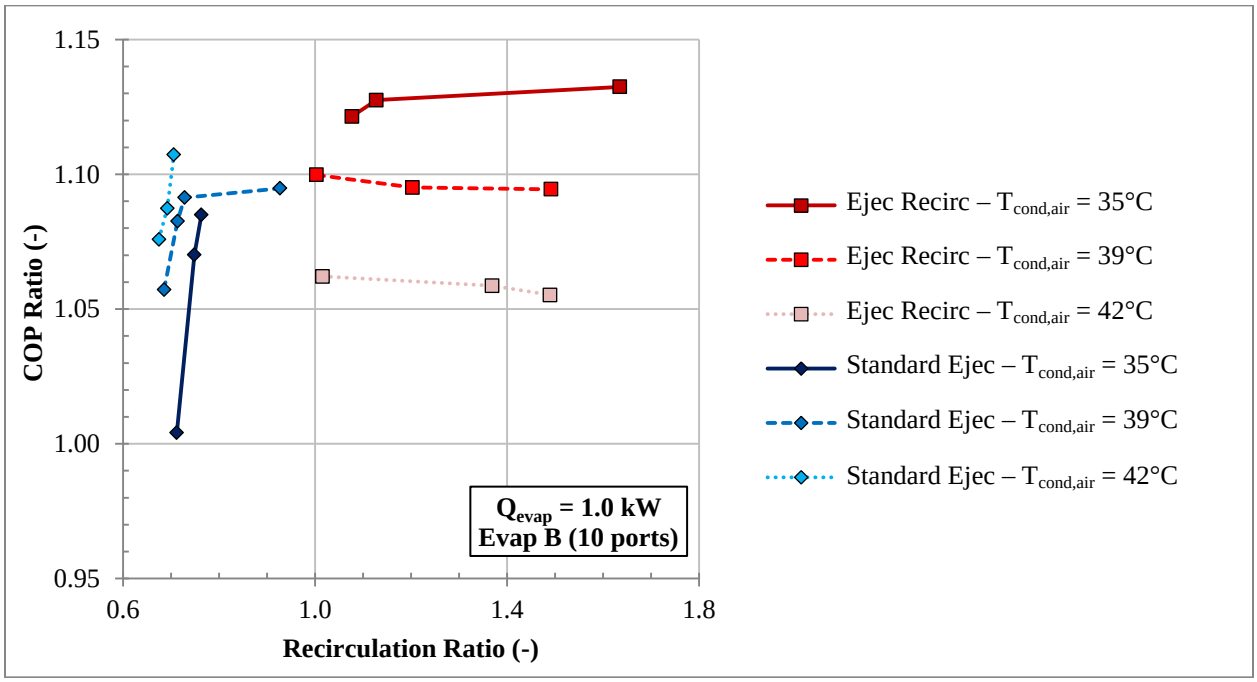

Figure 7.8: Comparison of ejector cycle performance at different ambient temperatures.

Interestingly, Figure 7.8 also shows that the COP improvement of the ejector recirculation cycle decreases as ambient temperature increases. As mentioned above, the ejector recirculation cycle uses the recovered expansion work to pump liquid through the evaporator but cannot use the ejector pressure lift to directly supplement compressor power. Thus, the ejector recirculation cycle can only use the additional expansion work to pump more liquid through the evaporator. However, it has been seen and discussed above that the COP of this cycle does not increase significantly once evaporator dryout is eliminated (beyond a recirculation ratio of approximately 1.1), meaning that pumping additional liquid does not necessarily provide improvement in COP for this cycle. This explains why, unlike the standard ejector cycle, the ejector recirculation cycle does not achieve greater COP improvement at higher ambient temperature.

Figure 7.9 compares the evaporation temperatures of the two ejector cycles and the ejector temperature lift of the standard ejector cycle at ambient temperatures of 35°C and 42°C. Theoretically, higher condenser pressure at higher ambient temperature should not affect the performance of the evaporator when capacity and evaporator air temperature and flow rate are fixed; this means that for the same cycle and evaporator conditions, the evaporation temperature should not change as ambient temperature is increased. Figure 7.9 shows that this is the case for the ejector recirculation cycle, as the evaporator temperature is approximately 11°C for all points at both 35°C and 42°C ambient temperatures. This means that the ejector recirculation cycle provides the same benefit to the evaporator (same increase in evaporation temperature) regardless of ambient temperature and work recovery. Figure 7.9 also shows that the standard ejector cycle does seem to achieve slightly higher evaporation temperature at higher ambient temperature. The reason for this is not clear, though this effect would ultimately have some effect on the comparison being presented. The greater ejector work recovery at higher ambient temperature can be seen through the higher ejector temperature lift at higher ambient temperature in Figure 7.9.

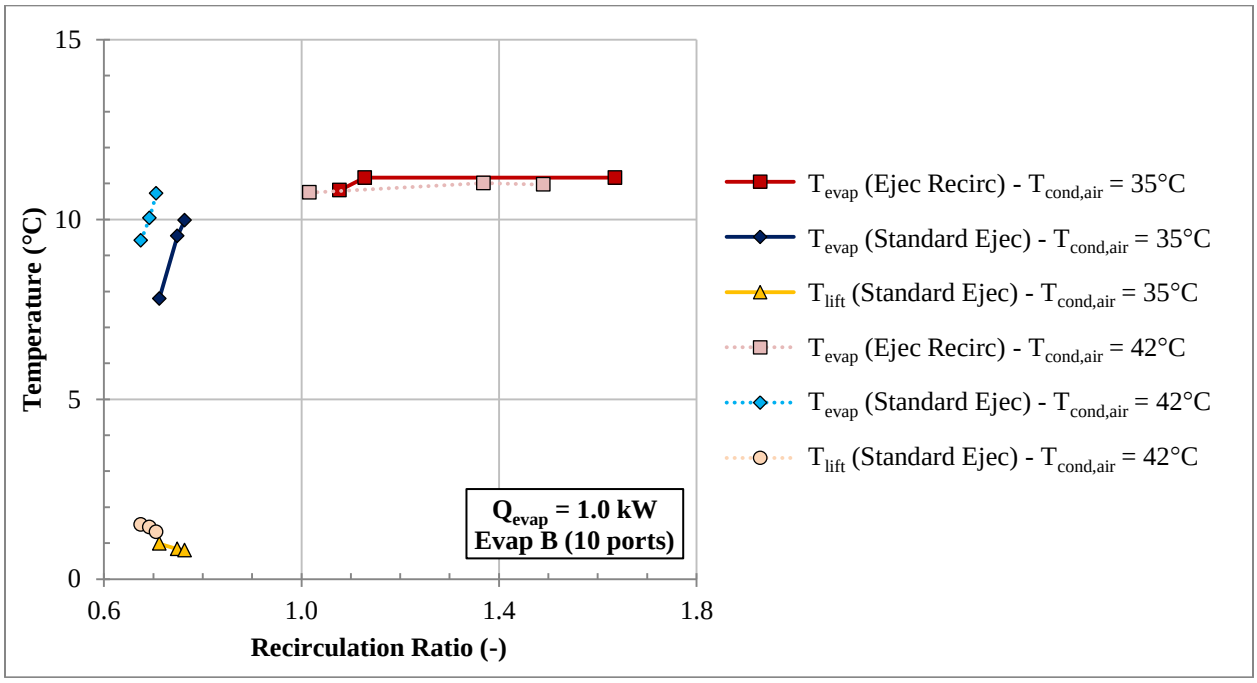

Figure 7.9: Evaporation temperature of ejector cycles and ejector temperature lift of standard ejector cycle at different ambient temperatures.

The above discussion shows why the ejector recirculation cycle does not offer greater COP improvement at higher ambient temperature. However, it may not be clear why the COP improvement of this cycle actually decreases as ambient temperature increases. The reason for this is that the same improvement in evaporator performance reduces compressor power by a smaller relative amount as ambient temperature

increases. To demonstrate this, the compressor power of the DX and ejector recirculation cycles is shown in Figure 7.10 for the different ambient temperatures. It can be seen from the figure that the absolute reduction in compressor power provided by the ejector recirculation cycle compared to the DX cycle is approximately the same for all ambient temperatures (approximately 30 W for 35°C and 39°C cases and slightly less for 42°C case); this is again due to the fact that the improvement in evaporator performance is the same regardless of ambient temperature. However, at higher ambient temperature, the compressor power required to achieve the higher condenser pressure is greater; this means that the same absolute reduction in compressor power offered by the ejector recirculation cycle results in less relative decrease of compressor power and thus less relative improvement in COP. This explains why the COP improvement of the ejector recirculation cycle decreases with increasing ambient temperature. Disawas and Wongwises (2004) also observed that COP improvement decreased with increasing ambient temperature with the standard ejector cycle when the cycle is operated with very large evaporator overfeed and very little direct compressor unloading. It can be concluded from these results that the ejector cycle that provides the highest COP depends on available work recovery (function of both external temperatures and working fluid) as well as evaporator design.

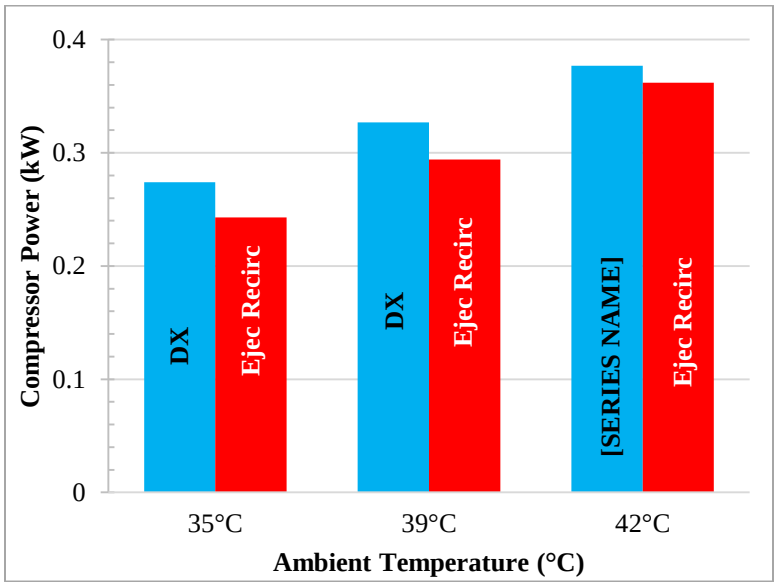

Figure 7.10: Compressor power of DX and ejector recirculation cycles for matched capacity at different ambient temperatures.

7.2 Numerical Investigation of Evaporator Design in Ejector Cycles with R410A

The previous section has shown experimentally that evaporator design can have a very significant effect on the performance of ejector cycles. This section aims to further the investigation of evaporator design in ejector cycles with numerical modeling. The effects of microchannel port hydraulic diameter, number of refrigerant-side passes, and evaporator liquid feeding rate are investigated, and guidelines for evaporator design and operation are presented and compared for the standard ejector and ejector recirculation cycles. The results of this section have been published previously in Lawrence and Elbel (2016c).

Details of the numerical model used in this section can be found in Chapter 4. The evaporator geometry was the same as Evaporator A used in the experimental investigation of Section 7.1 and presented in Table 5.1 except that the heat exchanger had 24 tubes and the microchannel port hydraulic diameter and the number of refrigerant-side passes were variable. R410A was the refrigerant. The capacity of the system was set to 1.0 kW for all cases. The condensing temperature was set to 45°C with 1 K of subcooling. Constant compressor isentropic and mechanical efficiencies of 70 and 80 %, respectively, were assumed. The evaporator air inlet state was set to be dry air at 27°C and 0.100 $m^3 s^{-1}$ flow rate. The efficiencies of the ejector motive nozzle, suction nozzle, and diffuser were assumed to be 0.60, 0.60, and 0.55, respectively, and the mixing pressure was assumed to be 20 kPa lower than the ejector suction pressure (corresponding to a 1 K drop in saturation pressure). The evaporator outlet superheat in the DX cycle was set to 3 K, while the evaporator outlet state was varied for different cases in the ejector cycles.

7.2.1 Effect of Microchannel Port Hydraulic Diameter

Figure 7.11 compares the COP Ratio of the standard ejector and DX cycles for varying microchannel port hydraulic diameter (same overall microchannel tube dimensions). In this section, the COP Ratio is defined as the COP at the point of interest divided by the maximum COP of the DX cycle. Figure 7.12 shows the UA of the evaporator and refrigerant-side pressure drop (ΔP) of the evaporator in the two cycles. Both refrigerant-side heat transfer coefficient and pressure drop increase as hydraulic diameter decreases due to a corresponding increase in mass flux. In comparison to the DX cycle, the ejector cycle has lower refrigerant mass flow rate and lower inlet quality to the evaporator due to the flash vapor being bypassed around the evaporator in the ejector cycle, resulting in lower mass flux and lower velocity throughout the evaporator of the ejector cycle. As a result, the ejector cycle has both lower refrigerant-side heat transfer coefficient (resulting in lower UA) and lower pressure drop compared to the DX cycle at a given hydraulic diameter. The net result is a lower evaporator outlet pressure (poorer overall evaporator performance) in the ejector cycle than in the DX cycle. This effect was also observed in the experimental results presented and discussed in the previous section. The standard ejector cycle is still

able to improve COP compared to the DX cycle due to the work recovery and pressure lift of the ejector. It can be seen from Figure 7.11 that there is an optimum microchannel port hydraulic diameter that results in maximum COP for each cycle due to the trade-off between increasing pressure drop and increasing UA as hydraulic diameter decreases (refrigerant mass flux increases).

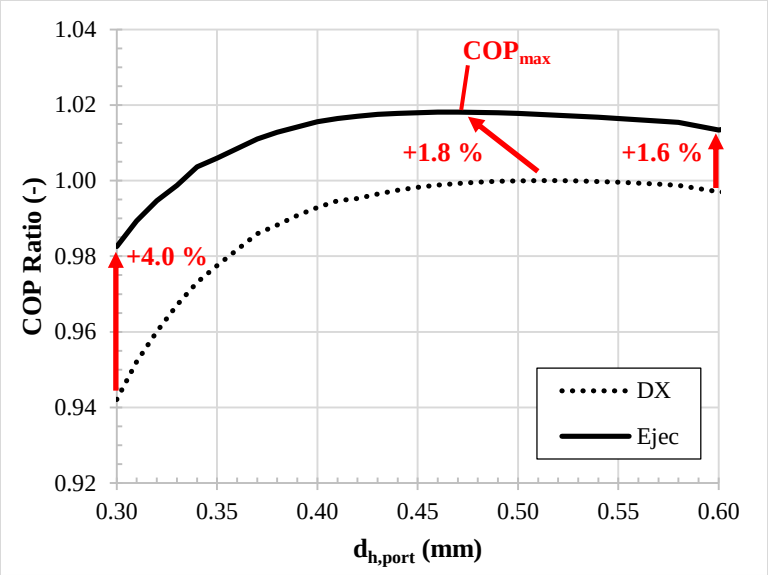

Figure 7.11: Comparison of standard ejector DX cycle COP with 3 K evaporator outlet superheat for both cycles; COP values are normalized by maximum DX cycle COP using R410A as the refrigerant.

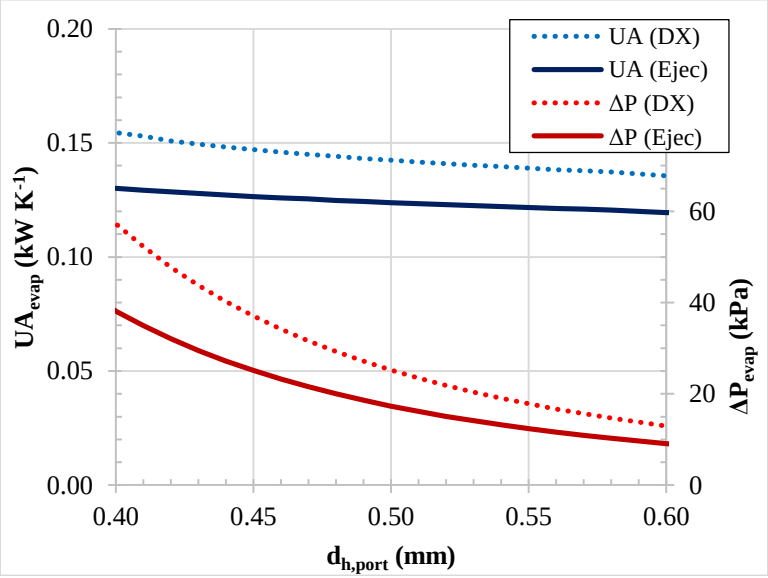

Figure 7.12: Comparison of standard ejector and DX cycle evaporator UA and refrigerant-side pressure drop with 3 K of superheat for both cycles using R410A as the refrigerant.

Figure 7.11 shows that the evaporator design that results in maximum COP for each cycle is not the same. The ejector cycle achieves its maximum COP at a hydraulic diameter of 0.47 mm with refrigerant-side mass flux (G_{ref}) equal to 64 kg m^{-2} s^{-1}; the DX cycle achieves its maximum COP at a hydraulic diameter of 0.51 mm (G_{ref} equals 72 kg m^{-2} s^{-1}). The DX cycle requires approximately 17 % greater refrigerant-side cross-sectional area to maximize COP than the ejector cycle. This is a considerable difference in optimal (COP-maximizing) evaporator design for these two cycles at the given conditions and indicates again that different cycles require different evaporator designs. The lower mass flow rate of the ejector cycle at a given hydraulic diameter means that the cycle is less sensitive to evaporator pressure drop and can tolerate a smaller hydraulic diameter in order to improve refrigerant-side heat transfer coefficient and evaporator UA. Additionally, Figure 7.11 shows that the amount of COP improvement obtained with an ejector cycle can be very dependent on the design of the evaporator. At the largest hydraulic diameter of 0.60 mm (where G_{ref} is 39 kg m^{-2} s^{-1} in the ejector cycle and 52 kg m^{-2} s^{-1} in the DX cycle), the ejector cycle only achieves 1.6 % higher COP than the DX cycle. At the smallest hydraulic diameter of 0.30 mm (where G_{ref} is 157 kg m^{-2} s^{-1} in the ejector cycle and 209 kg m^{-2} s^{-1} in the DX cycle), the ejector cycle achieves 4.0 % higher COP than the DX cycle. This is due to the vapor being bypassed around the evaporator in the ejector cycle, resulting in less sensitivity to pressure drop with the ejector cycle as mass flux increases. These results again show that evaporator design has a significant effect on not just the COP of the cycles but also the COP improvement of the ejector cycle compared to its baseline, as was also seen in the experimental results. Note also that the hydraulic diameter that maximizes ejector cycle COP is not that same as the hydraulic diameter that maximizes ejector cycle COP improvement.

The results presented in Figure 7.11 suggest that systems with smaller evaporators for the given capacity (resulting in greater refrigerant mass flux) would benefit more from implementing the standard ejector cycle. However, the objective should be to maximize ejector cycle COP, not to maximize COP improvement compared to a baseline cycle. Using a much smaller microchannel port size would result in greater COP improvement, as shown by the highest COP improvement (4.0 %) at the lowest hydraulic diameter (0.30 mm). However, greater COP improvement compared to the baseline at the given hydraulic diameter does not necessarily mean greater COP, as noted above. By increasing the hydraulic diameter to 0.47 mm (where G_{ref} equals 64 kg m^{-2} s^{-1}), the COP improvement offered by the ejector cycle decreases to 1.8 %, but the actual COP of the ejector cycle would increase by 3.6 %. Again, if one is free to design the evaporator in a system, it makes the most sense to maximize COP (and reduce system energy consumption), not to maximize COP improvement by comparing to a poorer baseline. The next section will focus on how to further improve evaporator design and performance in order to further increase ejector cycle COP.

7.2.2 Effect of Number of Passes and Evaporator Flow Rate

The above section has shown that changing refrigerant mass flux by adjusting hydraulic diameter can be used to maximize the COP of the standard ejector cycle. This section will investigate further improvement of the ejector cycle evaporator by increasing the number of refrigerant-side passes and by overfeeding the evaporator in order to increase refrigerant mass flux. Figure 7.13 shows four different evaporator configurations that were investigated, labeled as Evaporator A through D. Each evaporator configuration had a different number of refrigerant-side passes (one through four) and thus a different number of microchannel tubes per pass, as shown in the figure. All evaporators still had 24 total microchannel tubes, and all air-side dimensions were the same for all evaporators. The refrigerant was R410A.

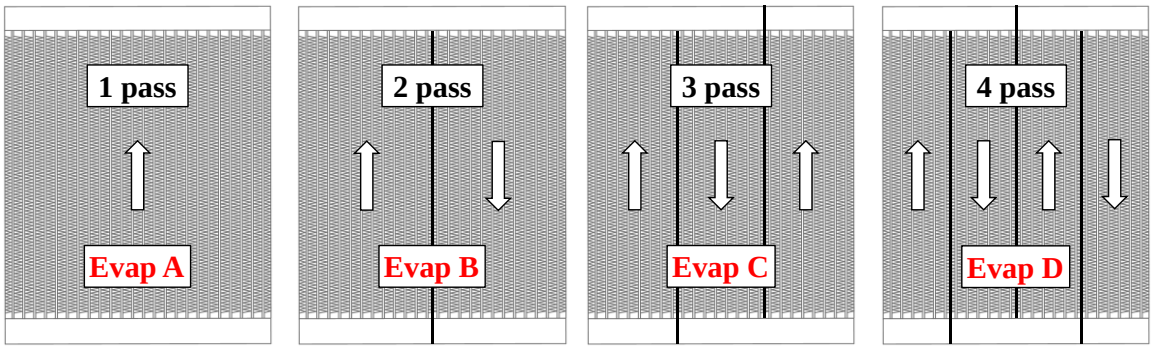

Figure 7.13: Configurations of Evaporator A (1 pass on refrigerant-side) through D (4 pass).

Figure 7.14 compares the relative COP of the standard ejector cycle as a function of circulation number for the four different evaporators, while Figure 7.15 shows the same for the ejector recirculation cycle. All the results shown in Figures 7.14 and 7.15 are for the optimum hydraulic diameter for the given evaporator configuration, circulation number, and system conditions, with the maximum possible hydraulic diameter assumed to be 0.98 mm due to the dimensions of the microchannel tube. All conditions were compared to the same baseline point (maximum DX cycle COP from Figure 7.11). It can be seen from Figure 7.14 that COP increases with increasing number of passes for the standard ejector cycle due to the increase of mass flux (increased heat transfer coefficient). As shown above, decreasing microchannel port hydraulic diameter can also be used to increase refrigerant mass flux and heat transfer coefficient (increases UA or effectiveness) in order to maximize COP. However, reducing hydraulic diameter also decreases refrigerant-side heat transfer area at the same time, which decreases UA or effectiveness, as can be seen in Equation (4.9). On the other hand, increasing the number of passes but keeping hydraulic diameter the same allows mass flux and heat transfer coefficient to be increased without decreasing refrigerant-side heat transfer area, offering the opportunity for greater improvement in COP. It can also be seen from Figure 7.14 that each evaporator has an optimum circulation number that

maximizes COP due to the trade-off between evaporator effectiveness, evaporator pressure drop, and ejector pressure lift. The standard ejector cycle can now achieve up to 9.5 % COP improvement if a larger number of refrigerant passes (4) is used and the hydraulic diameter and circulation number are optimized.

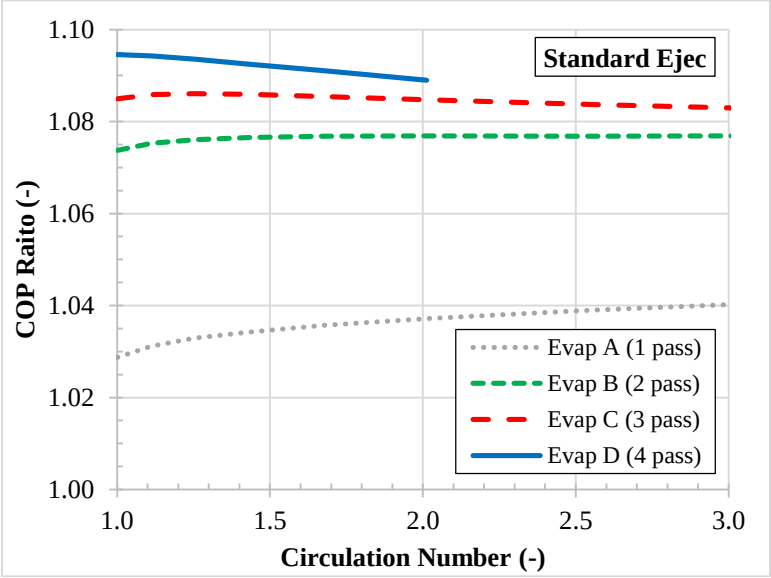

Figure 7.14: COP Ratio of standard ejector cycle as function of circulation number for different evaporator configurations (compared to DX cycle with Evaporator A).

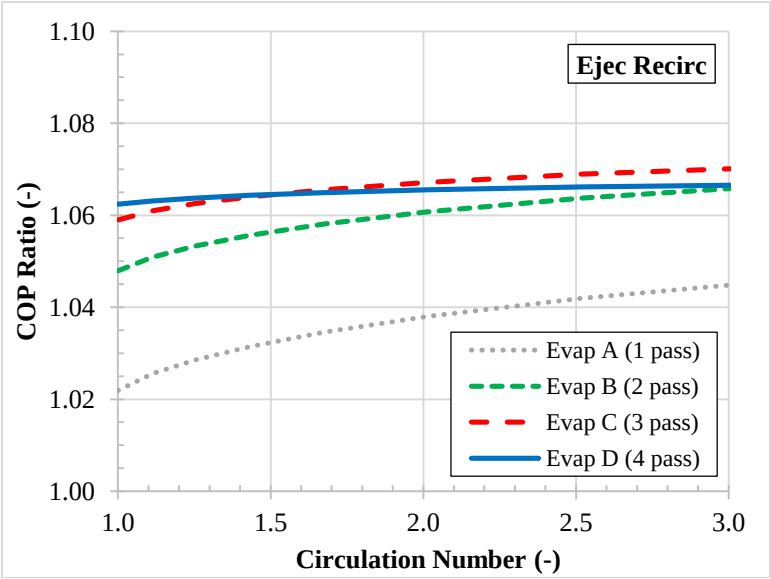

Figure 7.15: COP Ratio of ejector recirculation cycle as function of circulation number for different evaporator configurations (compared to DX cycle with Evaporator A).

Figure 7.15 shows that the ejector recirculation cycle COP increases with increasing circulation number for all evaporators. As mentioned above, increasing the mass flux through liquid overfeed will increase refrigerant heat transfer coefficient and evaporator UA or effectiveness, though refrigerant-side pressure drop will also increase at higher mass flux. At high enough circulation number, excessive pressure drop would eventually outweigh improved heat transfer performance, resulting in an eventual maximum in COP at some optimal circulation number. Interestingly, it is seen that unlike the standard ejector cycle, the highest COP, and thus the best evaporator performance, is obtained with Evaporator C (3 passes) and high circulation number (up to 7 % COP improvement for the range of circulation numbers considered here). The higher pressure drop obtained due to greater mass flux with Evaporator D outweighs the higher heat transfer coefficient, indicating that similar to optimizing circulation number, there is an optimum number of refrigerant-side passes that will maximize COP.

Figure 7.15 also shows that at low circulation number (less than 1.7), Evaporator D yields higher ejector recirculation cycle COP than Evaporator C. This means that if evaporator design (number of passes and tube diameter) were first optimized at low circulation number, and then evaporator operation (circulation number) were optimized for the chosen evaporator design, the maximum possible COP would not necessarily be achieved; the best evaporator design at circulation number less than 1.7 is Evaporator D, but the highest COP when for any evaporator design and any circulation number is achieved with Evaporator C. In order to achieve the highest obtainable COP, how the evaporator is designed and how the evaporator is operated must be considered simultaneously to find the optimal balance of refrigerant-side heat transfer coefficient and pressure and drop thus achieve the highest COP.

Comparing Figures 7.14 and 7.15 shows that with Evaporator A, the COP of both cycles increases with increasing circulation number; however, the ejector recirculation cycle achieves higher COP than the standard ejector cycle at high circulation number (above 2.5), while the standard ejector cycle achieves higher COP than the ejector recirculation cycle at lower circulation number. Since the circulation number can be freely set in a system, it would make sense to choose the ejector recirculation cycle and operate at high circulation number when using Evaporator A, which means that the ejector recirculation cycle is more favorable when using Evaporator A. On the other hand, the standard ejector cycle achieves higher COP than the ejector recirculation cycle when using any of the other evaporators. This shows that the standard ejector cycle can ultimately achieve higher COP than the ejector recirculation cycle if the evaporator design and circulation number are optimized for each cycle. However, if these important parameters of evaporator design and circulation number are not thoroughly investigated for the given system, one may not necessarily choose the most favorable ejector cycle, resulting in less benefit from use

of the ejector than could ideally be achieved. These results also show that the two ejector cycles have different optimal evaporator designs and also different optimal circulation numbers corresponding to their optimal evaporator designs. This will be discussed further in the following section.

Figure 7.16 shows the effectiveness of the different standard ejector cycle evaporator configurations, while Figure 7.17 shows the refrigerant-side pressure drop. As discussed above, the refrigerant-side heat transfer coefficient and evaporator effectiveness (or UA) increase with increasing circulation number due to increasing mass flux. A greater number of passes also increases mass flux and yields further improvement in evaporator effectiveness. Both of these effects are clear from Figure 7.16. Interestingly, Figure 7.17 shows that the pressure drop does not necessarily increase with increasing circulation number for all evaporators. At higher mass flux, as obtained with Evaporators C and D, pressure drop always increases with circulation number, but the pressure drop of Evaporator B shows a minimum while the pressure drop of Evaporator A decreases monotonically for increasing circulation number. This may be attributed a greater amount liquid and lower average quality throughout the tube as circulation number increases. Similar to the numerical results shown here, the experimental results of Section 7.1 (using the same evaporator) showed that overfeeding the evaporator in an ejector cycle to a moderate extent could noticeably improve heat transfer performance without noticeably increasing refrigerant-side pressure drop. Note again that maximum standard ejector cycle COP is achieved by properly balancing evaporator heat transfer performance, evaporator pressure drop, and ejector pressure lift.

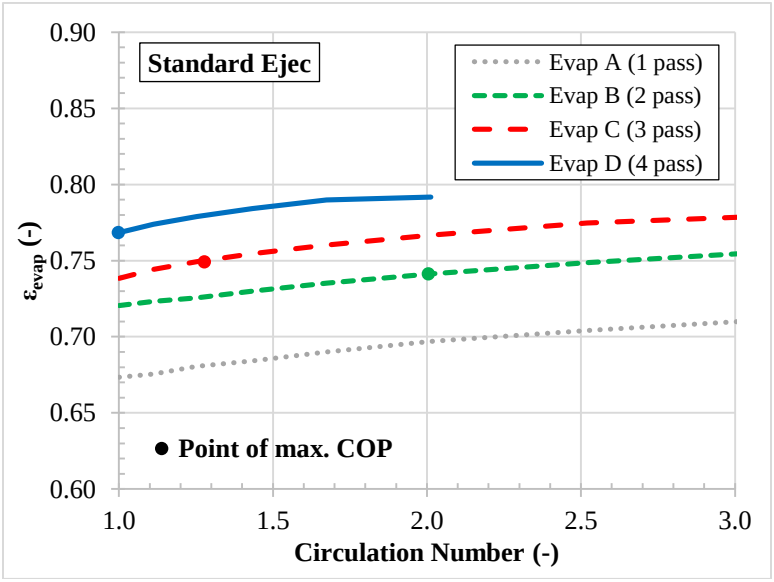

Figure 7.16: Evaporator effectiveness in standard ejector cycle as a function of circulation number for different evaporator configurations.

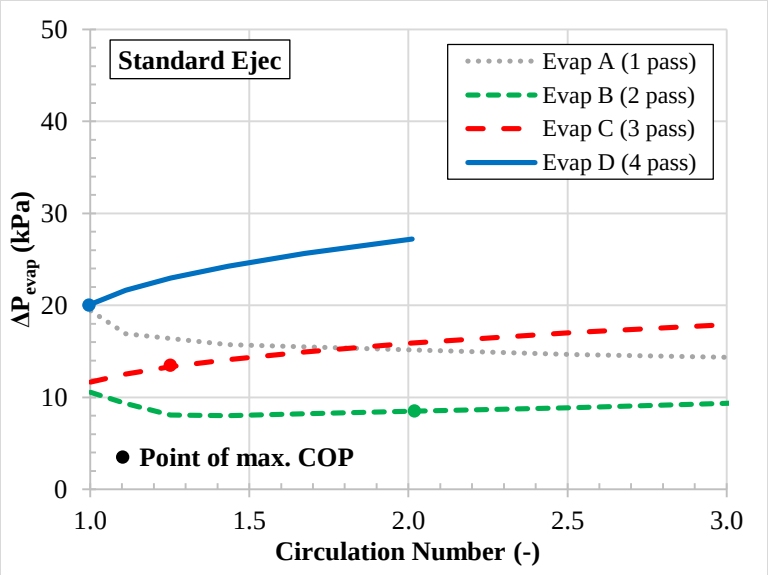

Figure 7.17: Evaporator refrigerant-side pressure drop in standard ejector cycle as a function of circulation number for different evaporator configurations.

It can also be seen from Figure 7.17 that Evaporator B has lower pressure drop than Evaporator A despite having noticeably better heat transfer performance. This is due to the fact that microchannel port hydraulic diameter is optimized for each point; Evaporator A must use much smaller hydraulic diameter compared to Evaporator B in order to improve heat transfer performance and maximize COP, but the smaller hydraulic diameter of Evaporator A also increases pressure drop. Evaporator B has double the flow rate through a given tube compared to Evaporator A and can achieve better heat transfer performance with a larger hydraulic diameter, allowing for a significant reduction in pressure drop. This again indicates that it is better to increase mass flux and improve evaporator heat transfer performance by increasing the number of refrigerant-side passes and overfeeding the evaporator than by reducing microchannel port hydraulic diameter. This also indicates how not properly optimizing evaporator design by using too few passes can drastically hurt evaporator and cycle performance.

Figure 7.18 shows the effectiveness of different ejector recirculation cycle evaporator configurations, while Figure 7.19 shows the refrigerant-side pressure drop. It can be seen that the trends are similar to those observed with the standard ejector cycle. Evaporator effectiveness increases with increasing circulation number and increasing number of refrigerant-side passes. Additionally, as also observed with the standard ejector cycle, the pressure drop shows a minimum with Evaporator B and continuously decreases with Evaporator A. Comparing the results for the standard ejector and ejector recirculation cycles shows that the ejector recirculation cycle generally achieves higher evaporator effectiveness; this is

due to the presence of vapor at the evaporator inlet in the ejector recirculation cycle, which increases velocity and refrigerant-side heat transfer coefficient throughout the evaporator, as discussed in relation to the experimental results in Section 7.1. The pressure drop is also higher in the ejector recirculation cycle (with the exception of Evaporator A), also due to the extra vapor.

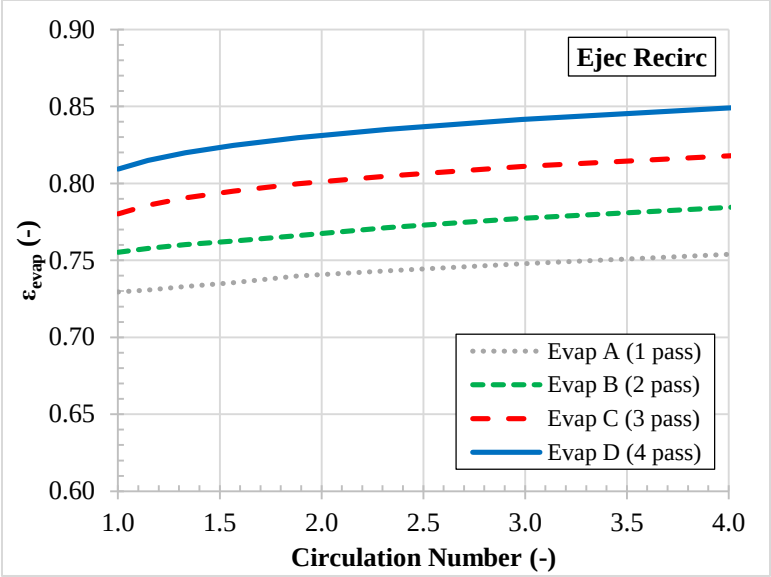

Figure 7.18: Evaporator effectiveness in ejector recirculation cycle as a function of circulation number for different evaporator configurations.

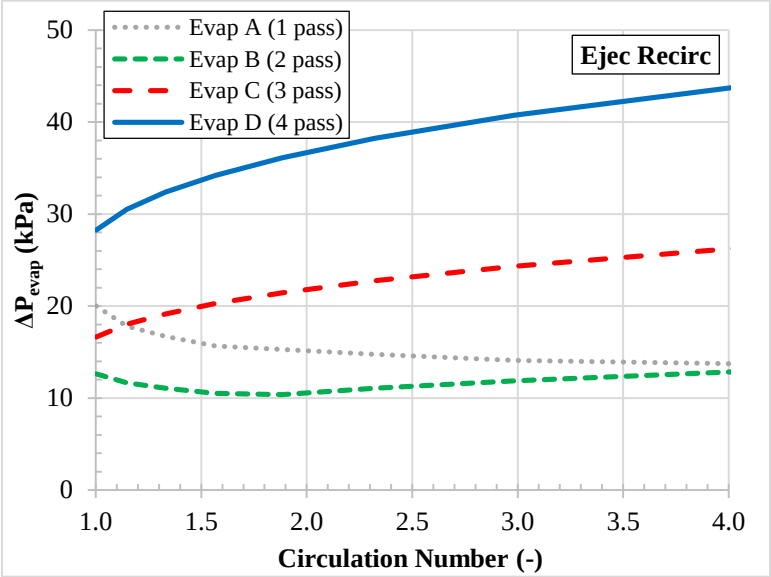

Figure 7.19: Evaporator refrigerant-side pressure drop in standard ejector cycle as a function of circulation number for different evaporator configurations.

Note that the numerical model did not account for the effect of refrigerant distribution among parallel microchannel tubes in a header; headers that have two-phase refrigerant entering them, such as inlet headers in DX and ejector recirculation cycles and any intermediate headers, may not achieve uniform distribution of liquid and vapor among all parallel tubes (Zou and Hrnjak, 2013), which would decrease the performance of the evaporator. The results presented in this paper do not investigate the effect of air-side dimensions on evaporator and cycle performance. Any change in dimensions that decreases air-side area or air-side heat transfer coefficient would clearly decrease COP for all cycles. More importantly, a decrease in air-side area or heat transfer coefficient will also increase air-side resistance, meaning that refrigerant-side changes would have less of an effect on overall evaporator and cycle performance; the opportunity to improve evaporator performance by optimizing (refrigerant-side) evaporator design or overfeeding is lower when the air-side performance is worse. This means that one cannot save on air-side area (lower cost heat exchanger) and expect to make up for it by improving the refrigerant side.

7.2.3 Guidelines for Ejector Cycle Evaporator Design and Operation

The numerical results in the previous section have shown specific evaporator dimensions and liquid feeding rates that optimize the performance of the ejector cycles for the specific system simulated in the model. However, these results are only necessarily applicable to the system considered in the previous section. It would be more useful if the results could be generalized in order to aid in the design and operation of any evaporator in any ejector system, as will be discussed in this section. Table 7.2 summarizes several evaporator performance parameters of the standard ejector and ejector recirculation cycles for the four different evaporator configurations at the point of maximum COP (or highest observed COP) for each case.

Table 7.2: Evaporator performance parameters of standard ejector and ejector recirculation cycles for four evaporator configurations at point of maximum (or highest observed) COP for each case.

	Standard Ejector Cycle				**Ejector Recirculation Cycle**		
	ε_{evap} (-)	**ΔP_{evap} (kPa)**	**G_{ref} (kg m^{-2} s^{-1})**	**$P_{lift,ejec}$ (kPa)**	**ε_{evap} (-)**	**ΔP_{evap} (kPa)**	**G_{ref} (kg m^{-2} s^{-1})**
Evap A	0.714	14.1	130.9	18.3	0.755	13.7	138.6
Evap B	0.741	8.5	59.6	26.1	0.785	12.9	127.8
Evap C	0.749	13.3	54.7	33.8	0.819	26.4	191.7
Evap D	0.768	20.1	58.4	37.2	0.850	43.9	255.6

It can be seen from Table 7.2 that the evaporator pressure drop at the optimal point for each evaporator configuration was in the range of 8 – 20 kPa for the standard ejector cycle and in the range of 14 – 44 kPa for the ejector recirculation cycle. The overall optimal point for the standard ejector cycle (Evaporator D) had a pressure drop of 20 kPa, while the overall optimal point for the ejector recirculation cycle (Evaporator C) had a similar pressure drop of 26 kPa; these pressure drops correspond to a drop in saturation temperature of approximately 0.6 – 0.7 K. This pressure drop at the optimal evaporator design and optimal circulation number is a consequence of the increased heat transfer coefficient-increased pressure drop trade-off that has been discussed above. Note that with the ejector recirculation cycle, the pressure drop of 44 kPa (1.2 K drop in saturation temperature) obtained with Evaporator D was seen to result in lower overall COP despite the higher effectiveness with this evaporator. Thus, it seems that there is a limiting pressure drop corresponding to at most a 1.0 K drop in saturation temperature (for R410A) that should not be exceeded when designing and operating an evaporator in an ejector cycle; theoretically, this 1.0 K limit could apply to all fluids, though it is not clear if this actually is the case.

Despite the similar pressure drop at the optimal points in the two ejector cycles, the cycles do have very different mass fluxes and circulation numbers at their optimal points. The performance of the standard ejector cycle is generally optimized when the mass flux through the given evaporator is in the range of 55 – 60 kg m^{-2} s^{-1} (for Evaporators B through D), while the performance of ejector recirculation cycle is optimized with a mass flux of 192 kg m^{-2} s^{-1} (Evaporator C). Furthermore, the optimal circulation number for the standard ejector cycle with Evaporator D was 1.0 (no overfeed), while the optimal circulation number for the ejector recirculation cycle was always at least 4.0 (very high overfeed) for each evaporator. This means that the way the ejector and evaporator should be operated is very different in the two different ejector cycles. It is not clear whether or not these optimal mass flux values would be applicable to other systems with microchannel heat exchangers as well.

As discussed in Chapter 6, the standard ejector cycle can use the work recovered in the ejector to either directly unload the compressor by lifting compressor suction pressure or to improve evaporator performance by liquid overfeed. Figure 7.14 demonstrates that each evaporator has a different optimum circulation number, corresponding to an optimum evaporator flow rate, that maximizes COP. This optimum is a result of the trade-off between improving evaporator performance and decreasing ejector pressure lift as circulation number increases. Increasing circulation number means more of the work recovered in the ejector is used to pump excess liquid through the evaporator and improve evaporator performance, but less work is available to lift the pressure of the vapor (which provides the capacity) and directly supplement compressor power. The highest observed COP with Evaporator D is achieved with a

circulation number of 1.0 (no overfeed). Thus, it seems most beneficial to use as much of the work as possible for pressure lift (direct compressor unloading) and use the design of the evaporator rather than overfeed to improve evaporator performance in the standard ejector cycle. Note that this is not the case in the ejector recirculation cycle. The ejector recirculation cycle can only use the ejector to pump excess liquid through the evaporator (not to directly supplement compressor power). Thus, it is beneficial to operate with a large amount of overfeed in the ejector recirculation cycle (in combination with an optimized evaporator design) to improve evaporator performance as much as possible.

Finally, the mass flux has been adjusted three different ways in the above results: Number of refrigerant-side passes; port hydraulic diameter; and circulation number. It is best to use the number of refrigerant-side passes to adjust the mass flux first and then use the circulation number in order to further control and achieve the desired mass flux; the number of refrigerant-side passes seems to have a greater effect on performance than circulation number. Comparing Evaporators C and D for the ejector recirculation cycle shows that too many passes results in too high mass flux and too high pressure drop, ultimately lowering cycle performance despite the higher effectiveness. However, comparing Evaporators A and B for each cycle shows that too few passes can severely hurt evaporator effectiveness; Evaporator B can achieve greater effectiveness than Evaporator A with a lower refrigerant-side pressure drop. There is an optimum number of passes to use for each cycle and condition. Because increasing mass flux by decreasing port hydraulic diameter also decreases refrigerant-side heat transfer area, it seems best to leave the hydraulic diameter large and use the number of passes and circulation number to achieve the desired mass flux.

Based on above discussion, the guidelines for the design and operation of microchannel evaporators in ejector cycles can be summarized as follows:

- The evaporator should be designed and operated so that the drop in saturation temperature due to refrigerant pressure drop does not exceed 1.0 K (not clear if this is fluid specific).
- For this system, the optimal mass flux seems to be around 55 – 60 kg m^{-2} s^{-1} for the standard ejector cycle, while the optimal mass flux for the ejector recirculation cycle is significantly higher (~200 kg m^{-2} s^{-1}); it is not clear if these guidelines apply to all systems and refrigerants.
- An increased number of refrigerant-side passes should be used first to adjust refrigerant mass flux; the amount of liquid overfeed should then be controlled to achieve the desired mass flux; the hydraulic diameter of the ports should generally be kept large to maximize heat transfer area.
- The ejector recirculation cycle should be operated with a large amount of overfeed and with an optimized number of refrigerant-side passes (balance heat transfer and pressure drop).
- The standard ejector cycle should be operated with a low amount of overfeed (maximize pressure lift of ejector) and should use a large number of refrigerant-side passes to improve evaporator heat transfer performance.

7.2.4 Comparison of Evaporator Design in CO_2 and R410A Ejector Cycles

All of the above results have used R410A as the refrigerant. This section will investigate the effect of microchannel port hydraulic diameter on the performance of a CO_2 ejector cycle and compare the results to those obtained with R410A. The conditions used in the simulations in this section with CO_2 were the same as with R410A (same evaporator geometry, evaporator conditions, compressor efficiency, system capacity) except that the gas cooler pressure and outlet temperature were set to 100 bar and 44°C, respectively. An IHX was not included in the CO_2 system. The efficiencies of the ejector motive nozzle, suction nozzle, and diffuser were kept at 0.60, 0.60, and 0.55, respectively, but the mixing pressure was assumed to be 100 kPa lower than the ejector suction pressure (corresponding to a 1 K drop in saturation pressure). The evaporator outlet superheat in the standard ejector cycle and DX cycle was set to 3 K.

The COP Ratio for the standard ejector and DX cycles is shown in Figure 7.20, while the evaporator UA and refrigerant-side pressure drop are shown in Figure 7.21 for the two cycles. It can be seen that similar to the R410A results, there is an optimum hydraulic diameter that maximizes COP, and the optimum hydraulic diameter is smaller for the ejector cycle (0.33 mm, G_{ref} equals 150 kg m^{-2} s^{-1}) than for the DX cycle (0.42 mm, G_{ref} equals 188 kg m^{-2} s^{-1}). Up to 6.4 % COP improvement is achieved with the ejector cycle when comparing the two cycles at optimum hydraulic diameter. Again, greater COP improvement (up to 9.0 %) can be achieved by comparing the two cycles with a hydraulic diameter that is too small for either cycle, though this ultimately results in lower ejector cycle COP.

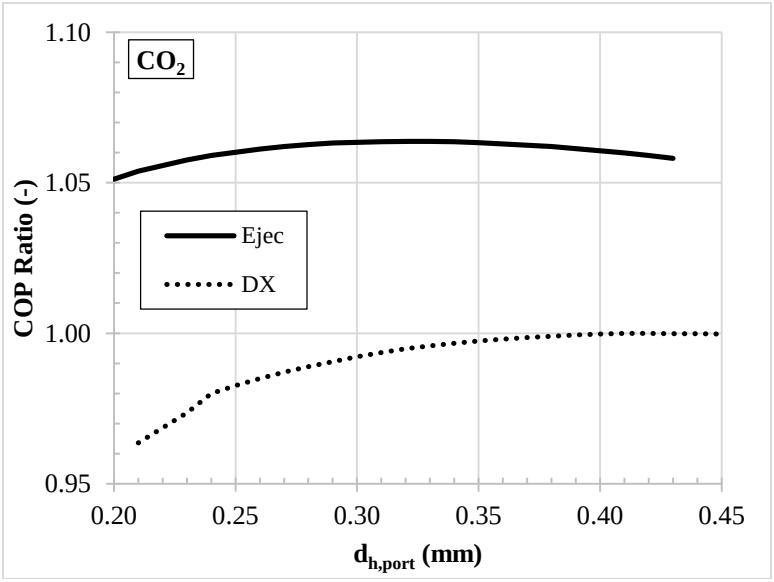

Figure 7.20: Comparison of standard ejector DX cycle COP with 3 K evaporator outlet superheat for both cycles using CO_2 as the refrigerant; COP values are normalized by maximum DX cycle COP.

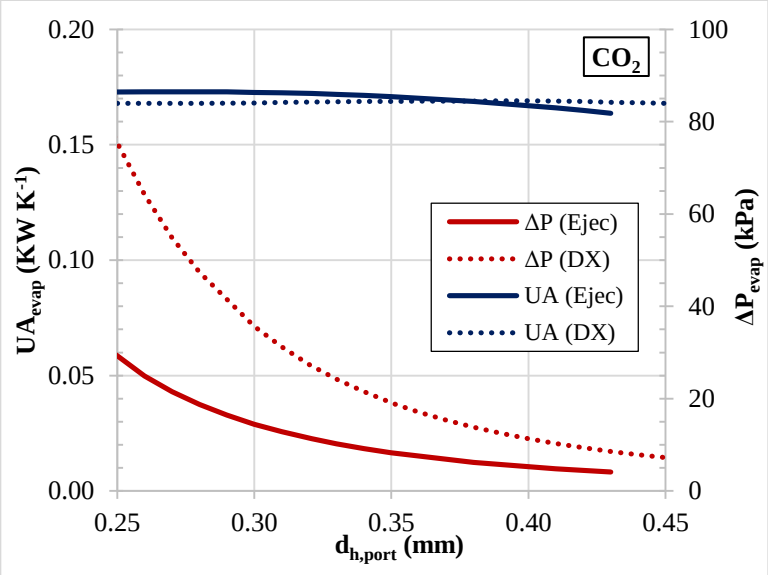

Figure 7.21: Comparison of standard ejector and DX cycle evaporator UA and refrigerant-side pressure drop with 3 K of superheat for both cycles using CO_2 as the refrigerant.

Figure 7.21 shows that the pressure drop behavior with CO_2 is similar to that observed with R410A, though because of its high working pressure, CO_2 is less sensitive to evaporator pressure drop compared to other refrigerants. This lower sensitivity to pressure drop allows CO_2 to use smaller hydraulic diameter to improve heat transfer. The evaporator UA trend with the CO_2 cycles differs significantly compared to what was observed with R410A. CO_2 achieves very high heat transfer coefficient at low quality because of its very strong nucleate boiling contribution. This means that the standard ejector cycle, which bypasses vapor around the evaporator and enters at very low quality, can actually achieve better heat transfer performance than the DX cycle despite the lower mass flux, as seen in Figure 7.21 for smaller hydraulic diameter. The evaporator UA trend also does not seem to vary significantly with hydraulic diameter. The reason for this is not clear, though it could be due to the flow boiling heat transfer coefficient of CO_2 being dominated by the very high nucleate boiling contribution, which should theoretically be independent of mass flux. It is also possible that the very high heat transfer coefficient of CO_2 makes refrigerant-side resistance nearly negligible compared to air-side resistance, as a result of little dependence of evaporator UA on refrigerant-side effects.

It can be seen from Figure 7.20 that the COP of the CO_2 ejector cycle is not as sensitive to hydraulic diameter as the COP of the R410A ejector cycle. The R410A results show that ejector cycle COP decreases by 3.6 % compared to its maximum as refrigerant-side cross-sectional area decreases by 59 % (from hydraulic diameter of 0.47 mm to 0.30 mm). The CO_2 results show that ejector cycle COP only

decreases by 1.0 % as refrigerant-side cross-sectional area decreases by the same amount (from hydraulic diameter of 0.33 mm to 0.21 mm). This is due to the lower sensitivity of CO_2 cycles to evaporator pressure drop, less dependence of evaporator UA on refrigerant-side geometry, and the larger ejector work recovery and pressure lift of the CO_2 ejector. As noted above, the high working pressure of CO_2 makes it less sensitive to evaporator pressure drop, and the evaporator UA does not seem to change significantly with evaporator geometry for these conditions. At the same time, as discussed in Chapter 6, the COP of the CO_2 standard ejector cycle is dominated by the pressure lift of the ejector cycle and the effect of improving evaporator performance is less significant in determining overall cycle performance. Further improvement of the CO_2 standard ejector cycle would, of course, be possible by adjusting the number of passes to optimize mass flux, though optimal mass flux would likely be greater for CO_2.

It can be concluded from the comparison of R410A and CO_2 results that evaporator design plays a critical role in the performance of ejector cycles for low-pressure refrigerants (R410A, hydrocarbons, ammonia, R134a) but does not seem to be as critical when operating the CO_2 standard ejector cycle. On the other hand, if this numerical investigation were extended to R134a or ammonia, refrigerants that are very sensitive to pressure drop in the evaporator, it is likely that evaporator design and overfeed rate would have an even more critical effect on ejector cycle COP than for R410A. It is also possible with a fluid such as R134a that after optimizing evaporator design for each ejector cycle, the ejector recirculation cycle would ultimately be more favorable because of the very small ejector pressure lift with R134a.

7.3 Chapter Summary and Conclusions

The experimental and numerical results of this chapter both demonstrate that evaporator design and operation (circulation number) can have a very significant effect on the COP improvement obtained with an ejector cycle. Thus, when designing an ejector system, it is important to understand how the design and operation of the evaporator can affect the COP of the ejector cycle in comparison to a DX cycle and to ensure that the COP improvement of the ejector cycle is not limited by an evaporator that is improperly designed or improperly supplied with refrigerant. The experimental results have shown that the most favorable evaporator design is different for different ejector cycles, as the ejector recirculation cycle favors an evaporator with larger refrigerant cross-sectional area while the standard ejector cycle favors an evaporator with smaller cross-sectional area. The experimental investigation presented in this chapter has used microchannel heat exchangers as evaporators. Using a different type of heat exchanger (round-tube, plate) when comparing these two ejector cycles may produce different results. However, it is likely that the majority of evaporator improvement in either cycle would still come from eliminating dryout regardless of the type of heat exchanger.

The numerical results have also shown that the evaporator should be designed and operated differently in the two different ejector cycles. It was recommended for both ejector cycles to keep microchannel port diameter large and use the number of refrigerant-side passes and circulation number to optimize mass flux. For the standard ejector cycle, the ejector should be used for pressure lift (directly supplementing compressor power) rather than liquid overfeed, meaning that circulation number should be kept as low as possible (while still avoiding dryout) and a larger number of refrigerant passes should be used to improve evaporator performance. On the other hand, for the ejector recirculation cycle, the ejector should be used to provide a large amount of overfeed to the evaporator and the number of refrigerant-side passes should be used to balance heat transfer and pressure drop to maximize cycle COP. It was also recommended that evaporator pressure drop be limited to approximately 1.0 K drop in saturation temperature for each cycle.

The numerical analysis has focused on optimizing the evaporator for ejector cycles, though the evaporator could also be improved for the baseline (DX) cycle. Though not investigated in detail here, the optimal geometry of the DX cycle evaporator would be very similar to the ejector recirculation cycle with no overfeed (n = 1), meaning Evaporator D would be the most favorable for the DX cycle. Note that while this results in the same number of passes for the standard ejector and DX cycles, the optimal mass flux is still different for the DX cycle (G_{ref} = 75 kg m^{-2} s^{-1} for DX cycle). Note also that the improvement in COP gained by improving evaporator design (Evaporator D compared to Evaporator A) in the standard ejector cycle is noticeably greater than what would be seen in the DX cycle, again indicating the importance of optimizing evaporator design in systems with ejectors, especially with low-pressure refrigerants.

While the experimental results showed that the ejector recirculation cycle could generally achieve higher COP with R410A and the given evaporator design, the numerical results showed that the standard ejector cycle could ultimately achieve higher COP once the refrigerant-side of the evaporator was optimized for each cycle. However, the ejector recirculation cycle would be expected to perform more favorably at conditions of lower ambient temperature or with a low work recovery fluid (R134a, ammonia) due to the lower pressure lift of the ejector. On the other hand, it was seen that CO_2 ejector cycle performance is much less sensitive to evaporator design, meaning that issues such as proper cycle control and design of efficient ejectors would have a more significant effect on the overall performance of a CO_2 ejector cycle. The issue of ejector cycle control will be investigated in the next chapter.

CHAPTER 8: EJECTOR CYCLE CONTROL METHODS AND STRATEGIES

This chapter investigates different control methods for the standard ejector cycle and provides experimental quantification of the performance losses encountered by not properly controlling the standard ejector cycle. The refrigerant of interest in this chapter is CO_2, and the majority of results are for a transcritical cycle. Control of evaporator flow rate and high-side pressure using an expansion valve and an adjustable ejector are investigated. Comparison is made between transcritical and subcritical cycles regarding their control. High-side pressure control strategies are developed and discussed. The results of this chapter have been previously published, as will be noted in the sections below.

8.1 Control of Ejector Cycles

The standard ejector cycle has two separate circuits, meaning that the flow rate through each can theoretically be controlled independently. The evaporator metering valve controls flow rate through the evaporator and the pressure lift of the ejector, as discussed in previous chapters. The experimental and numerical results in Chapter 7 have shown for a single working condition that control of evaporator flow rate can have a significant effect on evaporator and cycle performance. This chapter will explore control of the evaporator metering valve over a range of conditions. Additionally, the high-side pressure and high-side flow rate of the system (which are not independent of one another) are set by the size of the restriction or opening in the expansion device. Conventional systems use an adjustable valve with a variable size opening (isenthalpic expansion) to control high-side pressure. However, a conventional ejector has only a fixed opening size, meaning that some additional means of control must be added to the ejector or the cycle to regain active control of high-side pressure. Different high-side pressure control methods for ejector cycles will be investigated in this chapter over a range of conditions.

Similar control concepts apply to the ejector recirculation cycle, as high-side pressure must still be optimized to maximize COP, and evaporator flow rate can be controlled with the metering valve. However, as shown in Figure 6.3, whereas the COP of the standard ejector cycle is very sensitive to circulation number (controlled by the metering valve), the COP of the ejector recirculation cycle is relatively insensitive to circulation number. This was also seen in the experimental results with R410A where the majority of COP improvement offered by the ejector recirculation cycle was due to eliminating dryout, and little further gain in COP was achieved by further overfeeding the evaporator. What this means is that it may not be necessary to actively control the metering valve in the ejector recirculation cycle. This makes this ejector cycle much more appealing for small-scale applications where complex controls are not practical.

For a subcritical cycle, phase change occurs during heat rejection, meaning that high-side (condensing) pressure is set by the condensing temperature, which is a very strong function of ambient temperature. However, for a transcritical cycle, the refrigerant remains single-phase, meaning that pressure and temperature are independent, and the high-side pressure can be controlled independent of the ambient temperature. As will be discussed later in this chapter, some control of high-side pressure and temperature is possible in a subcritical cycle, but the effect of controlling high-side pressure is much more dramatic for a transcritical cycle. Figure 8.1 demonstrates the importance of controlling and optimizing high-side pressure of a transcritical cycle. As high-side pressure (P_2, P_3) is increased, both cooling capacity ($q, h_1 - h_4$) and compressor work ($w, h_2 - h_1$) increase. This means that there will be a maximum COP at some optimum high-side pressure. In order to operate at maximum COP as operating conditions vary, the expansion device must be able to control and optimize high-side pressure. This is also demonstrated in Equations (8.1) and (8.2). Equation (8.2) shows with a Taylor series expansion (neglecting higher order terms) how increased capacity and work affect COP (Domanski *et al.*, 1994).

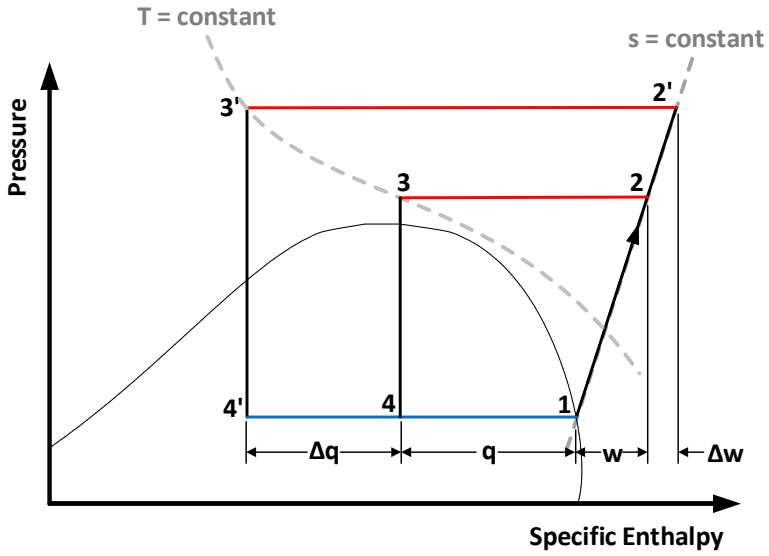

Figure 8.1: Variation of high-side pressure in a transcritical cycle has a significant effect on both capacity and compressor work.

$$COP = \frac{q}{w} \qquad (8.1)$$

$$COP' = \frac{q + \Delta q}{w + \Delta w} \approx COP\left(1 + \frac{\Delta q}{q} - \frac{\Delta w}{w}\right) \qquad (8.2)$$

In order to find a relation between maximum COP and optimal high-side pressure, the expression for COP can be differentiated with respect to high-side pressure. This analysis was first performed by Inokuty (1928), though many details of the derivation were not shown. Equation (8.3) gives the expression for COP using the numbering of Figure 8.1. Equations (8.4) through (8.7) show the details of the differentiation. It is assumed in Equation (8.5) that as high-side pressure changes, the temperature at state 3, which is the temperature that the refrigerant in the gas cooler is cooled to by the ambient fluid, remains the same. Additionally, Equation (8.5) assumes that the compression process occurs isentropically. These assumptions are not perfectly accurate for a real system but are justifiable for a theoretical derivation.

$$COP = \frac{h_1 - h_4}{h_2 - h_1} \qquad (8.3)$$

$$\frac{\partial}{\partial P_2}(COP) = \frac{\partial}{\partial P_2}\left(\frac{h_1}{h_2 - h_1}\right) - \frac{\partial}{\partial P_2}\left(\frac{h_3}{h_2 - h_1}\right) \qquad (8.4)$$

$$\frac{\partial}{\partial P_2}(COP) = -h_1\left(\frac{\partial h_2}{\partial P_2}\right)_s (h_2 - h_1)^{-2} - \left(\frac{\partial h_3}{\partial P_2}\right)_T \frac{1}{h_2 - h_1} + h_3\left(\frac{\partial h_2}{\partial P_2}\right)_s (h_2 - h_1)^{-2} \qquad (8.5)$$

$$\frac{\partial}{\partial P_2}(COP) = -\left(\frac{\partial h_2}{\partial P_2}\right)_s (h_2 - h_1)^{-2}[h_1 - h_3] - \left(\frac{\partial h_3}{\partial P_2}\right)_T \frac{1}{h_2 - h_1} \qquad (8.6)$$

$$\frac{\partial}{\partial P_2}(COP) = -\left(\frac{\partial h_2}{\partial P_2}\right)_s \left[\frac{h_1 - h_3}{(h_2 - h_1)^2}\right] - \left(\frac{\partial h_3}{\partial P_2}\right)_T \left[\frac{h_2 - h_1}{(h_2 - h_1)^2}\right] \qquad (8.7)$$

COP is maximized when the partial derivative with respect to high-side pressure is set equal to 0, as shown in Equations (8.8) through (8.11). The final result in Equation (8.11) is a relation between optimal high-side pressure (P_2) and COP of a transcritical cycle based on the above idealizations.

$$0 = -\left(\frac{\partial h_2}{\partial P_2}\right)_s \left[\frac{h_1 - h_3}{(h_2 - h_1)^2}\right] - \left(\frac{\partial h_3}{\partial P_2}\right)_T \left[\frac{h_2 - h_1}{(h_2 - h_1)^2}\right] \qquad (8.8)$$

$$\left(\frac{\partial h_2}{\partial P_2}\right)_s (h_1 - h_3) = -\left(\frac{\partial h_3}{\partial P_2}\right)_T (h_2 - h_1) \qquad (8.9)$$

$$\left(\frac{\partial h_3}{\partial P_2}\right)_T = -\frac{h_1 - h_3}{h_2 - h_1}\left(\frac{\partial h_2}{\partial P_2}\right)_s = -\frac{h_1 - h_4}{h_2 - h_1}\left(\frac{\partial h_2}{\partial P_2}\right)_s \qquad (8.10)$$

$$\left(\frac{\partial h_3}{\partial P_2}\right)_T = -COP\left(\frac{\partial h_2}{\partial P_2}\right)_s \qquad (8.11)$$

As mentioned above, a conventional (fixed geometry) ejector cannot actively control high-side pressure on its own, meaning that some additional means of control must be added to the cycle. Figure 8.2 shows several options for controlling the ejector in order to control high-side pressure. Figure 8.2(a) shows the adjustable ejector, while Figure 8.2(b) shows parallel ejectors; both of these options were discussed in the literature review in Chapter 2. High-side pressure control with an adjustable ejector will be investigated in Section 8.3. Figure 8.2(c) shows an expansion valve in series with the ejector (to increase high-side pressure) and an expansion valve in parallel with the ejector (to decrease high-side pressure). The use of an expansion valve to control ejector cycle high-side pressure will be investigated in Section 8.5.

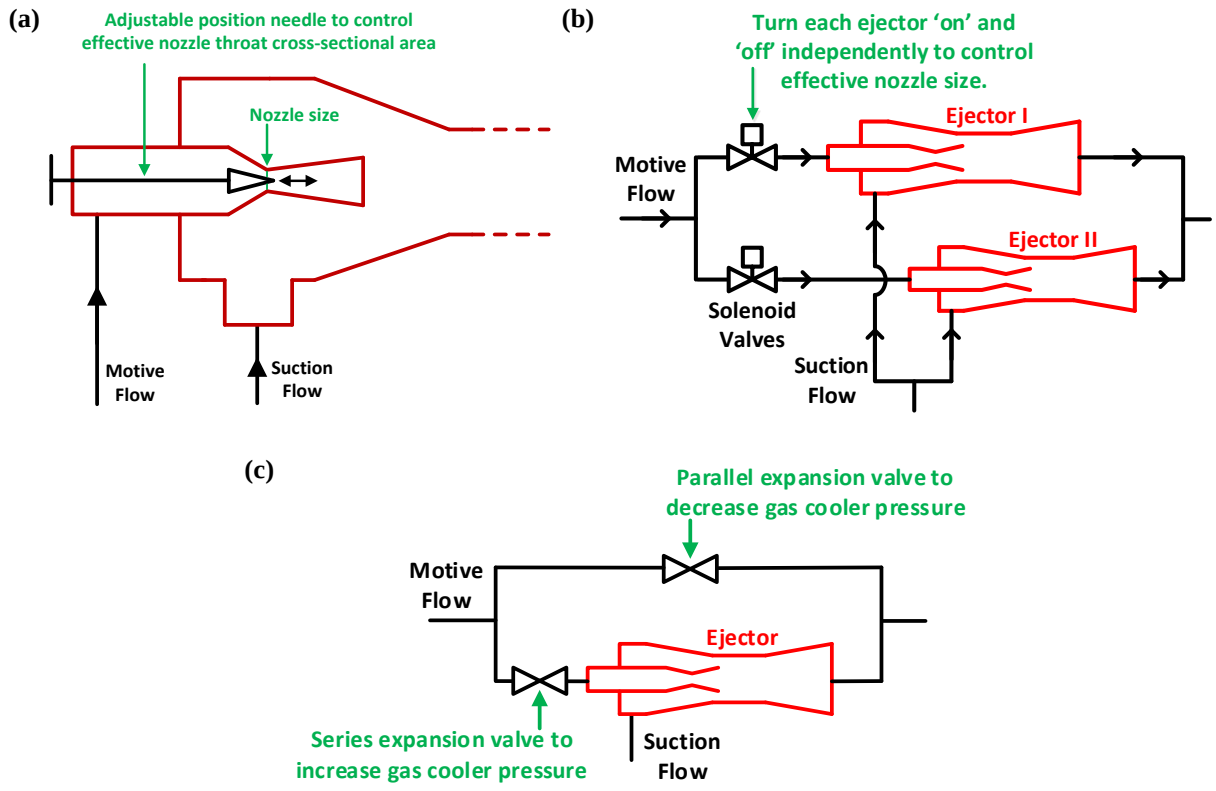

Figure 8.2: Diagrams of methods to control high-side pressure in an ejector cycle using (a) adjustable ejector, (b) parallel ejector arrangement, and (c) expansion valve in series or parallel with ejector.

8.2 Evaporator Metering Valve Control

As system operating conditions vary (especially compressor speed or cooling capacity), a different flow rate through the evaporator will be required, which will require a different metering valve setting if the optimal flow rate is desired at each condition. A flow rate that is too low for the given conditions will result in dryout and severely decreased evaporator performance. A flow rate that is too high for the given conditions will not necessarily result in much difference in evaporator performance, but it will result in lower ejector pressure lift. The CO_2 experimental facility described in Chapter 5 was used to investigate metering valve control experimentally. The results of this section have been previously published in Lawrence and Elbel (2016d). The test conditions are shown in Table 8.1. Compressor speed and ambient (gas cooler air inlet) temperature were varied for different tests. High-side pressure was not actively controlled in these experiments.

Table 8.1: Operating conditions used for CO_2 experiments.

Parameter	Unit	Value
$T_{evap,air,in}$	°C	27
$\dot{V}_{evap,air}$	$m^3\ s^{-1}$	0.250
$T_{gc,air,in}$	°C	30, 35, 40
$\dot{V}_{gc,air}$	$m^3\ s^{-1}$	0.500
N_{cp}	min^{-1}	900, 1200, 1500, 1800
ε_{IHX}	-	0.6

Figure 8.3 shows that there is an optimum entrainment ratio, corresponding to an optimum evaporator outlet state and optimum metering valve setting, which maximizes the COP of the ejector cycle. The optimum evaporator outlet state for this system at the given conditions is a quality of approximately 1.0. Figure 8.4 shows that this optimum in COP is due to a trade-off between increasing evaporator UA and decreasing ejector pressure lift as entrainment ratio increases. Compared to the optimum outlet state of saturated vapor, lower mass flow results in dryout (superheat) in the evaporator and lower evaporator UA; while ejector pressure lift is higher for the case of a superheated outlet, the decrease in evaporator UA has a more significant effect on overall cycle performance, resulting in a decrease in COP. Mass flow rate that is too high results in lower ejector pressure lift, as the ejector must pump more mass flow but with the same power, while evaporator UA does not change significantly once dryout is eliminated; this also results in decreased cycle performance. Note that the optimum outlet state will not be an outlet quality of

1.0 for every system. The numerical results in Chapter 6 showed that the optimum evaporator outlet quality for the standard ejector cycle with CO_2 was between 0.9 and 1.0, while the optimum outlet quality for low-pressure fluids could be much lower. This can also be seen by comparing the results for CO_2 presented here to the experimental results for R410A, which showed a much lower optimal outlet quality of the standard ejector cycle. Additionally, evaporator design, ejector efficiency, and operating conditions could have small but noticeable effects on the optimal evaporator outlet quality for a given ejector system.

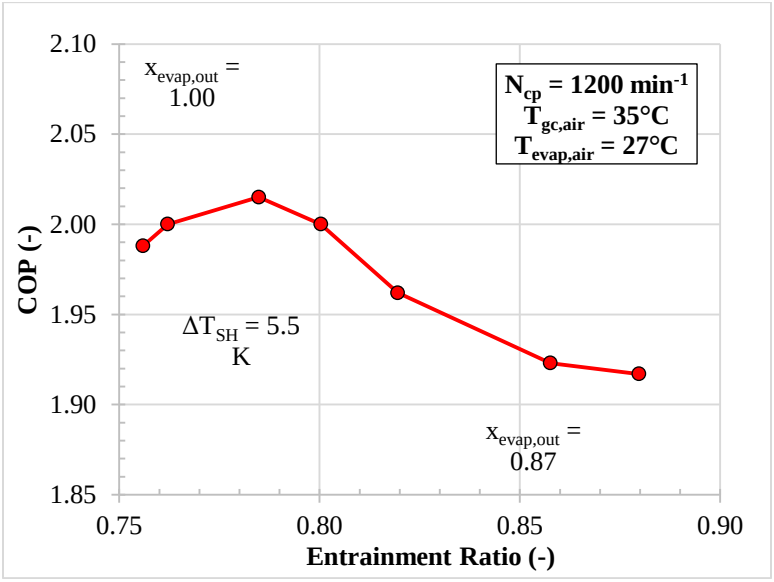

Figure 8.3: Effect of entrainment ratio (evaporator outlet state) on standard ejector cycle COP.

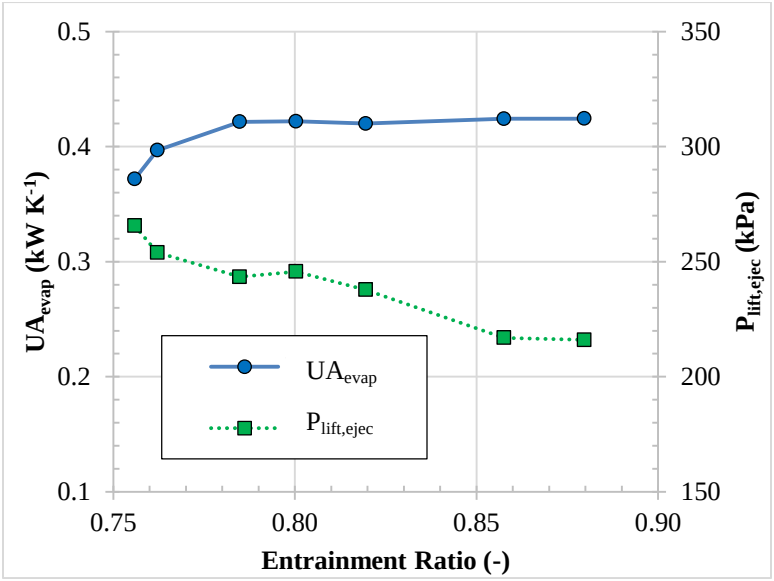

Figure 8.4: Effect of entrainment ratio (evaporator outlet state) on evaporator UA and ejector pressure lift.

Figure 8.5 demonstrates the performance penalty for not actively controlling the evaporator metering valve while capacity varies. Two cases are considered here: Valve fixed at 50 % opening (corresponding to the optimal valve setting at 900 min^{-1} compressor speed and 35°C ambient temperature) and valve fixed at 86 % opening (corresponding to the optimal valve setting at 1800 min^{-1} compressor speed and 35°C ambient temperature). The valve was fixed at each of these two settings while the compressor speed and ambient temperature were varied. The resulting COP's and corresponding evaporator outlet states for varying compressor speed tests are shown in Figure 8.5. Comparison is made to the optimal case (metering valve adjusted to achieve evaporator outlet quality of 1.0) at each speed.

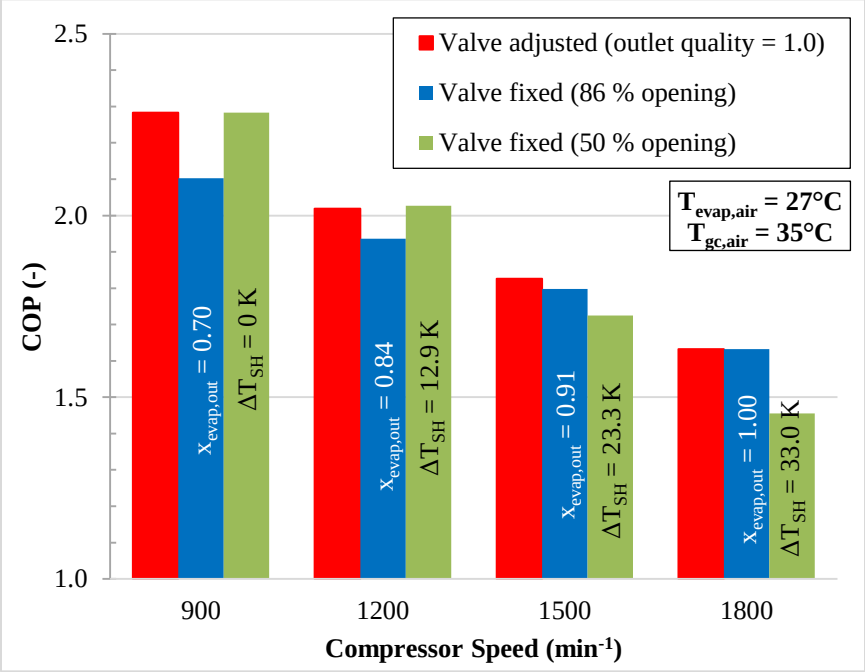

Figure 8.5: COP obtained by leaving evaporator metering valve fixed at two settings compared to optimal case (metering valve adjusted to achieve outlet quality of 1.0) for different compressor speeds; evaporator outlet state is indicated for each case.

Figure 8.5 shows that for the case of 50 % valve opening, the evaporator superheat increases (up to 33 K) with increasing compressor speed. At higher capacity, the evaporator requires greater flow rate; the smallest valve setting does not allow enough mass flow to the evaporator, resulting in significant dryout and decrease in COP compared to the optimal case. Similarly, for the case of 86 % valve opening, the evaporator outlet quality decreases (down to 0.70) with decreasing compressor speed. At lower capacity, the evaporator requires less flow rate; the largest valve setting allows too much mass flow to the evaporator, which does not necessarily hurt evaporator performance but does decrease the pressure lift of the ejector, ultimately decreasing COP.

Table 8.2 reports the percent change in COP and capacity for each of the valve settings compared to the optimal case for each condition (metering valve adjusted to achieve outlet quality of 1.0). It can be seen that very significant COP and capacity penalties result from not adjusting the evaporator metering valve. Up to 11 and 17 % penalties in COP and capacity, respectively, are observed if the smallest valve setting (50 % valve opening) is used at the highest compressor speed. Similarly, up to 8 % penalty each in COP and capacity are observed if the largest valve setting (86 % valve opening) is used at lower compressor speed. Note that the high-side pressure was not actively controlled for the results reported in this section but generally varied by 2 to 3 bar or less for results at the same compressor speed and ambient temperature. A 2 to 3 bar change in high-side pressure could have a small effect on COP and capacity depending on operating conditions. However, as will be shown below, the change in COP and capacity as high-side pressure varies by 2 to 3 bar would not be nearly as large as the losses reported here, meaning that these very large losses are due to improper metering valve control (dryout or lower pressure lift).

Table 8.2: Change in COP and capacity for two cases of fixed evaporator metering valve compared to optimal case (metering valve adjusted to achieve outlet quality of 1.0) for different conditions.

N_{cp} (min^{-1})	$T_{gc,air}$ (°C)	Valve fixed (50 % opening)		Valve fixed (86 % opening)	
		COP Change	Capacity Change	COP Change	Capacity Change
900	35	-	-	-8.1 %	-7.9 %
1200	40	+2.7 %	+1.5 %	-5.2 %	-5.2 %
1200	35	0.0 %	-2.0 %	-4.2 %	-4.1 %
1200	30	-7.2 %	-9.3 %	-1.7 %	-2.6 %
1500	35	-5.5 %	-9.7 %	-0.1 %	-1.5 %
1800	35	-10.8 %	-16.9 %	-	-

It can be seen from Table 8.2 that the performance penalty for using a valve setting that is too large is less than for using a valve setting that is too small, meaning that it is better to sacrifice pressure lift and operate with a flow rate that is too large than to allow significant dryout in the evaporator. Note that the performance penalty for overfeeding too much would likely be even lower for a system with a low-pressure refrigerant. This could be important for small-scale systems that require simpler system controls. Note also that for 40°C ambient temperature, a smaller valve setting actually improves COP and capacity slightly compared to the outlet quality of 1.0 case; this may be because of the greater potential work recovery at higher ambient temperature, which gives pressure lift a more dominant effect on COP and would shift the optimal flow rate to a lower value where pressure lift is higher.

8.3 High-side Pressure Control with Adjustable Ejector

This section investigates the use of an adjustable ejector to control high-side pressure. The results of this section have been previously published in Lawrence and Elbel (2016d). Figure 8.6 compares the COP and capacity of the transcritical ejector and DX cycles as functions of high-side pressure; note that the operating conditions of the results shown in this figure differ slightly from those used in the other results of this section and the previous section. It can be seen for both cycles that a maximum in COP is achieved, at 86 bar for the ejector cycle and 88 bar for the DX cycle, while capacity continues to increase with high-side pressure. The capacity of a transcritical cycle will eventually begin to decrease at high enough high-side pressure due to reduced compressor mass flow rate; compressor mass flow rate decreases because suction pressure (density) and volumetric efficiency decrease as high-side pressure increases. It can also be seen that the COP and capacity of the ejector cycle are generally greater than for the DX cycle, which is the objective of using the ejector cycle. By comparing at each cycle's optimum high-side pressure, simultaneous improvements of 5.6 % in COP and 2.6 % in capacity are achieved by the ejector cycle.

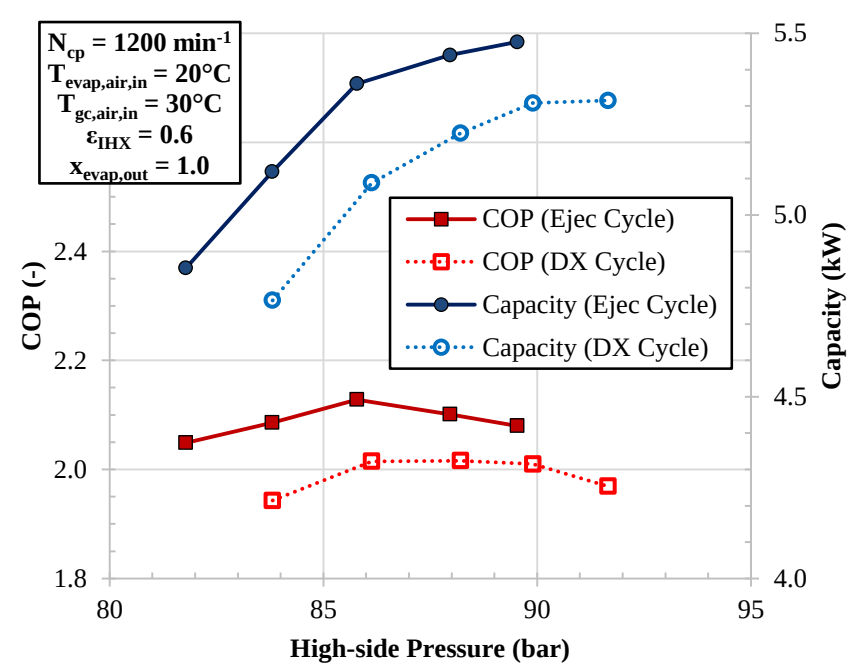

Figure 8.6: Comparison of ejector and DX cycle COP and capacity as functions of high-side pressure for transcritical operation.

It is very commonly observed in transcritical CO_2 systems that improving the cycle and increasing COP by adding an ejector results in lower optimal high-side pressure, though the reason for this is never discussed. The reason can be seen in the relation between optimal high-side pressure and COP, Equation

(8.11). A higher COP means that the partial derivative $\left(\frac{\partial h_3}{dP}\right)_T$ must also be higher. This partial derivative represents the slope of the isotherm at point 3 on the pressure-specific enthalpy diagram. Note that it can be seen from experimental observations that the change in the value of the partial derivative $\left(\frac{\partial h_2}{dP}\right)_s$, which represents the slope of the isentrope along which compression occurs on the pressure-specific enthalpy diagram, is noticeably smaller between ejector and DX cycles than the change in the COP. A larger value of $\left(\frac{\partial h_3}{dP}\right)_T$ physically means that the change in specific enthalpy for a given change in pressure at constant temperature is larger. Figure 8.7 shows that the sensitivity of specific enthalpy to pressure is generally higher at lower pressure. This means that the ejector cycle, which has a higher COP, needs to operate at lower high-side pressure, where specific enthalpy is more sensitive to changes in pressure, in order to balance Equation (8.11).

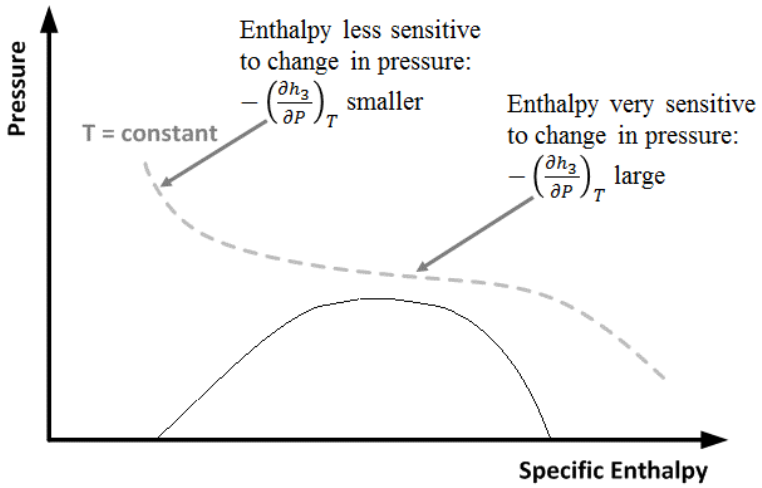

Figure 8.7: Slope of isotherm on pressure-specific enthalpy diagram changes dramatically as a function of pressure.

The adjustable ejector can be used to optimize high-side pressure over a range of conditions. Figure 8.8 presents the ejector cycle COP as a function of high-side pressure for different compressor speeds at constant ambient temperature, while Figure 8.9 presents the ejector cycle COP as a function of high-side pressure for different ambient temperatures at constant compressor speed. The operating conditions for these results are shown in Table 8.1; additionally, the evaporator outlet quality was adjusted to be 1.0 at each data point, which was found to generally be the optimal outlet state for this system (see Section 8.2). For each condition, the point of lowest high-side pressure is the operating point of the system when high-side pressure is not actively controlled (needle fully withdrawn from nozzle). The high-side pressure is increased by using the needle to decrease effective nozzle size.

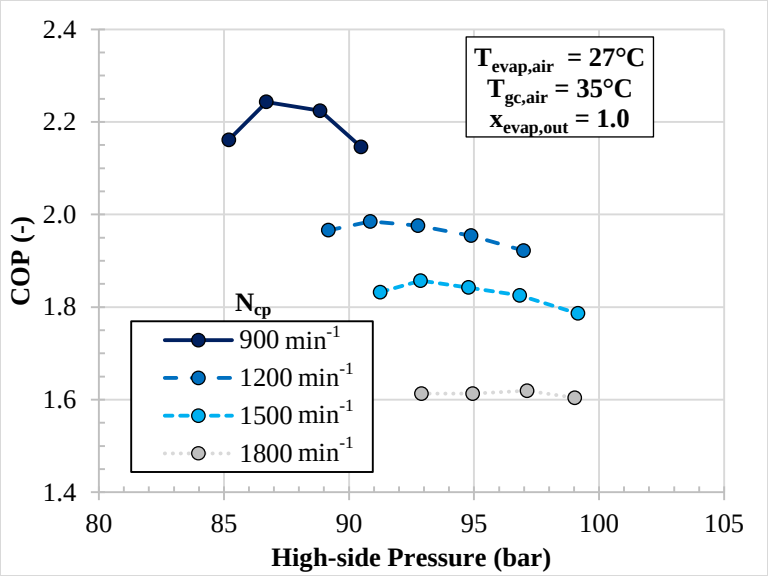

Figure 8.8: COP maximization with adjustable ejector at different conditions for varying compressor speed (constant ambient temperature).

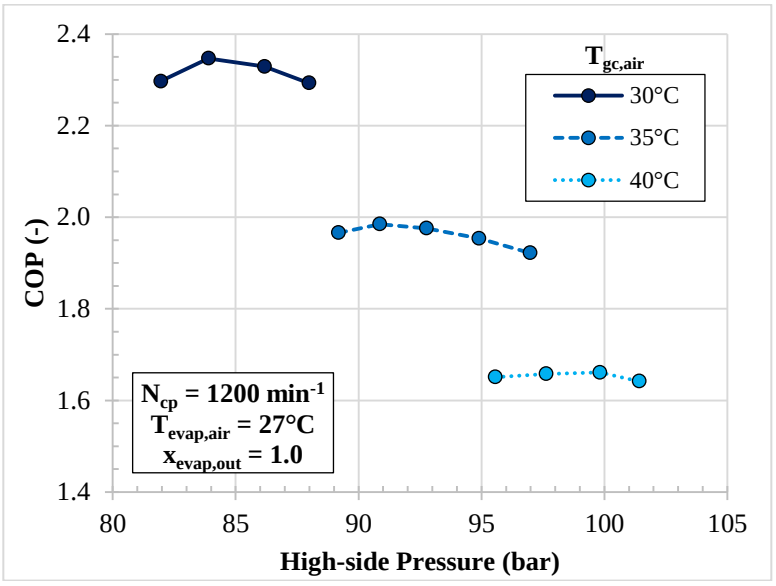

Figure 8.9: COP maximization with adjustable ejector at different conditions for varying ambient temperature (constant compressor speed).

It can be seen that for every condition, a maximum ejector cycle COP is achieved by increasing high-side pressure, meaning that the nozzle without the needle is oversized. However, for some conditions, particularly conditions of greater compressor speed (capacity) or greater ambient temperature where high-side pressure is greater, the variation of COP with respect to high-side pressure is very small. The COP of a transcritical CO_2 cycle is more sensitive to high-side pressure in the vicinity of the critical point

(approximately 31°C and 74 bar for CO_2), meaning that high-side pressure control is particularly important when operating at conditions of lower compressor speed (capacity) or lower ambient temperature, where the high-side pressure is nearer to the critical pressure. Accordingly, the opportunity to improve COP with an adjustable ejector (or another high-side pressure control method) is greater at conditions nearer to the critical pressure. Table 8.3 shows the COP improvement of the ejector cycle at optimum high-side pressure compared to the ejector cycle with no active control for each condition. It can be seen that in general, this COP improvement gained by controlling high-side pressure is greater at lower compressor speed and lower ambient temperature.

Table 8.3: COP improvement of ejector cycle (at optimum high-side pressure compared to ejector cycle with no active control) and maximum ejector efficiency (observed with no use of needle).

N_{cp} (min^{-1})	$T_{gc,air}$ (°C)	COP Improvement	$\eta_{ejec,max}$
900	35	3.8 %	16.6 %
1200	30	2.3 %	25.9 %
1200	35	1.0 %	22.8 %
1200	40	0.6 %	21.3 %
1500	35	1.4 %	27.2 %
1800	35	0.4 %	25.8 %

The ejector work recovery efficiency for the results presented above is shown in Figures 8.10 and 8.11. For every operating condition, the highest ejector efficiency is observed at the lowest high-side pressure where the needle is fully withdrawn from the nozzle. Inserting the needle into the nozzle increases high-side pressure but also results in increased frictional losses, meaning that the efficiency of the nozzle and ejector would be expected to decrease with greater use of the needle (greater increase in high-side pressure). This is seen clearly in Figures 8.10 and 8.11 where ejector efficiency continually decreases with increasing high-side pressure for almost every condition. However, despite the continuous decrease in ejector efficiency, the adjustable ejector still offers some opportunity to increase COP by moving to a more favorable high-side pressure, indicating that the effect of high-side pressure on cycle performance can be stronger than the effect of ejector efficiency. This was also observed by Elbel and Hrnjak (2008) and Xu *et al.* (2012).

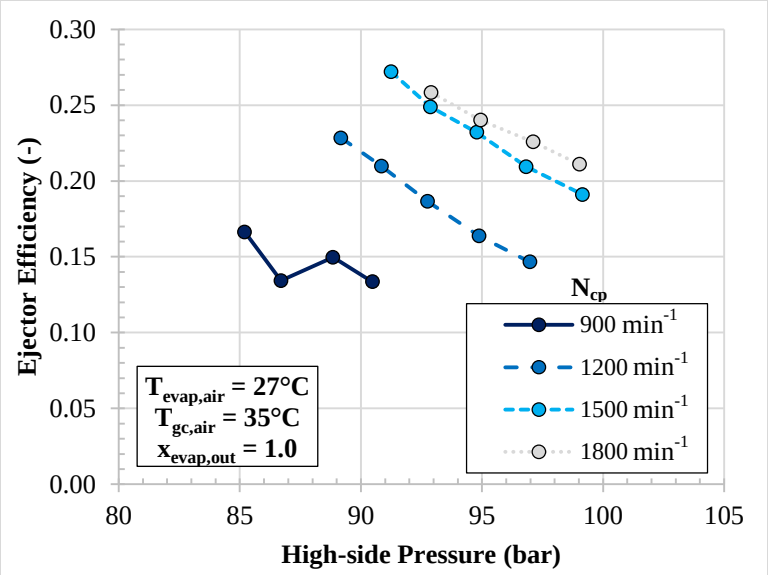

Figure 8.10: Ejector work recovery efficiency as a function of high-side pressure for different compressor speeds (constant ambient temperature).

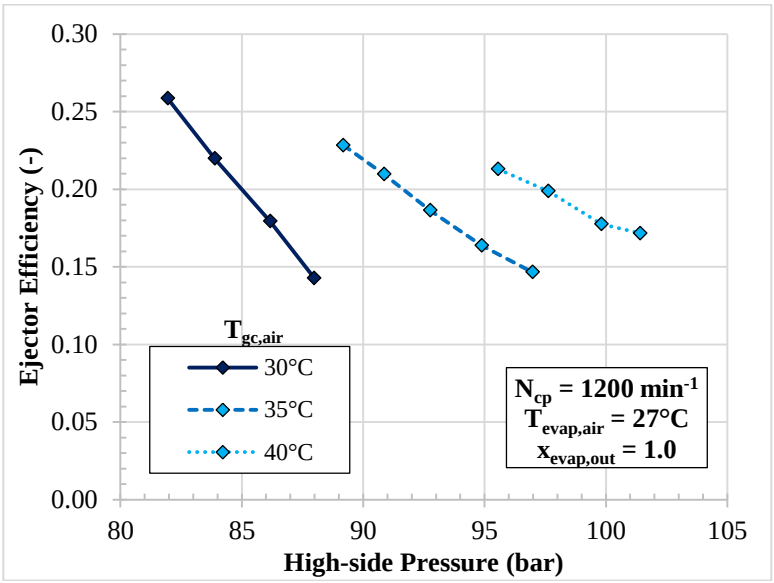

Figure 8.11: Ejector work recovery efficiency as a function of high-side pressure for different ambient temperatures (constant compressor speed).

Figure 8.10 shows that the efficiency of the ejector generally increases as compressor speed increases, though it is similar for the two highest compressor speeds. The nozzle diameter was sized for operation at the highest flow rate (compressor speed) and is likely too large for lower flow rate conditions. Similarly, Figure 8.11 shows that ejector efficiency is highest at the lowest ambient temperature, where flow rate is the highest. This decrease in ejector efficiency as mass flow rate decreases represents the loss in ejector

efficiency due to ejector off-design operation. For the points of no needle use, efficiency decreases from a maximum of 27.2 % at 1500 min^{-1} to 16.6 % at 900 min^{-1}, and from 25.9 % at 30°C to 21.3 % at 40°C, indicating significant losses in ejector efficiency due to off-design operation. Further decrease in ejector efficiency is incurred due to use of the needle. Furthermore, Figure 8.11 shows that the efficiency of the fixed ejector decreases from 22.8 % at 89 bar high-side pressure to 21.3 % at 95 bar high-side pressure as ambient temperature changes; this is the efficiency loss due to off-design. On the other hand, using the adjustable ejector to increase high-side pressure to 95 bar (at 35°C ambient temperature) causes efficiency to drop to 16.4 %, indicating far more significant loss caused by the needle than by off-design operation.

8.4 High-side Pressure Control Strategy

In order to ensure that a transcritical cycle is always operating at or near optimal high-side pressure as conditions vary in a real application, a control strategy must be implemented. The most common control strategy is to correlate optimal high-side pressure as a linear function of gas cooler refrigerant outlet temperature, as shown in Equation (8.12). Using the optimal high-side pressure values obtained in the previous section, separate control equations can be developed for the two cases of varying ambient temperature at constant compressor speed and varying compressor speed at constant ambient temperature. The results are shown in Figure 8.12.

$$P_{gc,opt} = C_1 T_{ref,out} + C_2 \qquad (8.12)$$

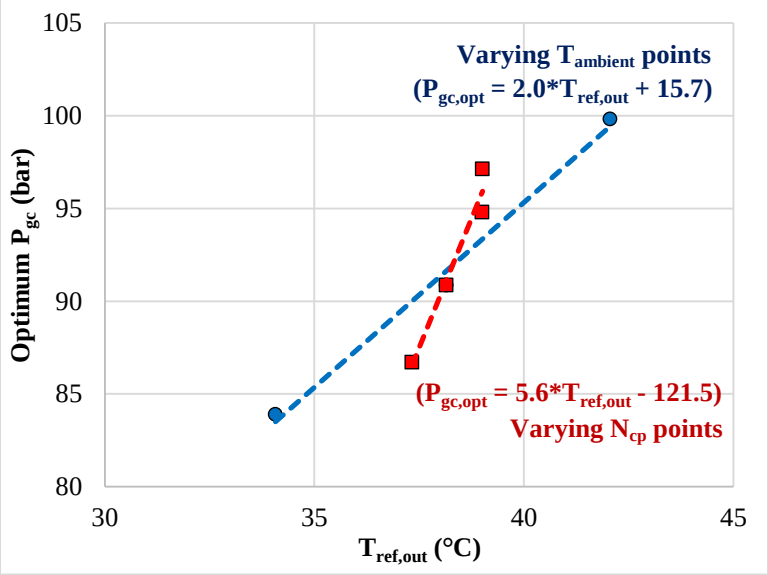

Figure 8.12: Relation between optimal high-side pressure and gas cooler refrigerant outlet temperature for cases of varying ambient temperature (blue circle) and varying compressor speed (red square).

It can be seen from Figure 8.12 that the two separate control strategies for varying ambient temperature and varying compressor speed each match their respective points well. However, the resulting control strategies for the two cases are very different. It would not be practical to implement separate high-side pressure control strategies, one to be used when ambient temperature is changing and one to be used when compressor speed is changing. Furthermore, implementing a single control strategy of the form shown in Equation (8.12) would not be very accurate. Figure 8.13 shows that if a single correlation for optimal high-side pressure as a linear function of gas cooler refrigerant outlet temperature were used to predict all points, the prediction would only match the experimental data to within 4 %. The constants C_1 and C_2 are 2.20 and 8.14, respectively, in the resulting control equation. While this accuracy may not seem unreasonable for predicting experimental data, it should be noted that a change of only several bar in high-side pressure can result in a very noticeable loss in system performance, especially for conditions where COP is more sensitive to high-side pressure (lower ambient temperature or lower compressor speed, closer to the critical point). Referring to Figure 8.8, at the lowest compressor speed, a change of 3 to 4 bar in high-side pressure could result in a COP loss of 5 % or greater.

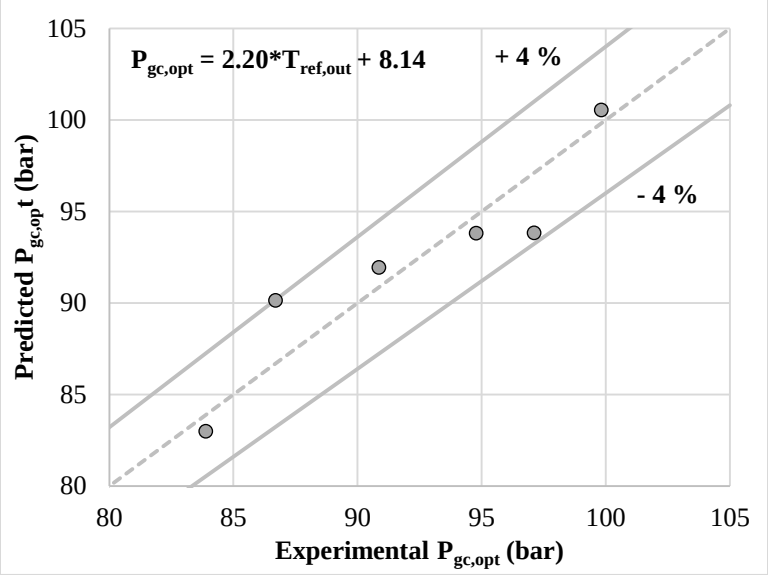

Figure 8.13: Comparison of curve fitted and experimental optimal high-side pressure as a linear function of gas cooler refrigerant outlet temperature; data points are predicted to within 4.0 % accuracy.

Using a linear relation between optimal high-side pressure and gas cooler refrigerant outlet temperature is generally meant for conditions of varying ambient temperature. In order to account for the effect of varying capacity at constant ambient temperature, an additional term that increases as capacity increases can be added to the control equation. This can be accomplished using the gas cooler approach temperature

(temperature difference between refrigerant outlet and air inlet), which is the smallest temperature difference in the gas cooler, as shown in Equation (8.13). A larger capacity means that the gas cooler will need to reject more heat, resulting in greater temperature difference throughout the gas cooler. Thus, higher capacity will result in higher gas cooler approach temperature, meaning that approach temperature can be used to account for capacity variation in the high-side pressure control equation.

$$\Delta T_{gc,app} = T_{ref,out} - T_{air,in} \qquad (8.13)$$

Equation (8.14) shows the form of the high-side pressure control equation with the addition of gas cooler approach temperature. Figure 8.14 shows that a when a control equation of the form shown in Equation (8.14) is used to predict optimal high-side pressure, much better prediction of the experimental data points is achieved, with the largest error between experiment and prediction being 1.3 %. The constants C_1, C_2, and C_3 are 2.74, 3.09, and -22.35, respectively, in the resulting control equation. Note that the larger the gas cooler is for the given system, the less significant the approach temperature would be in predicting optimal high-side pressure. The system in this study had gas cooler approach temperatures in the range of 2 – 5 K. For a larger system that can operate with approach temperature closer to 1 K over a range of conditions, accounting for varying capacity in the control equation may not be as important.

$$P_{gc,opt} = C_1 T_{ref,out} + C_2 \Delta T_{gc,app} + C_3 \qquad (8.14)$$

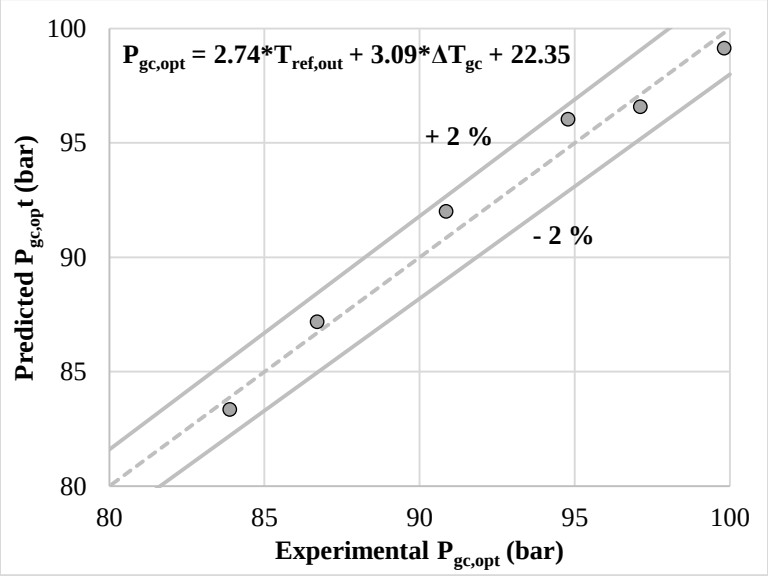

Figure 8.14: Comparison of curve fitted and experimental optimal high-side pressure as a function of gas cooler refrigerant outlet temperature and gas cooler approach temperature; data points are predicted to within 1.3 % accuracy.

8.5 High-side Pressure Control with Expansion Valve

The results of the previous two sections have shown that an adjustable ejector is an effective means for controlling high-side pressure. In this section, the use of an expansion valve in series or parallel with a fixed ejector, which may present a simpler and less expensive cycle control option, will be investigated experimentally. The results of this section have been previously published in Lawrence and Elbel (2016d, 2016e). The experimental conditions used in the tests of this section are shown in Table 8.1, and the evaporator outlet quality was 1.0 for all tests. Figure 8.15 shows the COP and capacity of the ejector cycle as high-side pressure is varied at the given conditions. High-side pressure can be increased by closing the expansion valve in series with the ejector, while high-side pressure is decreased by opening the expansion valve in parallel with the ejector. The results show that the series and parallel expansion valves are effective at controlling high-side pressure. The trends observed here are similar to those observed with the adjustable ejector, as COP shows a maximum at the optimal high-side pressure and capacity continues to increase with high-side pressure, though an adjustable ejector cannot decrease high-side pressure.

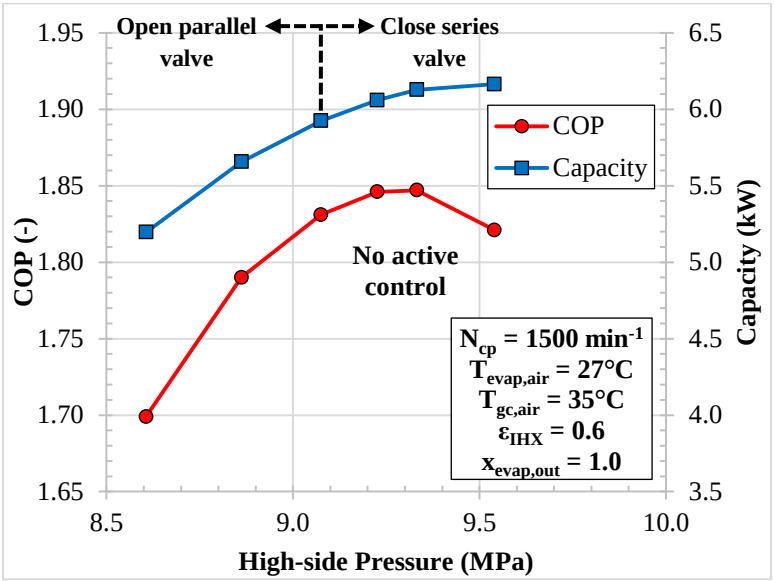

Figure 8.15: COP and capacity of ejector cycle using expansion valves in series and parallel with fixed ejector to control high-side pressure.

Figure 8.16 shows the actual work recovered by the ejector, maximum available ejector work recovery (based on the ejector motive inlet state), and total available work recovery for the entire expansion process (before loss in expansion valve) for different high-side pressures. The actual work recovered by the ejector was calculated assuming an isentropic compression of the suction stream. The difference between the maximum total and maximum ejector work recovery is due to the loss in the expansion valve,

and it can be seen from the figure that this loss is significant, even for moderate changes in high-side pressure. However, it can also be seen that the majority of loss during the expansion process still occurs in the ejector itself. Note that the maximum total expansion work and maximum ejector expansion work at the point of no control are the same because neither valve is being used for control at this point (series valve fully open and parallel valve fully closed). As the series expansion valve is closed and high-side pressure is increased, pressure loss in the series valve reduces available ejector work recovery. As the parallel expansion valve is opened and high-side pressure is decreased, the ejector inlet pressure is not reduced compared to the high-side pressure but a portion of the mass that would be ejector motive flow is bypassed around the ejector through the parallel valve instead, which reduces the available ejector work recovery.

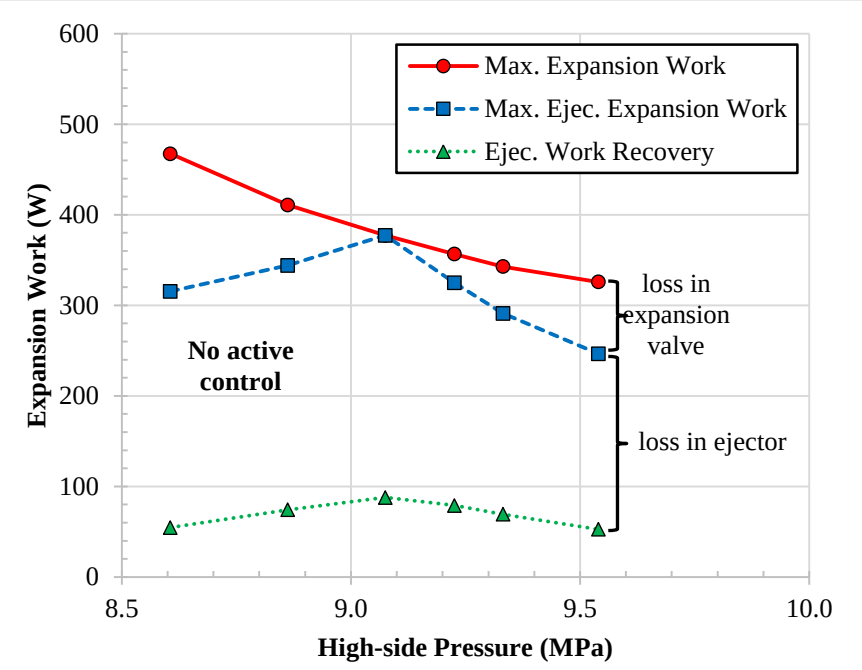

Figure 8.16: Comparison of maximum total work recovery potential, work recovery potential of ejector, and actual work recovery of ejector; data points are the same as those shown in previous figure.

Expansion work recovery efficiency can be defined two different ways for the control method considered here. The ejector work recovery efficiency (η_{ejec}) is defined as the actual ejector work recovery divided by the maximum available ejector work recovery, taking the motive inlet state as the point between the series expansion valve and ejector and using the actual mass flow rate through the ejector. The total work recovery efficiency (η_{exp}) is defined as the actual work recovery divided by the total available work recovery, taking the motive inlet state at the point upstream of the series expansion valve and using the

total high-side mass flow rate. The difference between the two efficiencies is the loss in the expansion valve. The two efficiencies are shown in Equations (8.15) and (8.16) and with the diagram in Figure 8.17.

$$\eta_{ejec} = \frac{\dot{m}_s}{\dot{m}_{ejec}} \frac{\left(h\left(P_{diff}, s_s\right) - h_s\right)}{\left(h_{ejec,in} - h\left(P_{diff}, s_{ejec,in}\right)\right)} \tag{8.15}$$

$$\eta_{exp} = \frac{\dot{m}_s}{\dot{m}_{tot}} \frac{\left(h\left(P_{diff}, s_s\right) - h_s\right)}{\left(h_{exp,in} - h\left(P_{diff}, s_{exp,in}\right)\right)} \tag{8.16}$$

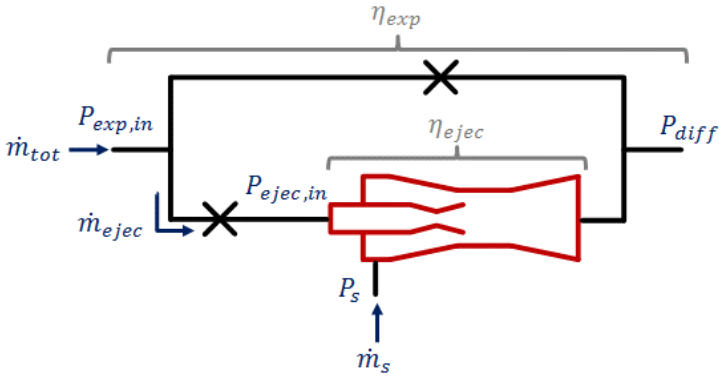

Figure 8.17: Diagram demonstrating ejector and total expansion work recovery efficiencies.

Figure 8.18 shows the ejector and total work recovery efficiencies. It can be seen that the total work recovery efficiency is always less than the ejector efficiency due to the loss in the valves described above, with the exception of the point where neither valve is used (no active control). Interestingly, when the pressure is increased by about 2 bar, the efficiency of the ejector actually improves slightly, meaning that the slight increase in inlet pressure is more favorable to ejector operation. However, total work recovery still decreases, meaning that the loss in the valve outweighs the gain in ejector efficiency. It is clear that both adjustable ejector and expansion valve control methods cause noticeable losses in expansion work recovery. A comparison of the adjustable ejector and series expansion valve control methods will be presented here. Figure 8.19 compares the COP of the ejector cycle at the same condition using the two control methods. When high-side pressure is not actively controlled (series expansion valve fully opened and needle fully retracted), the results should theoretically be the same for the two cases. It can be seen from Figure 8.19 that the COP is within 1 % for the two cases at the lowest high-side pressure where no losses are caused by the valve or needle. As high-side pressure is increased, there is a slight deviation in COP when comparing the two control methods, with the expansion valve cycle having up to 1.5 % lower

COP as high-side pressure is increased by up to 8 bar. However, the maximum COP, achieved by increasing high-side pressure by 2 bar, is very similar for the two control methods.

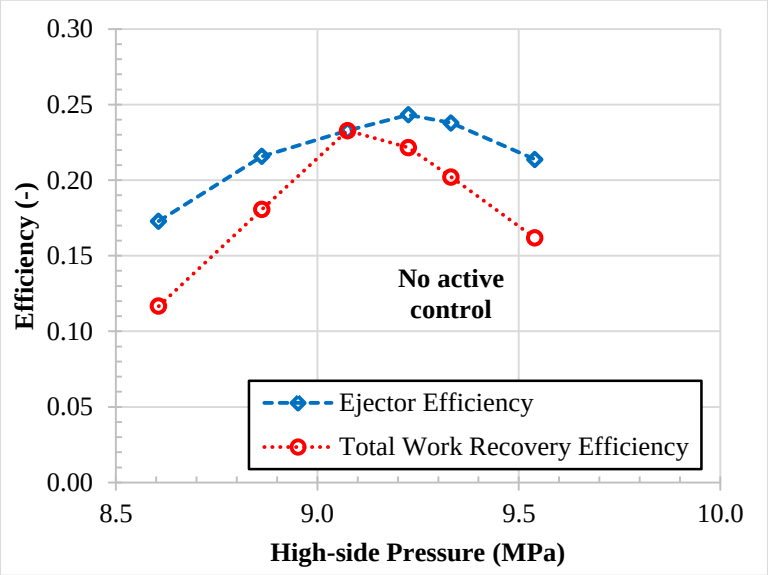

Figure 8.18: Comparison of ejector and total expansion work recovery efficiencies; data points are the same as those shown in figures above.

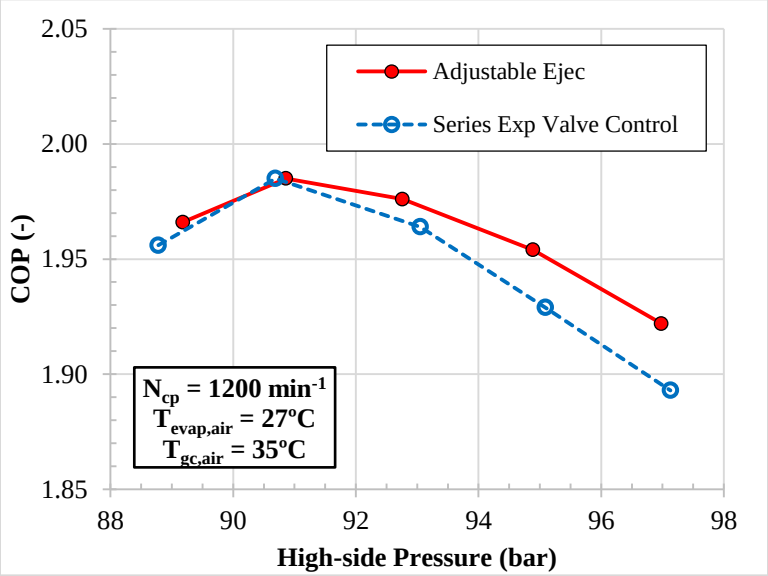

Figure 8.19: Comparison of COP with adjustable ejector control and series expansion valve control.

Figure 8.20 compares the expansion work recovery efficiency observed with the two control methods. For the system with series expansion valve control, the motive inlet state was taken as the point upstream of the expansion valve, meaning that the loss in the expansion valve contributed to lower work recovery

efficiency as calculated here; this is consistent with work recovery efficiency as defined in Equation (8.16). It can be seen from the figure that at the lowest high-side pressure where no active control is used, the work recovery efficiency observed is within 1.0 percentage point for the two different control methods. This is because when neither control method is used (series expansion valve fully opened and needle fully retracted), there is no loss due to the needle or expansion valve, and the work recovery efficiency is just the efficiency of the fixed geometry ejector. However, a small but noticeable difference in work recovery efficiency between the adjustable ejector and expansion valve control methods can be observed as high-side pressure increases, with the expansion valve control method yielding up to 2.3 percentage points lower work recovery efficiency. This indicates that the loss due to the needle in the adjustable ejector results in only slightly less loss than the series expansion valve. The expansion valve control represents the worst case situation (an adiabatic expansion process cannot be worse than isenthalpic). It can also be seen from Figure 8.20 that the difference in work recovery efficiency increases with greater increase of high-side pressure. Similarly, Figure 8.19 shows that the difference in COP between the two control methods also increases with greater increase of high-side pressure due to the increasing difference in work recovery efficiency. It can be concluded from these results that the use of an expansion valve in series or parallel with the ejector may offer a simpler option (lower cost) compared to the adjustable ejector with only a slight decrease in ejector and cycle efficiency. Ideally, the ejector nozzle could be sized such that only one expansion valve is needed (either oversize nozzle and use only series expansion valve or undersize nozzle and use only parallel expansion valve).

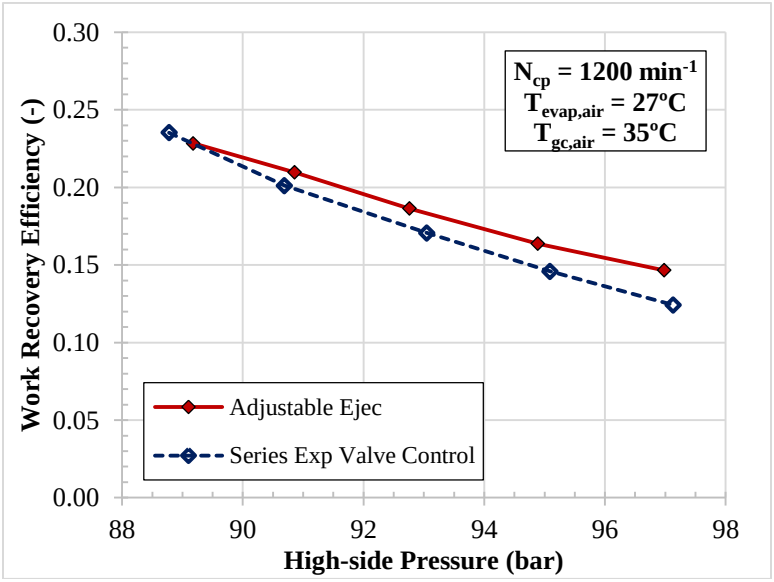

Figure 8.20: Comparison of expansion work recovery efficiency with adjustable ejector control and series expansion valve control.

8.6 Comparison of Transcritical and Subcritical Operation and Control

Control of subcritical CO_2 ejector cycles and the transition from transcritical to subcritical operation are generally not considered in experimental studies. The high-side pressure in a subcritical system is set by the condensing temperature, which is a strong function of ambient temperature. However, high-side pressure can still be controlled, albeit over a much smaller range compared to a transcritical cycle, and used to optimize cycle COP. Similar to a transcritical cycle, decreasing the expansion device restriction size will increase the condensing pressure, which simultaneously decreases condenser outlet specific enthalpy (increases capacity) and increases compressor outlet specific enthalpy (increases compressor power). This is shown in the diagram of Figure 8.21. Thus, similar to a transcritical cycle, there is an optimum condensing pressure that will result in maximum COP, and this optimum pressure is also determined by Equation (8.11). This method of cycle control has been described as subcooling control for DX cycles previously (Pottker and Hrnjak, 2015b), though in principle it is the same as high-side pressure control of transcritical cycles.

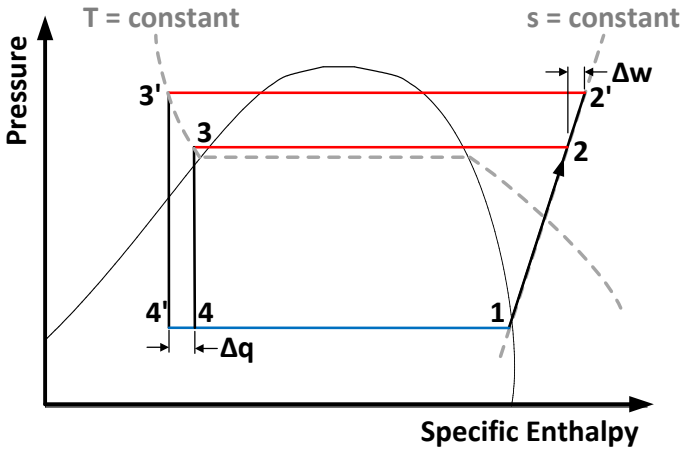

Figure 8.21: High-side (condensing) pressure of a subcritical system affects capacity and compressor work of a subcritical cycle and can be used to optimize COP, similar to a transcritical cycle.

An experimental investigation on a CO_2 ejector system was performed in order to investigate control and optimization of high-side pressure in subcritical cycles and compare to transcritical operation of the same system. The results of this section have been previously published in Lawrence and Elbel (2016f). Table 8.4 lists the operating conditions used in the CO_2 experiments comparing transcritical and subcritical operation and control. These operating conditions differ from those used in the previous sections in this chapter as a lower evaporator air temperature was used in order to allow the cycle to operate at subcritical conditions in addition to transcritical conditions. The cycle operated in subcritical mode at ambient temperatures of 20 and 22°C and in transcritical mode at ambient temperatures of 25, 30, and 35°C.

Table 8.4: Operating conditions used for CO_2 experiments comparing transcritical and subcritical operation.

Parameter	Unit	Value
$T_{evap,air,in}$	°C	20
$\dot{V}_{evap,air}$	$m^3\ s^{-1}$	0.250
T_{amb}	°C	20, 22, 25, 30, 35
$\dot{V}_{amb,air}$	$m^3\ s^{-1}$	0.500
N_{cp}	min^{-1}	1200
ε_{IHX}	-	0.6
$x_{evap,out}$	-	1.0

Figure 8.22 shows the COP of the ejector cycle as a function of high-side pressure at ambient temperatures of 20 and 22°C, for which the cycle operates in subcritical mode. The figure notes the amount of subcooling or outlet state of the condenser for each point. If the needle is fully retracted from the nozzle throat (no active control of high-side pressure), then the outlet of the condenser is at some two-phase condition (not fully condensed). Inserting the needle into the throat and increasing condensing pressure causes the outlet to become subcooled.

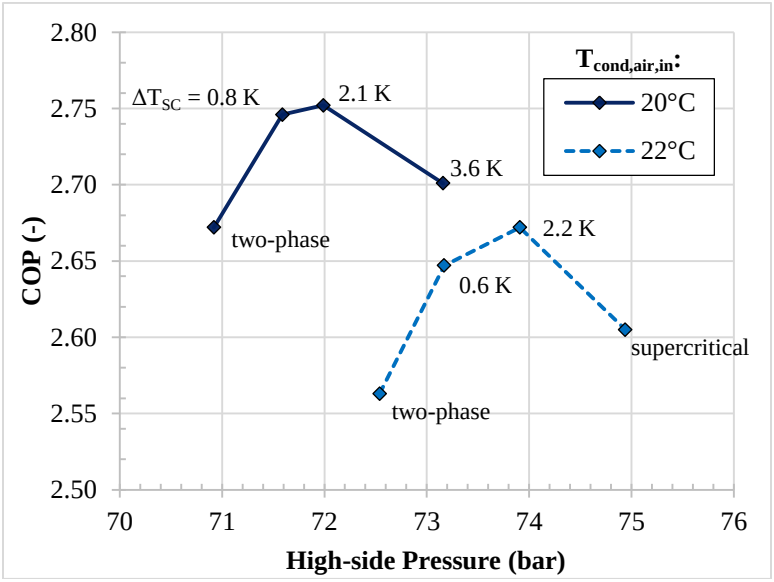

Figure 8.22: COP of subcritical ejector cycle for different ambient temperatures with condenser outlet subcooling or fluid state noted for each point.

It can be seen from Figure 8.22 that similar to transcritical operation, the ejector cycle shows an optimum in COP with respect to high-side (condensing) pressure for subcritical operation as well. These results clearly indicate that the concept of COP maximization by high-side pressure optimization can be applied to subcritical cycles. There is a corresponding subcooling for each optimal high-side pressure, indicating that subcooling control is ultimately the same as high-side pressure optimization. The optimum COP seems to occur when subcooling is approximately 2 K for both cases. For reference, the outlet state that resulted in maximum COP of the DX cycle was approximately 4 K subcooling for the 20°C ambient temperature case and supercritical for the 22°C ambient temperature case. Note that while the optimal subcooling seems small in this system, the fluid still passed through an IHX after the condenser, meaning that the enthalpy was still reduced substantially (and subcooling increased) before expansion.

High-side pressure optimization was determined for the transcritical operating points (25, 30, and 35°C ambient temperature) as well. Figure 8.23 shows the COP trends for all ambient temperatures (both subcritical and transcritical operation). As discussed in Section 8.3, the COP shows greater sensitivity to high-side pressure at lower ambient temperature due to the properties of CO_2. It can be seen from the figure that this trend continues into the subcritical region as well where COP seems to be very sensitive to high-side pressure.

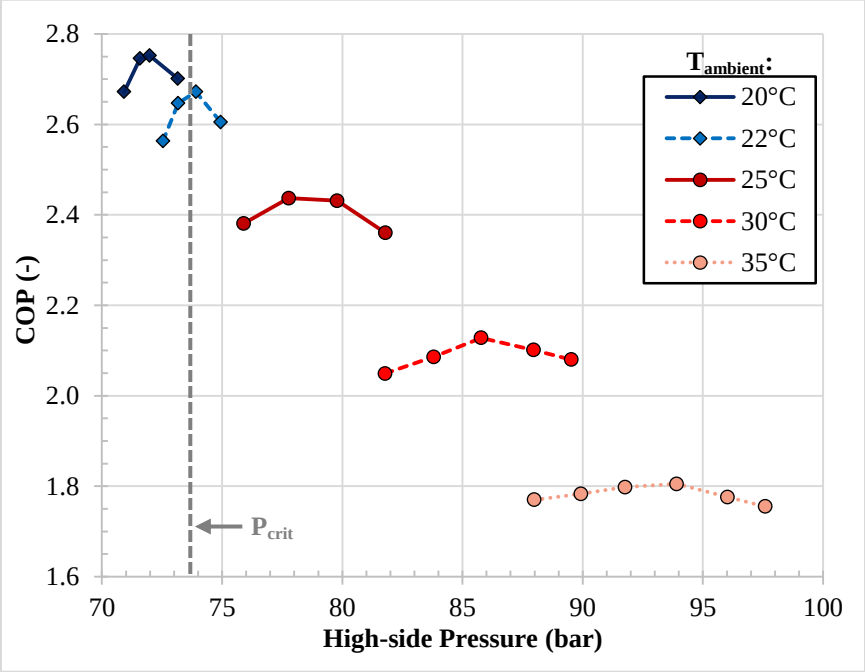

Figure 8.23: COP of ejector cycle for all ambient temperatures (subcritical and transcritical operation).

Figure 8.24 shows the variation of ejector work recovery efficiency for different ambient temperatures. For a given ambient temperature, it can be seen that the ejector efficiency consistently decreases as high-side pressure increases due to increased frictional losses when the needle is inserted further into the nozzle. Interestingly, the rate of decrease in ejector efficiency seems to be lower at higher ambient temperature. This implies that at higher pressure, less use of the needle (meaning less loss in ejector efficiency) is needed to increase high-side pressure by the same amount.

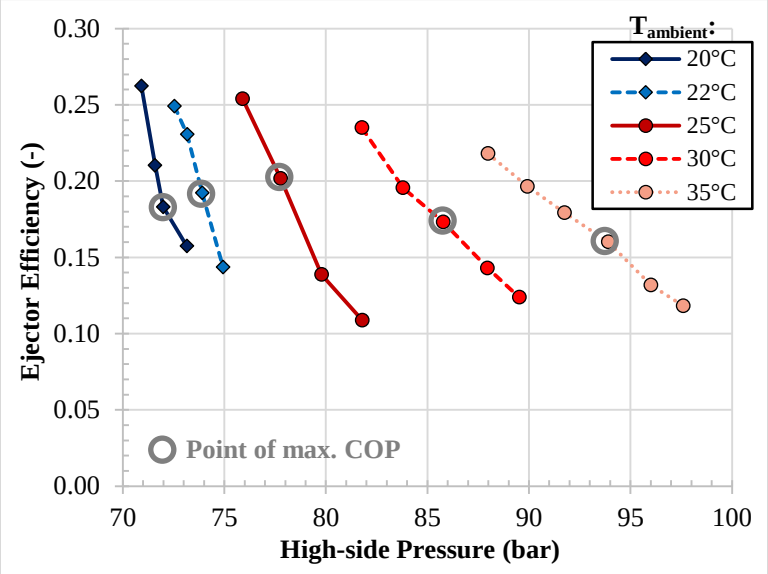

Figure 8.24: Variation of ejector work recovery efficiency with high-side pressure for ambient temperatures.

Table 8.5 shows the ejector cycle COP improvement gained by adjusting high-side pressure (compared to the ejector cycle with no active control of high-side pressure) at each ambient temperature. This COP improvement generally ranges from 2 to 4 %, which is similar to the results of Section 8.3 and to what was observed in the studies of Elbel and Hrnjak (2008) and Xu *et al.* (2012). The COP seems to be particularly sensitive at an ambient temperature of 22°C, where 4.3 % COP improvement can be gained by increasing high-side pressure by just 1.4 bar; this is because the high-side pressure is very close to the critical pressure at this condition. It also seems that a greater change in high-side pressure is needed to maximize COP at higher ambient temperature despite the lower COP gain from controlling high-side pressure, as shown in the table; for the subcritical conditions, 3 to 4 % is gained in COP by increasing high-side pressure by about 1 bar, while at the highest ambient temperature, only 2 % improvement in COP is achieved even though high-side pressure is increased by 6 bar.

Table 8.5: COP improvement of ejector cycle from use of adjustable ejector (needle) and COP and capacity improvement of ejector cycle compared to DX cycle.

$T_{ambient}$ (°C)	COP Improvement from Use of Needle	$P_{gc,opt} - P_{NoControl}$ (bar)	COP Improvement Compared to DX Cycle	Capacity Improvement Compared to DX Cycle
20	3.0 %	1.1	3.0 %	2.1 %
22	4.3 %	1.4	2.3 %	3.0 %
25	2.4 %	1.9	3.3 %	1.5 %
30	3.9 %	4.0	5.6 %	2.6 %
35	2.0 %	5.9	7.4 %	6.4 %

High-side pressure optimization at the same test conditions was repeated with the DX cycle. Table 8.5 also shows the COP and capacity improvements of the ejector cycle compared to the DX cycle with each cycle operating at its point of maximum COP. It can be seen that COP and capacity improvements of the ejector cycle are greater at higher ambient temperature due to the greater amount of work available for recovery in the ejector at higher temperature and pressure. Interestingly, it also seems that the COP increase from controlling ejector cycle high-side pressure is similar to or greater than the COP improvement over the DX cycle for some conditions, especially at lower ambient temperature. In other words, the ejector cycle has the opportunity to improve COP compared to a DX cycle at all conditions, but if the cycle is not controlled properly, any opportunity for COP improvement may be lost, particularly at lower ambient temperature. This point combined with the fact that COP is even more sensitive to high-side pressure near the critical point means that it is particularly important to actively control high-side pressure at lower ambient temperature (near the critical point) in order to ensure the ejector cycle is always performing better than the DX cycle.

The above results have shown that the same adjustable ejector can be used to control and optimize high-side pressure of the same ejector system for both transcritical and subcritical operation. Studies on transcritical CO_2 cycles commonly correlate the optimum high-side pressure as a function of refrigerant gas cooler outlet temperature, as shown in Equation (8.12); because only one compressor speed was used for these tests, the effect of condenser/gas cooler approach temperature was not considered here. Figure 8.25 shows the optimum high-side pressure plotted against the corresponding gas cooler/condenser outlet temperature at each condition. The solid line in the figure is the line of best fit for the three transcritical points. It can be seen from the figure that the same linear trend can be extended to fit the subcritical points as well, as shown by the dotted line in the figure. This finding is important because it means that there is

no need to switch between high-side pressure control and subcooling control or to determine an ambient temperature at which it becomes more beneficial to operate in transcritical mode. The high-side pressure control strategy applied to transcritical CO_2 ejector systems can actually be extended to subcritical operation of the same system as well using the same control equation.

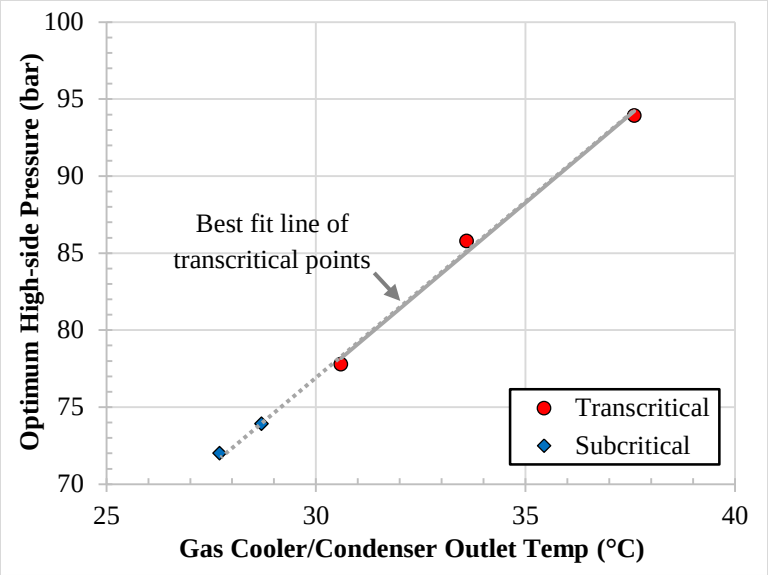

Figure 8.25: Linear trend of optimum high-side pressure as a function of condenser/gas cooler outlet temperature for subcritical and transcritical conditions.

8.7 Chapter Summary and Conclusions

This chapter has presented the results of an experimental investigation on the control of a CO_2 ejector cycle, with a particular emphasis on transcritical cycles. Options to control high-side pressure in a transcritical cycle include an adjustable ejector, parallel ejectors, or an expansion valve in series or parallel with the ejector, with the adjustable ejector and expansion valve control methods the focus of the experimental investigation. Additionally, control of evaporator flow rate has been investigated.

The results in Sections 8.3 and 8.5 have shown that both control methods, adjustable ejector and expansion valve in series with the ejector, are effective at controlling high-side pressure in order to maximize COP. The adjustable ejector did yield slightly higher work recovery efficiency and COP, especially at points of greater increase in high-side pressure where greater use of the control device is needed. However, the differences were small, meaning that the expansion valve control may offer a simple, inexpensive alternative to the adjustable ejector that can be controlled and used in the same manner. The results in Section 8.2 demonstrate the significant effect that control of the evaporator

metering valve can have on cycle performance. For every system and operating condition, there is an optimum evaporator outlet state and corresponding optimum evaporator metering valve setting. In order to optimize system performance as conditions vary, this valve must be actively controlled.

The results presented in Sections 8.3 and 8.6 have shown that upwards of 4 % in COP can be lost due to not properly controlling high-side pressure (assuming the ejector is properly designed for the system). However, it was seen in Section 8.2 that improper control of the evaporator metering valve can result in upwards of 11 % loss in COP, which is noticeably larger than the loss in COP due to not properly controlling high-side pressure. While the exact numbers presented here are not necessarily representative of all systems, these results show that for some systems, proper control of evaporator flow rate can be far more important than proper control of high-side pressure. For small-scale systems for which only one active control device can be used in the system, a decision must be made as to whether it is more important to control high-side pressure or evaporator flow rate for that system. This is an important point because, as seen from the literature review, almost all research on control of ejector systems focuses on high-side pressure control but neglects the important effect of evaporator control.

Control strategies (equations) for determining optimal high-side pressure at different conditions have been presented. Previous experimental studies have developed control strategies for high-side pressure as a function of only gas cooler refrigerant outlet temperature, as ambient temperature was the only operating condition that was actively varied. The results in Section 8.4 have shown that if significant capacity variations at the same ambient temperature are possible in the system, some additional variable, such as approach temperature, should be added to the control equation for more accurate prediction. Section 8.5 showed that the high-side pressure control concept and strategy can be extended to subcritical operation, which is essentially the same as the subcooling control concept for subcritical cycles. It was found that control of high-side pressure is particularly important at lower ambient temperature where COP is more sensitive to high-side pressure and the improvement compared to the DX cycle is lower. This means that when designing an ejector for a system, it would be best to design the ejector to optimize performance at lower ambient conditions and rely more on cycle control to achieve reasonable COP at higher ambient conditions, where the consequences of improper ejector design and control are not as significant.

CHAPTER 9: SUMMARY, CONCLUSIONS, AND RECOMMENDED FUTURE WORK

9.1 Summary of Research and Findings

This dissertation has presented an experimental and numerical investigation into factors affecting the performance of vapor-compression cycles using ejectors for expansion work recovery. Previous research has mainly focused on the design and performance of the ejector and the impact ejector performance has on cycle performance. However, important factors such as cycle architecture (or choice of cycle), evaporator design and operation, and cycle control also have a very significant impact on ejector cycle performance, though these points have been discussed only marginally in previous ejector studies. Thus, the aim of this dissertation has been to provide a more thorough investigation of these factors.

Two different uses of the expansion work recovered by an ejector in a vapor-compression system have been identified, namely directly supplementing compressor work by directly lifting compressor suction pressure with the ejector and improving evaporator performance by using the ejector for liquid recirculation. A finite volume model of a microchannel evaporator was developed and combined with thermodynamic state-point models of the ejector cycles to compare cycle performance with different refrigerants (CO_2, R410A, and R134a). The numerical results have shown that fluids with very large throttling loss (such as CO_2) should use the ejector to directly supplement compressor power with the standard ejector cycle, while low-pressure fluids (such as R134a) that do not achieve very large pressure lift with the ejector but can gain noticeable benefit from liquid recirculation should use the ejector for liquid recirculation. The ejector recirculation cycle COP does not depend on ejector efficiency as long as the ejector can overcome the pressure drop in the evaporator; this aspect of the cycle makes it particularly appealing for systems with low-pressure refrigerants and smaller, less expensive systems due to the opportunity for simplified cycle controls and simplified ejector design.

Experimental results with R410A ejector cycles using microchannel evaporators have demonstrated that evaporator design and operation (overfeed rate) can have a very significant effect on the COP improvement obtained with an ejector cycle. The standard ejector cycle initially achieved only 6 % COP improvement while the ejector recirculation cycle achieved up to 16 % COP improvement compared to the same baseline; however, when an evaporator with the same air-side resistance but half the refrigerant-side cross-sectional area and heat transfer area was used, the standard ejector cycle COP improvement increased to 9 %, while the ejector recirculation cycle COP improvement decreased to 13 %. Thus, the experimental results have shown that the most favorable evaporator design is different for different ejector cycles. The improved heat transfer coefficient due to increased mass flux with the second

evaporator improved performance in the standard ejector cycle, while the reduced heat transfer area outweighed the improved heat transfer coefficient and hurt evaporator performance in the ejector recirculation cycle. It should also be noted that the majority of evaporator improvement in either cycle was gained by eliminating dryout. This means that when designing an ejector system, it is important to understand how the design and operation of the evaporator can affect the COP of the ejector cycle in comparison to a DX cycle.

The numerical model was used to further investigate evaporator design in ejector cycles. It was recommended for both ejector cycles to keep microchannel port diameter large and use the number of refrigerant-side passes and circulation number to optimize mass flux. For the standard ejector cycle, the evaporator design should be used to improve the evaporator performance for a low overfeed rate, and the ejector should be used for pressure lift (directly supplementing compressor power). On the other hand, for the ejector recirculation cycle, the ejector should be used to provide a large amount of overfeed to the evaporator and the number of refrigerant-side passes should be used to balance heat transfer and pressure drop. It was also recommended that evaporator pressure drop be limited to a 1.0 K drop in saturation temperature for each cycle (at least for R410A). While the experimental results showed that the ejector recirculation cycle could generally achieve higher COP with R410A and the given evaporator, the numerical results showed the standard ejector cycle could ultimately achieve higher COP once the refrigerant-side of the evaporator was optimized for each cycle. Finally, it was seen that for a higher-pressure fluid that is less sensitive to pressure drop in the evaporator (CO_2), evaporator design does not have as significant of an effect on cycle performance compared to a low-pressure fluid.

A CO_2 ejector system was used to investigate ejector cycle control experimentally. Control was investigated for both high- and low-pressure sides of the system. It was seen that upwards of 4 % in COP can be lost due to not properly controlling high-side pressure, while improper control of the evaporator metering valve can result in upwards of 11 % loss in COP. The loss in COP for not properly controlling the evaporator metering valve is noticeably larger than the loss in COP for not properly controlling high-side pressure. This means that in order to optimize ejector cycle performance as conditions vary, the evaporator flow rate (metering valve) must be actively controlled, a point that is generally neglected in ejector studies. Two different methods were investigated for controlling high-side pressure, the adjustable ejector and expansion valve control. It was seen that both methods were effective at controlling high-side pressure, but both methods also resulted in significant losses caused by the control mechanism. The adjustable ejector did yield slightly higher work recovery efficiency and COP compared to the series expansion valve control. Control strategies (equations) for determining optimal high-side pressure at

different conditions have been presented. It has been shown that systems with simultaneous variations in ambient temperature and capacity should account for both variations with separate variables in the control strategy (equation). Control was found to be particularly important near the critical point, where fluid properties make COP very sensitive to high-side pressure. Additionally, it was seen that the high-side pressure control concept and strategy can be extended to subcritical operation, which is essentially the same as the subcooling control concept for subcritical cycles, and that the same control strategy can be used for both sub- and transcritical operation.

The contributions to the field of ejector technology unique to this dissertation are as follows:

- Identification of two different uses of the expansion work recovered in the ejector.
- Comparison of the two uses of expansion work recovered in ejector via numerical modeling (CO_2, R410A, and R134a) and experiments (R410A).
- Demonstration of the effect of evaporator design and operation (overfeed rate) on standard ejector and ejector recirculation cycle performance with R410A through use of experiments and numerical modeling.
- Development of guidelines for the design and operation of the evaporator in standard ejector and ejector recirculation cycles.
- Experimental investigation of high-side pressure control methods (adjustable ejector, series and parallel expansion valves) and development of transcritical CO_2 system control strategies for conditions of simultaneously varying ambient temperature and capacity.
- Experimental comparison of losses in work recovery efficiency and cycle efficiency encountered with adjustable ejector and series expansion valve control methods in a transcritical CO_2 ejector system.
- Experimental quantification of the potential gain in COP by properly controlling evaporator flow rate and high-side pressure under conditions of varying ambient temperature and capacity in a transcritical CO_2 ejector system.
- Investigation of subcritical CO_2 ejector cycle operation and development of a control strategy for both sub- and transcritical cycle operation.

9.2 Conclusions Regarding Ejector System Design

The objective of the research presented in this dissertation has been to investigate proper design and control of ejector cycles in order to gain the most benefit from the use of the ejector in the system. Conclusions that can be extracted from the results presented in this dissertation on how to best design an ejector system and gain the most benefit from the ejector will be discussed here. Much of this dissertation has focused on a comparison of two different ejector cycles, the standard ejector cycle and the ejector recirculation cycle. Analysis of these two cycles has shown that there are two fundamentally different ways in which to use the expansion work recovered in the ejector to improve the system, namely directly

increasing compressor suction pressure to supplement compressor power and recirculating liquid to improve the performance of the evaporator. The standard ejector cycle can utilize the ejector both ways simultaneously (though there is a trade-off between the two benefits) while the ejector recirculation cycle can only use the ejector to recirculate liquid. Which of these uses of the recovered work is more beneficial depends strongly on the refrigerant, evaporator design, and operating conditions. As a result, the most favorable ejector cycle for a given system is also strongly dependent on these factors. For conditions of lower expansion work recovery (using a low-pressure working fluid while operating at lower ambient temperature and/or higher evaporator temperature) or for systems in which the system is relatively sensitive to pressure drop in the evaporator, using the ejector to recirculate liquid is a better way to apply the recovered work. When a large amount of expansion work is available for recovery (higher-pressure fluid or more extreme operating conditions), it is better to use the large work recovery to directly supplement compressor power.

Control issues may also play a role in deciding which ejector cycle is better for the given system. It has been shown how the majority of benefit from overfeeding the evaporator is gained from eliminating dryout rather than further increasing mass flux after dryout is eliminated. This means that precise control of the evaporator flow rate in the ejector recirculation cycle is not critical for optimizing cycle performance as long as the evaporator operates without dryout at all conditions. This is not the case for the standard ejector cycle because the evaporator flow rate still has a significant effect on ejector pressure lift and how much the ejector can directly supplement compressor power. This means that the ejector recirculation cycle may allow for a simplified system control strategy, which would be a great benefit for small-scale applications that are driven by lower initial cost.

The ejector recirculation cycle also does not suffer a capacity loss compared to a DX cycle even if the ejector fails to function and entrain mass properly. Furthermore, the amount of expansion work that must actually be recovered in the ejector recirculation cycle to provide a small amount of overfeed to the evaporator is small in comparison to the amount of expansion work that must be recovered in the standard ejector cycle, in which the ejector must provide compression to the entire capacity (vapor) of the evaporator. This again makes the ejector recirculation cycle more favorable for conditions of lower expansion work recovery.

In principle, the standard ejector cycle would offer greater potential for many systems, assuming that the evaporator can be designed to perform well without requiring too much overfeed, because it can simultaneously use the ejector work recovery both ways, as was demonstrated by the numerical results

investigating evaporator design. However, reasons that the ejector recirculation cycle may be chosen over the standard ejector cycle when designing a system would include:

- Use of a low-pressure fluid for which directly supplementing compressor power would only offer a small benefit due to the low work recovery.
- Systems with significant variations in capacity and operating temperatures, for which ejector efficiency would drop due to off-design operation.
- Small-scale applications which do not allow for complex controls or complicated (expensive) ejector designs.
- Systems in which the evaporator could benefit significantly from overfeeding liquid (such as a shell-and-tube evaporator) or systems in which the evaporator design cannot be modified.

Once the ejector cycle has been chosen, evaporator design and operation (rate at which refrigerant is supplied to the evaporator) must be considered. These factors have been seen to have very significant effects on the COP improvement that an ejector cycle can achieve in comparison to a baseline cycle. Evaporator design and operation are particularly important for low-pressure fluids, which are very sensitive to pressure drop on the low-pressure-side of the system. The benefit of overfeeding an evaporator is that it allows for an improvement in heat transfer with a lower pressure drop penalty compared to modifying the evaporator geometry in order to improve heat transfer. This is why low-pressure fluids can gain the most benefit from overfeeding the evaporator.

Furthermore, the optimal design and operation of an evaporator would be different for the two different ejector cycles, even in the same system. The evaporator in an ejector cycle should be designed and operated with the following points in mind:

- Refrigerant-side mass flux should be adjusted to properly balance pressure drop and heat transfer performance for the given system; this should be accomplished by adjusting the number of refrigerant-side passes and the overfeed rate, leaving the tube diameter relatively large.
- The evaporator in the standard ejector cycle should be designed with a lower refrigerant-side cross-sectional area in order to increase mass flux without increasing mass flow rate significantly; the amount of overfeed should be kept low in order to maximize the pressure lift of the ejector.
- The evaporator in the ejector recirculation cycle should be designed with a larger (though still optimized) refrigerant-side cross-sectional area and should make as much use of overfeed provided by the ejector as possible.

Regardless of which ejector cycle is chosen, control of the high-pressure side of the system remains an issue. As the ejector is a fixed geometry device, some additional means of active control must be added to the system to regain control over high-side pressure/flow rate. For systems that only operate in subcritical mode, it does not matter if the system is controlled to obtain an optimal subcooling or if it is controlled to

obtain an optimal high-side pressure, as the two control strategies are essentially equivalent. However, for systems that operate in both sub- and transcritical modes, it may make sense to use only one control strategy (to optimize high-side pressure) rather than switch between control strategies as ambient temperature varies.

High-side pressure control is most important near the critical point. For fluids such as R134a and R410A (at lower ambient temperatures), which operate well below their critical pressure, active control of the high-side pressure or subcooling would not be so important. Though not ideal, it may be possible to allow systems with low-pressure fluids to use just a fixed ejector (with a properly sized nozzle) and no additional component to control the high-pressure-side of the system without suffering significant losses in cycle capacity and COP. On the other hand, for a fluid that operates near its critical point, such as CO_2, there is far more incentive to add some additional means of control, despite the potential drop in ejector component efficiency, in order to optimize cycle performance as conditions vary. This is especially true for a CO_2 system that operates in both sub- and transcritical modes.

High-side pressure control in the standard ejector cycle must be considered carefully, as any loss in ejector efficiency due to either off-design or loss from the control mechanism can have a noticeable impact on cycle performance. The ejector control method should be chosen based on the size and complexity of the system. Parallel ejectors offer the potential to control high-side pressure without any loss in efficiency; however, this control method is also expensive, large in size, and potentially difficult to design and control, meaning it may not be practical for anything smaller than a refrigeration plant. Despite its lower efficiency, the adjustable ejector offers a simpler and more compact control option, which is likely more practical for small- and medium-scale applications. The expansion valve control method may offer a somewhat less expensive option, though its lower efficiency does not make it appealing for use in the standard ejector cycle. On the other hand, the ejector recirculation cycle does not require a significant amount of work recovery in order to offer significant performance improvement. This means that a simple expansion valve upstream of the ejector to control the cycle could be a very reasonable option in this cycle; despite the loss in the expansion valve, there would still be enough available work recovered to pump a small amount of liquid and eliminate dryout in the evaporator.

9.3 Recommended Future Work

It is recommended that future work in the field of ejector technology continue to focus on investigation of alternate ejector cycles, cycle control methods, and evaporator performance. This dissertation has presented a thorough comparison of the standard ejector and ejector recirculation cycles; however, there

are additional alternate ejector cycle options that may be of interest in future studies. Of greatest value are cycles that offer practical advantages in real applications, such as reduced penalty for ejector off-design performance. Simplified ejector control methods or control methods that result in little or no losses due to the controlling mechanism would also greatly advance the field of ejector technology. Additionally, understanding how to design and control evaporators in ejector cycles requires further research. The results of this dissertation have shown how significant evaporator design can be in ejector cycles and have provided guidelines on how to design and operate evaporators for these cycles. The results reported here can be expanded for a wider range of heat exchanger types and refrigerants, and it is recommended that this also be a significant area of future ejector research.

Ejectors have already been successfully applied to large-scale CO_2 refrigeration plants. This is a natural application of ejectors because the large size of the system allows for a complex ejector control strategy (these systems use parallel ejectors), and the use of CO_2 offers large opportunity for performance improvement. However, further research is needed in order to successfully apply ejectors to smaller applications with low-pressure refrigerants. A simplified control strategy (or a cycle that requires no active control) would be needed for many of these applications, indicating the need for further research on ejector cycles with practical advantages in real applications as well as simpler ejector control methods. It is also important to understand what the losses in cycle performance due to these design simplifications would be. This dissertation has quantified the penalty for improper cycle control for a CO_2 system. However, applications with low-pressure refrigerants could yield very different penalties for improper control; further research is needed to quantify these penalties for small-scale systems and systems with low-pressure refrigerants. The ultimate goal of the future research on ejectors should be to understand the best way to incorporate an ejector into a given system for a wide range of applications.

REFERENCES

American Society of Heating Refrigeration, and Air Conditioning Engineers (ASHRAE), 1983, *Equipment Handbook*, Chapter 13 Steam-jet Refrigeration Equipment, Atlanta, GA, USA.

American Society of Heating, Refrigeration, and Air Conditioning Engineers (ASHRAE), 2014, *Refrigeration Handbook*, Chapter 4 Liquid Recirculation, Atlanta, GA, USA.

Banasiak, K., Hafner, A., 2011, 1D computational model of a two-phase R744 ejector for expansion work recovery, *Int. J. Therm. Science*, 50: 2235-2247.

Banasiak, K., Hafner, A., Andresen, T., 2012, Experimental and numerical investigation of the influence of the two-phase ejector geometry on the performance of the R744 heat pump, *Int. J. Refrigeration*, 35: 1617-1625.

Banasiak, K., Hafner, A., 2013, Mathematical modelling of supersonic two-phase R744 flows through converging-diverging nozzles: the effects of phase transition models, *Appl. Therm. Engr.*, 51: 635-643.

Banasiak, K., Palacz, M., Hafner, A., Buliński, Z., Smołka, J., Nowak, A.J., Fic, A., 2014, A CFD-based investigation of the energy performance of two-phase R744 ejectors to recover the expansion work in refrigeration systems: An irreversibility analysis, *Int. J. Refrigeration*, 40: 328-337.

Banasiak, K., Hafner, A., Palacz, M., 2015a, State of the art in the identification of two-phase transonic flow phenomena in transcritical CO_2 ejectors, 24th IIR International Congress of Refrigeration, Yokohama, Japan, Paper 45.

Banasiak, K., Hafner, A., Kriezi, E.E., Madsen, K.B., Birkelund, M., Fredslund, K., Olsson, R., 2015b, Development and performance mapping of a multi-ejector expansion work recovery pack for R744 vapour compression units, *Int. J. Refrigeration*, 57: 265-276.

Besagni, G., Mereu, R., Inzoli, F., 2016, Ejector refrigeration: a comprehensive review, *Renew. Sustain. Energy Reviews*, 53: 373-407.

Bilir Sag, N., Ersoy, H.K., Hepbasli, A., Halkaci, H.S., 2015, Energetic and exergetic comparison of basic and ejector expander refrigeration systems operating under the same external conditions and cooling capacities, *Energy Conv. Management*, 90: 184-194.

Boumaraf, L., Haberschill, P., Lallemand, A., 2014, Investigation of a novel ejector expansion refrigeration system using the working fluid R134a and its potential substitute R1234yf, *Int. J. Refrigeration*, 45: 148-159.

Brodie, B.R., Takano, Y., Gocho, M., 2012, Evaporator with integrated ejector for automotive cabin cooling, SAE Technical Paper 2012-01-1048.

Carey, V.P., 2008, *Liquid-Vapor Phase-Change Phenomena*, Chapter 10 Introduction to Two-phase Flow, 2nd Ed., Taylor & Francis Group, New York, NY, USA.

Chen, J.C., 1966, Correlation for boiling heat transfer to saturated fluids in convective flow, *Ind. Eng. Chem. Proc. Des. Dev.*, 5(3): 322-339.

Chen, J., Jarall, S., Havtun, H., Palm, B., 2015, A review on versatile ejector applications in refrigeration systems, *Renew. Sustain. Energy Reviews*, 49: 67-90.

Cheng, L., Ribatski, G., Wojtan, L., Thome, J.R., 2006, New flow boiling heat transfer model and flow pattern map for carbon dioxide evaporating inside horizontal tubes, *Int. J. Heat Mass Transfer*, 49: 4082-4094.

Chunnanond, K., Aphornratana, S., 2004, Ejectors: applications in refrigeration technology, *Renew. Sustain. Energy Reviews*, 8: 129-155.

Churchill, S.W., 1977, Friction factor equations spans all fluid-flow regimes, *Chem. Engr.*, 84(24): 91-92.

Colarossi, M., Trask, N., Schmidt, D.P., Bergander, M.J., 2012, Multidimensional modeling of condensing two-phase ejector, *Int. J. Refrigeration*, 35: 290-299.

Deng, J., Zhang, Y., He, Y., Zheng, L., 2016, Visual investigation on effect of structural parameters and operation condition of two-phase ejector, 16th International Refrigeration and Air Conditioning Conference at Purdue, West Lafayette, IN, USA, Paper 2155.

Disawas, S., Wongwises, S., 2004, Experimental investigation on the performance of the refrigeration cycle using a two-phase ejector as an expansion device, *Int. J. Refrigeration*, 27: 587-594.

Dittus, F.W., Boelter, L.M.K., 1930, Heat transfer in automobile radiator of the tubular type, *Pub. Engr.*, 2: 443-461.

Domanski, P., 1995, Theoretical evaluation of the vapor-compression cycle with a liquid-line/suction-line heat exchanger, economizer, and ejector, National Institute of Standards and Technology (NIST), Report NISTIR 5606, Gaithersburg, MD, USA.

Domanski, P.A., Didion, D.A., Doyle, J.P., 1994, Evaluation of suction-line/liquid-line heat exchanger in the refrigeration cycle, *Int. J. Refrigeration*, 17: 487-493.

Dopazo, J.A., Fernández-Seara, J., 2011, Experimental evaluation of an ejector as liquid re-circulator in an overfeed NH_3 system with a plate evaporator, *Int. J. Refrigeration*, 34: 1676-1683.

Elbel, S.W., Hrnjak, P.S., 2004a, Effect of internal heat exchanger on performance of transcritical CO_2 systems with ejector, 10th International Refrigeration and Air Conditioning Conference at Purdue, West Lafayette, IN, USA, Paper R166.

Elbel, S., Hrnjak, P., 2004b, Flash gas bypass for improving the performance of transcritical R744 systems that use microchannel evaporators, *Int. J. Refrigeration*, 27: 724-735.

Elbel, S., 2007, Experimental and analytical investigation of a two-phase ejector used for expansion work recovery in a transcritical R744 air-conditioning system, University of Illinois at Urbana-Champaign, Ph.D. Dissertation, Urbana, IL, USA.

Elbel, S., Hrnjak, P., 2008, Experimental validation of a prototype ejector designed to reduce throttling losses encountered in transcritical R744 system operation, *Int. J. Refrigeration*, 31: 411-422.

Elbel, S., 2011, Historical and present developments of ejector refrigeration systems with emphasis on transcritical carbon-dioxide air-conditioning applications, *Int. J. Refrigeration*, 34: 1545-1561.

Elbel, S., Lawrence, N., 2016, Review of recent developments in advanced ejector technology, *Int. J. Refrigeration*, 62: 1-18.

Ersoy, H.K., Bilir Sag, N., 2014, Preliminary experimental results on the R134a refrigeration system using a two-phase ejector as an expander, *Int. J. Refrigeration*, 43: 97-110.

F-Chart Software, 2015, Engineering Equation Solver Academic Profession V9.908, Middleton, WI, USA.

Fredslund, K., Kriezi, E.E., Madsen, K.B., Birkelund, M., Olsson, R., 2016, CO_2 installations with a multi ejector for supermarkets, case studies from various locations, 12th IIR Gustav Lorentzen Conference on Natural Refrigerants, Edinburgh, UK, Paper 1105.

Friedel, L., 1979, Improved friction pressure drop correlations for horizontal and vertical two-phase pipe flow, European Two Phase Flow Group Meeting, Ispra, Italy, Paper E2.

Gay, N.H., 1931, Refrigerating system, U.S. Patent 1,836,318.

Gnielinski, V., 1976, New equations for heat and mass transfer in turbulent pipe and channel flow, *Int. Chem. Engr.*, 16(2): 359-367.

Hafner, A., Försterling, S., Banasiak, K., 2014, Multi-ejector concept for R-744 supermarket refrigeration, *Int. J. Refrigeration*, 43: 1-13.

Hafner, A., Banasiak, K., Herdlitschka, T., Fredslund, K., Girotto, S., Haida, M., Smołka, J., 2016, R744 ejector system case: Italian supermarket, Spiazzo, 12th IIR Gustav Lorentzen Conference on Natural Refrigerants, Edinburgh, UK, Paper 1078.

Haida, M., Banasiak, K., Smołka, J., Hafner, A., Madsen, K.B., 2016, Experimental analysis of the R744 vapour compression rack equipped with the multi-ejector expansion work recovery module, 12th IIR Gustav Lorentzen Conference on Natural Refrigerants, Edinburgh, UK, Paper 1079.

Harrell, G.S., Kornhauser, A.A., 1995, Performance tests of a two phase ejector, 30th Intersociety Energy Conversion Engineering Conference, Orlando, FL, USA, Paper CT-69.

Henry, R.E., Fauske, H.K., 1971, The two-phase critical flow of one-component mixtures in nozzles, orifices, and short tubes, *ASME J. Heat Transfer*, 92(2), 179-187.

Hu, J., Shi, J., Liang, Y., Yang, Z., Chen, J., 2014, Numerical and experimental investigation on nozzle parameters for R410A ejector air conditioning system, *Int. J. Refrigeration*, 40: 338-346.

Incropera, F.P., DeWitt, D.P., Bergman, T.L., Lavine, A.S., 2007, *Fundamentals of Heat and Mass Transfer*, Chapter 11 Heat Exchangers, 6th Ed., John Wiley & Sons, Hoboken, NJ, USA.

Inokuty, H., 1928, Graphical method of finding compression pressure of CO_2 refrigerating machine, 5th IIR International Congress of Refrigeration, Rome, Italy, 185-192.

Kornhauser, A.A., 1990, The use of an ejector as a refrigerant expander, 1990 USNC IIR-Purdue Refrigeration Conference, West Lafayette, IN, USA.

Lawrence, N., 2012, Analytical and experimental investigation of two-phase ejector cycles using low-pressure refrigerants, University of Illinois at Urbana-Champaign, M.S. Thesis, Urbana, IL, USA.

Lawrence, N., Elbel, S., 2012, Experimental and analytical investigation of automotive ejector air-conditioning cycles using low-pressure refrigerants, 14th International Refrigeration and Air Conditioning Conference at Purdue, West Lafayette, IN, USA, Paper 2118.

Lawrence, N., Elbel, S., 2013, Theoretical and practical comparison of two-phase ejector refrigeration cycles including First and Second Law analysis, *Int. J. Refrigeration*, 36: 1220-1232.

Lawrence, N., Elbel, S., 2014a, Experimental investigation of a two-phase ejector cycle suitable for use with low-pressure refrigerants R134a and R1234yf, *Int. J. Refrigeration*, 38: 310-322.

Lawrence, N., Elbel, S., 2014b, Review and analysis of the effect of ejector geometry on the performance of two-phase CO_2 ejectors, 11th IIR Gustav Lorentzen Conference on Natural Refrigerants, Hangzhou, China, Paper 53.

Lawrence, N., Elbel, S., 2014c, Numerical investigation of two-phase ejector liquid recirculation cycles with natural refrigerants, 11th IIR Gustav Lorentzen Conference on Natural Refrigerants, Hangzhou, China, Paper 52.

Lawrence, N., Elbel, S., 2015, Mathematical modeling and thermodynamic investigation of the use of two-phase ejectors for work recovery and liquid recirculation in refrigeration cycles, *Int. J. Refrigeration*, 58: 41-52.

Lawrence, N., Elbel, S., 2016a, Experimental investigation on the effect of evaporator design and application of work recovery on the performance of two-phase ejector liquid recirculation cycles with R410A, *Appl. Therm. Engr.*, 100: 398-411.

Lawrence, N., Elbel, S., 2016b, Implementation of a two-phase ejector cycle for R744 glass door merchandisers, 12th IIR Gustav Lorentzen Conference on Natural Refrigerants, Edinburgh, UK, Paper 1082.

Lawrence, N., Elbel, S., 2016c, Numerical study on the design of microchannel evaporators for ejector refrigeration cycles, 16th International Refrigeration and Air Conditioning Conference at Purdue, West Lafayette, IN, USA, Paper 2092.

Lawrence, N., Elbel, S., 2016d, Experimental study on control methods for transcritical CO_2 two-phase ejector systems at off-design conditions, 12th IIR Gustav Lorentzen Conference on Natural Refrigerants, Edinburgh, UK, Paper 1083.

Lawrence, N., Elbel, S., 2016e, Experimental investigation of control strategies for off-design operation of a transcritical CO_2 two-phase ejector refrigeration system for the cold chain, 4th IIR Conference on Sustainability and the Cold Chain, Auckland, New Zealand.

Lawrence, N., Elbel, S., 2016f, Experimental comparison of the performance of a CO_2 ejector cycle for transcritical and subcritical operation, 12th IIR Gustav Lorentzen Conference on Natural Refrigerants, Edinburgh, UK, Paper 1085.

Lee, J.S., Kim, M.S., Kim M.S., 2011, Experimental study on the improvement of CO_2 air conditioning system performance using an ejector, *Int. J. Refrigeration*, 34: 1614-1625.

Lee, J.S., Kim, M.S., Kim, M.S., 2014, Studies on the performance of a CO_2 air conditioning system using an ejector as an expansion device, *Int. J. Refrigeration*, 38: 140-152.

Li, D., Groll, E.A., 2005, Transcritical CO_2 refrigeration cycle with ejector-expansion device, *Int. J. Refrigeration*, 28: 766-773.

Li, Y., Tan, L., Zhang, X., Du, K., 2014, Experimental evaluation of an ejector as a liquid re-circulator in falling film water chiller, *Int. J. Refrigeration*, 40: 309-316.

Little, A.B., Garimella, S., 2016, A critical review linking ejector flow phenomena with component and system-level performance, *Int. J. Refrigeration*, 70: 243-268.

Liu, F., Li, Y., Groll, E.A., 2012a, Performance enhancement of CO_2 air conditioner with a controllable ejector, *Int. J. Refrigeration*, 35: 1604-1616.

Liu, F., Groll, E.A., Li, D., 2012b, Investigation on performance of variable geometry ejectors for CO_2 refrigeration cycles, *Energy*, 45: 829-839.

Liu, F., Groll, E.A., 2013, Study of ejector efficiencies in refrigeration cycles, *Appl. Therm. Engr.*, 52: 360-370.

Lorentzen, G., 1983, Throttling, the internal haemorrhage of the refrigeration process, *Proc. Inst. Refrigeration*, 80: 39-47.

Lucas, C., Koehler, J., 2012, Experimental investigation of the COP improvement of a refrigeration cycle by use of an ejector, *Int. J. Refrigeration*, 35: 1595-1603.

Lucas, C., Koehler, J., Schroeder, A., Tischendorf, C., 2013, Experimentally validated CO_2 ejector operation characteristic used in a numerical investigation of ejector cycle, *Int. J. Refrigeration*, 36: 881-891.

Lucas, C., Rusche, H., Schroeder, A., Koehler, J., 2014, Numerical investigation of a two-phase CO_2 ejector, *Int. J. Refrigeration*, 43: 154-166.

Menegay, P., Kornhauser, A.A., 1996, Improvements to the ejector expansion refrigeration cycle, 31st Intersociety Energy Conversion Engineering Conference, Washington D.C., USA, Paper 96157.

Minetto, S., Brignoli, R., Banasiak, K., Hafner, A., Zilio, C., 2013, Performance assessment of an off-the-shelf R744 heat pump equipped with an ejector, *Appl. Therm. Engr.*, 59: 568-575.

Minetto, S., Brignoli, R., Zilio, C., Marinetti, S., 2014a, Experimental analysis of a new method for overfeeding multiple evaporators in refrigeration systems, *Int. J. Refrigeration*, 38: 1-9.

Minetto, S., Girotto, S., Salvatore, M., Rossetti, A., Marinetti, S., 2014b, Recent installations of CO_2 supermarket refrigeration systems for warm climates: Data from the field, 3rd IRR International Conference on Sustainability and the Cold Chain, London, UK.

Moran, M.J., Shapiro, H.N., Boettner, D.D., Bailey, M.B., 2014, *Fundamentals of Engineering Thermodynamics*, Chapter 7 Exergy Analysis, 8th Ed., John Wiley & Sons, Hoboken, NJ, USA.

Nakagawa, M., Matumi, T., Takeuchi, H., Kokubo, N., 1996, Mixing of the confined jet of mist flow, *JSME Int. J. B*, 39(2): 381-386.

Nakagawa, M., Takeuchi, H., 1998, Performance of two-phase ejector in refrigeration cycle, 3rd International Conference on Multiphase Flow, Lyon, France, Paper 382.

Nakagawa, M., Marasigan, A.R., Matsukawa, T., Kurashina, A., 2011a, Experimental investigation on the effect of mixing length on the performance of two-phase ejector for CO_2 refrigeration cycle with and without heat exchanger, *Int. J. Refrigeration*, 34: 1604-1613.

Nakagawa, M., Marasigan, A.R., Matsukawa, T., 2011b, Experimental analysis on the effect of internal heat exchanger in transcritical CO_2 refrigeration cycle with two-phase ejector, *Int. J. Refrigeration*, 34: 1577-1586.

Oshitani, H., Gocho, M., Takano, Y., 2008, Ejector-type cool box, SAE Technical Paper 2008-01-0734.

Padilla Fuentes, Y., Hrnjak, P., 2012, Charge reduction potentials of several refrigerants based on experimentally validated micro-channel heat exchangers performance and charge model, 14th International Refrigeration and Air Conditioning Conference at Purdue, West Lafayette, IN, USA, Paper 2292.

Palacz, M., Smołka, J., Fic, A., Buliński, Z., Nowak, A.J., Banasiak, K., Hafner, A., 2015, Application range of the HEM approach for CO_2 expansion inside two-phase ejectors for supermarket refrigeration systems, *Int. J. Refrigeration*, 59: 251-258.

Park, C.Y., Hrnjak, P.S., 2007, CO_2 and R410A flow boiling heat transfer, pressure drop and flow pattern at low temperatures in a horizontal smooth tube, *Int. J. Refrigeration*, 30: 166-178.

Park, Y., Jacobi, A.M., 2009, Air-side heat transfer and friction correlations for flat-tube louver-fin heat exchangers, *ASME J. Heat Transfer*, 131, 021801.

Phillips, H.A., 1938, Refrigeration system, U.S. Patent 2,123,021.

Pottker, G., Hrnjak, P., 2015a, Ejector in R410A vapor-compression systems with experimental quantification of two major mechanisms of performance improvement: Work recovery and liquid feeding, *Int. J. Refrigeration*, 50: 184-192.

Pottker, G., Hrnjak, P., 2015b, Effect of condenser subcooling on the performance of vapor-compression systems, *Int. J. Refrigeration*, 50: 156-164.

Sarkar, J., 2012, Ejector enhanced vapor-compression refrigeration and heat pump systems – a review, *Renew. Sustain. Energy Reviews*, 16: 6647-6659.

Schönenberger, J., Hafner, A., Banasiak, K., Girotto, S., 2014, Experience with ejectors implemented in a R744 booster system operating in a supermarket, 11th IIR Gustav Lorentzen Conference on Natural Refrigerants, Hangzhou, China, Paper 19.

Schoenenberger, J., 2016, Experience with R744 refrigerating systems and implemented multi ejectors and liquid overfeed, 12th IIR Gustav Lorentzen Conference on Natural Refrigerants, Edinburgh, UK, Paper 1107.

Smołka, J., Buliński, Z., Fic, A., Nowak, A.J., Banasiak, K., Hafner, A., 2013, A computational model of a transcritical R744 ejector based on a homogeneous real fluid approach, *Appl. Math. Modeling*, 37: 1208-1224.

Stoecker, W.F., 1958, *Refrigeration and Air Conditioning*, Chapter 13 Steam-jet Refrigeration, 1st ed., McGraw-Hill, New York, NY, USA.

Stoecker, W.F., 1989, *Design of Thermal Systems*, Chapter 6 System Simulation, 3rd Ed., McGraw-Hill, New York, NY, USA.

Stoecker, W.F., 1998, *Industrial Refrigeration Handbook*, Chapter 8 Liquid Recirculation, McGraw-Hill, New York, NY, USA.

Sumeru, K., Nasution, Ani, F.N., 2012, A review on two-phase ejector as an expansion device in vapor-compression refrigeration cycle, *Renew. Sustain. Energy Reviews*, 16: 4927-4937.

Xu, X., Chen, G., Tang, L., Zhu, Z., 2012, Experimental investigation on performance of transcritical CO_2 heat pump system with ejector under optimum high-side pressure, *Energy*, 44: 870-877.

Yamada, E., Nishijima, H., Matsui, H., Ueno, T., Taniguchi, M., Fujita, A., 2009, Next generation ejector cycle for truck-transport refrigerator, SAE Technical Paper 2009-01-0973.

Yazdani, M., Alahyari, A.A., Radcliff, T.D., 2012, Numerical modeling of two-phase supersonic ejectors for work recovery applications, *Int. J. Heat Mass Transfer*, 55: 5744-5753.

Yazdani, M., Alahyari, A.A., Radcliff, T.D., 2014, Numerical modeling and validation of supersonic two-phase flow of CO2 in converging-diverging nozzles, *J. Fluids Engr.*, 136: 014503.

Zhang, Z., Ma, Y., Wang, H., Li, M., 2013, Theoretical evaluation on effect of internal heat exchanger in ejector expansion transcritical CO_2 refrigeration cycle, *Appl. Therm. Engr.*, 50: 932-938.

Zou, Y., Hrnjak, P.S., 2013, Refrigerant distribution in the vertical header of the microchannel heat exchanger – measurement and visualization of R410A flow, *Int. J. Refrigeration*, 36: 2196-2208.

APPENDIX A: LIST OF EJECTOR PUBLICATIONS BY AUTHOR

Numerous publications on the use of ejectors in vapor-compression systems have been published by the author in his time as a graduate student. The author's publications on ejectors in technical journals are as follows:

- Lawrence, N., Elbel, S., 2016, Experimental investigation on the effect of evaporator design and application of work recovery on the performance of two-phase ejector liquid recirculation cycles with R410A, *Appl. Therm. Engr.*, 100: 398-411.
- Elbel, S., Lawrence, N., 2016, Review of recent developments in advanced ejector technology, *Int. J. Refrigeration*, 62: 1-18.
- Lawrence, N., Elbel, S., 2015, Mathematical modeling and thermodynamic investigation of the use of two-phase ejectors for work recovery and liquid recirculation in refrigeration cycles, *Int. J. Refrigeration*, 58: 41-52.
- Lawrence, N., Elbel, S., 2015, Analysis of two-phase ejector performance metrics and comparison of R134a and CO_2 ejector performance, *Sci. Tech. Built Environment* (formerly *HVAC&R Research*), 21(5): 515-525.
- Lawrence, N., Elbel, S., 2014, Experimental investigation of a two-phase ejector cycle suitable for use with low pressure refrigerants, *Int. J. Refrigeration*, 38: 310-322.
- Lawrence, N., Elbel, S., 2013, Theoretical and practical comparison of two-phase ejector refrigeration cycles including First and Second Law analysis, *Int. J. Refrigeration*, 36(4): 1220-1232.

The author's publications on ejectors in conference proceedings are as follows:

- Lawrence, N., Elbel, S., 2016, Implementation of a two-phase ejector cycle for R744 glass door merchandisers, 12th IIR Gustav Lorentzen Conference on Natural Refrigerants, Edinburgh, UK, Paper 1082.
- Lawrence, N., Elbel, S., 2016, Experimental study on control methods for transcritical CO_2 two-phase ejector systems at off-design conditions, 12th IIR Gustav Lorentzen Conference on Natural Refrigerants, Edinburgh, UK, Paper 1083.
- Lawrence, N., Elbel, S., 2016, Numerical modeling of the off-design performance of a transcritical CO_2 two-phase ejector cycle, 12th IIR Gustav Lorentzen Conference on Natural Refrigerants, Edinburgh, UK, Paper 1084.
- Lawrence, N., Elbel, S., 2016, Experimental comparison of the performance of a CO_2 ejector cycle for transcritical and subcritical operation, 12th IIR Gustav Lorentzen Conference on Natural Refrigerants, Edinburgh, UK, Paper 1085.
- Lawrence, N., Elbel, S., 2016, Numerical study on the design of microchannel evaporators for ejector refrigeration cycles, 16th International Refrigeration and Air Conditioning Conference at Purdue, West Lafayette, IN, USA, Paper 2092.
- Lawrence, N., Elbel, S., 2016, Performance improvements of R744 glass door merchandiser using low-cost two-phase ejector, 4th IIR Conference on Sustainability and the Cold Chain, Auckland, New Zealand.

- Lawrence, N., Elbel, S., 2016, Experimental investigation of control strategies for off-design operation of a transcritical CO_2 two-phase ejector refrigeration system for the cold chain, 4th IIR Conference on Sustainability and the Cold Chain, Auckland, New Zealand.
- Lawrence, N., Elbel, S., Numerical investigation of evaporator design in the ejector refrigeration cycle with R134a and CO_2, 24th IIR International Congress of Refrigeration, Yokohama, Japan, Paper 193.
- Lawrence, N., Elbel, S., 2015, Experimental investigation of two-phase ejector liquid recirculation cycles with R410A, 24th IIR International Congress of Refrigeration, Yokohama, Japan, Paper 194.
- Lawrence, N., Elbel, S., 2015, Study on the use of ejectors for capacity modulation and performance improvement in CO_2 commercial refrigeration systems, 24th IIR International Congress of Refrigeration, Yokohama, Japan, Paper 195.
- Lawrence, N., Elbel, S., 2015, Numerical investigation of the effect of microchannel evaporator design on the performance of two-phase ejector automotive air-conditioning cycles, SAE Tech. Paper 2015-01-0362.
- Lawrence, N., Elbel, S., 2014, Numerical investigation of two-phase ejector liquid recirculation cycles with natural refrigerants, 11th IIR Gustav Lorentzen Conference on Natural Refrigerants, Hangzhou, China, Paper 52.
- Lawrence, N., Elbel, S., 2014, Review and analysis of the effect of ejector geometry on the performance of two-phase CO_2 ejectors, 11th IIR Gustav Lorentzen Conference on Natural Refrigerants, Hangzhou, China, Paper 53.
- Lawrence, N., Elbel, S., 2014, Experimental and numerical study on the performance of R410A liquid recirculation cycles with and without ejectors, 15th International Refrigeration and Air Conditioning Conference at Purdue, West Lafayette, IN, USA, Paper 2187.
- Lawrence, N., Elbel, S., 2014, Analysis and comparison of two-phase ejector performance metrics for R134a and CO_2 ejectors, 15th International Refrigeration and Air Conditioning Conference at Purdue, West Lafayette, IN, USA, Paper 2188.
- Lawrence, N., Elbel, S., 2014, Comparison of R134a and CO_2 two-phase ejector performance for use in automotive air conditioning applications, SAE Tech. Paper 2014-01-0689.
- Lawrence, N., Elbel, S., 2013, Experimental and analytical investigation of two-phase ejector air-conditioning cycles using low-pressure refrigerants R134a and R1234yf, SAE Tech. Paper 2013-01-1495.
- Lawrence, N., Elbel, S., 2012, Experimental and analytical investigation of automotive ejector air-conditioning cycles using low-pressure refrigerants, 14th International Refrigeration and Air Conditioning Conference at Purdue, West Lafayette, IN, USA, Paper 2118.

APPENDIX B: DETAILS OF EVAPORATOR MODEL

This appendix provides further details of the finite volume evaporator model used in the numerical investigations of this study. Detailed information on empirical correlations, model grid independence, and model validation is provided.

B.1 Empirical Correlations

Air-side heat transfer coefficient was predicted using the empirical correlation of Park and Jacobi (2009) for louvered-fin, flat-tube heat exchangers. The equation listing to calculate the Chilton-Colburn j-factor for the correlation of Park and Jacobi (2009) can be seen in Equations (B.1) through (B.5). The j-factor can be related to heat transfer coefficient as shown in Equation (B.6). Air-side pressure drop was not calculated as part of the model. See the Nomenclature section for description of the symbols used in this section.

$$j = 0.872\, j_{Re}\, j_{low}\, j_{louver}\, {\theta_{louver}}^{0.219}\, {N_{louver}}^{-0.0881} \left(\frac{h_{fin}}{P_{louver}}\right)^{0.149} \left(\frac{d_{fin}}{P_{fin}}\right)^{-0.259} \left(\frac{L_{louver}}{h_{fin}}\right)^{0.540} \left(\frac{h_{fin}}{P_{tube}}\right)^{-0.902} \left(\frac{P_{louver}}{P_{fin}}\right)^{0.301} \qquad (B.1)$$

$$Re = \frac{v_{air}\, \rho_{air}\, P_{louver}}{\mu_{air}} \qquad (B.2)$$

$$j_{Re} = Re^{\left[-0.458 - 0.00874 \cosh\left(\frac{P_{fin}}{P_{louver}} - 1\right)\right]} \qquad (B.3)$$

$$j_{low} = 1 - \sin\left(\frac{P_{louver}}{P_{fin}}\, \theta_{louver}\right)\left(\frac{1}{\cosh\left(\frac{0.0490\, Re - 0.142\, d_{fin}}{N_{louver}\, P_{fin}}\right)}\right) \qquad (B.4)$$

$$j_{louver} = 1 + 0.0065 \tan(\theta_{louver}) \left(\frac{d_{fin}}{N_{louver}\, P_{fin}}\right) \cos\left(2\pi \left(\frac{d_{fin}}{P_{louver} \tan(\theta_{louver})}\right) - 1.8\right) \qquad (B.5)$$

$$h_{air} = j\, Pr^{-\frac{2}{3}}\, c_{p,air}\, \rho_{air}\, v_{air} \qquad (B.6)$$

The refrigerant-side single-phase heat transfer coefficient was predicted using the empirical correlation of Gnielinski (1976), as shown in Equation (B.7). This correlation requires knowledge of the friction factor. The friction factor was determined using a curve fit of the Moody Chart from Churchill (1977). The Moody Chart is a graphical method for determining friction factor as a function of Reynolds number and the ratio of absolute roughness of the tube (ε) to the diameter of the tube, also known as the relative roughness; Churchill (1977) provides a simple curve fit to allow the Moody Chart to be used in equation form. The equation listing for Churchill (1977) can be seen in Equations (B.8) through (B.10). The friction factor from Churchill (1977) was also used to determine single-phase pressure drop.

$$h_{ref} = \left(\frac{k}{d_{tube}}\right)\left(\frac{f}{2}\right)\frac{(Re - 1000)\,Pr}{1 + 12.7\left(\frac{f}{2}\right)^{0.5}(Pr^{-0.67} - 1)} \qquad (B.7)$$

$$f = \left[\left(\frac{8}{Re}\right)^{12} + \frac{1}{(A+B)^{\frac{3}{2}}}\right]^{\frac{1}{12}} \qquad (B.8)$$

$$A = \left[2.457 \ln\left(\frac{1}{\left(\frac{7}{Re}\right)^{0.9} + 0.27\,\frac{\varepsilon}{d_{tube}}}\right)\right]^{16} \qquad (B.9)$$

$$B = \left(\frac{37530}{Re}\right)^{16} \qquad (B.10)$$

The refrigerant-side two-phase heat transfer coefficient for R134a and R410A was predicted using the flow boiling heat transfer correlation of Chen (1966). This correlation, with equation listing shown in Equations (B.11) through (B.18), calculates evaporation heat transfer coefficient as the sum of a nucleate boiling contribution (h_{micro}) and a convective contribution (h_{macro}). The convective contribution is based on the Dittus and Boelter (1930) heat transfer correlation for single-phase fluid but is empirically modified for a two-phase turbulent flow. The nucleate boiling contribution is a function of the temperature difference between the bulk refrigerant and the wall (ΔT_w), which must be determined iteratively with the effectiveness-NTU heat exchanger method as a function of refrigerant- and air-side resistances as well as air temperature. The nucleate boiling contribution also accounts for nucleate boiling suppression at higher refrigerant mass flux through the boiling suppression factor (S).

$$h_{ref} = h_{micro} + h_{macro} \qquad (B.11)$$

$$h_{macro} = \frac{k_l}{d_{tube}}\ 0.023\ {Re_{tp}}^{0.8}\ {Pr_l}^{0.4} \qquad (B.12)$$

$$Re_{tp} = Re_l\ F^{1.25} \qquad (B.13)$$

$$Re_l = \frac{\rho_l\ v_l\ d_{tube}}{\mu_l}\ (1 - x) \qquad (B.14)$$

$$F = \begin{cases} 1 & \text{for} \quad \frac{1}{X_{tt}} \leq 0.1 \\ 2.35\ \left(0.213 + \frac{1}{X_{tt}}\right)^{0.736} & \text{for} \quad \frac{1}{X_{tt}} > 0.1 \end{cases} \qquad (B.15)$$

$$X_{tt} = \left(\frac{1 - x}{x}\right)^{0.9}\ \left(\frac{\rho_v}{\rho_l}\right)^{0.5}\ \left(\frac{\mu_l}{\mu_v}\right)^{0.1} \qquad (B.16)$$

$$h_{micro} = 0.00122\ \frac{{k_l}^{0.79}\ {c_{p,l}}^{0.45}\ {\rho_l}^{0.49}}{\sigma^{0.5}\ {\mu_l}^{0.29}\ {h_{fg}}^{0.24}\ {\rho_v}^{0.24}}\ {\Delta T_w}^{0.75}\ (P_{sat}(T_w) - P)^{0.75}\ S \qquad (B.17)$$

$$S = \frac{1}{1 + 2.56 * 10^{-6}\ {Re_{tp}}^{1.17}} \qquad (B.18)$$

There are numerous additional correlations that can be used to predict two-phase flow boiling heat transfer coefficient for conventional refrigerants. The correlation of Chen (1966) was chosen because it provides a realistic trend of how flow boiling heat transfer coefficient is understood to behave with respect to varying conditions. Figure B.1 demonstrates how flow boiling heat transfer coefficient varies with respect to quality. At low quality, where the fluid is almost all liquid and velocity is low, heat transfer is nucleate boiling dominated. As quality increases and the amount of vapor and velocity increase, convective heat transfer becomes more significant, resulting in a substantial increase in heat transfer coefficient. At very high quality, the there is too little remaining liquid to properly cover the walls of the tube (referred to as dryout), resulting in a dramatic decrease in heat transfer coefficient.

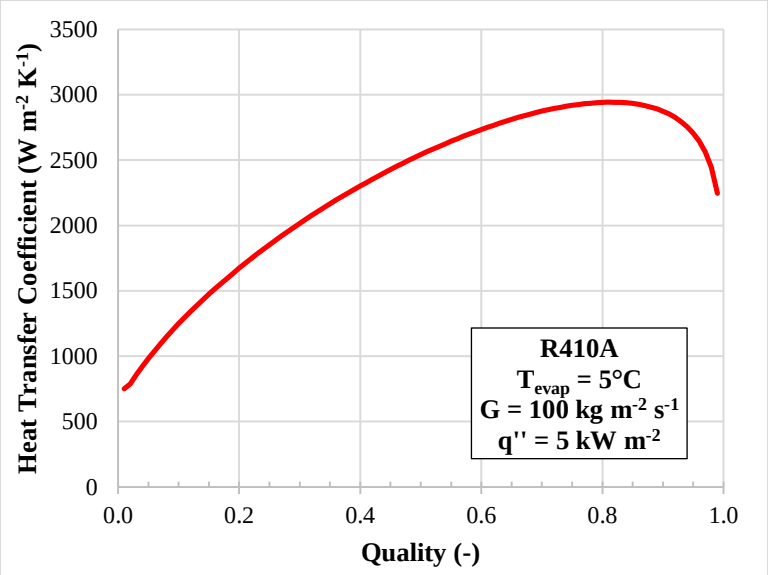

Figure B.1: Variation of flow boiling heat transfer coefficient with refrigerant quality at given conditions using correlation of Chen (1966).

Because CO_2 displays very different flow boiling heat transfer behavior compared to more conventional refrigerants, a different correlation, Cheng *et al.* (2006), was used to predict the flow boiling heat transfer coefficient of CO_2. The correlation of Cheng *et al.* (2006) first determines the flow regime of the refrigerant flow based on the given conditions and then applies different correlations to calculate heat transfer coefficient for different flow regimes. The specific listing of equations for the correlation is fairly extensive and will not be given here but can be found in the reference.

For demonstration, Figure B.2 shows a flow map that is generated using the correlation of Cheng *et al.* (2006). The flow pattern map is generated as a function of evaporation temperature and heat flux. The particular flow regime encountered in the tube is then a function of mass flux and quality; as flow proceeds through a tube, mass flux would stay constant but quality would increase, generally resulting in changes in flow regime. Figure B.3 demonstrates how flow boiling heat transfer coefficient varies with quality for the given conditions. It can be seen that the heat transfer coefficient of CO_2 is very large at low quality (in comparison to conventional refrigerants). CO_2 evaporation occurs at relatively high reduced pressure (close to the critical pressure), meaning that surface tension is small and nucleate boiling can be very significant; this leads to high heat transfer coefficient at low quality. As quality increases (more vapor), the heat transfer coefficient increases, but only slightly in comparison to conventional refrigerants; this is because the large vapor density of CO_2 results in only a moderate increase in velocity as quality increases, meaning that the convective heat transfer contribution is not as significant for CO_2.

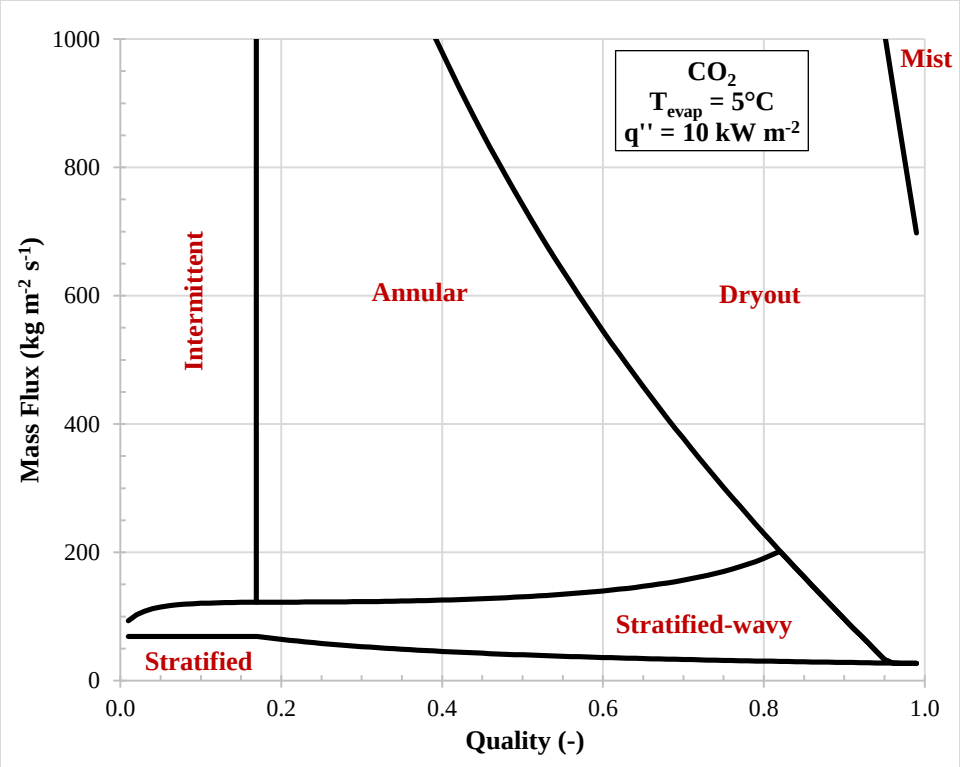

Figure B.2: Flow pattern map for flow boiling of CO_2 for a specified quality and mass flux at given conditions using correlation of Cheng *et al.* (2006).

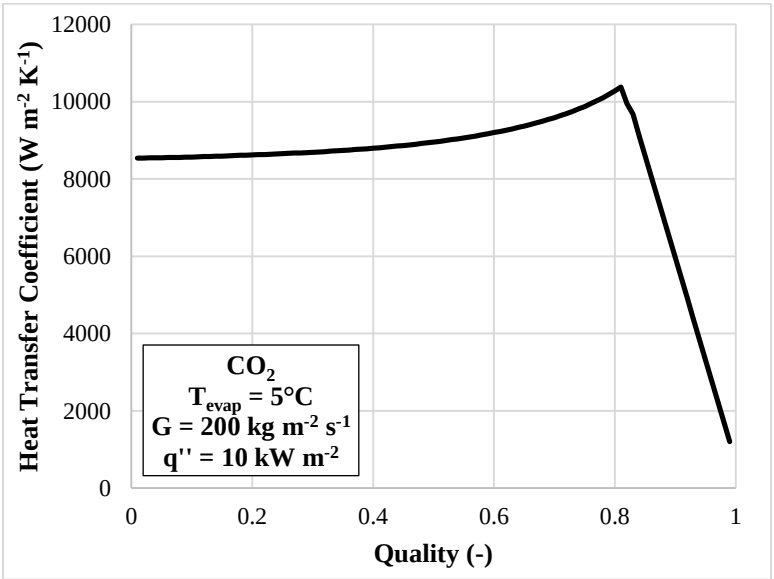

Figure B.3: Variation of CO_2 flow boiling heat transfer coefficient with refrigerant quality at given conditions using correlation of Cheng *et al.* (2006).

Refrigerant-side two-phase pressure drop was predicted using the two-phase flow multiplier correlation of Friedel (1979), with equation listing shown in Equations (B.19) through (B.25). This correlation

empirically calculates a two-phase multiplier, which is multiplied by the pressure gradient of a pure liquid flow to predict the two-phase pressure gradient. The correlation of Friedel (1979) is recommended when the ratio of liquid to vapor dynamic viscosity is less than 1000 (Carey, 2008), which is valid for the fluids and conditions considered in this study; there does not seem to be a recommended limit on the diameter of the tube for which this correlation is valid. The average density ($\bar{\rho}$) in Equations (B.24) and (B.25) is a quality-weighted average of saturated liquid and vapor densities.

$$\left(\frac{dP}{dz}\right)_{fr} = {\phi_{lo}}^2 \left(\frac{dP}{dz}\right)_{lo} \qquad (B.19)$$

$${\phi_{lo}}^2 = C_{F1} + \frac{3.24\, C_{F2}\, C_{F3}}{Fr^{0.045}\, We^{0.035}} \qquad (B.20)$$

$$C_{F1} = (1-x)^2 + x^2 \left(\frac{\rho_l\, f_{vo}}{\rho_v\, f_{lo}}\right) \qquad (B.21)$$

$$C_{F2} = x^{0.78}\,(1-x)^{0.24} \qquad (B.22)$$

$$C_{F3} = \left(\frac{\rho_l}{\rho_v}\right)^{0.91} \left(\frac{\mu_l}{\mu_v}\right)^{0.19} \left(\frac{1-\mu_v}{\mu_l}\right)^{0.7} \qquad (B.23)$$

$$Fr = \frac{G^2}{g\, d_{tube}\, \bar{\rho}^2} \qquad (B.24)$$

$$We = \frac{G^2\, d_{tube}}{\bar{\rho}\, \sigma} \qquad (B.25)$$

B.2 Grid Independence

The number of finite volumes or elements per tube in the evaporator model was chosen in order to ensure sufficient accuracy of the model. A larger number of elements is more computationally expensive but may be necessary to produce a more accurate result. In order to determine the proper number of elements, a grid independence study was conducted. Figure B.4 shows the predicted evaporator capacity at the given conditions for different numbers of evaporator elements. It can be seen from the figure that beyond 160 elements, the predicted heat transfer does not change noticeably as the number of elements is increased. Based on this analysis, it was concluded that the model was grid independent at 200 elements.

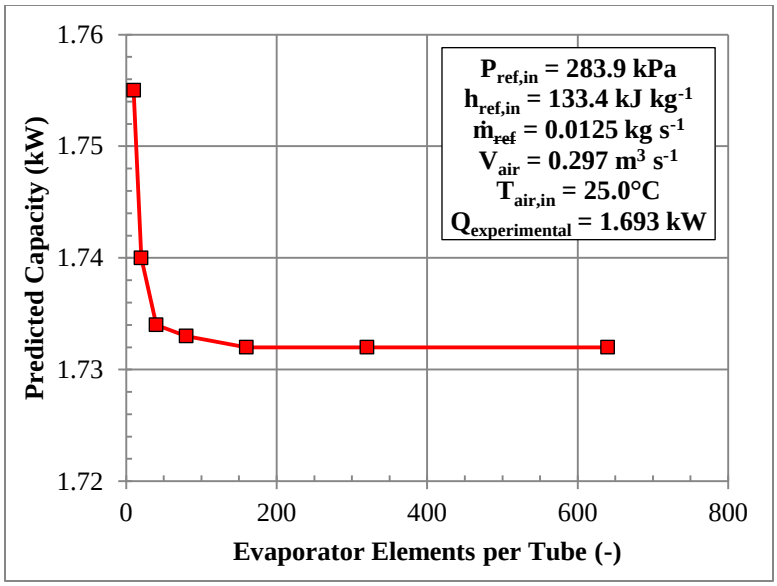

Figure B.4: Results of grid independence study show that the predicted evaporator capacity at the given conditions does not change significantly beyond 160 elements, meaning that the model is grid independent at the number of elements (200) used in the results of this study.

B.3 Evaporator Model Validation

The evaporator performance (capacity and refrigerant pressure drop) predicted by the model were compared against experimental data in order to validate the accuracy of the model. Figures B.5 and B.6 compare the predicted capacity and refrigerant pressure drop to experimental R134a data from the study of Lawrence (2012) and Lawrence and Elbel (2014a); the evaporator geometry used in this study was the same as Evaporator A from Table 5.4. Figures B.7 and B.8 compare the predicted capacity and refrigerant pressure drop to experimental CO_2 data from the present study; the evaporator geometry can be seen in Table C.5.

It can be seen from the comparison of the model and experimental data that capacity is generally predicted to within 5 % accuracy, which is an acceptable accuracy. A constant value multiplier of the form $C * \Delta P_{Friedel}$ was added to the refrigerant pressure drop correlation to improve the accuracy of the model compared to the experiments. It can be seen that refrigerant pressure drop is generally predicted to within 30 %. Very accurate prediction of refrigerant pressure drop in microchannels is difficult due to large variations in the exact geometry of individual microchannels in a given heat exchanger as a result of the manufacturing process of these heat exchangers; accurate prediction to within 30 % for microchannel heat exchangers of often considered acceptable.

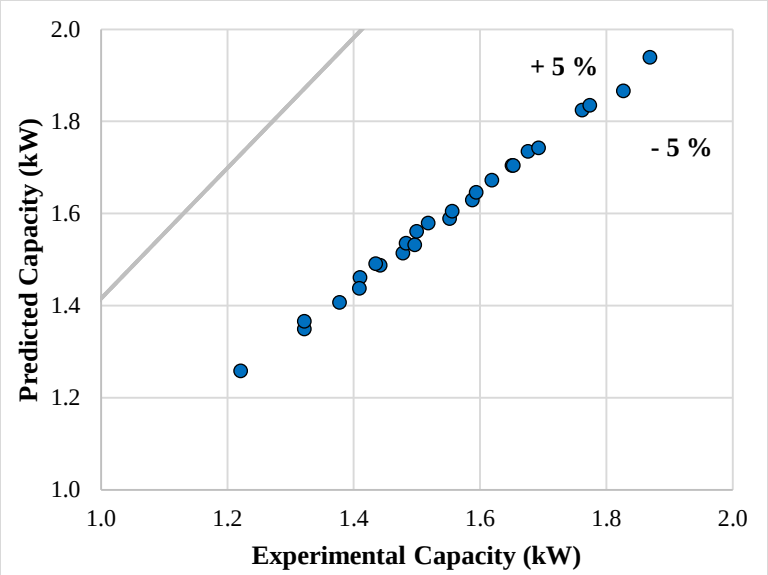

Figure B.5: Comparison of predicted and experimentally determined capacity shows that model predicts capacity to within 5 % accuracy with R134a as the refrigerant; experimental data is from the study of Lawrence and Elbel (2014a) with the geometry of Evaporator A.

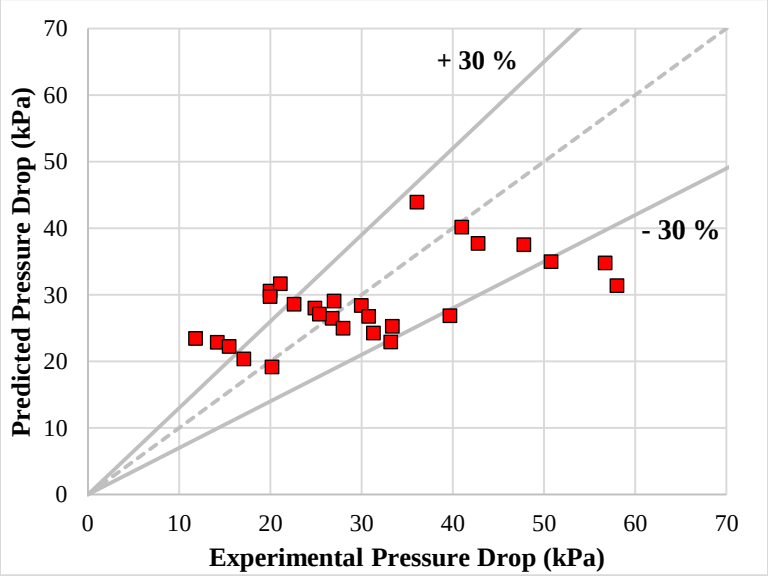

Figure B.6: Comparison of predicted and experimentally determined refrigerant pressure drop shows that model generally predicts pressure drop to within 30 % accuracy with R134a as the refrigerant; experimental data is from the study of Lawrence and Elbel (2014a) with the geometry of Evaporator A.

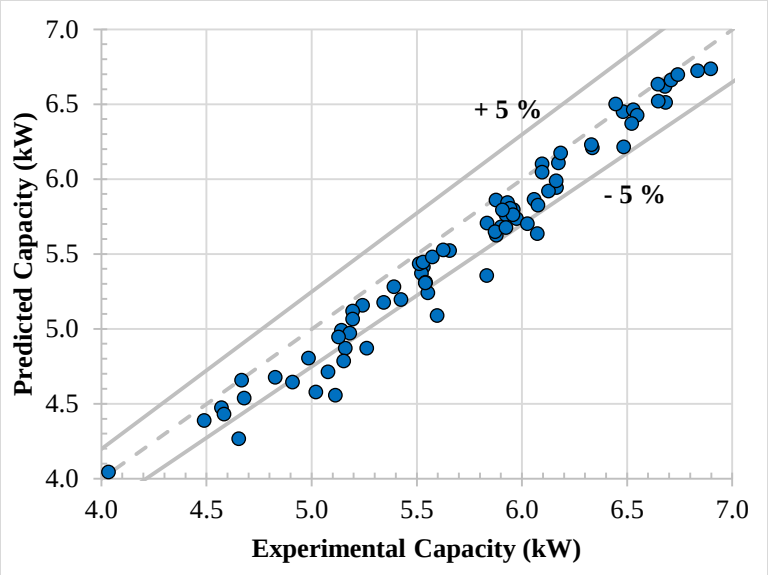

Figure B.7: Comparison of predicted and experimentally determined capacity shows that model generally predicts capacity to within 5 % accuracy with CO_2 as the refrigerant; experimental data is from the present study with the CO_2 evaporator.

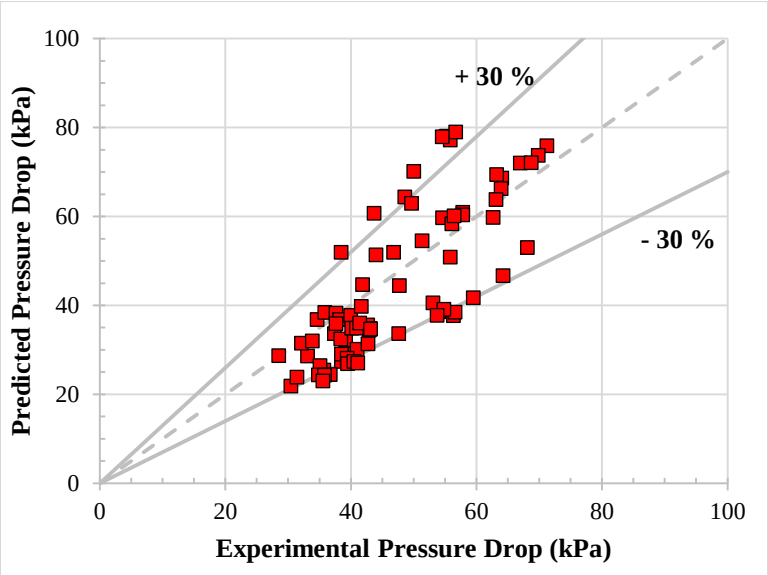

Figure B.8: Comparison of predicted and experimentally determined refrigerant pressure drop shows that model generally predicts pressure drop to within 30 % accuracy with CO_2 as the refrigerant; experimental data is from the present study with the CO_2 evaporator.

APPENDIX C: DETAILS OF EXPERIMENTAL FACILITY

This appendix provides further details of the components and uncertainty of the sensors used in the experimental R410A and CO_2 experimental facilities.

C.1 Details of R410A Experimental Facility

C.1.1 Compressor

The compressor used in the R410A experimental facility was of the hermetic, rolling-piston type. The compressor was sized to provide a maximum capacity of approximately 2 kW at a maximum speed of 80 Hz. Compressor speed was controlled with a variable frequency drive (VFD). Input power to the VFD was measured with a power transducer; losses in the VFD were not accounted for when measuring compressor power. PVE oil was used for compressor lubrication. A picture of the compressor can be seen in Figure C.1.

Figure C.1: Rolling-piston compressor used in R410A experimental facility.

C.1.2 Condenser

The condenser used in the R410A experimental facility was of the round-tube-plate-fin type. A picture of the condenser can be seen in Figure C.2. The condenser was constructed in an L-shape. The condenser was oriented in the wind tunnel in order to maximize face area. The refrigerant was split into two separate circuits through the condenser. The geometry of the condenser can be seen in Table C.1. The condenser included a high-pressure receiver at the outlet, meaning that the refrigerant generally exited the condenser as saturated liquid. A subcooling pass was not used after the receiver.

Figure C.2: Round-tube-plate-fin condenser used in R410A experimental facility.

Table C.1: Geometric dimensions and overall heat exchanger areas of round-tube-plate-fin condenser used in R410A experimental facility.

Parameter	Value
Number of tube passes per slab	24
Number of slabs	2
Number of circuits	2
Tube length per pass	800 mm
Tube outer diameter	7.9 mm
Tube pitch	20.6 mm
Fin pitch	2.3 mm
Fin depth (parallel to flow)	17.5 mm
Overall height	504 mm
Overall width (perpendicular to flow)	673 mm
Face area	0.339 m^2
Air-side area	7.050 m^2
Refrigerant-side area	0.243 m^2

C.1.3 Experimental Uncertainty of Sensors

The experimental uncertainty of the sensors used in the R410A experimental facility can be seen in Table C.2. The total uncertainties of the calculated parameters are listed in Table 5.2.

Table C.2: Summary of uncertainties of air- and refrigerant-side sensors used in R410A experimental facility.

Sensor	Range	Units	Uncertainty
Air-side sensors			
Type-T thermocouples	-200 to 220	ºC	±0.5 absolute
Differential pressure transducer (evap. to amb. and cond. to amb.)	0 to 3738	Pa	±0.14 % full scale
Differential pressure transducer (cond. nozzle and evap.)	-1246 to 1246	Pa	±0.25 % full scale
Differential pressure transducer (evap. nozzle)	0 to 1246	Pa	±0.25 % full scale
Differential pressure transducer (cond.)	0 to 623	Pa	±0.25 % full scale
Differential pressure transducer (cond. nozzle to amb.)	0 to 7475	Pa	±0.14 % full scale
Refrigerant-side sensors			
Type-T thermocouples	-200 to 220	ºC	±0.5 absolute
Absolute pressure transducer (cond. inlet and outlet and comp. outlet)	0 to 6891	kPa	±0.13 % full scale
Absolute pressure transducer (comp. inlet)	0 to 6891	kPa	±0.11 % full scale
Absolute pressure transducer (evap. outlet)	0 to 3446	kPa	±0.13 % full scale
Absolute pressure transducer (ejector diffuser outlet)	0 to 13790	kPa	±0.25 % full scale
Differential pressure transducer (sep. to comp. inlet)	-345 to 345	kPa	±0.25 % full scale
Differential pressure transducer (evap.)	-552 to 552	kPa	±0.25 % full scale
Differential pressure transducer (ejector motive inlet to diffuser outlet)	-690 to 690	kPa	±0.1 % full scale
Coriolis-type mass flow meter	0 to 333	$g\ s^{-1}$	±0.2 % reading
Power transducer	0 to 5600	W	±0.2 % reading

C.2 Details of CO_2 Experimental Facility

C.2.1 Compressor

The compressor used in the CO_2 experimental facility was of the semi-hermetic, reciprocating type. A picture of the compressor can be seen in Figure C.3, and the manufacturer specifications of the compressor can be seen in Table C.3. Compressor speed was controlled with a variable frequency drive (VFD). Input power to the VFD was measured with a power transducer; losses in the VFD were not accounted for when measuring compressor power. 400 mL of PAG oil was used in the system for

compressor lubrication. The compressor contained an internal oil separator, and oil circulation rate (OCR) was estimated to be less than 1 % by the manufacturer (Elbel, 2007).

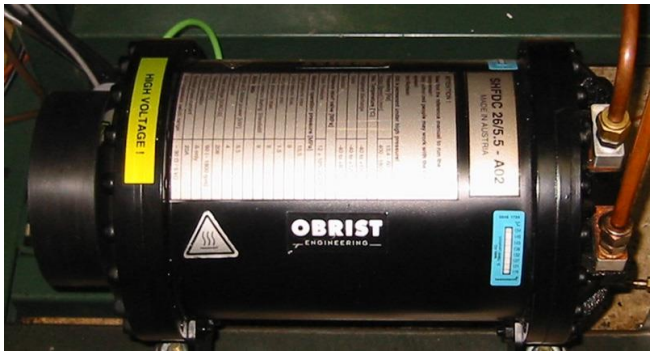

Figure C.3: Semi-hermetic, reciprocating compressor used in CO_2 experimental facility.

Table C.3: Specifications of reciprocating compressor used in CO_2 experimental facility.

Parameter	Value
Nominal speed	1800 min^{-1}
Nominal power	5.5 kW / 20 A / 208 V / 3 Ø
Maximum pressure	135 bar
Maximum temperature	160°C
Displacement	26 cm^3 rev^{-1}
Nominal flow rate	63 g s^{-1}

C.2.2 Evaporator and Gas Cooler

The evaporator and gas cooler used in the CO_2 experimental facility were both microchannel heat exchangers. When the system operated in subcritical mode, the same gas cooler would be used as a condenser; while the gas cooler design may not be ideal for a condenser, it would not be practical to switch to a different heat exchanger when switching between subcritical and transcritical operation. The geometric dimensions of the evaporator and gas cooler/condenser can be found in Table C.4, while the overall heat exchanger areas of the evaporator and gas cooler/condenser can be found in Table C.5. Both heat exchangers were constructed in such a way that refrigerant in separate tubes would not mix between slabs. A picture of the evaporator can be found in Figure C.4, and a picture of the gas cooler/condenser can be found in Figure C.5. An intercooler was placed alongside the gas cooler but was not used in the experiments (blocked off from air flow).

Table C.4: Geometric dimensions of microchannel evaporator and microchannel gas cooler/condenser used in CO_2 experimental facility.

	Evaporator	Gas Cooler
Height	202 mm	490 mm
Width	302 mm	402 mm
Number of MC tubes per pass	36	41
Number of refrigerant-side passes	4	4
MC tube pitch	8.2 mm	9.7 mm
MC tube port hydraulic diameter	0.81 mm	0.89 mm
Number of ports per MC tube	6	4
Length of MC tube per pass	177.8 mm	460.4 mm
MC tube thickness (perpendicular to air flow)	1.7 mm	1.7 mm
MC tube depth (parallel to air flow)	7.9 mm	6.4 mm
Louver angle	27°	27°
Louver pitch	1.3 mm	1.2 mm
Number of louver sets per fin	2	4
Fin pitch	1.4 mm	1.4 mm
Length of MC tube surface with fins	169.1 mm	460.4 mm
Fin thickness	0.1 mm	0.1 mm
Fin depth (parallel to air flow)	43.8 mm	35 mm
Fin height (perpendicular to air flow)	6.8 mm	8.1 mm

Table C.5: Overall heat exchanger areas of microchannel evaporator and microchannel gas cooler/condenser used in CO_2 experimental facility.

	Evaporator	Gas Cooler
Total air-side heat transfer area	3.067 m^2	8.798 m^2
Face area (air-side)	0.061 m^2	0.197 m^2
Total refrigerant-side heat transfer area	0.391 m^2	0.844 m^2
Refrigerant-side cross-sectional area	111.3 mm^2	102.0 mm^2

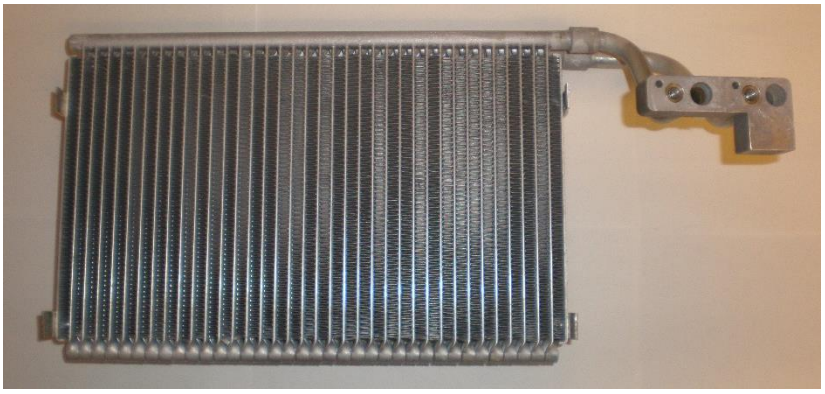

Figure C.4: Microchannel evaporator used in CO_2 experimental facility.

Figure C.5: Microchannel gas cooler/condenser used in CO_2 experimental facility.

C.2.3 Internal Heat Exchanger

A microchannel-plate heat exchanger was used as the internal heat exchanger (IHX). A valve was placed in parallel with the IHX on the low-pressure side to control IHX effectiveness. A picture of the IHX can be seen in Figure C.6.

Figure C.6: Microchannel internal heat exchanger used in CO_2 experimental facility.

C.2.4 Experimental Uncertainty of Sensors

The experimental uncertainty of the sensors used in the CO_2 experimental facility can be seen in Table C.6. The total uncertainties of the calculated parameters are listed in Table 5.3.

Table C.6: Summary of uncertainties of air- and refrigerant-side sensors used in CO_2 experimental facility.

Sensor	Range	Units	Uncertainty
Air-side sensors			
Type-T thermocouples	-200 to 220	ºC	±0.5 absolute
Differential pressure transducer (evap. to amb. and cond. to amb.)	0 to 3738	Pa	±0.14 % full scale
Differential pressure transducer (cond. nozzle and evap.)	-1246 to 1246	Pa	±0.25 % full scale
Differential pressure transducer (evap. nozzle)	0 to 1246	Pa	±0.25 % full scale
Differential pressure transducer (cond.)	0 to 623	Pa	±0.25 % full scale
Differential pressure transducer (cond. nozzle to amb.)	0 to 7475	Pa	±0.14 % full scale
Capacitive relative humidity sensor	0.2 – 100	%	±1 % absolute
Refrigerant-side sensors			
Type-T thermocouples	-200 to 220	ºC	±0.5 absolute
Absolute pressure transducer (cond. inlet and outlet and comp. outlet)	20684	kPa	±0.13 % full scale
Absolute pressure transducer (comp. inlet)	6895	kPa	±0.11 % full scale
Absolute pressure transducer (evap. outlet)	6895	kPa	±0.13 % full scale
Absolute pressure transducer (ejector diffuser outlet)	13790	kPa	±0.1 % full scale
Absolute pressure transducer (ejector nozzle inlet)	20684	kPa	±0.5 % full scale
Differential pressure transducer (sl.-IHX)	-689 to 689	kPa	±0.1 % full scale
Differential pressure transducer (evap.)	-552 to 552	kPa	±0.25 % full scale
Coriolis-type mass flow meter	0 to 333	g s^{-1}	±0.2 % reading
Power transducer	0 to 5600	W	±0.2 % reading

APPENDIX D: SAMPLE EXPERIMENTAL DATA

This appendix provides a sample of the experimental data obtained with the CO_2 experimental facility investigating the standard ejector cycle with the adjustable ejector. The data can be seen in Table D.1. The data is taken under the operating conditions of 27°C evaporator air temperature, 35°C gas cooler air temperature, and 1200 min^{-1} compressor speed for five different gas cooler pressures.

Table D.1: Sample experimental data taken at $T_{evap,air,in}$ = 27°C, $T_{gc,air,in}$ = 35°C, N_{cp} = 1200 min^{-1} for gas cooler pressures of 89 – 97 bar.

Variable	Units	Data Point #1	Data Point #2	Data Point #3	Data Point #4	Data Point #5
COP_{air}	-	1.96	1.98	1.97	1.95	1.92
Date & Time	-	2016 Jan 28 11:20 a.m.	2016 Jan 28 11:45 a.m.	2016 Jan 28 12:05 p.m.	2016 Jan 28 12:35 p.m.	2016 Jan 28 1:00 p.m.
$\Delta P_{evap,amb}$	Pa	-72.0	-72.0	-71.6	-72.1	-71.7
$\Delta P_{gc,amb}$	Pa	0.5	0.5	0.6	0.7	0.8
$\Delta P_{gc,n,amb}$	Pa	45.1	43.0	43.0	46.2	46.7
$\Delta P_{evap,air}$	Pa	151.1	151.2	151.1	152.0	152.2
$\Delta P_{evap,n}$	Pa	111.7	112.3	112.2	112.9	111.8
$\Delta P_{gc,air}$	Pa	7.4	7.4	7.4	7.4	7.4
$\Delta P_{gc,n}$	Pa	233.6	233.6	233.6	234.4	234.2
$\Delta P_{evap,ref}$	kPa	41.1	42.3	41.5	41.0	40.2
$\Delta T_{gc,app}$	K	3.4	3.2	2.6	2.1	1.6
$\Delta T_{SH,evap,out}$	K	0.0	0.1	0.1	0.1	0.2
$\Delta T_{SH,cp,in}$	K	18.9	19.4	19.5	19.5	19.6
ε_{evap}	-	0.74	0.74	0.74	0.74	0.74
ε_{gc}	-	0.94	0.95	0.96	0.97	0.98
ε_{IHX}	-	0.59	0.59	0.59	0.59	0.59
η_{cp}	-	0.70	0.70	0.68	0.68	0.68
η_{ejec}	-	0.228	0.209	0.186	0.163	0.146
η_{mech}	-	0.67	0.66	0.66	0.65	0.65
η_{vol}	-	0.70	0.68	0.67	0.66	0.65

Table D.1 (cont'd.)

Variable	Units	Data Point #1	Data Point #2	Data Point #3	Data Point #4	Data Point #5
$h_{cp,ref,in}$	kJ kg^{-1}	-47.9	-47.0	-46.7	-46.7	-46.4
$h_{cp,ref,out}$	kJ kg^{-1}	3.6	8.2	12.6	15.6	18.8
$h_{diff,out}$	kJ kg^{-1}	-159.3	-162.1	-164.4	-165.7	-166.4
$h_{evap,air,in}$	kJ kg^{-1}	36.5	36.7	36.8	36.9	37.0
$h_{evap,air,out}$	kJ kg^{-1}	19.4	19.0	18.8	18.7	18.5
$h_{evap,ref,in}$	kJ kg^{-1}	-287.8	-290.8	-292.9	-294.4	-295.7
$h_{evap,ref,out}$	kJ kg^{-1}	-78.8	-78.4	-78.1	-78.0	-77.8
$h_{gc,air,in}$	kJ kg^{-1}	308.7	308.6	308.6	308.7	308.7
$h_{gc,air,out}$	kJ kg^{-1}	318.5	318.7	318.9	319.1	319.1
$h_{gc,ref,in}$	kJ kg^{-1}	0.7	4.9	8.8	11.5	14.6
$h_{gc,ref,out}$	kJ kg^{-1}	-176.2	-186.9	-195.8	-202.0	-207.2
$h_{IHX,low,in}$	kJ kg^{-1}	-80.7	-79.8	-79.1	-78.8	-78.4
$h_{mn,in}$	kJ kg^{-1}	-217.2	-227.2	-235.3	-241.0	-245.3
$LMTD_{evap}$	K	12.4	12.8	13.0	13.1	13.3
$LMTD_{gc}$	K	17.8	18.2	18.1	17.6	17.1
$LMTD_{IHX}$	K	18.7	18.6	18.2	17.9	17.6
$\dot{m}_{cp,ref}$	g s^{-1}	33.7	31.9	30.5	29.3	28.4
$\dot{m}_{evap,air}$	kg s^{-1}	0.294	0.296	0.296	0.297	0.295
$\dot{m}_{evap,ref}$	g s^{-1}	24.2	24.8	25.1	25.2	25.3
$\dot{m}_{gc,air}$	kg s^{-1}	0.559	0.559	0.559	0.560	0.560
N_{cp}	min^{-1}	1200	1200	1200	1200	1200
P_{atm}	kPa	99.3	99.3	99.3	99.3	99.3
$P_{cp,ref,in}$	kPa	4140	4024	3943	3894	3839
$P_{cp,ref,out}$	kPa	8978	9149	9304	9542	9735
$P_{diff,out}$	kPa	4228	4108	4023	3964	3913
$P_{evap,air,in}$	kPa	99.4	99.4	99.4	99.4	99.4
$P_{evap,air,n}$	kPa	99.1	99.1	99.1	99.1	99.1

Table D.1 (cont'd.)

Variable	Units	Data Point #1	Data Point #2	Data Point #3	Data Point #4	Data Point #5
$P_{evap,air,out}$	kPa	99.3	99.3	99.3	99.3	99.2
$P_{evap,ref,in}$	kPa	3951	3893	3855	3832	3804
$P_{evap,ref,out}$	kPa	3910	3851	3814	3791	3764
$P_{gc,air,in}$	kPa	99.3	99.3	99.3	99.3	99.3
$P_{gc,air,n}$	kPa	99.3	99.3	99.3	99.3	99.3
$P_{gc,air,out}$	kPa	99.3	99.3	99.3	99.3	99.3
$P_{gc,ref,in}$	kPa	8946	9101	9287	9507	9708
$P_{gc,ref,out}$	kPa	8889	9070	9265	9471	9688
$P_{lift,ejec}$	kPa	318	257	209	173	149
$P_{mn,in}$	kPa	8808	8983	9174	9392	9603
$P_{r,cp}$	-	2.17	2.27	2.36	2.45	2.54
Φ_m	-	0.72	0.78	0.82	0.86	0.89
Π_s	-	1.08	1.07	1.06	1.05	1.04
$\dot{\mathbf{Q}}_{evap,air}$	kW	5.07	5.26	5.38	5.45	5.51
$\dot{\mathbf{Q}}_{evap,air,dry}$	kW	4.98	5.15	5.25	5.3	5.31
$\dot{\mathbf{Q}}_{evap,latent}$	kW	0.09	0.11	0.14	0.15	0.19
$\dot{\mathbf{Q}}_{gc,air}$	kW	5.47	5.63	5.73	5.78	5.80
$\dot{\mathbf{Q}}_{gc,ref}$	kW	5.96	6.11	6.24	6.27	6.29
$\dot{\mathbf{Q}}_{IHX}$	kW	1.11	1.04	0.99	0.94	0.91
Refrigerant	-	R744	R744	R744	R744	R744
$RH_{evap,in}$	-	0.16	0.16	0.17	0.17	0.17
$RH_{evap,out}$	-	0.45	0.46	0.47	0.48	0.49
T_{amb}	°C	25.6	25.8	26.0	26.1	26.2
$T_{cp,ref,in}$	°C	25.6	24.9	24.2	23.7	23.3
$T_{cp,ref,out}$	°C	98.6	102.8	106.8	110.1	113.4
$T_{evap,air,in}$	°C	27.0	27.1	27.1	27.1	27.1
$T_{evap,DP,in}$	°C	-0.6	-0.5	-0.3	-0.1	0.0

Table D.1 (cont'd.)

Variable	Units	Data Point #1	Data Point #2	Data Point #3	Data Point #4	Data Point #5
$T_{evap,air,out}$	°C	10.4	10.0	9.7	9.5	9.4
$T_{evap,ref,in}$	°C	4.6	4.0	3.7	3.5	3.2
$T_{evap,ref,out}$	°C	4.4	3.9	3.5	3.3	3.2
$T_{gc,air,in}$	°C	35.0	35.0	35.0	35.1	35.1
$T_{gc,air,out}$	°C	44.8	45.0	45.2	45.4	45.4
$T_{gc,ref,in}$	°C	96.4	100.2	104.0	107.0	110.3
$T_{gc,ref,out}$	°C	38.5	38.2	37.6	37.2	36.7
$T_{IHX,low,in}$	°C	6.7	5.6	4.8	4.3	3.8
$T_{lift,ejec}$	K	3.1	2.5	2.1	1.7	1.5
$T_{mn,in}$	°C	32.8	30.8	28.9	27.5	26.3
UA_{evap}	kW K^{-1}	0.409	0.411	0.414	0.415	0.414
UA_{gc}	kW K^{-1}	0.309	0.309	0.316	0.329	0.340
UA_{IHX}	kW K^{-1}	0.059	0.056	0.054	0.053	0.051
$\dot{\mathbf{V}}_{evap,air}$	m^{-3} s^{-1}	0.243	0.243	0.243	0.242	0.242
$\dot{\mathbf{V}}_{gc,air}$	m^{-3} s^{-1}	0.499	0.499	0.499	0.500	0.500
$\dot{\mathbf{W}}_{cp,elec}$	kW	2.58	2.65	2.73	2.80	2.87
$\dot{\mathbf{W}}_{cp,ref}$	kW	1.74	1.76	1.81	1.83	1.85
$\dot{\mathbf{W}}_{rec}$	W	66.5	56.3	47.0	39.6	34.6
$\dot{\mathbf{W}}_{rec,max}$	W	291.9	268.9	252.8	242.7	236.6
$x_{evap,ref,in}$	-	0.032	0.025	0.019	0.015	0.013
$x_{evap,ref,out}$	-	1.00	1.00	1.00	1.00	1.00